Numerical and Experimental Study of Dynamic Solar Cooling System with a Liquid Piston Converter

GAMAL HASHEM

PhD

2016

Numerical and Experimental Study of Dynamic Solar Cooling System with a Liquid Piston Converter

GAMAL HASHEM

A thesis submitted in partial fulfilment
of the requirements of the
University of Northumbria at Newcastle for
the degree of Doctor of Philosophy

Research undertaken in the

School of Engineering and Environment

July 2016

Abstract

Solar energy has been actively used to drive cooling cycles for domestic and industrial applications, especially in remote areas with a lack of electricity supply for running conventional refrigeration or air-conditioning systems. A number of solar cooling technologies exists but their market penetration level is relatively low due to the high capital costs involved and a long pay-back period. Extensive R & D activities are underway at Universities and industrial companies across many countries to improve performance and reduce capital and running costs of solar cooling systems.

Systems based on application of a liquid piston converter for solar water pumping and dynamic water desalination have been developed at Northumbria University. Some preliminary work has been completed on the development of a new solar cooling system built around the above fluid piston converter. In this work, the task is to experimentally and numerically investigate performance of the solar cooling system with the fluid piston converter. The developed theoretical model then can be used for determination of its rational design parameters.

Experimental tests were conducted in the Energy Laboratory of the Faculty. The test rig consisted of a solar simulator and evacuated tube solar collector, coupled to the liquid piston converters, equipped with a heat exchanger. Three different configurations of the solar cooling unit were tested and a data acquisition system with pressure, temperature and liquid piston displacement sensors was used to evaluate the experimental performance on the cooling capacity.

In the theoretical part of the study, the thermodynamic model of the solar cooling system was developed. In the calculation scheme, the system was split into a number of control volumes and ordinary differential equations of energy and mass conservation were used to describe mass and heat transfer in each such volume. The system of ordinary equations then was solved numerically in MATLAB/Simulink environment and information on the variations of pressure and temperatures in the control volumes of the system over the cycle were obtained.

Calibration of the mathematical model with the use of experimental data demonstrated that the model predicts the performance of the system with accuracy acceptable for engineering purposes.

Experimental investigations showed that laboratory prototypes of the system demonstrate a stable operation during the tests with an amplitude and frequency of liquid piston oscillations being about 4- 6 cm and 3 Hz, respectively. The reduction in the air temperature in the cooling space was about 1 and 2 K, compared to the ambient temperature. The cooling effect increases with the raise in the heat input into the solar collector and in the flow rate of cooling water. The developed mathematical model of the system describes the pressure variation in the cycle, amplitude and frequency of oscillation of pistons with a level accuracy sufficient for performing engineering design calculations.

Overall, both experimental and theoretical investigations confirm that the system demonstrates a capacity to produce a cooling effect with utilisation of solar energy. However, further R & D is required to enhance its performance.

List of Contents

List of Figures

List of Tables

Acknowledgment

First of all, I would like to thank Almighty Allah for giving me the courage, determination and guidance in conducting this research work.

I would like to express my heartily gratefulness to my supervisor, Professor Khamid Mahkamov, for his continuous support, patience, motivation, and invaluable help during my Ph.D.

My sincere thanks also go to my parents, my wife, my siblings and my children for their encouragement, support, prayer and patience during the period of my study.

I wish to express my sincere thanks to Dr Basim Belgasim for his support and help.

I take this opportunity to express my gratitude to the Ministry of Education and the Culture Affairs Department of the Libyan Embassy in London for providing the managerial and financial support during my Ph.D. study at Northumbria University.

Last but not the least: my warm thanks should go to the colleagues, the academic and technical staff at Northumbria University for their support and encouragement.

Declaration

I declare that the work contained in this thesis has not been submitted for any other award and that it is all my own work. I also confirm that this work fully acknowledges opinions, ideas and contributions from the work of others.

Name: Gamal Hashem

Signature:

Date: July 2016

Nomenclature

A	area, m^2
C	damping coefficient, $N.s.m^{-1}$
C_p, C_v	specific heat at constant pressure and volume, $Jkg^{-1}K^{-1}$
D	diameter, m
G	solar radiation, Wm^{-2}
H	water column height, m
K	gas spring stiffness, Nm^{-1}
M	mass, kg
NTU	number of heat transfer unit
P	pressure, Pa
Q_r	heat rejected, W
Q_{in}	heat input, W
R	gas constant, $Jkg^{-1}\ K^{-1}$
R_b	geometric factor
T	temperature, K

t time, second

U overall convection heat transfer coefficient, $Jm^{-2}s^{-1}K^{-1}$

V volume, m^3

X displacement of water level in the liquid piston, m

g gravity acceleration, ms^{-2}

h_o, h_i outer and inner convection heat transfer coefficients, $Jm^{-2}s^{-1}K^{-1}$

$\dot{m}$ mass flow rate, kgs^{-1}

Subscripts

a air

b brine

c condenser of the engine part or cooler of the cooling part

cool cooling water

cp interface between condenser and liquid piston

e evaporator of the engine part or cooling space of the cooling part

ec interface between condenser and evaporator

p liquid piston cylinder

sw seawater

v vapour

1 inner cylinder

2 outer cylinder

Greek symbols

γ isentropic index

ε effectiveness

μ viscosity, $kgm^{-1}s^{-1}$

ρ density, kgm^{-3}

Chapter 1 Introduction

Solar energy is one of the most important clean sources of renewable energy, which can be used to produce electricity, heating or cooling indoors etc. Seitz and Hite [1] state that the Earth receives energy over a one year period which is equal to about ten times of that reserved in the form of all fossil fuels and uranium. Hassan et al. [2] highlight that the total amount of solar energy reaching the Earth's surface is much greater than the global energy demand on the planet over a year period. The energy rate incoming from the Sun is 82×10^{15} W and this value is about 5200 times greater than the overall energy requirement of the world was in 2006 [2]. In addition, the International Energy Agency (IEA) reported that, in 2010, the world's total final energy consumption was 8,677 million tonnes of oil equivalent (Mtoe) or 363 Exajoules EJ [3, 4]. In 2011, the International Energy Outlook predicted that the world's energy consumption expected to rise from 533 EJ in 2008 to 812 EJ in 2035 [5]. The growth of energy demand which takes place in countries outside of the Organization for Economic Cooperation and Development (non-OECD) from 2008 to 2035 is 85%, while the 15% growth occurs in the OECD countries. Based on the report issued by the Renewable Energy Policy Network for the 21st Century, currently about 81% of the world's energy consumption is satisfied by using fossil fuels, while 16% comes from renewable sources and the remainder covered by nuclear energy, as demonstrated in Figure 1.1. The report shows that renewable energy replaces fossil and nuclear fuels in some market sectors, including power production, heating and cooling, and rural/off-grid energy services [5].

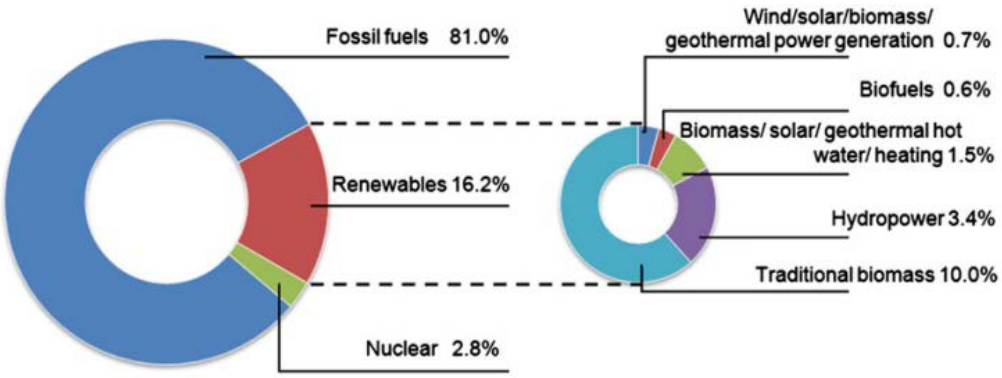

Figure 1.1 Renewable energy and the global final energy consumption, 2009 [5]

Solar energy is extensively used to heat indoors or domestic water by using solar collectors, which receive the sunlight by reflection from mirrors or lenses on the absorption surface of a pipe carrying fluid. Whilst the fluid (mainly water) passes through the pipe it is heated and sometimes changes its phase to steam which can be used in heating applications. Solar energy has also been used for the cooling purposes by actuating cooling cycles for two main purposes. The first is to provide refrigeration which can be used in applications such as in the food and pharmaceutical industries, especially in the remote places where there is a lack of electricity. Secondly, it may be used in air-conditioning systems to provide a living comfort in areas where the climate is too hot or/and humid (the sub-Sahara and tropical regions) [6]. The use of solar energy for cooling in some particular places is sufficient which makes this source of energy very attractive for government or private sector investments [7].

Although several types of solar cooling systems have been proven to be feasible, their market penetration level is relatively low due to the high capital cost, long pay-back period and low coefficient of performance when compared to the conventional vapour compression cycles. Figure 1.2 shows the coefficient of performance of different kind of the solar thermal cooling systems as a function of the heat source temperature.

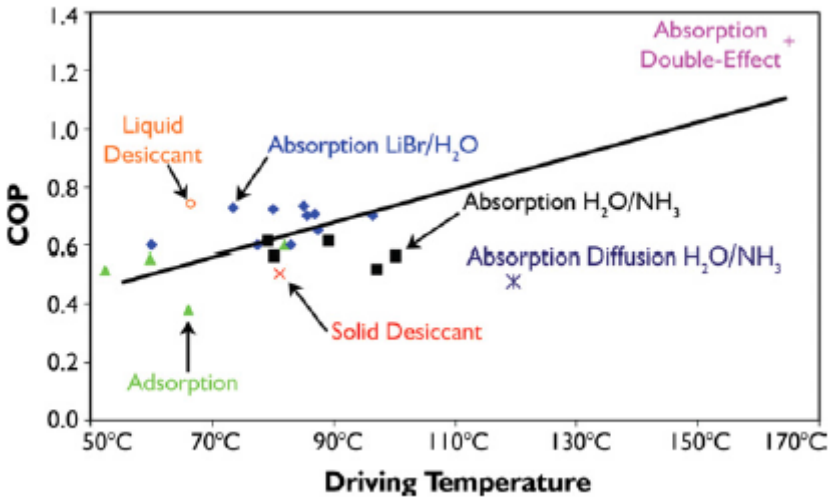

Figure 1.2 COP as a function of heat source temperature [8]

1.1 Problem Statement

Extensive R & D activities are underway at a number of universities and industrial companies to reduce the capital and running costs of solar desalination systems. Operational principles of the systems for solar water pumping and dynamic water desalination test rigs were developed and built at Northumbria University and described previously in a number of papers [9]. These systems are built around the fluid piston converter with a simple design and made of low-cost materials. In the water pump and desalination systems, the fluid piston converter works as an engine driven by solar thermal energy accumulated by flat- plate or evacuated tube collectors. Such the test rig contains solar evacuated tube collector to heat an evaporator. In addition, it contains condenser and fluid piston engine as shown in Figure 1.3. The solar collector receives heat from a solar simulator contained 110 halogen floodlight, and uses this energy to evaporate water. The produced steam drives the fluid piston engine which actuates the circulation pump and increases the vaporisation process [9].

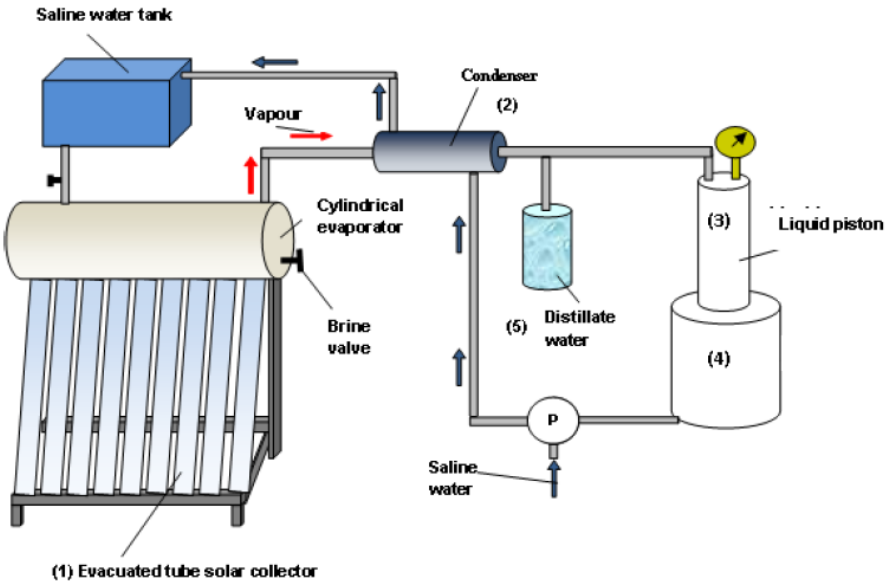

Figure 1.3 Schematic diagram of dynamic solar desalination unit [9]

If in a design the fluid piston is driven using an external source of energy without heat input then such a converter works as a cooling device. In this study, the solar fluid piston converter/engine is coupled to the cooling unit and the fluid piston of the latter is driven by the solar fluid piston converter/engine. The resulting effect is producing of a cooling effect using solar energy. The task in this study was to investigate operation of such the system theoretically and experimentally. For this, the thermodynamic model, consisting of a system of ordinary differential equations, was developed in MATLAB/Simulink environment to simulate the operation of this thermal auto-oscillation system. Experimentally, tests have been conducted on the developed test rig in the Energy Laboratory of the Faculty. Experimental facilities allow estimating the instantaneous parameters of the cycle in the engine and cooling machine sides (pressures and temperatures) and also the cooling effect. The obtained experimental data was used to evaluate the accurateness of the developed mathematical model and for its improvement.

1.2 Aims and Objectives

The overall aim of this research is to build the design of a novel solar cooling unit based on a fluid piston converter and create its accurate mathematical model.

The main objectives of this research can be summarised as follows:

- To accomplish a comprehensive literature review related to the different types of the solar thermal driven cooling systems to analyse the state-of-art in the field.
- Develop the mathematical model of the solar cooling system with the governing equations, describing energy transfer processes in the physical model.
- Develop a computer programme in the Simulink/Matlab environment to solve equations of the mathematical model and simulate the performance of the unit.
- To build the test rig of the proposed system and acquire experimental data on the performance of the unit to validate the simulation results.
- To perform a parametric analysis in order to determine the design parameters which have significant effects on the operation performance of the cooling unit and define their values.

1.3 Contribution to knowledge

This research is an investigation of the working process of a novel small-scale dynamic solar cooling unit. The unit is actuated by a liquid piston engine which is driven by a solar energy.

- Three different physical models have been proposed in this and the main factors which influence the performance of the system were studied.
- The thermodynamic model of the unit for its various configurations has been derived and their operation was simulated and analysed for the first time. In the calculation

scheme, the engine and cooling parts are split into control volumes by means of control surfaces. The theoretical model has been derived, consisting of the mass and energy conservation equations applied to all control volumes.

- The three prototypes, which are theoretically simulated in the first part of the research, have been built and the experimental data have been obtained for the first time to validate theoretical results. A parametric analysis has been conducted in order to find the rational design parameters of the system.

1.4 Research outcomes

The findings of this research were partially described in the following conference papers:

1- K. Mahkamov, G. Hashem, B. Belgasim, and I. Makhkamova. A Novel Solar Cooling system Based on a Fluid Piston Convertor. *Proceedings of the 16th International Stirling Engine Conference(ISEC)*, Bilbao, Spain, 2014.

2- K. Mahkamov and G. Hashem. Development of a Solar Cooling System Based on a Fluid Piston Convertor. *Proceedings of The European Conference on Sustainability, Energy & the Environment 2015*, Brighton, UK, 2015.

3- K. Mahkhamov, G. Hashem, B. Belgasim, K Hossin, I. Mahkamova. Parametric Analysis of Dynamic Solar Cooling System Based on Liquid Piston Converter. *Proceedings of the 17th International Stirling Engine Conference(ISEC)*, Newcastle upon Tyne, UK, 2016.

1.5 Thesis Construction

This research has been split into several phases and, therefore, the structure of the thesis reflects the logical sequence of the research process. The thesis has been divided into Chapters as follows:

- **Chapter 2 Solar Cooling Technologies.** This Chapter presents results of the comprehensive literature review of publications on the solar cooling systems. The review concentrates on the operation principle of such systems, design and

components, advantages and drawbacks and latest achievements in the solar cooling technologies. At the end of this Chapter, the summary part discusses the main findings and research issues in the subject area.

- **Chapter 3 Mathematical Modelling of the Cooling Part of the System.** This Chapter describes the thermodynamic mathematical model of the dynamic solar cooling unit with liquid piston cooling device. The physical model is described including its design and operational principle. Thereafter, the mathematical model derivation is presented. The mathematical model is based on mass and energy balance equations applied to the unit components, including the liquid piston cooling device, cooler and cooling space. Then, the resulting governing equations are solved in the Matlab/Simulink environment. Lastly, the results from the theoretical model are presented and discussed.
- **Chapter 4 Experimental Study of the Dynamic Solar Cooling System.** This chapter describes three different configurations of dynamic solar cooling system prototypes. Additionally, the main components of each experimental set with these three proposed configurations and their operational principles are described. All sensors and data acquisition system, that were utilised during experiments to record data, are described. Finally, the procedures of the experiments and the examples of experimental data obtained are presented and discussed.
- **Chapter 5 Development and Validation of the Whole System Mathematical Model.** The mathematical models of the whole system were developed in this Chapter and validated against experimental data. A comparison between theoretical and experimental results was performed and results were discussed in terms of the

oscillation amplitudes of the liquid pistons, pressures and temperatures in both the engine and cooling part.

- **Chapter 6 Parametric Analysis of the Dynamic Solar Cooling System for Designing Purpose.** In this Chapter, a parametric analysis of the solar cooling system was performed. The effects of the cooling water flow rate and temperature and the effect of the heat input into the cooling system are discussed.

- **Chapter 7 Conclusions and Future Recommendations.** This Chapter presents the main findings and conclusions from the performed research work and describes recommendations for future research.

Chapter 2 Solar Cooling Technologies

A comprehensive review related to the solar thermal driven refrigeration systems are presented in this Chapter. The review concentrates on the operation principle of a number of systems, their design and components, advantages and drawbacks and latest research achievements in the solar cooling technologies. Lastly, the Chapter discusses the main research questions and describes the contribution of this study in this subject area.

2.1 Introduction

There are numerous technologies which use the solar energy as a main source in order to produce a cooling effect for particular purposes. These technologies could be defined as solar cooling systems which are considered to be the best alternative to the conventional vapour compression cycles and which may reduce the consumption of the electric power [10]. Figure 2.1 illustrates a classification of the different kinds of the solar cooling systems which are either solar thermal or solar electric driven processes. In this review, the study is concentrated on the solar thermal cooling technologies [11]. The solar electric driven cooling technologies are powered by a Photo- voltaic (PV) panels. In solar thermal driven cooling technology, the sunlight caught by a solar collector can be used to generate mechanical power to compress a working fluid in a conventional vapour compression cycle or as a heat source for the generator of a sorption cooling cycle.

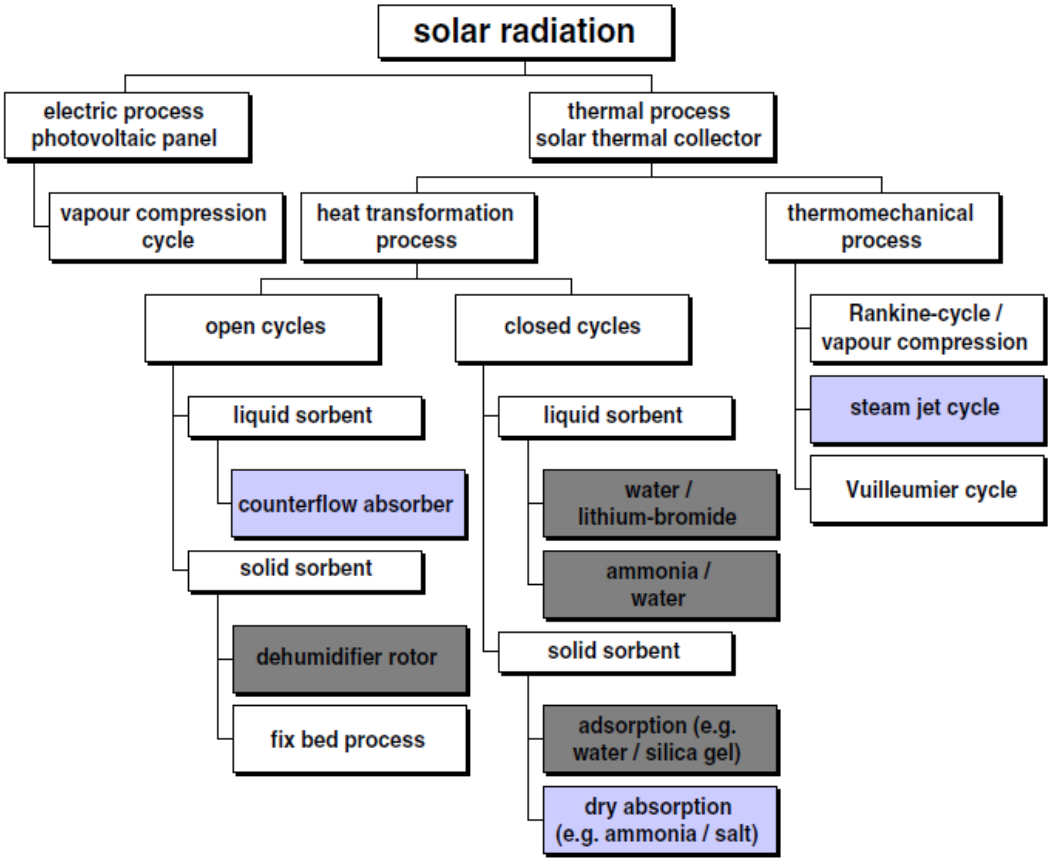

Figure 2.1 Classification of the solar cooling technology [11]

2.2 Solar sorption systems

In solar sorption cycles, the driving power is the thermal power instead of the electrical one supplied to the compressor of a conventional refrigeration machine. Such cycles use physical or chemical affinity between a pair of substances (the sorbent and the sorbate) to generate the cooling effect. The systems can be split into two types of processes, namely: closed and open cycles. The closed sorption system's principle is illustrated in Figure 2.2.

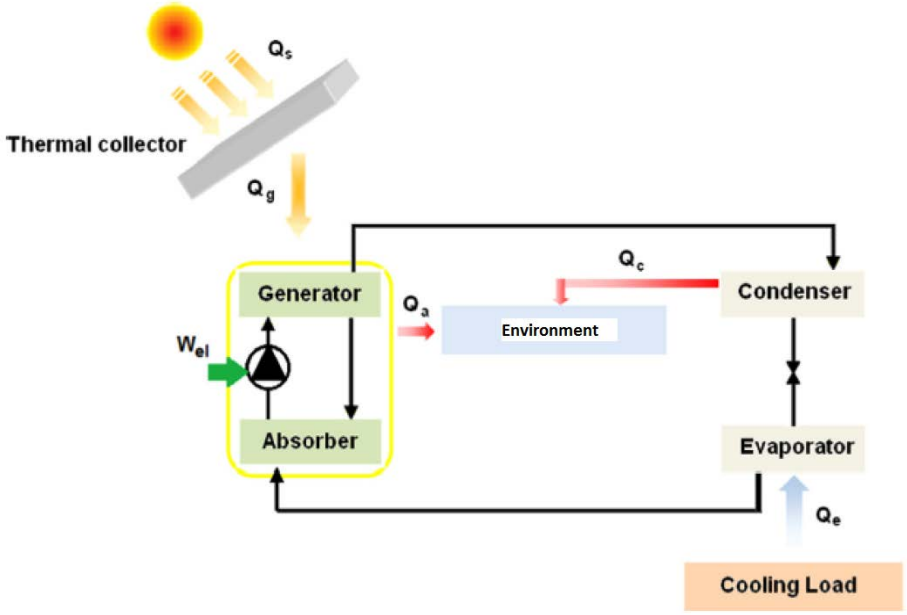

Figure 2.2 Solar sorption refrigeration processes [12]

The generator receives the heat from the solar collector in order to heat up the sorbent with the absorbed refrigerant. The refrigerant is vaporized and afterwards condensed in the condenser by rejecting of the condensation heat to the environment. Meantime, the regenerated sorbent flows back to the absorber in which the sorbent absorbs the refrigerant vapour from the evaporator. This process is followed by a rejection of sorption heat to the ambient. The liquefied refrigerant, which comes out from the condenser, evaporates in the evaporator by consuming heat from the cooling space. In the adsorption systems, the sorbent is porous material such as activated carbon that is able to desorb the refrigerant. In such systems, the coefficient of performance (COP) is [12]:

$$COP = \frac{Q_e}{Q_g + W_{el}} \tag{2.1}$$

where W_{el} denotes to the additional electrical work done by the pump, Q_e is the heat extracted in the evaporator, Q_g is the regeneration heat received by solar collector.

2.2.1 Solar absorption cooling systems

The phenomenon of absorption has been used widely in solar cooling along the last century. By using the absorption systems, it is possible to produce a cooling effect for applications in the range between -60 and 5˚C [13]. The absorption cycle contains a pair of fluids that works as a refrigerant, such as ammonia/water or water/Lithium Bromide (LiBr). The secondary fluid, absorber, absorbs the vapour of the main fluid so that the result of both fluids is a dilute solution that can be pumped by a pump which cause the circulation in the cycle. Solar energy is the source of heat which is required to circulate the refrigerant rather than electrical compressor as in the conventional vapour compression cycle. On the other hand, in both last mentioned refrigeration technologies there is a condenser at higher pressure side for rejection of heat from the refrigerant also there is an evaporator to heat the refrigerant at the lower pressure side of the cycle. There are many configurations of the absorption systems such as half, single or double effect [14]. In addition, there are two other absorption refrigeration systems, hybrid systems and Diffusion Absorption Refrigeration (DAR), which can carry out better performance [15].

2.2.1.1 The single effect solar absorption cooling cycle

The basic single effect absorption cooling cycle consists of a generator, condenser, evaporator, absorber and economizer [10]. In the solar absorption system, in addition, to the previous components, there is a solar collector as seen in Figure 2.3. The heat collected in the solar collector is exchanged in the generator where the refrigerant is extracted from the working fluid mixture. The volatile refrigerant flows to the condenser in which it is cooled and expands in the throttling valve. In the evaporator, heat transfer from the surrounding to

the cooled and expanded refrigerant so that the desired cooling effect can be produced. After that, the absorber receives the refrigerant from the evaporator and the strong solution from the generator. This mixing of the two fluids causes heat released in the absorber. The mixture, week solution, flows out from the absorber to the generator by means of a pump. Before the generator, the mixture receives heat in the solution heat exchanger, economizer, to be preheated and so on.

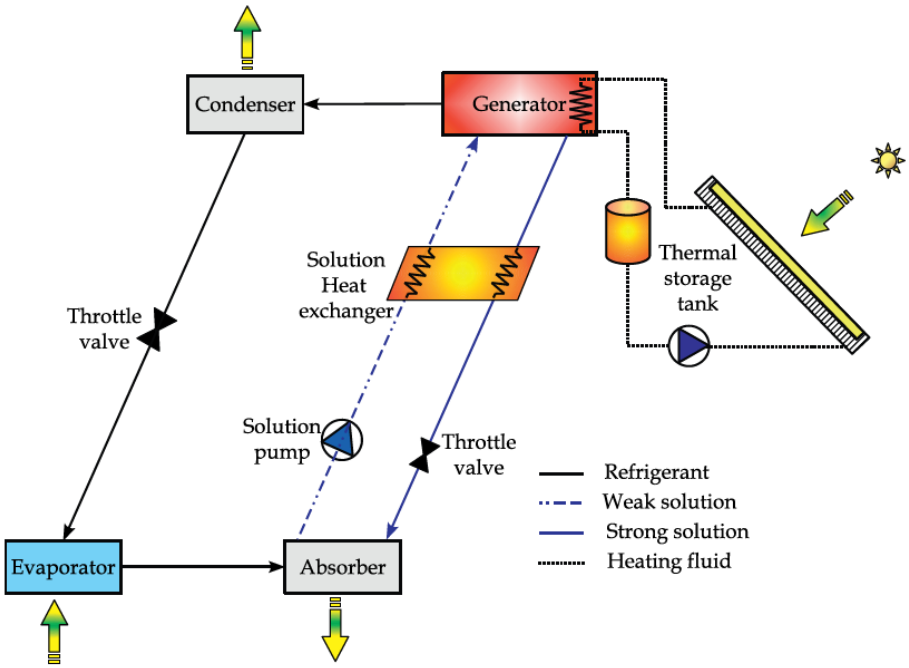

Figure 2.3 A basic diagram for the single effect solar absorption cycle [10]

Nakahara et al. [16] developed a system aimed to use solar energy for supplying a building with cooling, heating and hot water. They used flat plate collectors with area of 80 m^2 and absorption chiller. The binary mixture was water and Lithium Bromide. During the summer time, the cooling capacity reached 6.5 kW but the coefficient of performance was 0.14. To investigate the feasibility of using a comfort solar cooling system in Hong Kong, Yeung et al. [17] designed and built an absorption air-conditioning unit driven by solar power on the

campus of the University of Hong Kong. The unit collects the sunlight by using a flat plate solar collector array with an area of 38.2 m^2 and the cooling capacity of the LiBr–H2O absorption chiller is 4.7 kW. In addition, the system has a hot storage water tank with a capacity of 2.75 m^3, a fan-coil unit, a cooling tower and is equipped with a data-acquisition system. This unit has been evaluated and compared to similar systems after two years of operation by Lazzarin et al. [18]. It is found that the assessed solar cooling unit had an annual efficiency of 7.8% and an average solar fraction of 55%. Vereda et al. [19] presented a numerical model of ammonia/Lithium Nitrate solution, which is able to produce cold at temperatures lower than 0°C. They chose a single effect absorption cycle including a liquid-vapour ejector to work as adiabatic absorber and compressor for refrigerator vapour. It was noticed that the cooling capacity improved remarkably. Some models of single effect cycles with and without refrigerant circulation were investigated analytically by Kim and Infante Ferriera [20]. The study focused on describing the cycle behaviour to predict the performance of new working fluids as a function of generation temperature. Yan et al. [21] presented a numerical study under the conditions of steady working for an arrangement with an absorption cycle, using water/Lithium Bromide as a working fluid. In this arrangement, they were able to reduce the waste gas discharged temperature by about 20˚C compared to the conventional single effect cycle. Furthermore, the cooling capacity per unit mass of waste gas achieved by novel arrangement was higher than for the conventional one at the same simulated conditions.

2.2.1.2 The half effect solar absorption cooling system

Single effect absorption systems need a minimum temperature of heat source at 100°C in order to produce a cooling effect at the temperature of about 0°C with a reasonable COP

[22]. The half effect systems can provide cooling effect with a relatively lower driving temperature than the single effect solar absorption cooling systems. Because its coefficient of performance is roughly half of the single effect system, it is called half effect solar absorption cooling system [10]. It is also called double-lift or two-stage cycle, see Figure 2.4.

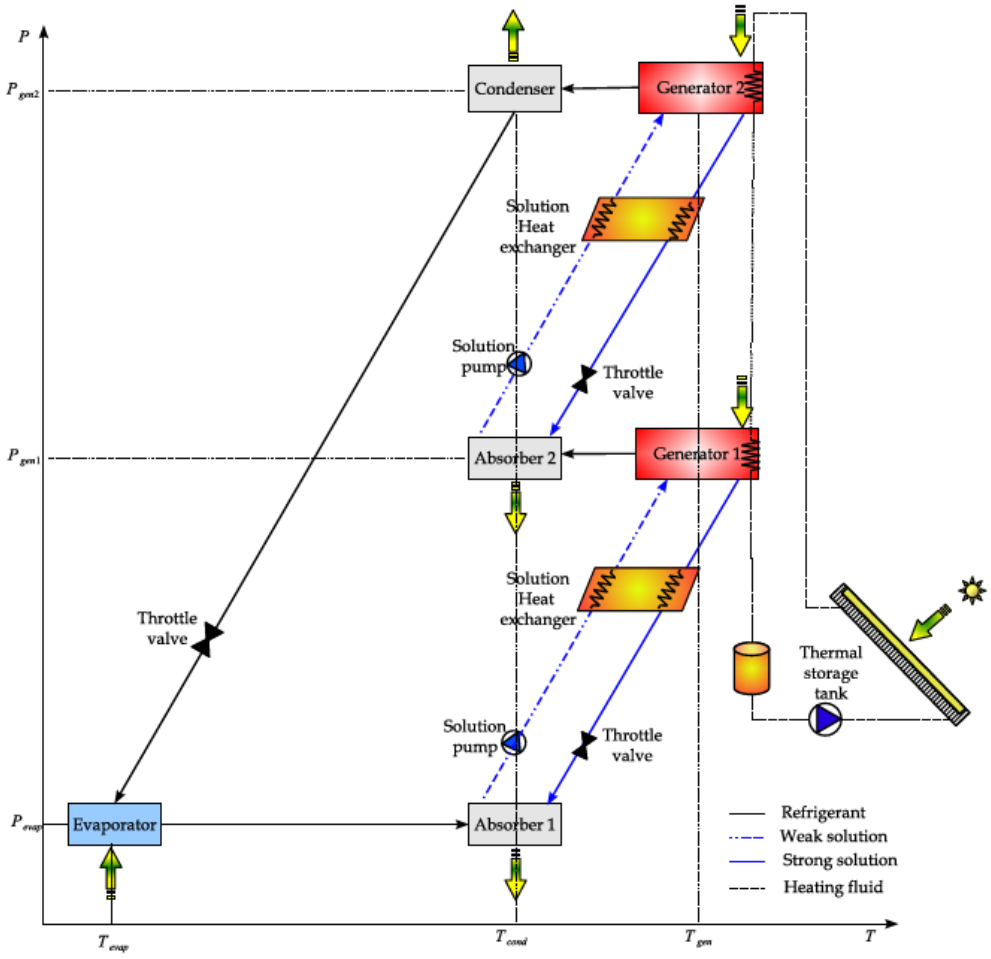

Figure 2.4 A basic diagram for the half effect solar absorption cooling system [10]

This system has been tested experimentally by Arivazhagan et al. [23] and studied numerically by Lin at al. [24]. Arivazhagan et al. [23] built a prototype to produce a cooling effect at the rate 1 kW utilizing HFC-based working fluids as shown in Figure 2.5. The system can lower the evaporative temperature of the system down to -7°C with generator temperature between 55 and 75°C. It is also found that the optimum generator temperature

was ranging between 65 and 70°C in order to have a coefficient of performance of 0.36. To examine the feasibility of low-price air-cooled solar absorption cooling system, Kim and Machielsen [25] compared many systems based on their manufacturing costs and performance. The comparison demonstrated that half effect systems might require about 40% more heat exchanger area and 10-60% more collector area compared to single effect system of the same cooling capacity. However, the half effect system is capable to produce the higher average cooling efficiency than a single effect system with the low cost flat plate collector. And the opposite is true in the case of the use of vacuum tube collectors. By comparing some working fluids, it was found that the NH3/LiNO3 mixture provides the better performance and lower cost than NH3/H2O while NH3/NaSCN is the most unfavourable because of the high pumping power requirement. Furthermore, numerical and experimental investigations of a two-stage lithium bromide absorption solar cooling system in south China is presented by Sumathy et al. [26]. They found that the low range of hot water temperature, which can be supplied by solar hot water generator, can drive the two-stage chiller. They constructed solar cooling and heating system with the two-stage chiller. The operating data of the proposed cycle showed that the cooling capacity reached 100 kW and its COP was nearly the same as for the conventional cooling cycles with a financial reduction of about 50% in the running costs.

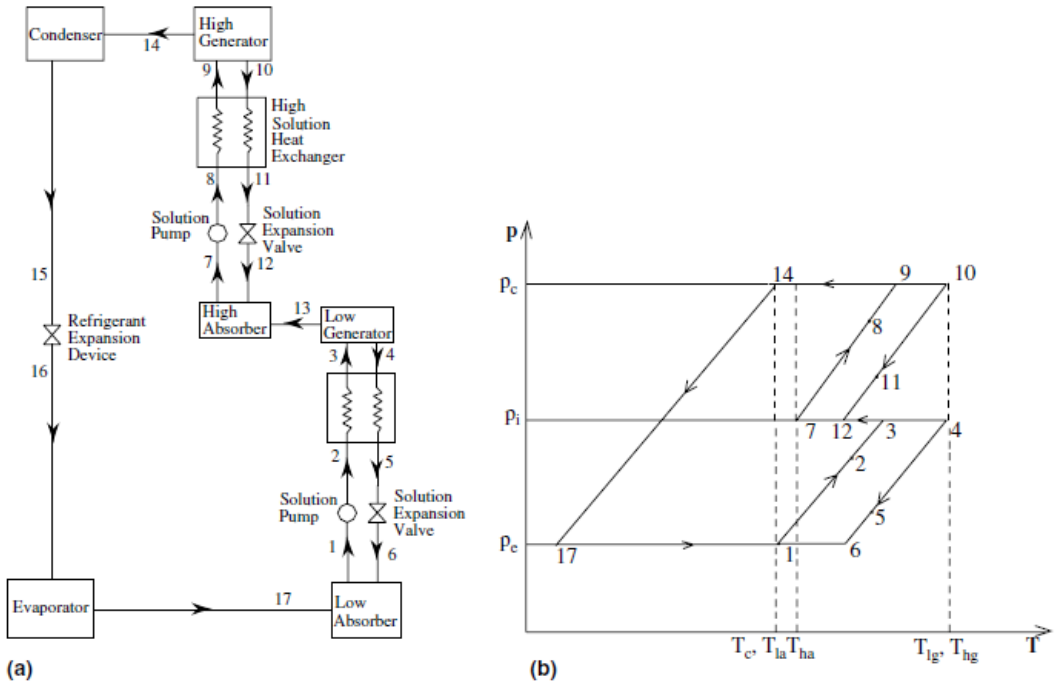

Figure 2.5 Half effect absorption refrigeration system. (a) Schematic; (b) PT diagram [23]

2.2.1.3 The double effect solar assisted absorption cooling systems

The double effect solar absorption cooling cycle consists of same components as the single effect cycle with an additional stage as a topping of the cycle. The double effect absorption chillers have a doubled coefficient of performance compared to the single effect systems. On the other hand, the double effect systems require a relatively high generation temperature, namely more than 130˚C [27], which eliminates the possibility of using many types of solar collector types that cannot fulfil this requirement. To overcome this limitation, the high-pressure generator should receive heat from another source of energy such as natural gas boiler, as seen in Figure 2.6. The low-pressure generator receives heat mainly from the solar collector. Beside that to have an efficient generation process, the system is supplied with heat released in the condenser from the vapour generated in the high-pressure generator. Liu and Wang [28] investigated a double effect solar cooling system with LiBr/H2O mixture in

Shanghai, China. The cooling capacity of the system was 10 kW. They considered the system driven by the solar energy and natural gas boiler. The hot water temperature, supplied to the low-pressure generator, is 90°C. Simulation results showed that this type of solar system is feasible and economical.

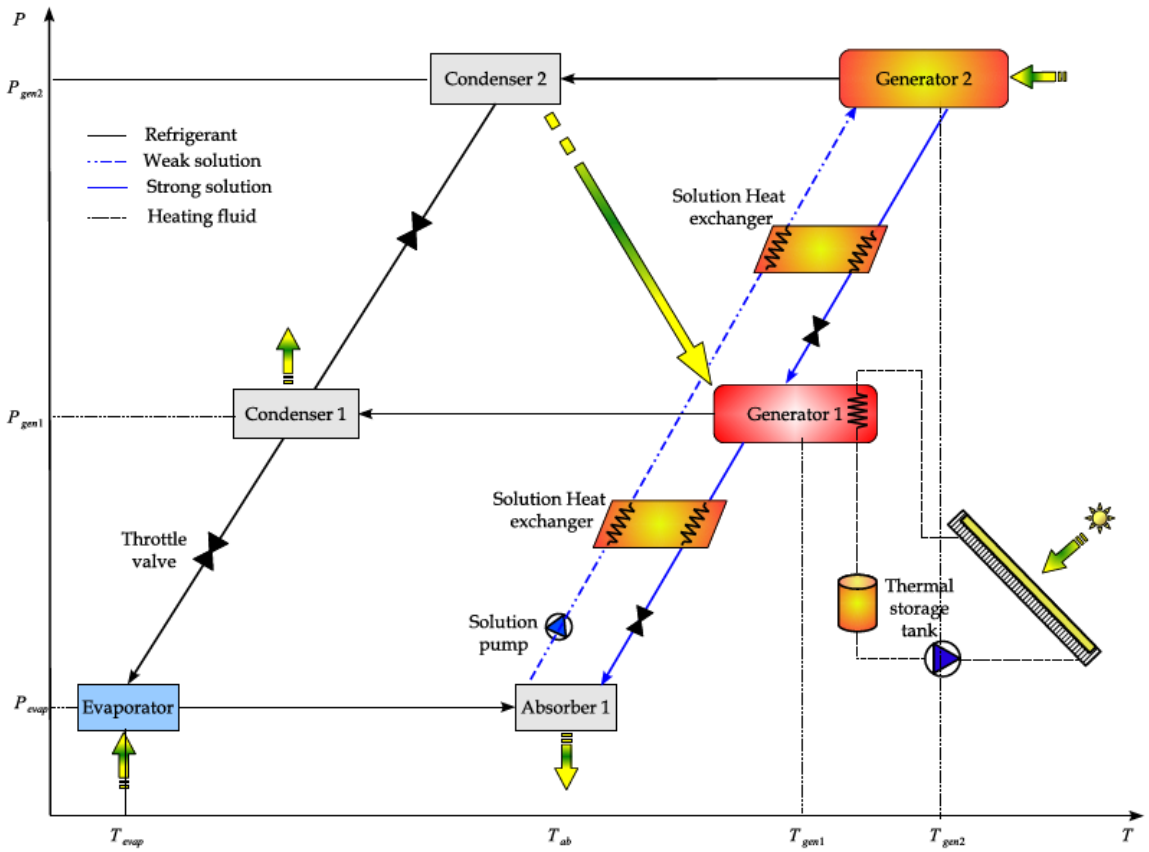

Figure 2.6 A basic diagram for the double effect solar absorption cooling system [10].

A dynamic simulation study for modelling a real double effect LiBr–H_2O absorption cooling systems was conducted by Shin et al. [29]. The mathematical model described the dynamic behaviour of the working mixture. Nonlinear differential equations were derived and solved in order to simulate the system. The simulation results were compared to test data and results showed a good agreement. It is found that ant-crystallization and control performance could be improved using the dilution cycle.

A comparison between single and double effect absorption cooling cycles with the same cooling effect production conditions was presented by Gomri[30]. Figures 2.7 and 2.8 show the schematic illustration of single and double effect absorption systems that have been studied in that research. In the theoretical part of study the effect of a number of operation factors, such as the thermal load and total change in exergy, on the coefficient of performance (COP) was investigated. A FORTRAN computer program was developed for thermodynamic analysis. The model was built on the use of energy balance equations and thermodynamic properties for each reference point. The initial conditions were described in the program including the ambient conditions, the component temperatures, pump efficiency, the effectiveness of heat exchangers and cooling load. The study concluded that the COP of the double effect arrangement was doubled compared to the single effect arrangement but the exergetic efficiency of the double effect is slightly higher compared to the single effect system. In addition, it was concluded that the total change in exergy for both arrangements was minimum when the generation temperature, depending on evaporator and condenser temperatures, was optimal. Moreover, it was proposed that the evaporator temperature and condenser temperature should be in the range of 4 to 10˚C and 33 to 39˚C, respectively, whilst the high-pressure generator temperature was between 60 and 190 ˚C. They also found that the maximum value of the COP for the single effect arrangement ranges between 0.73 and 0.79 and for double effect arrangement this value was between 1.22 to 1.42. The maximum exergetic efficiency values of the single effect absorption systems are in the range between 12.5 and 23.2% while for the double effect absorption systems these values are in the range of 14.3 to 25.1%.

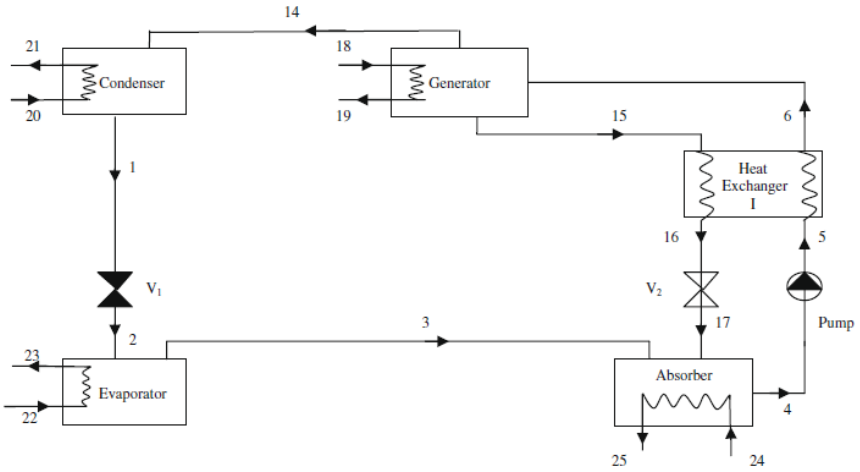

Figure 2.7 The schematic illustration of single effect absorption refrigeration system [30]

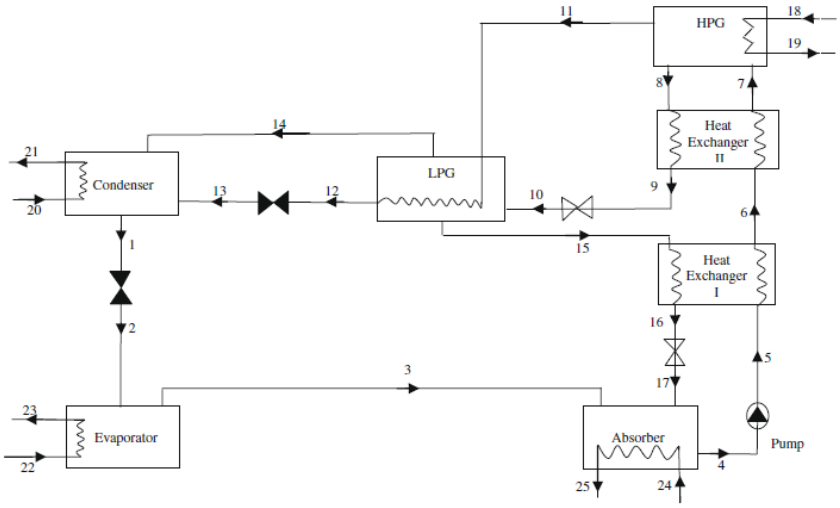

Figure 2.8 The schematic illustration of double effect absorption refrigeration system [30]

Xu et al. [31] presented a simulation study of a novel arrangement of the absorber, generator and condenser with multi-pressure levels. They stated that the proposed arrangement (Absorber Generator heat exchanger, AGX) had a relatively simpler configuration than classic absorption cycles. In addition, the AGX had a wider range of the generation temperature which enabled AGX with higher COP. In this cycle, the H2O/LiBr mixture has been used as a working fluid, with single and double effect. The AGX absorption cycle can

work at generation temperatures ranging between 85 and 150°C with an evaporation temperature of 5°C, absorption temperature of 35°C and condensation temperature of 40°C. The results of simulations revealed that the proposed cycle could work in single and double effect modes when the generation temperatures were in the ranges between 85 and 93°C, 93 and 140°C and 140 and 150°C, with achieving a COP of 0.75, between 0.75 and 1.08 and between 1.08 and 1.25, respectively.

2.2.1.4 Properties of working fluids for solar absorption cooling systems

The binary mixture should have some certain properties [32]. Firstly, the refrigerant should have a high latent heat in order to reduce the circulation rate of both fluids in the cycle. Secondly, the volatility of the refrigerant should be higher than that for the absorbent so the mixture can be separated easily to avoid the need for a rectifier. Thirdly, the solid-phase should not be present in the range of temperatures, composition and concentrations of the working mixture. Fourthly, the affinity of the absorbent for the refrigerant should be strong to optimise the absorption process, decrease sensible heat losses and reduce the absorbent circulation rate. Finally, the working pressure should be moderate to avoid designing problems caused by high pressures such as thick wall equipment or high electric power necessary for the pump. At the same time, the low working pressure requires large volume equipment. Although many refrigerant/absorbent mixtures have been suggested and investigated recently, the two mixtures, namely ammonia/water and water/Lithium-Bromide are the most common working fluids [33, 34]. Each binary mixture has its own thermodynamic and physical properties which distinguish every mixture among other working fluids. Masheiti [13] presented a comparison of working fluids summarized in Table 2.1. In general, types of working fluids and effect of the system arrangement (half

effect, single effect, or double effect), have been investigated recently in a number of works, namely [35-40].

Table 2.1: Comparison between H_2O/LiBr and N3O/H_2O mixture properties [13]

Property		Water/Lithium Bromide	Ammonia/Water
Refrigerant			
1	High latent heat	Excellent	Good
2	Moderate vapour pressure	Too low	Too high
3	Low freezing temperature	Limited applications	Excellent
4	Low viscosity	Good	Good
5	Toxicity	No	Yes
6	Flammability	No	No
7	Non-Volatility	Excellent	Poor
Absorbent			
1	Low vapour pressure	Excellent	Poor
2	Low viscosity	Good	Good
3	Toxicity	No	No
4	Flammability	No	No
5	Non-Volatility	Excellent	Poor
Solution			
1	No solid phase	Limited application	Excellent
2	Low toxicity	Good	Poor
3	Solution circulation flow rate	Low	High
4	Odour	No	Yes
Features			
1	Coefficient of performance (COP) at low heat input	Higher	Lower
2	Need for rectifier (Separator)	No	Yes
3	Lower equipment cost	Yes	No
4	Performance at low driving temperature (<100 ºC)	Excellent	Poor
5	Less system complications	Good	Poor

2.2.2 Solar adsorption cooling system

The adsorption technology was first used for refrigeration and heat pump applications in the early 1990s,. The main difference between the adsorption and absorption process is that the absorption is a volumetric phenomenon, whereas adsorption is a surface phenomenon [41].

2.2.2.1 Principles of adsorption

In general, the adsorption systems can be divided according to processes taking place into the physical [42-44] and chemical adsorption [45-47]. The physical adsorption occurs as a result of the Van de Walls force acting between the molecules of the adsorbent and the refrigerant, adsorbate, [48]. There are not any changes in the chemical composition of the adsorption pair. The enthalpy of adsorption is of the same order as the heat of condensation of the gas. The binding molecules can be split by applying heat, which usually does not exceed 80 kJ/mol [49]. Physical adsorbents with mesopores can adsorb consecutive layers of adsorbate while those with micropores have the volume of the pores filled with the adsorbate. Physical adsorbents develop the selectivity to the adsorbate after the former undergo specific treatments, such as reaction with a gas stream or with certain agents. The kind of treatment will depend on the type of sorbents [50].

The chemical adsorption is caused by the reaction between the adsorbate and surface molecules of the absorbent. This includes the atoms rearrangement, electron transfer, and fracture or the chemical bond [51]. Only one layer of adsorbate reacts with the surface molecules of the chemical adsorbent. The chemisorption process includes valence forces caused by sharing of electrons between the adsorbent and the adsorbate atoms. This results in the chemical reaction and formation of a complex surface compound. The forces of these

formed bonds are much stronger than the Van der Waals force in the physical adsorption. Consequently, much more heat of adsorption is required to release the adsorbate, up to 800 kJ/mol [49]. The adsorbate and adsorbent molecules after adsorption never retain their original state, for instance, a complexation occurs between chlorides and ammonia. Moreover, salt swelling and agglomeration may be present which are critical to heat and mass transfer performance [48].

The adsorption characteristics of particular pairs mainly depend on the nature of the adsorbate, the nature of the adsorbent, the reactivity of the surface, the surface area and the temperature and pressure of adsorption. When a solid surface of the absorbent is exposed to a gas, the molecules of the gas come in contact with the surface of the solid. Some of these molecules are adsorbed by the solid surface, whereas others remain unattached. At the beginning, the rate of adsorption is high because the whole surface is uncoated. The rate continues to decline as more and more of the solid surface is covered by the adsorbate molecules. The rate of desorption increases because desorption occurs on the covered surface. The system will reach equilibrium when the rate of adsorption and the rate of desorption are equal. At this stage, the gas–solid system can be described to be in adsorption dynamic equilibrium in which the number of molecules bonded to the surface and the number of molecules freeing from the surface is the same [52]. In both physical and chemical adsorption, the adsorption process is an exothermic process while the desorption process is an endothermic process. Therefore, the solar adsorption cooling systems use these processes to produce a cooling effect [49].

2.2.2.2 Adsorption cooling technologies

In the physical adsorption system, the primary component is a solid porous surface, with a large surface area and a large adsorptive capacity. In the beginning of the process, this surface remains unsaturated. When a vapour molecule of the refrigerant contacts the surface of the adsorbent, an interaction occurs between the surface and the gas molecules, and as a consequence, the porous material adsorbs the gas molecules. This phenomenon is used in the solar adsorption refrigeration machines which generally consist of a generator, condenser, pressure relief valve and evaporator. The adsorbent material is supplied by solar energy heat by means of integrating with a solar collector bed in order to activate the desorption process of the refrigerant as shown in Figure 2.9[53].

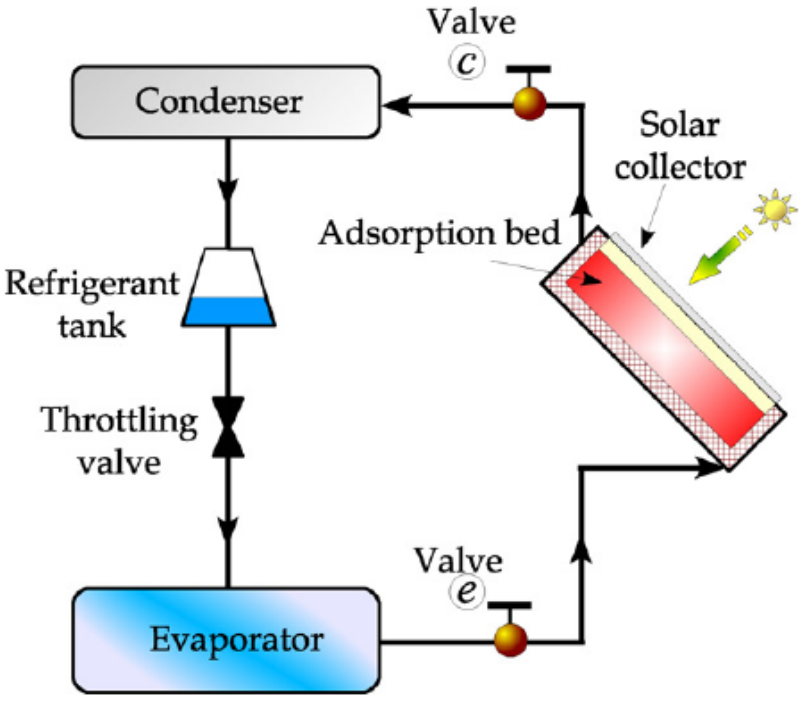

Figure 2.9 Schematic diagram of the solar adsorption cooling system [49]

The solar adsorption cycle can be operated without any compression device such as a pump or compressor. This type of cycles is silent, highly reliable, mechanically simple and has very long lifetime [6]. However, the basic one-bed cycle performance, see Figure 2.9, varies because of the alternating adsorption and desorption processes, resulting in a decrease in the COP. In order to have a continuous cooling effect, two or more beds are suggested to exchange their functions periodically, as shown in Figure 2.10. In this cycle, the generation and the cooling effect are shifted between the beds to ensure the continuity of production of the cooling effect in the cycle.

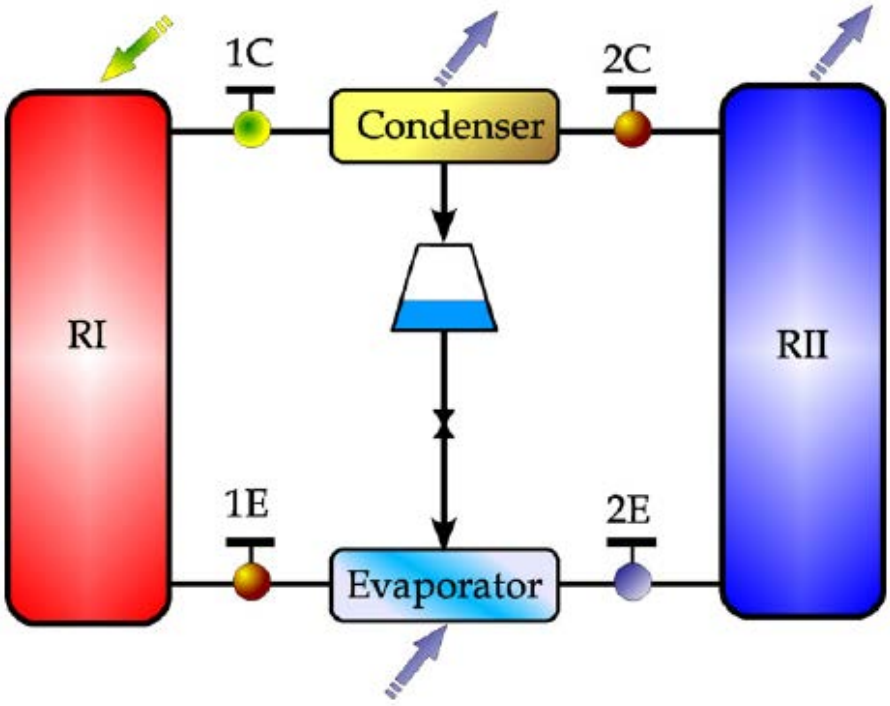

Figure 2.10 Schematic diagram of the continuous two-bed adsorption cooling system [49]

In the cycle shown in Figure 2.9, the first half of the cycle starts when the first bed (RI) is isolated from the evaporator by closing the valve 1E and heated to start the desorption process. Then the refrigerant vapour flows from RI to the condenser through the open valve 1C. Meantime the cooling effect occurs and the refrigerant flows to the second bed (RII)

where the valve 2E is opened and the valve 2C is closed. The second half of the cycle happens by reversing the refrigerant flow direction and so reversing the heating and cooling steps. The cold production in the evaporator is due to the condensed vapour flowing from the second reactor RII [49].

2.2.2.3 Advantages and drawbacks of the adsorption over absorption systems

Although both the adsorption and absorption refrigeration systems can be powered by a low-grade heat source, the adsorption systems have a wider operational temperature range. A heat source with a temperature of 50˚C can be used to power the adsorption cycle while in the absorption cycle, the heat source should be at least 70˚C. In addition, a source with a 500˚C may be used directly in the adsorption process without producing any kind of corrosion problem, whereas in the absorption cycles, intense corrosion may commence at the temperature more than 200˚C [48]. Moreover, in the conditions of strong vibration such as present in fishing boats or locomotives, the adsorption refrigeration systems, which use solid absorbent, are more suitable compared to the absorption systems [54]. Due to vibrations, the liquid absorbent used in the absorption systems might flow from the generator to the evaporator or from the absorber to the condenser. In this case, the refrigerant would be polluted which may affect the system performance [48]. Adsorption cooling machines do not require any extra cooling equipment at high ambient temperatures because they have high storage capacity and energy density. There are fewer problems associated with corrosion and crystallization and these machines are more appropriate for working in dry and hot areas than absorption ones [49].

On the other hand, the main drawbacks of the adsorption cooling systems are the need of special designs to maintain high vacuum, the large volume and weight relative to

traditional refrigeration systems. Also, the coefficient of performance COP is lower for the adsorption systems compared to absorption systems under the same operational conditions which limit the wide application of this technology [55].

2.2.2.4 Adsorption working pairs

The working pairs, adsorbents and refrigerants, affect essentially the coefficient of performance and the technical specification of the solar adsorption cycles because each working pair has specific physical and thermodynamic properties. One of these properties is the latent heat of the refrigerant. The high refrigerant latent heat ensures the low circulation rate of the working fluid in he cycle. In addition, the volatility of the refrigerant should be higher than that for the absorbent in order to separate them easily without the use of a rectifier. Besides, the affinity between the absorbent and the refrigerant should be strong under the sorption conditions to have less absorbent to be circulated to achieve the same refrigeration effect, to use a smaller liquid heat exchanger and reduce the sensible heat losses [49]. Furthermore, the operating pressure should be moderated to avoid a thick-walled devices. The most widely used working pairs which satisfy the above requirements are activated carbon-methanol, activated carbon fibres–methanol, activated carbon-ethanol, activated carbon–ammonia, silica gel–water, and zeolite–water. The results obtained by Anyanwu and Ogueke [56] showed that zeolite/water was the best pair for air conditioning application while activated carbon–ammonia was preferred for ice making, deep freezing and food preservation. The maximum possible net solar COP was found to be 0.3, 0.19 and 0.16 for zeolite–water, activated carbon–ammonia and activated carbon-methanol, respectively, when a conventional flat plate solar collector was used. Choudhury [8] stated that the pair of

zeolite–water cannot produce cooling below 0˚C but its adsorption capacity is three times of that of silica gel which makes the zeolite based systems more compact.

2.2.3 Solar desiccant cooling systems

The evaporative cooling system was invented about 2500 B. C. in ancient Egypt. They used porous clay jars filled with water and located them in the buildings for cooling purposes [57]. In the modern age, in the late 1930s, air conditioning machines, based on direct or indirect evaporative coolers, were invented for application in the southern west of the United States of America. In general, the solar desiccant cooling systems are an open-cycle dehumidification/ humidification process. The desiccant system needs heat and water to actuate the system. The water is the most common working fluid since it is environmentally friendly and cheap. The desiccant cooling cycle generally consists of three main processes, namely, dehumidification process, regeneration process and humidification process. All these three processes take place at the atmospheric pressure. To achieve these processes, three components, namely a dehumidifier, regenerator and cooling unit are used side by side as shown in Figure 2.11 [58]. In addition to these components, heat exchangers are used within the cycle in order to increase the cycle efficiency. The solar desiccant systems utilise the solar energy for generation of the desiccant material. Several cycles have been described and some of them are briefly discussed in this section.

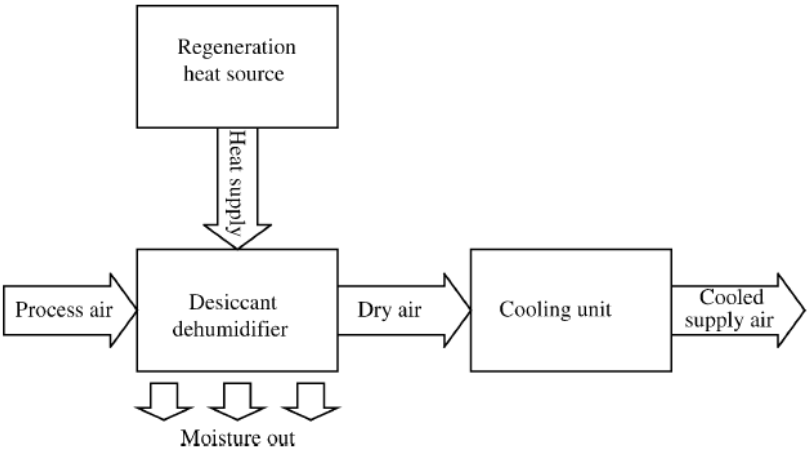

Figure 2.11 Principle of desiccant cooling [58]

The process of dehumidification and regeneration of a desiccant dehumidifier is shown in Figure 2.12 [57]. The desiccant removes moisture from the air (1–2) and the desiccant is regenerated by removing moisture from it using hot air (2–3). During process (3-1) the desiccant is cooled down again.

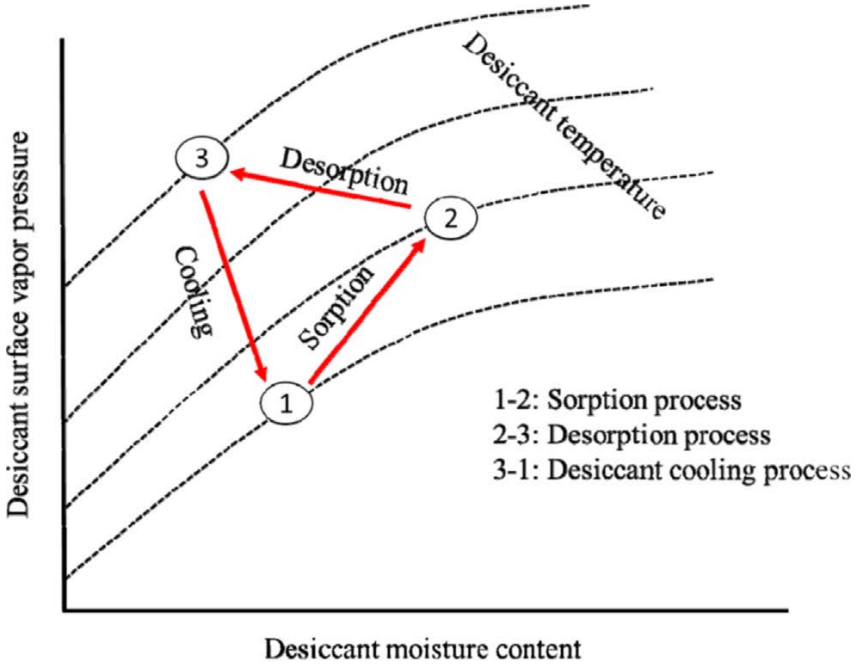

Figure 2.12 Dehumidification and regeneration process of a desiccant dehumidifier [57]

2.2.3.1 The desiccant dehumidifier

The desiccant dehumidifier contains a desiccant material in solid or liquid state. The most common configurations of the solid-state dehumidifier are the rotating wheel or the absorbent bed. In the case when the desiccant material is in the liquid state, the process air stream is brought into contact with the liquid desiccant which is contained in the dehumidifier (absorber). This absorber could be in the form of a finned-tube surface, spray tower, coil-type absorber and packed tower [59].

2.2.3.2 The cooling unit

The cooling unit may be an evaporator of a conventional air conditioner, an evaporative cooling system or a cold coil. The cooling unit is used in the desiccant cooling systems to handle the sensible load; meantime, the latent load is removed from the process air by means of the desiccant material. In the systems, containing a desiccant wheel (solid state), a heat exchanger is commonly needed in tandem with it in order to provide an initial cooling of the dry and heat up of the air stream before its additional cooling by an evaporative cooler or a cold coil, etc. In such case, the combination of the heat exchanger and the cold coil or the evaporator cooler constitutes the cooling unit. The process air stream through different configurations of the cooling unit is illustrated on psychrometric chart in which the deployment of an evaporative cooler is shown as a line 3–4 while the use of the heat exchanger cooler in tandem with the cooling coil is shown as a line 2–3 and 3–4' respectively, see Figure 2.13[58].

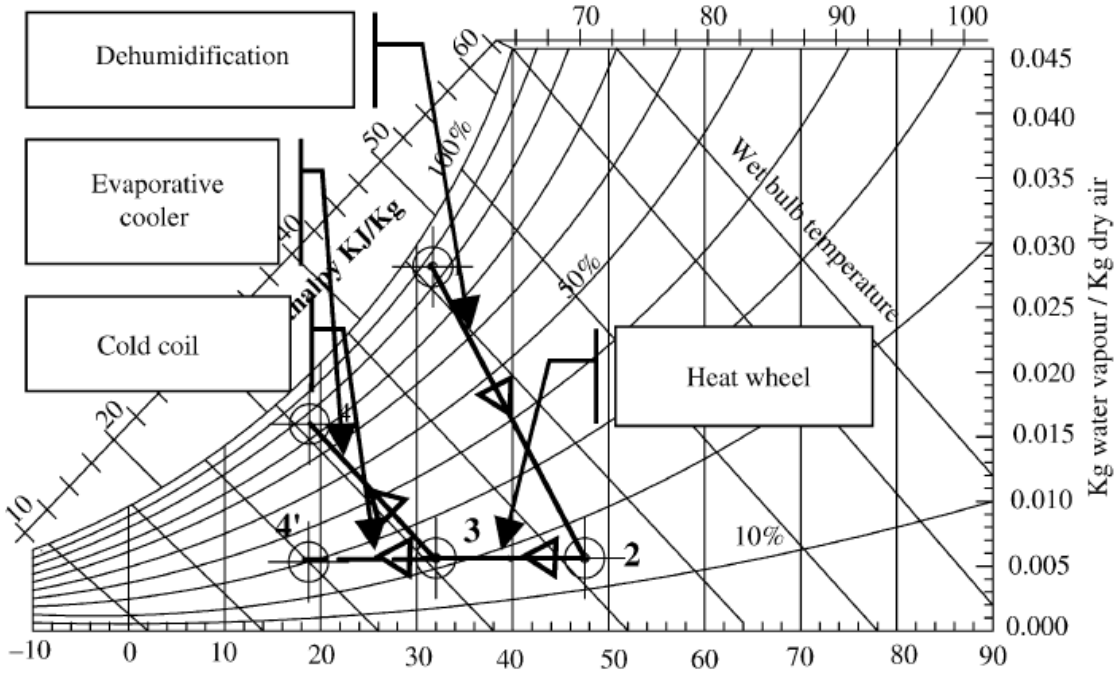

Figure 2.13 Psychrometric chart illustrating the principle of desiccant cooling [58]

2.2.3.2.1 Basic principle of evaporative cooler

Evaporative cooling units are fit for dry and hot climatic conditions [60]. These cooling units may be used as a direct contact evaporative cooling unit [61, 62], indirect contact evaporative cooling [63] or as a combination of both. In the indirect evaporative cooling, the evaporative cooler is used to reduce the temperature of air without adding moisture content to it [60]. In the indirect evaporative system, the treated air stream does not mix directly with the cooling fluid stream however it is cooled sensibly. The psychrometric chart shown in Figure 2.14 shows the cooling process inside an indirect evaporative cooler. The temperature of air is reduced by using different types of heat exchanges in which primary air loses sensible heat that absorbed by the secondary air stream. Meantime, the secondary air is cooled by means of the effect of the water spray. In the indirect evaporative cooling system, both dry and wet

bulb temperatures of the air are lowered [57]. The schematic arrangement inside the indirect evaporative cooler is shown in Figure 2.15.

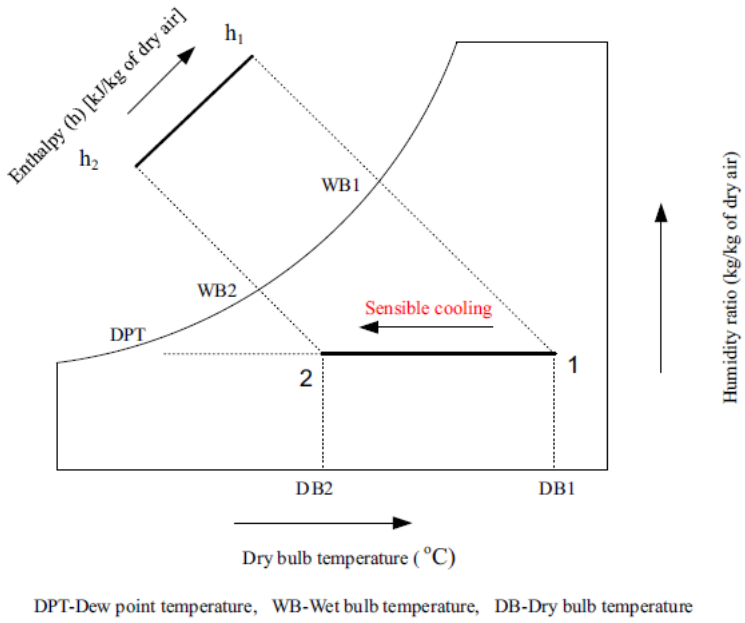

Figure 2.14 Cooling process representation of indirect evaporative cooler [57]

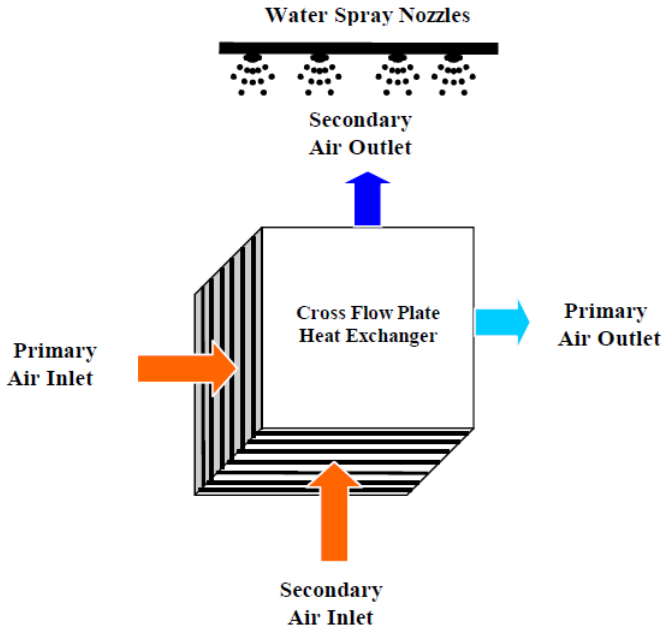

Figure 2.15 The schematic of the indirect evaporative cooler [64]

In the direct evaporative system, humidification process takes place by adding moisture to the cooled air stream where the treated air stream moves across the spray of the cooling water, see Figure 2.16 [57]. In this cooling unit, high moisture content in the air causes a drop in the temperature of the treated air. Therefore, the process is adiabatic which is appropriate for the climate of the hot and dry areas while for hot and humid areas indirect evaporative cooler is more suitable. In the direct evaporative cooling process, dry bulb temperature of the air is lowered but wet bulb temperature remains constant. The effectiveness of a well-made direct evaporative cooler may reach the level of 85% [57]. Figure 2.16 shows both the schematic and psychrometric process of the direct evaporative cooler.

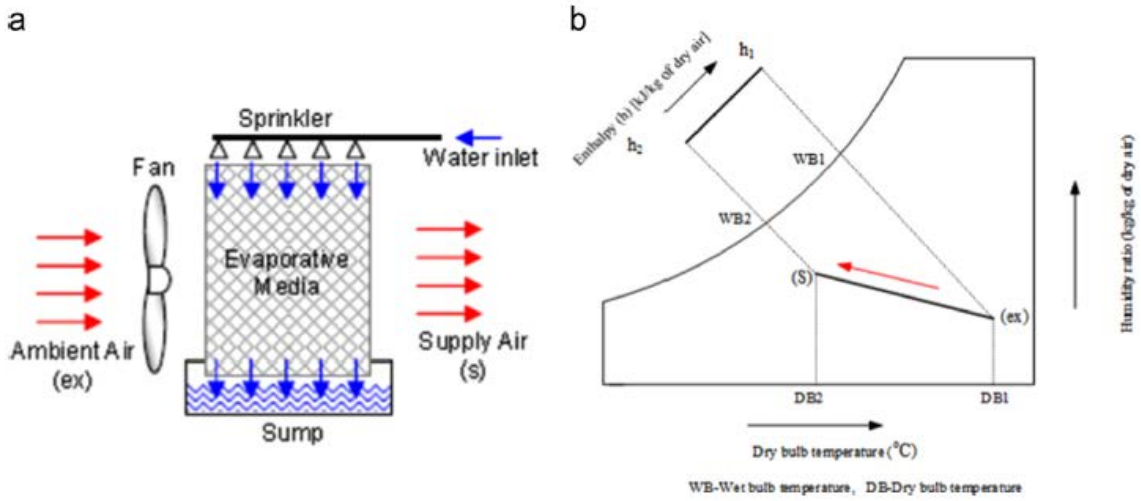

Figure 2.16 The direct evaporative cooler (a) schematic diagram (b) and psychrometric process [57]

The outdoor air mixes in direct contact with the sprayed water which drops the temperature of the supply air and increases the content of the moisture in it, see the psychrometric chart. The operational principle of a direct evaporative cooling process during the summer time to provide the human thermal comfort conditions is studied by Camargo et al. [65]. Riffat and

Zhu [66] presented the study describing the fundamental processes in the indirect evaporative cooler based on porous ceramics. The study concluded that a high cooling capacity of the system can be achieved in the dry and windy cooling space. The increase of air velocity by about 0.6 m/s significantly enhances the thermal conductivity and thus increases the heat transfer in the heat exchanger. The dimensions of the air flow passage, velocity of air and intake air ratio are the main parameters that affect the effectiveness of the heat exchanger. On the other hand, the effectiveness is affected to a lesser extent by the supply of water [67]. Figure 2.17 illustrates the difference in the cooling processes between the direct evaporative cooler and conventional air conditioning unit plotted on the psychrometric chart [68]. The difference in the enthalpy in the evaporative cooler is smaller than the difference in the enthalpy of the conventional unit which results in the evaporative cooler requiring the much greater value of mass flowrate to achieve the same cooling load which is produced by the conventional unit. Figure 2.17 shows that under the same operation conditions, the air supplied by the evaporative cooling unit has higher humidity than the air supplied by the conventional unit.

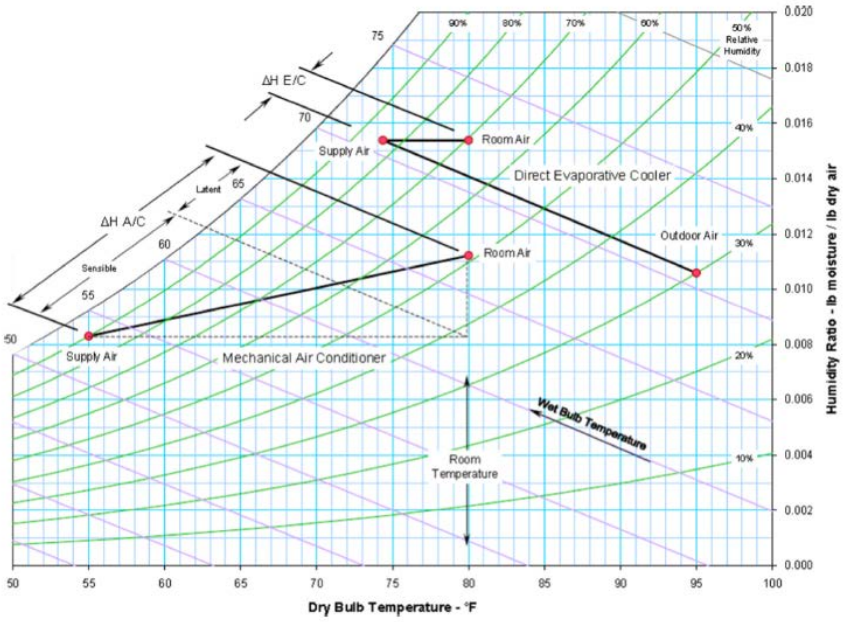

Figure 2.17 Psychrometric chart of air supplied by the evaporative cooling unit [68]

2.2.3.3 The regeneration heat source

The regeneration heat source provides the system with the thermal energy needed to extract the moisture which the desiccant material had absorbed during the sorption process. There are a number of sources of the thermal energy which can be used to drive the system including solar energy, waste heat and natural gas burning. In the systems equipped with a liquid desiccant, the regeneration heat is supplied to the desiccant solution in the structure of a regenerator into which a hot air stream is blown in order to separate the moisture from the solution. The various aspects of the liquid and solid desiccant solar cooling systems have been intensively studied by researchers. The feasibility, performance of the system, material of the desiccant and the optimization of the cycle are the most common topics reported in publications, see for example [69].

2.2.3.4 Feasibility studies

The feasibility of the desiccant cooling systems was intensively investigated to evaluate these systems operating in different hot and humid outdoor climatic conditions. Jain et al. [70] examined four solid desiccant cycles, namely the ventilation cycle, the recirculation cycle, the Dunkle cycle and the wet surface heat exchangers cycle. Figure 2.18 shows the ventilation cycle in which the fresh air is dehumidified and then sensibly and evaporatively cooled before being sent to the conditioned space. The return air, after heating, is used for regeneration. In the recirculation cycle, the return air is re-circulated through the dehumidifier while the outdoor air is used for regeneration of the desiccant wheel as shown in Figure 2.19. The Dunkle cycle, see Figure 2.20, which in a certain sense is a crossover between the above two cycles, has an additional sensible heat exchanger for improving the cycle performance. The recirculation cycle and the Dunkle cycle have 100% of the air re-circulated which does not fully take the health considerations. Therefore, the study proposed the ratio of ventilation air to be 10%.

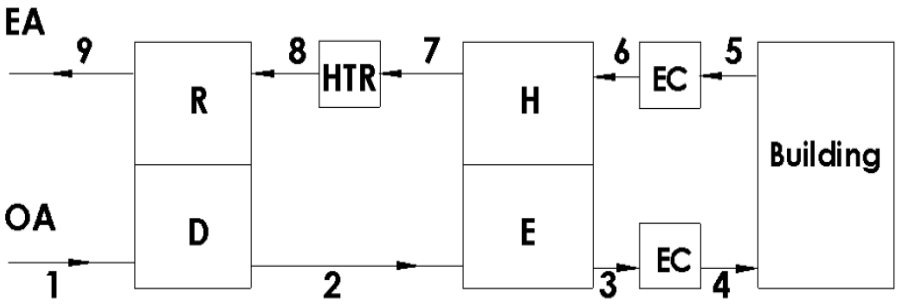

Figure 2.18 Schematic of ventilation cycle [70]

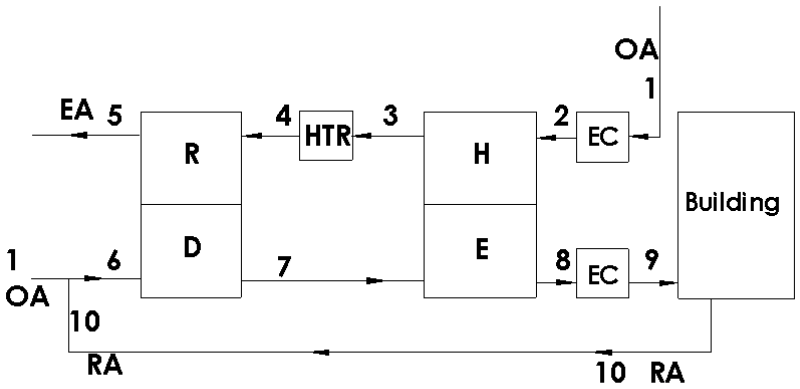

Figure 2.19 Schematic of recirculation cycle [70]

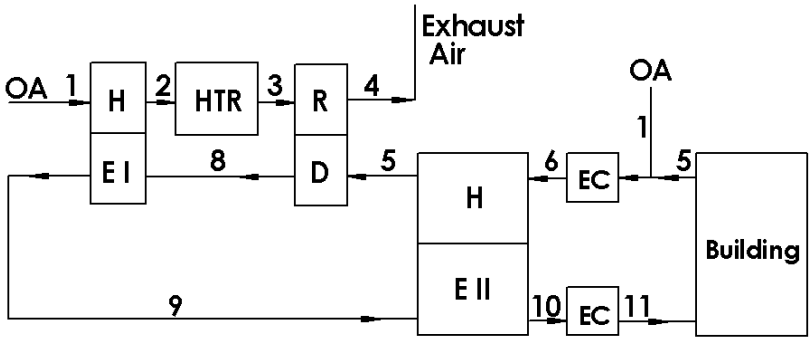

Figure 2.20 Schematic of Dunkle cycle [70]

The forth proposed cycle uses a wet surface heat exchanger in which the supply air is cooled to its dew point temperature. In this cycle, the percentage of the re-circulated air in the supply air is 50%. The study is done for various outdoor wet-bulb temperature and dry-bulb temperature of 16 cities in India. The influence of the effectiveness of evaporative coolers and heat exchangers on the COP and the volumetric circulation rate of the air in the chosen cities were the main aims of this study. It is found that the Dunkle cycle achieved a better coefficient of performance compared to ventilation and recirculation cycles in the most of the climatic conditions. However, the cycles equipped with wet surface heat exchangers achieved

the best performance. Mavroudaki et al. [71] and Halliday et al. [72] described two separate feasibility studies of desiccant cooling for many European cities, representing different climate condition across the continent. The proposed cycle uses the solar energy as the source of the regeneration. The solar collectors were indirectly connected to the desiccant system by using a water storage tank as shown in Figure 2.21. In addition, some solar coils were inserted in the incoming and exhaust airstreams, see Figure 2.22.

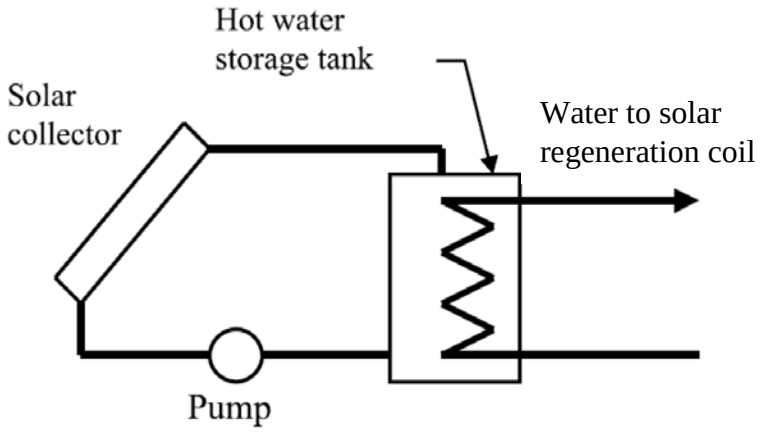

Figure 2.21 Solar collector arrangement [72]

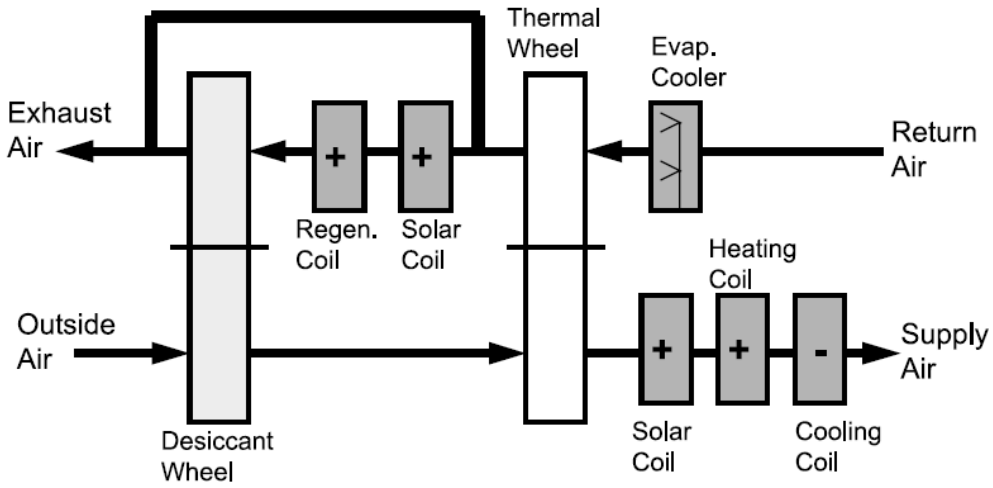

Figure 2.22 Solar desiccant cooling system [72]

The authors in both studies concluded that in the dry zones in the continent the energy savings were achieved while in the humid zones, in which the energy saving was a primary task, a decline in the saving was noticed. This decline was related to the high temperature needed to regenerate the desiccant in the climates with the high content of moisture.

2.2.3.5 Performance studies

A simulation model was developed to predict the thermal performance of a forced parallel flow solar collector/regenerator system by Alizadeh and Saman [73]. The system proposed uses a liquid desiccant of Calcium Chloride. The moisture is removed from the desiccant liquid solution as a result of absorption of solar energy in the collector/regenerator by using forced air stream that flows in counter or parallel direction to the weak solution film. The effect of climatic conditions and the system variables such as Reynolds number of the air flow, regenerator length, solution concentration and flow rate are investigated. It is found that the preheating of the air and the solution improves the regenerator performance to a large extent. In addition to this analytical study, Alizadeh and Saman [74] described an experimental study of the forced flow solar collector/regenerator system. The test rig was designed, optimized and built to compare the results of the described above model with the same aqueous solution as a desiccant. The effect of the climatic conditions and the system variables on the performance of the regenerator was studied. The authors concluded that the increase in the air flow rate enhances the performance of the regenerator and the solar collector efficiency as well. Furthermore, the study revealed that the introduced system worked satisfactorily under the summer climatic conditions corresponding to that in Adelaide, Australia.

A hybrid cooling system which consisted of a conventional vapour compression cycle combined with a liquid desiccant dehumidifier based on a solar regeneration source was simulated by Yadav [75].The liquid-desiccant cycle is employed to keep the humidity within the desirable range by partially converting the latent heat load to a sensible heat load and then meeting this load with a conventional vapour compression (VC) cycle. In such system, the heat rejected from the condenser of the VC cycle is used to regenerate partially the liquid desiccant which enhances the COP of the system. The study concluded that the hybrid system was promising in the high ambient humidity conditions, as the energy savings reached 80% when the latent heat load was 90% of the cooling load. The hybrid cycle made of VC and liquid desiccant dehumidifier was experimentally studied by Dai et al. [76]. The cycle was linked to an evaporative cooling. The cold production and COP of three cycles, namely standalone VC cycle, the liquid desiccant associated with the VCS and the desiccant and evaporative cooling associated with VCS, were compared. The study concluded that the hybrid system with evaporative cooling had an increase in the COP by 20-30% compared to the standalone VC cycle. It was also found that the electric coefficient of performance (ECOP), which was defined as the ratio of cooling production to the electric power consumption, was increased by 39-76% depending on the relative humidity of the outside air. Consequently, the electric power consumption and size of vapour compression system could be further reduced.

Mazzei et al. [77] presented a theoretical study to compare the operating costs of the desiccant and conventional cooling systems to cool a commercial building. They used three software codes to simulate and predict the cost savings. The study showed that, in the Italian summer conditions, the use of the desiccant cycle might save up to 35% of the operating costs and the thermal cooling power could be reduced by 52%. Furthermore, the use of the

waste heat for the regeneration could increase the savings up to 87%. In addition, the authors found that the use of the indirect evaporative cooling, associated with desiccant dehumidification, emphasized the reduction of the cooling power and cost savings. At that point, it was necessary to take into account that the local electricity fares, which varied from one country to another, affected the operating costs savings.

Techajunta et al. [78] presented indoor experimental and analytical study to evaluate the performance of a solar soliddesiccant cooling system in which the desiccant material was silica gel. Six incandescent electric bulbs of 120 Watts each were utilised to simulate the solar radiation in the laboratory where a light intensity meter (solarimeter) was used to measure the radiation from the solar simulator. The collector was 400x200 mm in dimensions and had a 3 mm thick single glazing. In addition, it contained a wire mesh to carry about 25 mm thick of spherical silica gel particles. A schematic diagram of the test rig for the air dehumidification process is shown in Figure 2.23.

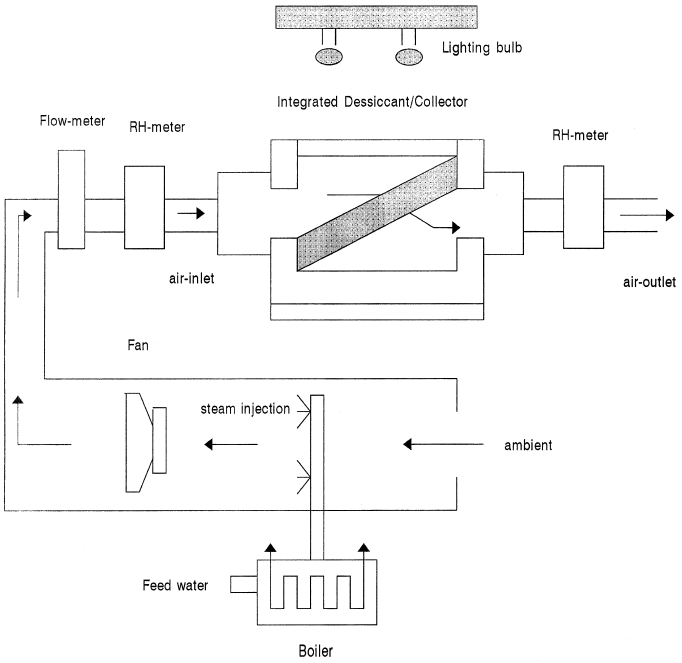

Figure 2.23 Experimental apparatus for air dehumidification by silica gel [78]

The authors found that the regeneration rate increased at high irradiation values and drops with the air flow rate. On the other hand, it was found that the dehumidification rate declined with irradiation and increased slightly with the air flow rate. The results also showed that the proposed cooling system was feasible in high humidity conditions when the regeneration process could be used in the daytime and the dehumidification process - in the night time.

2.2.3.6 Desiccant material studies

The desiccant material may be categorized as solid or liquid desiccants, physisorption or chemisorption desiccants, natural or artificial desiccants, bio or rock based desiccants, composite and polymer based desiccants etc. The term physisorption or chemisorption refers to the strength of the bond between the adsorbate and adsorbent. The removal of water vapour from the air is normally considered as physisorption because of a low bond strength between adsorbate and adsorbent. In the desiccant air-conditioning system, the bond strength is kept optimally low for an efficient regeneration process. Novel desiccants are also developed, including composite materials, which give better results compared to conventional desiccant silica gel [79, 80].

The performance and the age quantifying of six desiccant materials were described by Belding et al. [81]. Adsorption isotherms for the every desiccant were determined by subjecting the materials to varying numbers of a set of thermal processes in a test unit specially designed to carry out adsorption/desorption cycling every 10 min, see Figure 2.24.

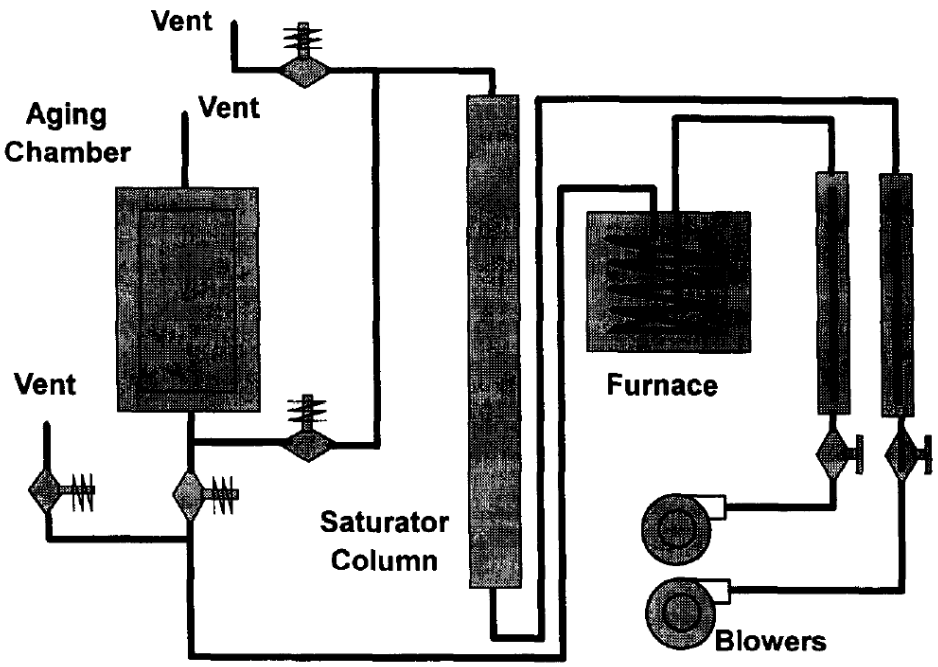

Figure 2.24 Desiccant aging apparatus [81]

The results showed that the desiccant materials exposed to cyclic hydrothermal adsorption/desorption processes deteriorated more quickly in the early time of its use and the degradation alleviated thereafter at an insignificantly small rate throughout a period of time depending on the desiccant. This period was trailed by a more noticeable deterioration tendency that directed the desiccant to the final decay. The deterioration in desiccant performance was detected by the drop in the equilibrium water adsorption rate. At adsorbing temperature of 200°C, it was concluded that Alumina and silica gel were ageing more severely after a large number of adsorption/desorption cycles. Therefore, the authors recommended that the use of Alumina and silica should be restricted to the applications with low regeneration temperatures. On the other hand, the desiccant named 13 X molecular sieve showed more stability and less severe loss of water adsorption capacity. The most stable amongst the proposed desiccants was the LCIX-Type 1M desiccant which had a large number of adsorption/desorption cycles at a desorption temperature of 250°C without

significant loss of its water vapour equilibrium capacity. Furthermore, the increase in the desiccant wheel rotational speed was also found to decrease the effect of desiccant ageing on the system performance. In this study, it was also concluded that the overall performance of desiccant cooling systems was not affected significantly by the slight decrease in adsorbent capacity of adsorption.

Factor and Grossman [82] concluded that the solid desiccants had a significantly higher degree of dehumidification than the liquid desiccants. The solid desiccant systems usually use fixed beds or movable rotary wheel beds in order to pack the desiccant materials in them. In the first system, two or more fixed desiccant beds are built with an arrangement of valves in order to make these fixed beds work alternately in the adsorption and regeneration phase. In the other system, the air to be desiccated flows through one side of the rotary wheel, whilst the heated air stream regenerates the desiccant on the opposite side of the wheel. The two air streams must be separated completely to maintain the functions of each stream. In both systems, solar air heaters are particularly suited to provide heat for regeneration of the desiccant because air is the regeneration medium.

2.2.3.7 Applications of desiccant air conditioning

In addition to the application for air conditioning of a particular space, the desiccant cooling systems can be used to for preservation of products and foods such as stored cereals. Thorpe [83] presented a mathematical model of a solar desiccant cooling device, which used the solar energy for regenerating the desiccant, in order to preserve stored grains. The author validated the results he found with experimental data which had been published earlier. In a subtropical climate, the presented cooling device can reduce the wet bulb temperature of ambient air from approximately 17.3°C to approximately 12.3°C. At these conditions the device was to

provide a cooling energy worth 50 times of the electrical energy consumed. Dai et al. [84] investigated a hybrid solar cooling system which consisted of a rotary dehumidifier wheel associated with a solar adsorption refrigeration to produce the cooling effect for preserving stored grains. The study concluded that an outlet temperature less than 20^{o}C regardless of any given entry humidity and temperature could be produced and the coefficient of performance of the hybrid system of 0.4 could be obtained. In addition, the authors analysed a number of parameters which could have an effect on the system performance, for instance, ambient conditions, evaporative cooler design, the effectiveness of the heat exchanger and mass air-flow rate.

Nagaya et al. [85] proposed a new type of air conditioning system for automobiles in which the energy loss was small compared to the previous system. For an automobile, any small reduction of the energy loss in the air conditioner is significant, because the compressor is driven by the engine. In the previous system, the air was cooled at a lower temperature and then reheated to produce dry air in the system, therefore, the energy efficiency declined and the humidity could not be controlled properly. In the new proposed system, a desiccant was mounted in the air conditioning system for controlling both temperature and humidity. The energy of the new system was compared with that of the traditional one at the same operating conditions. Results demonstrated that the desiccant system controlled the temperature and humidity and achieved the much higher energy efficiency.

2.2.3.8 Comparison between conventional and desiccant air conditioning systems

The thermally driven desiccant air conditioning (DAC) systems have many advantages over the conventional vapour compression air conditioning (VAC) systems. The advantages mentioned in the next section reflect the increasing importance of the DAC.

2.2.3.8.1 Green technology

The traditional VAC systems are the main cause of the depletion of the ozone layer, global warming and greenhouse gas effect [86], however, DAC is a green technology which warrants the environmental safety [87]. Bolaji et al. [88] stated that CFCs and HCFCs were found harmful to the earth's protective ozone layer. Accordingly, their production was banned by the Montreal Protocol and other international agreements. HFC refrigerants have been replacing CFC and HCFC refrigerants. But, they are still similar to CFCs and HCFCs and a much preferable option is to utilise natural refrigerants, which are environmentally friendly. The authors presented the environmental effects of some common refrigerants on the ODP (Ozone Depletion Potential) and GWP, see Table 2.2, where GWP is the amount of infrared radiation that the gas can absorb, relative to carbon dioxide (which has GWP of 1), over a period of 100 years.

Table 2.2 Environmental effect of some common refrigerants on ODP and GWP

Compositional group	Refrigerants	Ozone depletion potential (ODP)	Global warming potential (GWP) (100 years' horizon)
CFCs	R11	1	3800
	R12	1	8100
	R113	0.8	4800
	R114	1	9000
	R115	0.6	9000
HCFCs	R22	0.055	1500
	R123	0.02	90
	R124	0.022	470
	R141b	0.11	630

	R142b	0.065	2000
HFCs	R23	0	11700
	R32	0	650
	R125	0	2800
	R134a	0	1300
	R143a	0	3800
	R152a	0	140
Natural Refrigerants	R290	0	3
	R600a	0	3
	R717	0	0
	R718	0	0
	R744	0	1

2.2.3.8.2 Control of temperature and humidity

Humidity control is clearly needed in the daily life, however, it is more needed in some sectors, e.g. hospital buildings in which the patients and working staff are under the risk of infection because the effect of humidity on microbes, bacteria or viruses evolution plays a vital role as shown in Figure 2.25 [89].

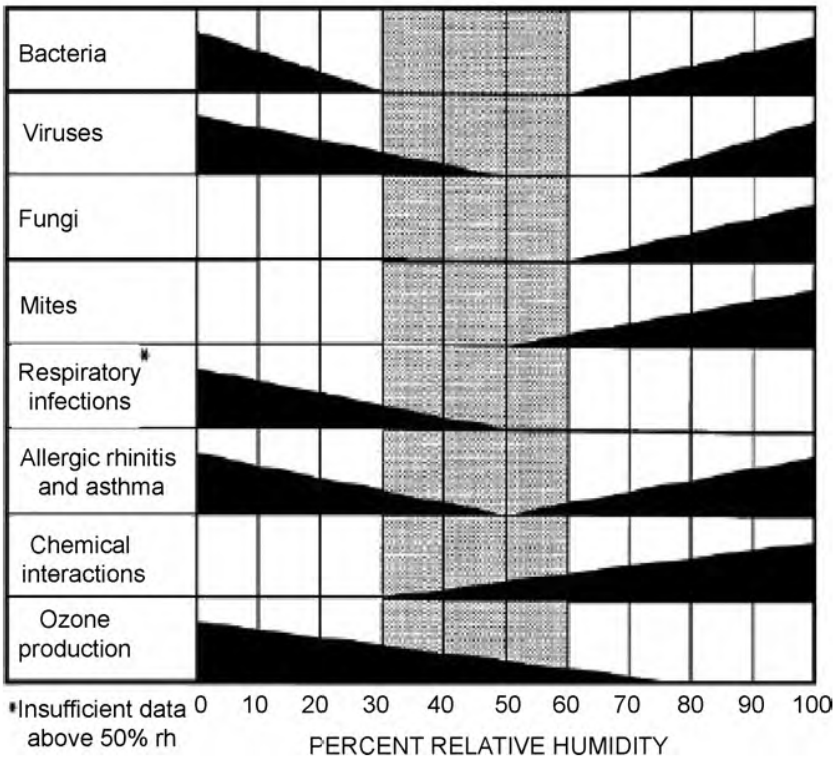

Figure 2.25 Relative humidity percentage associated with different health issues [89]

The VAC systems control the humidity by keeping the temperature of the supply air lower than dew point, thus, the heating is required to achieve the wanted conditions of temperature and humidity as shown in Figure 2.26 through processes (1–3–4–5) [80, 90]. Therefore, the VAC system cannot handle the sensible load and latent load of AC. On the other hand, in the case of DAC systems, the latent load of AC is transformed into the sensible load by using a desiccant dehumidification through processes (1–2–5) as shown in Figure 2.26. Moreover, the indoor air quality may be enhanced significantly by using high ventilation, air flow rate and the capability of removing airborne pollutants.

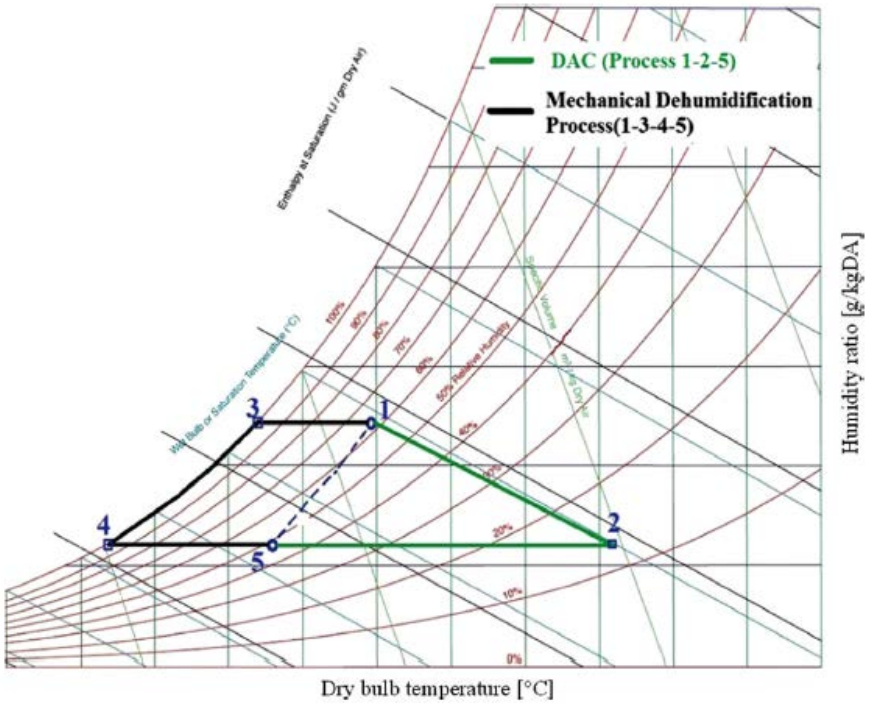

Figure 2.26 The operation of production of VAC and DAC system [80]

2.2.3.8.3 Energy conservation

As in the VAC the humidity is controlled by keeping the temperature of the supply air below the dew point, then an additional amount of energy is required to achieve the desired conditions of temperature and humidity [91]. As it was shown in Figure 2.26, it is possible to avoid overcooling the air and then reheat it in DAC systems compared to VAC ones. Saving energy is also important for avoiding depletion of fossil fuels. Lee and Lee [92] presented a parametric study involving a number of ventilation rates in wet markets in hot and humid conditions of Hong Kong. The study indicated that the use of DAC system in such environmental conditions could lead to energy savings, as well as CO2 emissions reduction of 13% depending mainly on the value of ventilation rate. Besides, a DAC system provided the electricity saving up to 24% in hot and humid climatic conditions of Thailand according to Hirunlabh et al. [93].

2.2.3.8.4 Waste energy or renewable energy

Unlike conventional VAC systems, heat is the main driving energy required to actuate DAC systems, which makes it possible to use low-grade waste heat and renewable energy. Hurdogan et al. [94] investigated the use of solar energy in DAC systems. Solar radiation data for the city of Adana in Turkey was used in their study. By applying the solar energy in the DAC system, an increase of the COP by 50–120% could be achieved.

2.2.3.8.5 Potential applications

The DAC system can be applied for various humidity conditions for air conditioners' applications in more efficient way, compared to VAC such as AC for automobiles [85], wet markets [92], drying grains [83, 84], greenhouses [95], marine ships [96], museums [97], and product storage hospitals. Figure 2.27 shows some of the humidity based AC applications plotted on psychometric charts [80]. The DAC systems are more effective in the lower humidity processes in manufacturing and storage facilities, which are shown in the red dotted lines in Figure 2.27 (a) and (b), respectively.

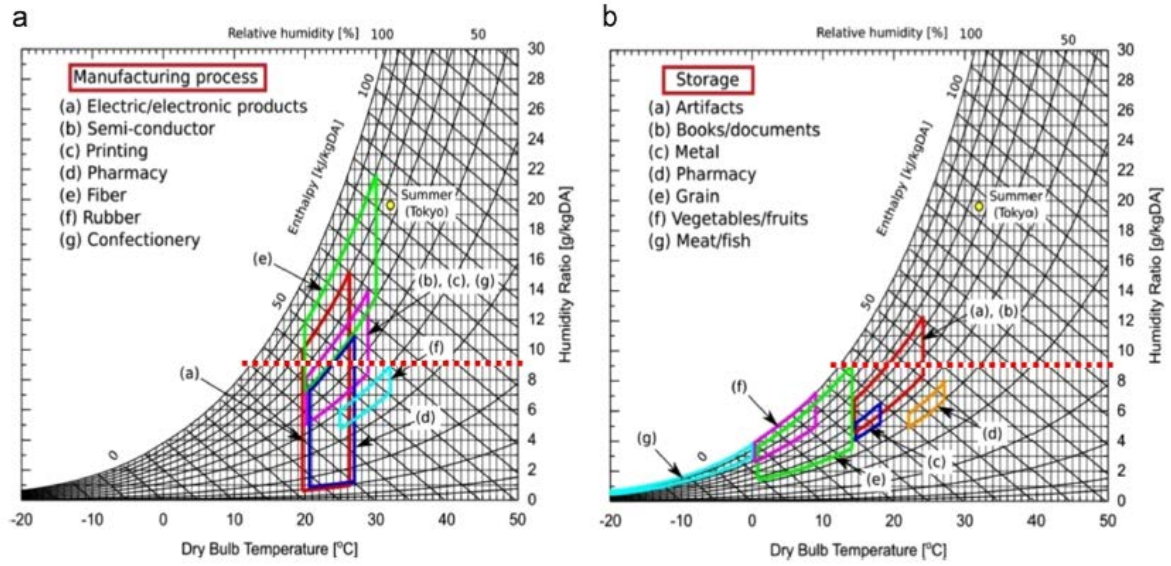

Figure 2.27 Temperature and RH for different kinds of storage and manufacturing processes [80]

2.2.3.9 Implementation of solar collectors in desiccant cooling systems

Solar powered Desiccant Systems are widely adopted in various sectors; the basic type of solar desiccant wheel cooling system is implemented in the cycles, containing rotary wheel and solid desiccant materials [98]. In such systems, the solar energy is absorbed by solar collectors and then is used to regenerate the wet desiccant. Many projects used flat plate or heat pipe vacuum tube solar collectors to drive the processes in the solid desiccant cooling systems.

2.2.3.9.1 Flat plate solar collector drives Desiccant system

Preisler et al. [99] experimentally studied the annual performance of an actual solar desiccant evaporative cooling system (SDECS). The experimental investigation was conducted in an administration building in Vienna, Austria, where the humidification of air was a big issue as

the outdoor air had a very low humidity (1 to 2 g/kg). Figure 2.28 illustrates the configuration of the proposed system.

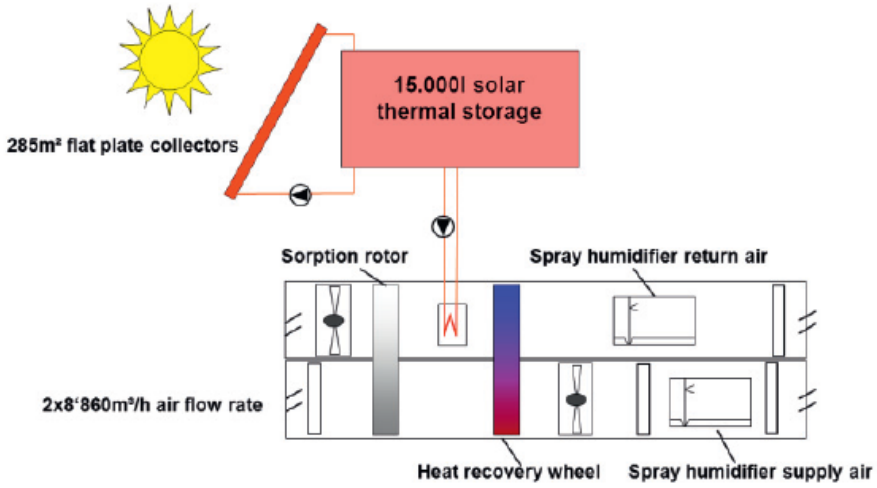

Figure 2.28 Schematic design of SDECS [99]

The data collected for the proposed system was compared with simulated results for a conventional compression chiller obtained with TRNSYS 17. Results showed that average COP*el of SDECS in the winter time could reach 7. In 2010, the SDECS provided the 60.5% primary energy savings compared to the reference system. The highest energy saving was found to be in the winter time when the system was used for heating and humidity recovery of fresh air. A moderate energy savings were shown in the summer time when system was used for a cooling and humidity control. In addition, Joudi and Dhaiban [100] evaluated the performance of the solar driven heating and desiccant cooling system deployed in a residential building in Baghdad, Iraq. A simulation model was developed to investigate both heating and cooling performance of the proposed system. They studied the effects of main operation parameters on the system performance. Results revealed that the use of the flat plate solar collector alone could produce a regeneration temperature of 62 °C and the use an additional heat source to reach higher regeneration temperature was necessary.

Furthermore, the solar desiccant cooling system could satisfactorily supply air to the conditioned area at local climatic conditions. The effectiveness of the evaporative cooler and sensible heat exchanger had a dominant effect on the performance of the desiccant cooling system while the effect of the dehumidifier was relatively small. The pre-cooling and final-cooling modes were developed by Guidara et al [101] in order to fulfil the required cooling capacity. Figure 2.29 shows the schematic diagram of the proposed system. The authors suggested two indirect evaporative coolers to be fitted into the system, one of them before ambient air entering desiccant wheel while the second one was used before the process air entering the cooling space. The analysis of the performance of the system was simulated for three different climatic conditions in Tunisia, namely Bizerte, Remada and Djerba. The simulation study included three modes of functioning for the three climatic conditions: relatively cold and humid in Bizerte, hot and dry in Remada and moderate in Djerba. The results showed that the basic DECS mode was feasible for the ambient temperature and humidity conditions in Bizerte. However, for the dry climate in Remada and moderate climate in Djerba, systems with pre-cooling mode and with both pre-cooling and final-cooling modes had to be installed to satisfy all demands.

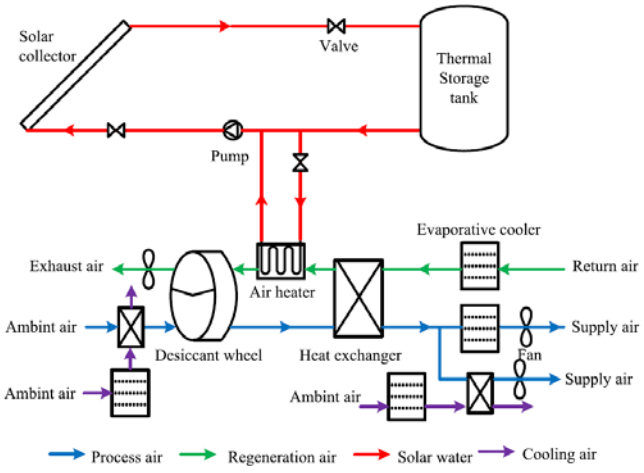

Figure 2.29 Solar desiccant cooling system with pre-cooling and final-cooling [101]

2.2.3.9.2 Heat pipe vacuum tube solar collector drives Desiccant system

Bourdoukan et al. [102] assumed that low efficiency of flat-plate collectors is the main cause of low potential of solar energy for the use in solid desiccant cooling, therefore, heat pipe vacuum tube (HPVT) collectors were introduced in the study to drive normal DECS. Mathematical models of HPVT collectors and water tank were used to simulate and validated in the study, and then the outputs of these models were integrated with existing desiccant wheel models [103, 104], see Figure 2.30. Based on this integrated model, the performance of the system was simulated to produce the cooling capacity for a building with an area of 1350 m^2 in three locations namely, La Rochelle, Bolzano and Berlin in order to investigate the potential of such configuration. The indoor comfort level temperature was assumed to be less than 26 ^oC and the humidity ratio less than 11.8 g/kg. Simulation results over a summer time revealed that the cooling system could maintain the conditioned space temperature and humidity at the comfort level for the three suggested locations. The daily efficiency of HPVT varied from 50% to 64% and the daily solar fraction varied from 87% to 97%, and the corresponding seasonal overall efficiency and solar fraction were higher than 51% and 90%, respectively.

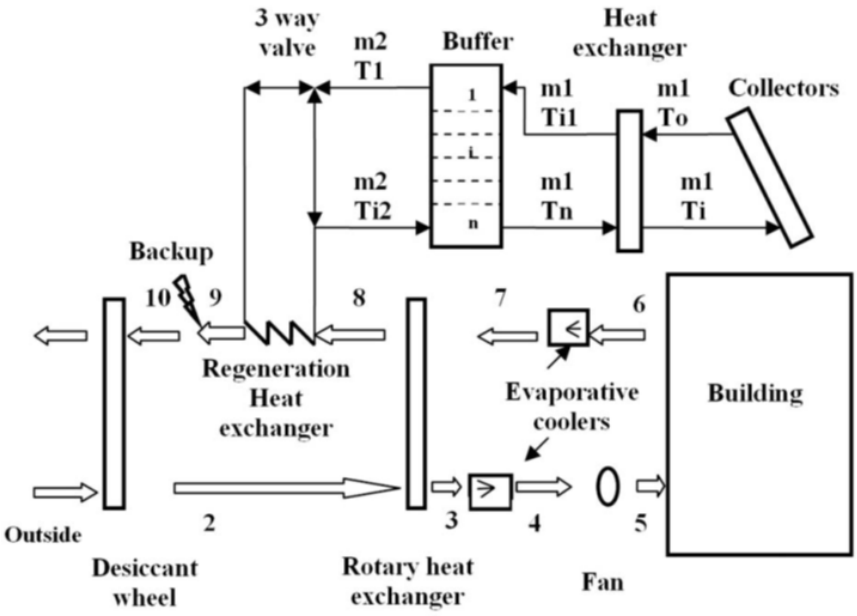

Figure 2.30 Desiccant cooling integrated with HPVT [105]

Improving the above study Bourdoukan et al. [102] developed an experimental test rig of the HPVT powered DECS. The actual operational data showed that the system was feasible and it was verified that HPVT collector could acquire the high-temperature level and steadily maintain the regeneration temperature. According to the study, the use of the solar energy as a sole regeneration source could satisfy maintaining the indoor temperature and humidity at comfortable conditions with the temperature at 26.5°C and humidity of 12–14 g/kg. The overall efficiency of the solar installation could reach the level of 55% whereas the thermodynamic coefficient of performance achieved was 0.45. The performance indicator based on the electrical energy consumption was 4.5 over the whole day. Besides, effects of outdoor and regeneration conditions were investigated, and the outdoor humidity ratio was shown to be the most sensitive parameter.

Ge et al. [106, 107] concluded that the performance of the rotary desiccant wheel decreased mainly as a result of the rejected adsorption heat in the dynamic dehumidification

process. Therefore, they developed an inter-cooling two-stage rotary desiccant wheel cooling system (TSDCS) to achieve an enhancement in the performance of the system. It was shown that TSDCS had the advantage of the high thermal COP as well as low regeneration temperature. Further study to enhance the performance of the solar powered TSDCS was conducted by Ge et al. [108] as illustrated in Figure 2.31.

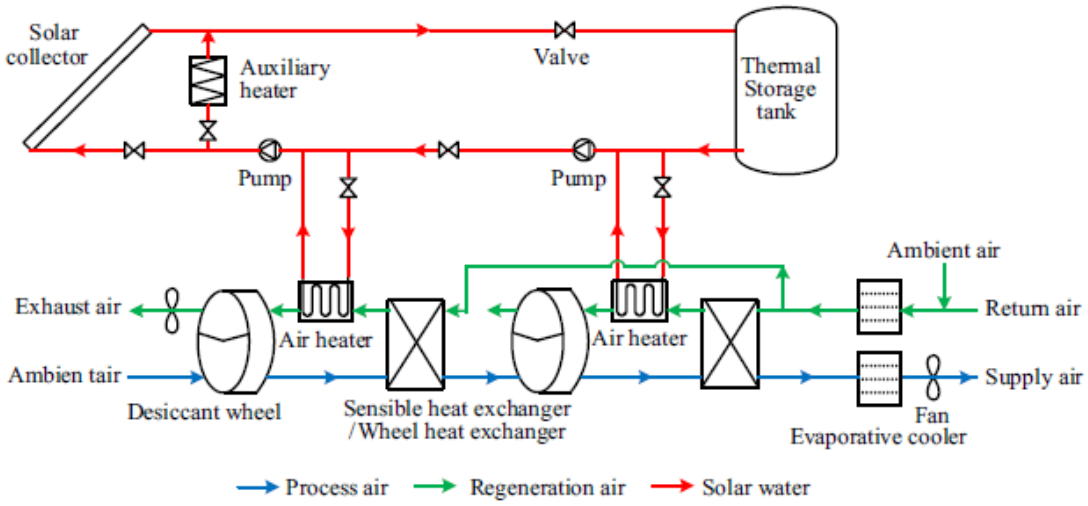

Figure 2.31 Schematic diagram of two-stage rotary desiccant wheel cooling system [108]

In the research, the performance of two different cooling systems including a solar driven TSDCS and vapour compression system were simulated to meet the cooling demand for one of stores in a commercial office building in two different cities with different climatic conditions, namely Berlin and Shanghai. The aims of the study were to evaluate and compare the thermodynamic and economic performance of the above two systems. The results showed that the desiccant cooling system could produce the needed cooling demand as well as to provide process air to create comfortable conditions in both cities. In Berlin, the required regeneration temperature was 55°C whilst it was 85°C in Shanghai. It was also found that the desiccant cooling system had a better supply air quality and consumed less electrical energy, compared to the vapour compression systems. The results of the financial

analysis revealed that the dynamic investment payback periods were 4.7 years for Berlin and 7.2 years for Shanghai.

2.3 Thermo-mechanical refrigeration

The main target in any solar thermo-mechanical refrigeration system is to use the solar energy to drive the compressor of the refrigerating cycle to produce the cooling effect as showing in Figure 2.32.

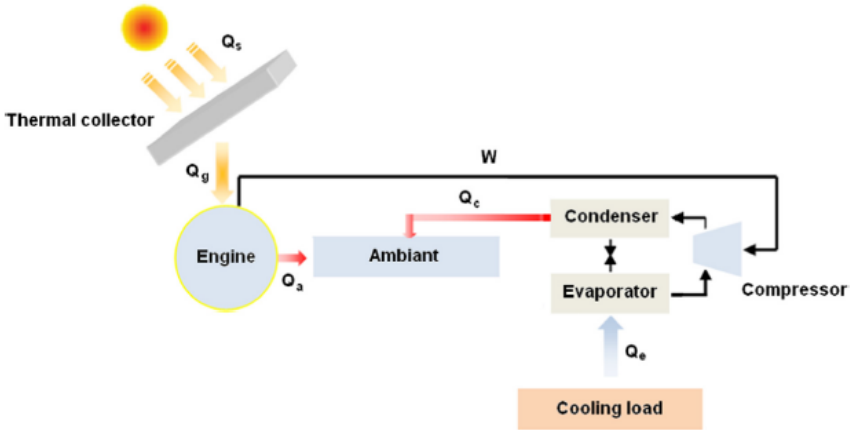

Figure 2.32 Solar thermo-mechanical refrigeration principle [12]

2.3.1 Rankine cycle

Most of the global electric power is produced using thermodynamic power cycles. These power cycles can be classified according to the used working fluid: gas power cycles, and vapour power cycles. In the gas cycles, the working fluid throughout the cycle is in the gaseous phase, e.g. the Brayton cycle. In a vapour power cycle, the working fluid that enters the turbine is in the gaseous phase, produced by vaporizing a liquid in the boiler [109].

Cogeneration, producing power and cooling effect, has improved the sustainability of the thermal power cycles, where it can increase the energy application efficiency significantly.

In the early 1950s, the use of Rankine cycle with a working fluid being ammonia–water as an absorption power cycle was proposed by Maloney and Robertson [110]. The binary component mixtures exhibit a boiling temperature that varies during the boiling process, and their use makes it possible to maintain a more constant temperature difference between the working fluid and variable temperature heat sources. This reduces exergy losses in the heat addition process [111]. Maloney and Robertson concluded that there was no significant advantage over the steam cycle operation for the conditions considered.

2.3.1.1 Kalina cycle

Kalina [112, 113] developed a combined power cycle which employs an ammonia/water mixture as the bottoming cycle working fluid, and solved the problem in the cycle by Maloney and Robertson by replacing the condensation process with an absorption process. In this cycle, as seen in Figure 2.33, the vapour solution stream from the distillation unit (stream 5) is combined with a bypass basic solution (stream 3). Thereafter, the mixed stream (stream 6) is cooled and condensed in the second condenser, which makes it possible for the distillation unit to work at a lower pressure than that of the boiler. The lower pressure minimises the amount of energy needed to separate the combined mixture, which enhances the performance of the cycle. Then, the mixture is heated, in the boiler, and superheated before it is directed to the turbine. The turbine exhaust is used to recover the energy and to heat the basic solution [35].

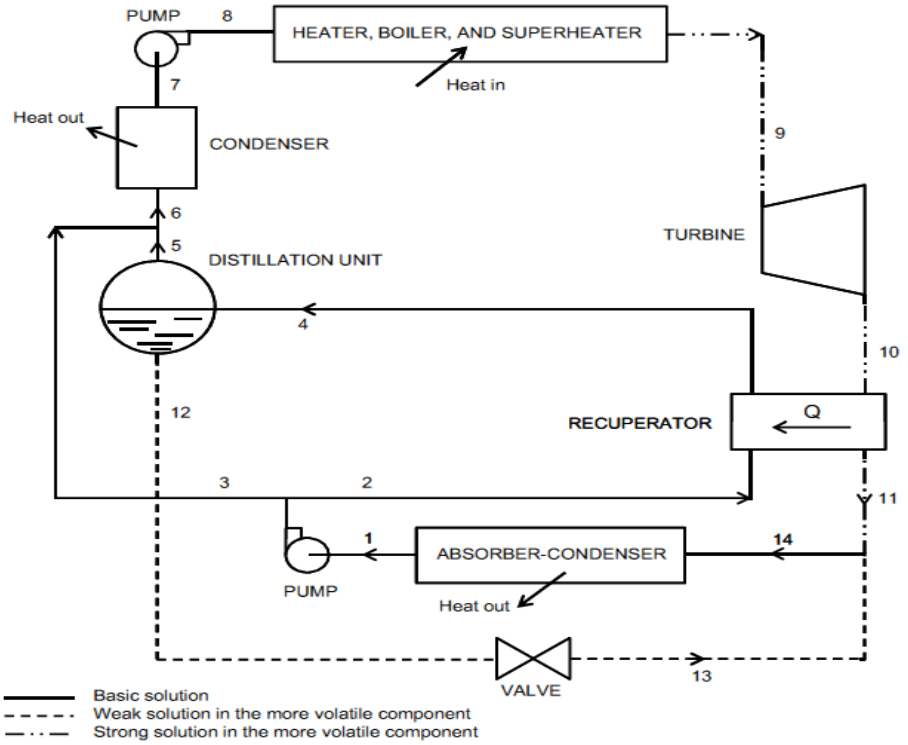

Figure 2.33 Schematic diagram of Kalina power cycle [35]

The Kalina cycle has been studied for many years [114, 115]. Recent appreciations of its advantages has renewed the interest in the ammonia/water absorption cooling cycle. Where the waste heat rejected from the power cycle, it is used to run the absorption process in the absorption refrigeration cycle for producing power and cooling simultaneously. In those combination cycles, the benefit of the energy-conversion criteria and the cycle characteristics may be different from one application to another. The absorption cycle is flexible for the use in a wide variety of practical process schemes [116, 117].

2.3.1.2 Goswami cycle

Goswami presented in [118, 119] a unique feature of the cycle (called the Goswami cycle) used to produce a combination of power and cooling cycle simultaneously in the same loop.

This cycle is a combination of a Rankin cycle and an absorption refrigeration cycle with a working fluid being ammonia–water mixture.

The Goswami cycle [120], see Figure 2.34, works in the following way: the basic solution, which is a mixture of ammonia and water, is pumped from the low pressure level in the absorber (state 1) to high pressure level (state 2) by the circulation pump. It is then split into two streams (state 2A and 2B) to recover heat (state 13 and 14), then the two streams mix together with the condensed liquid from the rectifier (state 5) into one stream and enter the desorber (state 3) which is called a boiler by Goswami and co-workers. The working fluid is partially boiled in the desorber where a vapour, rich in ammonia, is produced as a result of this process (state 4) together with a hot, weak-in-ammonia, liquid solution (state 10). The vapour, rich in ammonia, passes through the rectifier to increase the percentage of the ammonia in the vapour by reducing the content of water in the vapour in the condensation process. The resulting rectified vapour (state 6) enters the super-heater (state 7) and then expands in the expander (state 8), which produces useful power. Power production is accompanied by a cooling effect in the case of expanding the vapour below ambient temperature (states 7–8). The expanded stream provides a refrigeration effect in the refrigeration heat exchanger by receiving a sensible heat from another fluid (states 8– 9). After recovering heat from it in the solution heat exchanger, the pressure of the weak liquid solution is reduced in a throttling valve before it flows back to the absorber (states 10–12). In the absorber, the heat is rejected from the cycle when the weak solution (state 12) and the vapour (state 9) are mixed together, generating the basic solution (state 1) [120]. As shown in Figure 2.33 for the condensate, that flows back from the rectifier (state 5), to be mixed with the basic solution after recovering heat, it may either be re-circulated into the desorber

[120-122] or be mixed with the weak solution after reducing its pressure in the throttling valve [123].

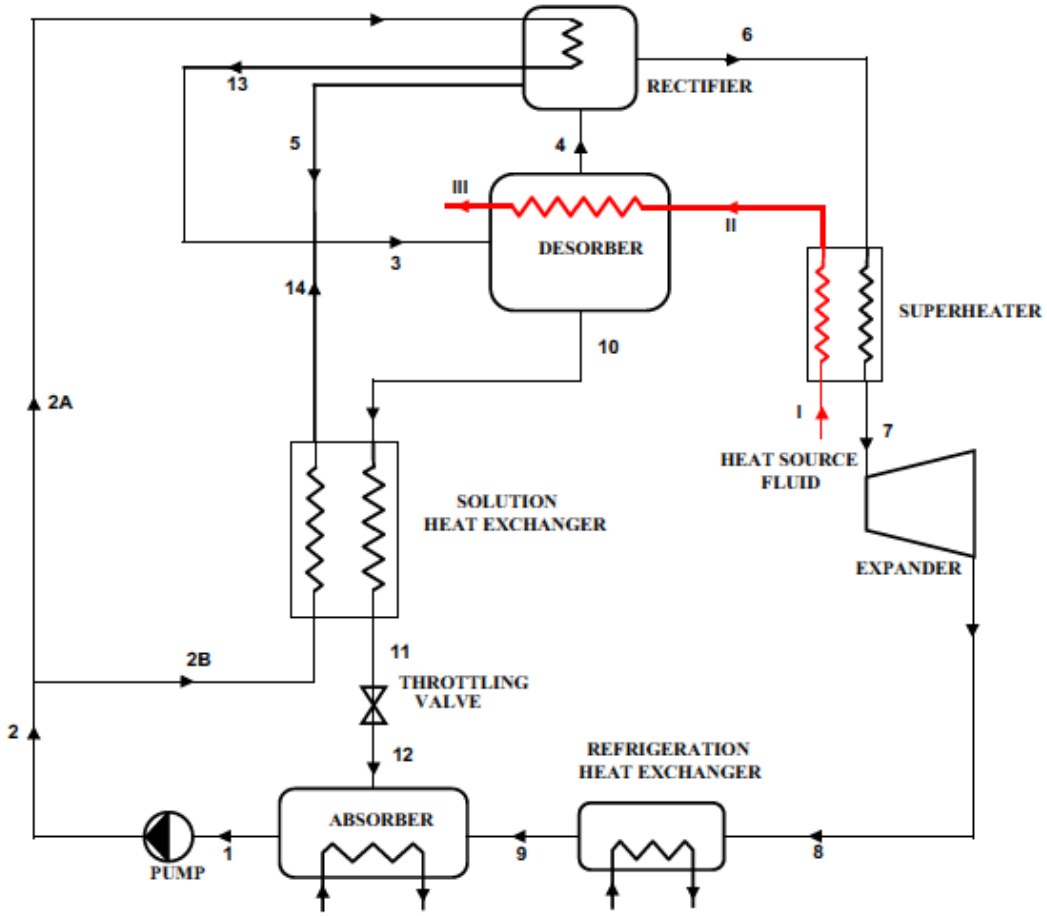

Figure 2.34 Schematic diagram of the Goswami cycle with internally cooled rectifier [35]

The heat source in this cycle could be geothermal energy, solar energy, waste heat, etc. In addition, the cycle may be a bottoming cycle for a conventional power cycle. The cooling effect can be accomplished because the working fluid is a mixture (ammonia and water) at the constant pressure. Also, the condensing temperature of the ammonia-rich vapour can be significantly lower than the saturation temperature of a lower concentration ammonia–water mixture. The ammonia can be expanded to a low temperature by increasing the concentration of the ammonia vapour that enters the expander and by decreasing the expander inlet

temperature, which negatively affects the power production. Accordingly, the superheating process of the vapour in the rectifier enhances power production but it lessens cooling production. Using the Goswami cycle, a number of studies were performed to take into account some specific features such as refrigeration output, cycle optimisation, parametric analysis and cycle development to enhance power and cooling production simultaneously. Goswami et al. [120] presented a thermodynamic parametric analysis of the Goswami cycle. The analysis was carried out with the assumption of the ideal conditions by neglecting the irreversibilities that might occur during the heat transfer and expansion processes. The results showed the possibility of using the low and medium temperature solar collectors to drive the cycle. In addition, the proposed cycle had a high thermal efficiency but the cycle had to be optimized to produce the maximum power, maximum cooling effect, or a maximum overall thermal efficiency. Another parametric analysis of a Goswami cycle was performed by Xu et al. [124], see Figure 2.35. The theoretical investigations of this cycle demonstrated that the combined cycle achieved a high thermal efficiency of about 23.5% with a heat source temperature of 137 ˚C. This value of the efficiency is higher than that of the conventional steam power cycle, working at the same operating conditions. Additionally, the output power production of the proposed cycle was 2 MW together with a cooling output of 700 kW for refrigeration. Also, it was found that the cycle was efficient thermally with a heat source temperature of 400 K, which could be provided by flat plate solar collectors or many other sources of the heat, including geothermal one.

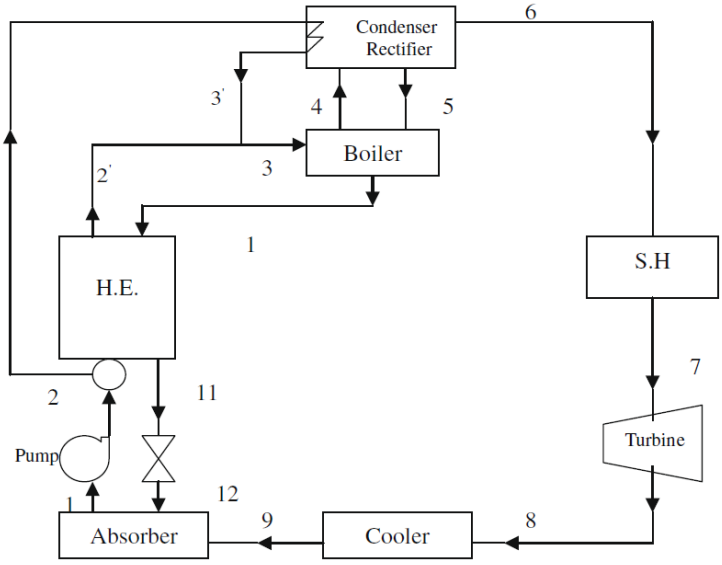

Figure 2.35 A modified ammonia-based combined power/cooling cycle [124]

The cycle which had been studied by Xu et al. [124] was optimised by Pouraghaie et al. [109]. The optimisation was carried by changing the value of superheat temperature, condenser temperature and turbine inlet pressure in a limited range. The objective functions considered in this study were turbine output work, cooling capacity and cycle thermal efficiency and the Pareto approach optimisation method was used. The first law of thermodynamic was applied to find the objective functions ignoring the irreversibilities. The obtained results demonstrated that two extreme points in the Pareto method included those of single-objective optimization results, therefore, provided more choices for optimal output designs.

Xu and Goswami [125] proposed a new method to calculate the thermodynamic properties of the working fluid, ammonia-water, by using Gibbs free energy equations and empirical bubble and dew point temperature equations when calculating the phase equilibria. The equations were solved iteratively and the results were compared to experimental data and showed good agreement. By using the first and second laws of thermodynamics, Hasan et

al. [126] optimised the thermodynamic performance of the cycle in order to maximise the second law efficiency using a commercial optimisation program using Generalised Reduced Gradient method (GRG2). The study considered the heat source temperature ranging between 57 and 197 ˚C which could be provided by low to medium temperature solar collectors. They concluded that the second law efficiency could be maximised up to 65.8%. Furthermore, it was found that the absorber had the largest (44%) contribution to the cycle irreversibility with the front of the rectifier and solution heat exchanger adding 16% and 24% to the total irreversibility, respectively. In some cases when the heat source had a very low temperature, the irreversibility in the boiler had a significant value. For Hasan–Goswami–Vijayaraghavan study [126], an exergy analysis was carried out by Vidal et al. [127]. They applied The Redlich–Kwong–Soave equation of state in order to evaluate the thermodynamic properties of the working fluid in the cycle simulation. The study included the effect of the irreversibilities caused by the different components of the cycle. The simulation of the cycle was done using the process simulator ASPEN Plus. When the heat source temperatures were between 125 and 150˚C, it was found that the exergy effectiveness was between 53% and 51% respectively. The production of cooling was less than the power production. The exergy analysis of the cycle revealed that both cooling effect and power could be generated using low-temperature heat sources even in the case of irreversible cycles.

Lu and Goswami [121, 122] studied the enhancement of the cooling effect by reducing the refrigeration temperature and the effect of the ambient temperature on the cooling effect. It was found that both first and second low efficiencies decreased as a function of the drop in the refrigeration temperatures. The results showed that a low refrigeration temperature of 205 K could be reached by using this cycle. Furthermore, they

showed that both cooling effect and power generation could be produced at optimum conditions with the source temperature of 360 K. Vijayaraghavan and Goswami [128, 129] developed a number of expressions to evaluate the total efficiency of the cycle which included effciencies for the refrigeration effect and the power production. Then, the cycle was optimised for the maximum efficiency by using Generalised Reduced Gradient. The definition of resource utilization efficiency (RUE) was presented to express the total desired effect needed from the combined power and cooling cycles. An improvement of RUE was achieved by adding a thermal distillation scheme to the cycle with two different configurations: namely, configurations 1 and 2, as shown in Figure 2.36 and Figure 2.37, respectively. By optimising RUE of the modified cycle, an enhancement of more than 25% was achieved.

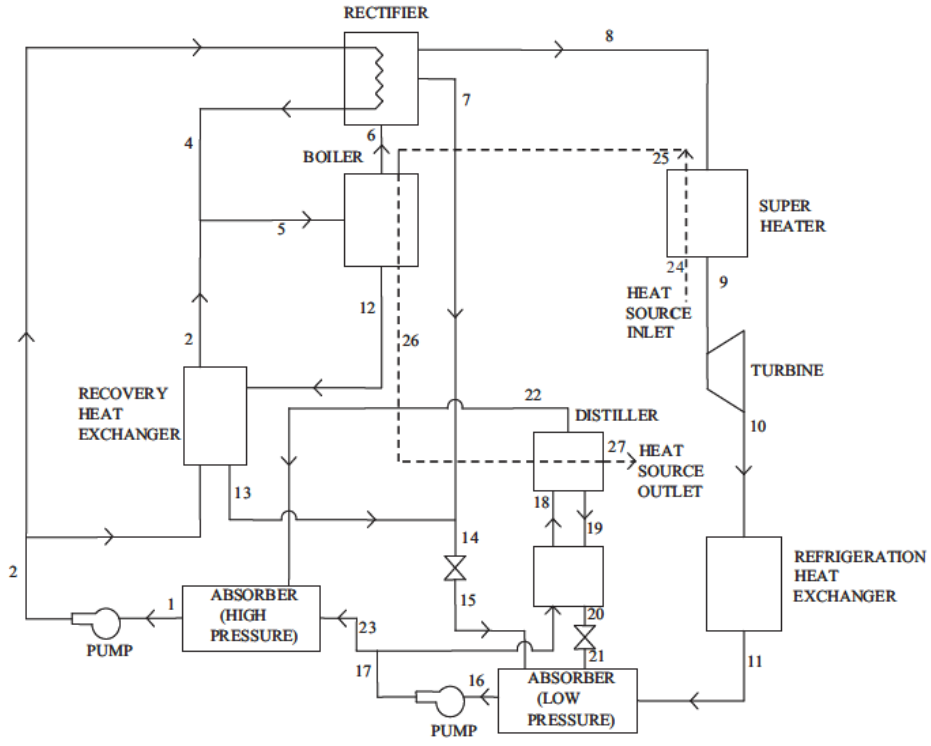

Figure 2.36 Modified power and cooling cycle configuration 1 [129]

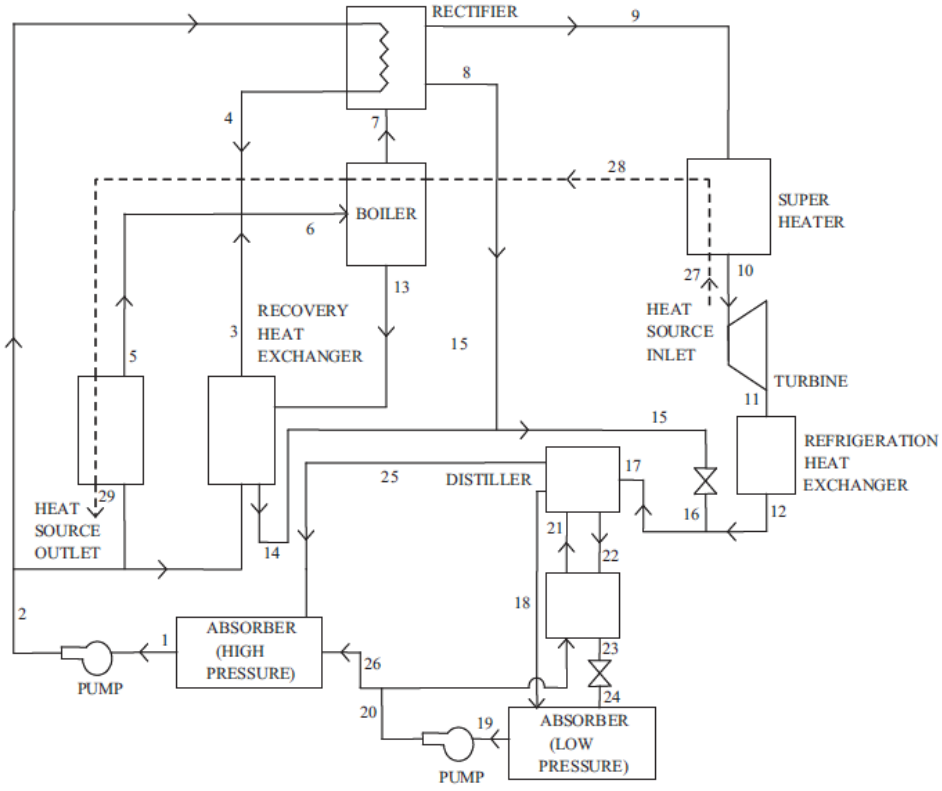

Figure 2.37 Modified power and cooling cycle configuration 2 [129]

A new parameter, called effective COP, was introduced by Goswami and co-workers [123, 130] to evaluate and optimise the gain in the cooling. This COP definition relates the cooling produced with this cycle and the theoretical amount of work production which was compromised in order to have combined cooling production:

$$\mathrm{COP}_{\mathrm{effective}} = \frac{\text{Cooling Produced}}{\text{Potential Work Lost}} \tag{2.2}$$

The rectifier conditions were optimised by using the effective COP value. Values of COP were achieved close to 5, when the parameter was used to optimise the gain in cooling. But this parameter was at the level 1.1 when combined operation was considered. The simulator in ASPEN was used to optimise the cycle to reduce the expenses of the work production

when the cycle was optimised for the cooling production [130]. The theoretical results were compared with experimental data and showed good agreement.

The Goswami cycle was also studied experimentally to prove the feasibility of the cycle and to validate the theoretical results [131, 132]. The authors included in these studies some realistic irreversibilities to improve agreement between theoretical and experimental results. A number of organic working fluids were proposed to substitute the ammonia-water mixture used in other studies [133]. The benefits and drawbacks of those organic fluids were discussed with comparison to the ammonia-water mixture. It was concluded that the efficiencies achieved by using organic mixture were lower than that shown with the ammonia-water mixture. Optimisation of operational conditions in terms of the boiler pressure, isentropic turbine efficiency for a range of ammonia concentration in the basic solution was carried out by Demirkaya et al. [134]. It was shown that the cycle can be optimized for the net work, cooling output, effective first law and exergy efficiencies. The effect of rectification of the cooling source on the cycle output was investigated, and it was found that an internal rectification of the cooling source always produced the higher efficiencies. Furthermore, they found that the superheating process of the ammonia vapour after the rectification process led to an increase in the cycle efficiency and to a decrease in the cooling output.

2.3.2 Stirling refrigeration cycle

Stirling engine can be driven by any thermal energy source including waste heat, rice husk combustion or solar energy. Basically, the Stirling refrigeration cycle produces the cooling effect based on volume changes caused by piston displacements which result in the gas pressure and temperature variations over the cycle. The working gas during the cycle does

not experience any phase changes [135]. Such the system is suggested to be used for certain applications in which heat sources are of a low-temperature range. By applying the condition of the ideal regeneration, the thermal efficiency of this refrigeration cycle is equal to the thermal efficiency of the Carnot cycle. Moreover, compared with all reciprocating piston heat engines working at the same conditions, the ideal Stirling engine has the maximum possible thermodynamic efficiency [136].

Chen et al. [137] modelled a solar-driven Stirling engine as a combined system. The system consists of a solar collector integrated with a Stirling engine, as shown in Figure 2.38. The authors investigated the performance of the system with the irreversibilities of heat conduction and regenerative losses.

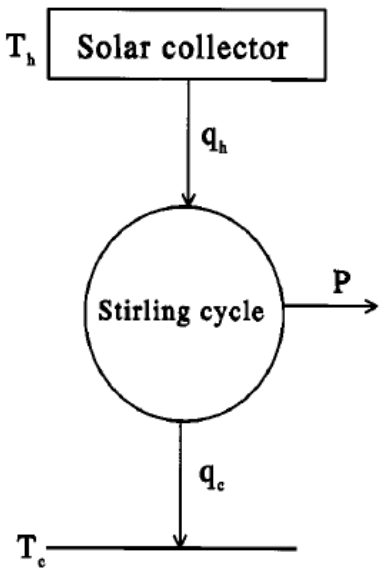

Figure 2.38 A solar-driven Stirling engine system [137]

Le'an et al [138] presented a theoretical and experimental study on the V-type integral Stirling refrigerator (VISR). The VISR consists of an expansion cylinder, a compression cylinder and a heat exchanger in-between as shown in Figure 2.39. Both the expansion and

compression cylinder pistons are driven by a crankshaft and the machine is a V-shaped. The authors concluded that the cooling capacity increased with the charged pressure of the working gas: up to 1.0 MPa for nitrogen and up to 1.3 MPa for helium.

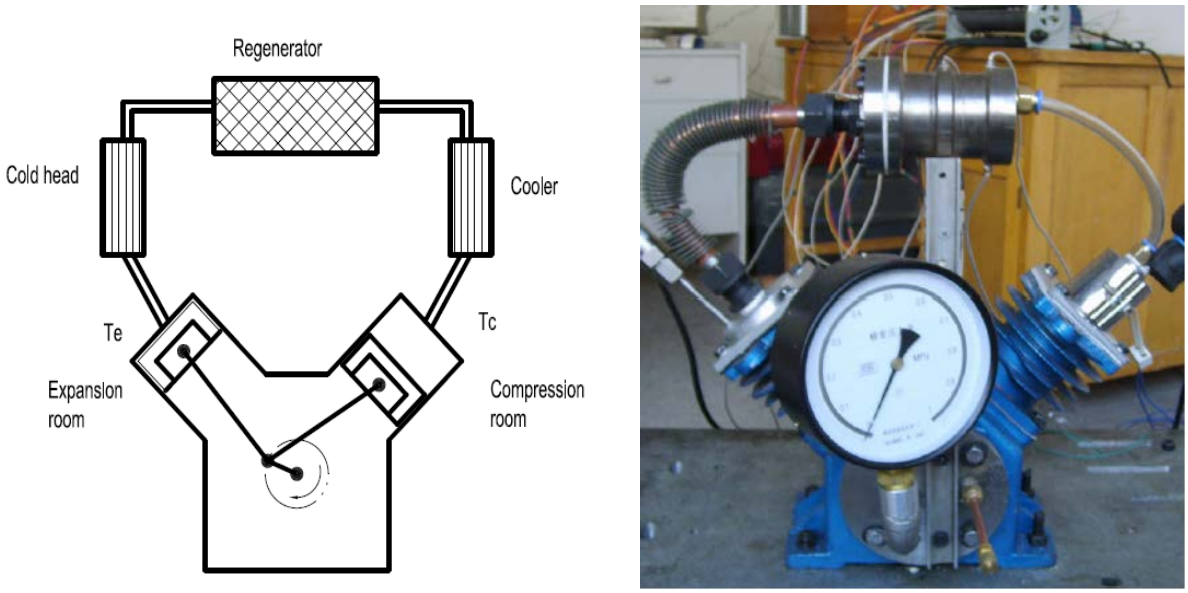

Figure 2.39 Schematic and prototype of the V-type integral Stirling refrigerator [138]

The main advantages of the solar-powered Stirling engine or cooling machine are firstly their high efficiency at low capacity and secondly its ability to generate both power and cold. On the other hand, the Stirling engines are quite complex and need a high-quality heat at temperatures between 600 and 700°C, therefore, the solar thermal energy should be of a very high grade. Lastly, this technology is practically restricted in terms of capacity since its efficiency is a decreasing function of the capacity [12].

2.3.3 Solar ejector refrigeration

The ejector refrigeration technology is generally driven by a low-grade thermal energy, including solar one. In this technology a set, made of a generator, ejector and pump, is used to replace the compressor in the vapour compression cycle [139]. The solar ejector

refrigeration technology could be classified into three main categories including single and multi-stage and hybrid systems in which the ejector technology is combined with other cooling technologies.

2.3.3.1 Single stage ejector refrigeration systems

The single-stage ejector systems are the simplest form of this technology and are widely used around the world. Figure 2.40 shows a single stage solar ejector cooling system which consists of three circulating loops, including solar loop, power loop and refrigeration loop. The solar loop comprises a solar collector, generator heat exchanger, heat storage tank and pump. The solar loop delivers thermal energy to the generator. In the power loop, the working fluid absorbs the heat offered in the solar loop in order to produce a vapour of high temperature and pressure (point 1).The high-pressure vapour, primary fluid, passes through the ejector in which it accelerates as moves through the nozzle part of the ejector, see Figure 2.41. Flow pressure reduces as its velocity rises. The primary fluid pressure, at the nozzle exit, becomes less than the flow pressure inside the evaporator. At this point, as a result of the pressures differences, the low (point 6) is sucked into a mixture of the flow and the primary flow. The fluid mixture emerges from the mixing chamber, and as it enters the diffuser its velocity drops and pressure increases. The pressure of the emerging flow (point 2) is slightly above the condenser pressure. In the refrigeration loop, the fluid inside the condenser becomes liquid by rejecting heat to the surroundings (point 3). A part of the liquid (point 7) is pumped to the generator in order to complete the power loop. While the rest of the liquid (point 4) is expanded by passing through a throttling valve (point 5) and enters the evaporator as a mixture of vapour and liquid. In the evaporator, the heat is transferred from

the cooling space to the refrigerant which is converted to vapour (point 6), and enters the ejector to complete the refrigeration cycle [140].

Although the performance of ejector cooling systems is less than 0.3 and lower in comparison with other heat-driven cooling systems, the simplicity of their construction, the absence of moving parts (which reduces the need for the maintenance) and their low operating and installation costs make them an attractive alternative. Their major disadvantages are the difficulty to run them over a wide range of the ambient temperature values and the complicated design of the ejector [141].

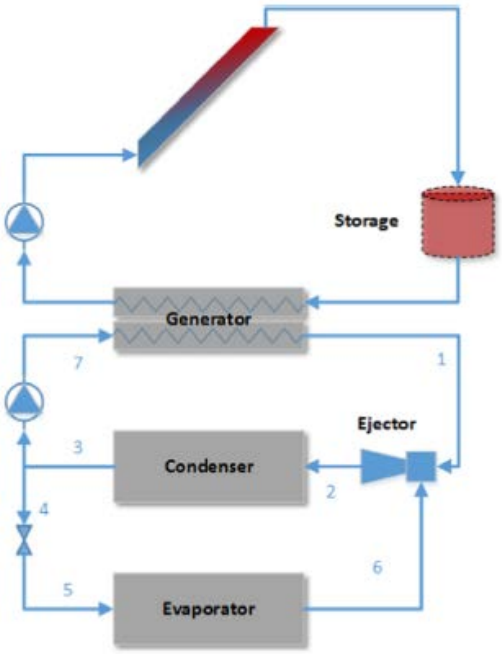

Figure 2.40 Schematic diagram of a solar ejector cooling system [140]

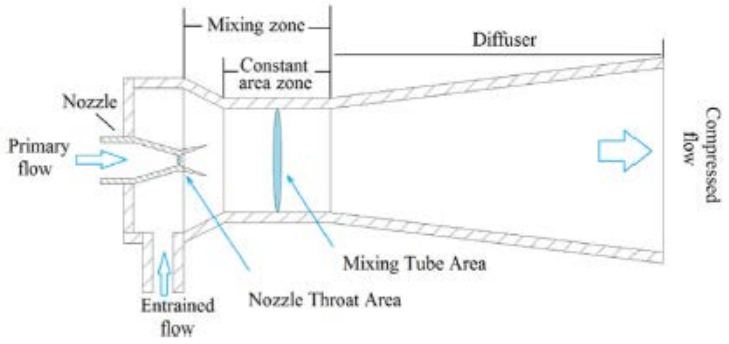

Figure 2.41 Schematic diagram of an ejector [140]

2.3.3.2 Multi-stage ejector refrigeration systems

Due to the variation of operation conditions, it is difficult to keep the single-stage ejector systems running at the optimum regime because the ejector, which is the main part of the ejector cooling cycle, is a static device. The cycle performs well for the designed regime but it is unable to deal with changes in operating conditions. For instance, an increase in the ambient temperatures above design conditions may lead to operation difficulties [142]. To give the refrigeration cycle more flexibility to work with a high COP at different operational conditions, Sokolov and Hershgal [143] recommended using a parallel array of ejectors positioned between a common inlet and a condenser, as shown in Figure 2.42. A number of ejectors with different dimensions are placed in parallel; the condenser pressure determines the selection of the ejector that will operate.

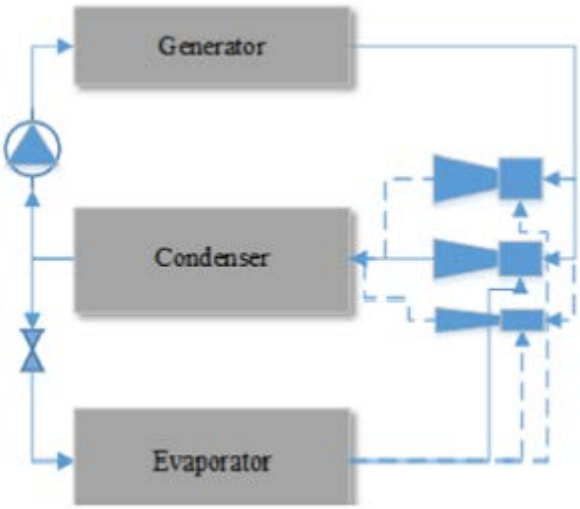

Figure 2.42 Schematic diagram of multi-stage ejector cooling system [140]

The overall entrainment ratio is illustrated in Figure 2.43. In this Figure, the ejector 1 works when the condenser pressure is higher than Pc1; the ejector 2 works at the condenser pressure in the range between Pc1 and Pc2; and the ejector 3 works at the condenser pressure higher than Pc2 and less than Pc3 [142].

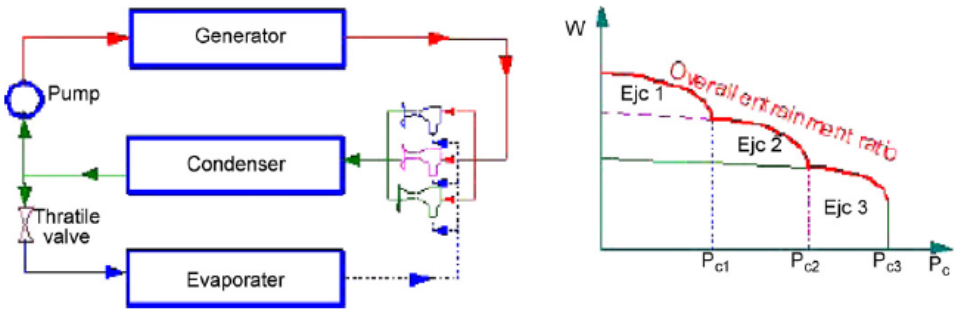

Figure 2.43 Performance of the multi-stage ejector refrigeration system [142]

2.3.3.3 Working fluid for the ejector refrigeration systems

The old fashion solar ejector cooling systems used CFC and HFCF refrigerants [144, 145], but in the recent years these were tested with more environmentally friendly refrigerants such

as hydrocarbon [146] or hydrofluoroether [147]. The characteristics of a working fluid affect the coefficient of performance, environmental impact, operating conditions and economic viability of the solar cooling system. The main characteristics which should be considered for choosing working fluids are [148-150]:

a) Thermodynamic and physical properties:

Working fluids with the high latent heat of vaporisation are preferred which reduce the size of the facility, the refrigerant flow rate per unit of the cooling capacity and consequently the pump consumption. In addition, refrigerants with a low viscosity and high thermal conductivity are preferred. Furthermore, working fluids with a large value of molecular weight require more compact ejectors and provide higher ejector efficiency and entrainment ratio.

b) Environmental aspects:

As to the environmental characteristics, the leading concerns include the ozone depletion potential (ODP), the atmospheric lifetime (ALT) and global warming potential (GWP).

c) Stability and compatibility with materials:

The working fluids should be chemically stable at the operation conditions especially at the high-temperature range, also should be non-reactive or corrosive to the materials in contact.

d) Safety considerations:

In general, they should be non-flammable, non-explosive, non-toxic and non-corrosive.

e) Economic viability:

The low-cost working fluids are the more favourable to be used in these systems.

2.3.3.4 Solar collectors for the ejector refrigeration systems

Many types of solar collectors have been proposed to deliver generation heat to the ejector refrigeration systems such as flat plate [143], evacuated tube [151] and parabolic trough [152]. Nehdi et al. [151] showed that for a solar ejector refrigeration systems with R717 as the working fluid, using evacuated solar collectors produced the higher cooling efficiency compared to both single glazed and double glazed flat plate collectors. Nevertheless, some other studies concluded that the use of high-temperature solar collectors it is not necessary in all cases. Pridasawas and Lundqvist [153] conducted an exergy analysis study of a solar driven ejector refrigeration cycle with the working fluid R600. The study showed that the highest exergy losses in the system occurred in the solar collectors and the ejector. In addition, it was found that there was no need to employ very high temperature solar collectors. In the case of solar insolation of 700 W/m^2, the generation temperature ranges between 80 and 100^{o}C was sufficient for operation of the system. Huang et al. [154] developed a high-performance ejector refrigeration system using R141b, as shown in Figure 2.44. They experimentally obtained a COP of 0.5 at a the generating temperature of 90^{o}C, and an evaporating temperature of 8^{o}C.

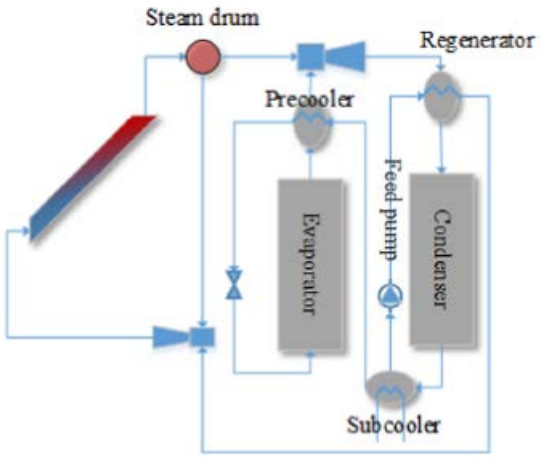

Figure 2.44 A solar ejector cooling system as proposed by Huang et al. [154]

To select the most suitable solar collector three different collector types were investigated by Huang et al. [155] including a conventional single glazed flat plate solar collector, a high efficiency single glazed flat plate with a selective surface and an evacuated tube collector. The study revealed that the optimum choice was the single glazed collector with a selective surface.

2.4 Passive solar cooling systems

One of the biggest consumers of the produced energy around the world is the building sector. In 2010, the fraction of energy consumption in this sector was 39.9% of the gross final energy consumption in the European Union (EU-27) [35]. Chan et al. [156] concluded that about 35.3% of the overall energy demand was consumed by the building sector. The main proportion was consumed for the heating or cooling of buildings.

2.4.1 Evaporative cooling

In this type of cooling, a stream of air is passed over the surface of water so that water absorbs heat from the air and turns into steam. In contrast, the air loses heat and becomes colder. According to Amer [157], the cooling effect of the evaporative cooling is very good if compared with the solar chimney cooling system. Chan et al. [156] described two types of evaporative cooling, Direct Evaporative Cooling (DEC) and Indirect Evaporative Cooling (IEC), as shown in Figure 2.45.

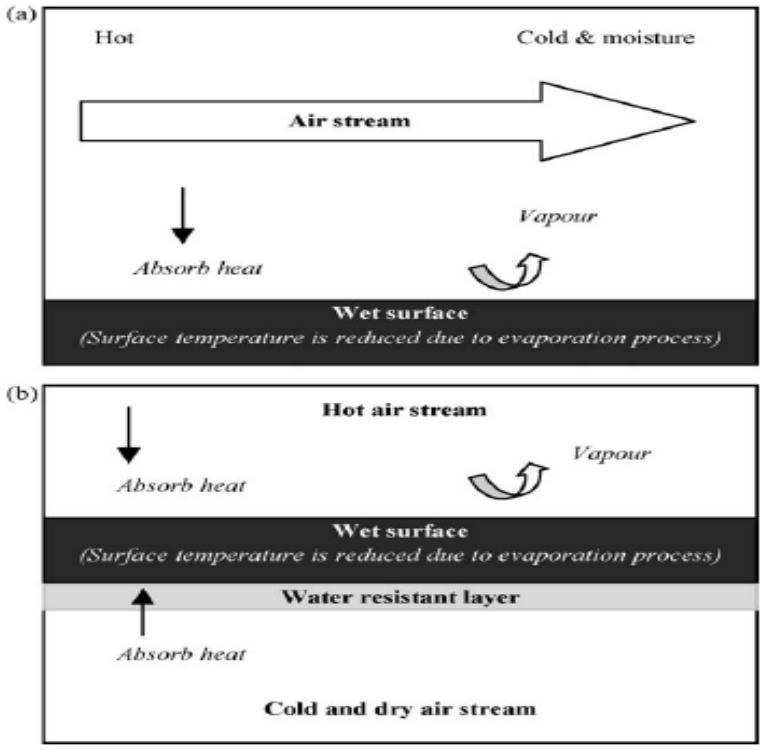

Figure 2.45 Evaporative process for (a) direct evaporative cooling and (b) indirect evaporative cooling [156]

The main principle in those two types is to transfer heat (sensible heat) from the air stream to the water leading to evaporation of some of it.

In DEC the evaporated water mixes with air which makes the treated air is more humid. This may reduce the efficiency of the cooling system and produce discomfort, especially in the humid regions around the world. That is why in such cooling systems, it is needed to install a dehumidifier by passing the air through a desiccant [58, 158]. While in IEC there is no direct contact between the air and water.

2.4.2 Porous roof layer

In this type of solar cooling systems, a porous layer is used to collect water during the rainfall. This water may be used for evaporation process when there is a strong irradiation. Because of the release of the latent heat, the temperature of the porous layer remains lower than that of ambient. During the nighttime or cloudy days when the humidity is rising up, the porous material absorbs water vapour from the surrounding, see Figure 2.46.

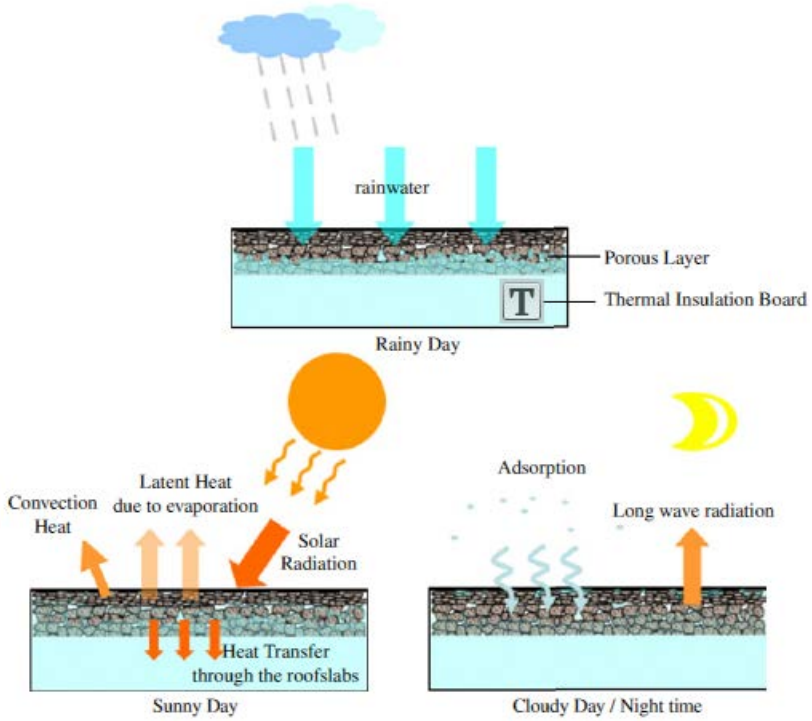

Figure 2.46 Mechanism of porous roof layer [159]

The performance of selected types of porous material was investigated experimentally by Wanphen and Nagano [159]. Because of its higher vapour absorption from the surrounding air, they found that siliceous shale had the best cooling performance among other studied materials which were silica sand, pebbles, volcanic ash and siliceous shale. In general, there are many other techniques are used to maintain cooling in buildings such as coating with reflective materials [160, 161] or using solar chimney [162, 163]. In addition to the above, Raman et al. [164] developed an integrated arrangement which consisted of both solar air heater and an evaporating cooling system.

2.5 Liquid piston engines

The liquid piston engine (Fluidyne) is a free-piston Stirling engine with liquid columns acting as pistons. Such the engine can be built using sections of pipes. Since the pistons are liquid then no additional sealing rings and high precision manufacturing is required. The liquid piston engines function at pressures close the atmospheric one, and have a low frequency which is typically between 1/2 and 1 Hz [165]. Consequently, the power density is low, and large machines are required if a significant power output is needed. Liquid piston engines usually used to pump water, particularly for drainage pumping or irrigation in developing countries, or for the generation of the electric power, if other means are not readily available. As any other Stirling machine, the liquid piston engine can be used as a heat pump or refrigerator and several studies proposed exploiting such the option [165]. Since the liquid piston eliminates gas leakage and need for a sliding seal mechanical loses are not significant [166].

Mahkamov and Belgasim [9, 167, 168] studied the laboratory solar water pumping and dynamic water desalination system based on the liquid piston engine, built by Mahkamov.

The liquid engine was made of two concentric acrylic cylinders with aluminium flanges on their top and bottom. These two cylinders were connected at the bottom and filled with a water to work as a liquid piston, as shown in Figure 2.47. Periodical oscillations of the fluid piston change the volume and pressure in the plant. For the duration of approximately half of the periodic cycle the pressure in the plant drops below the atmospheric level causing flash boiling of saline water in the manifold of the solar collector. Generated vapour is turned into fresh water in the condenser which surrounds the cooling jacket with saline water. The flash boiling effect improves the fresh water production capacity of the plant. Additionally, the fluid piston converter drives a pump which provides lifting of saline water from a well and pumps this through the cooling jacket of the condenser to a saline water storage tank.

Figure 2.47 The liquid piston engine [9]

A theoretical study on a liquid piston concept was proposed to improve the efficiency of gas compression and expansion by Van de Ven and Li [166]. The liquid was used as a medium to carry heat into and out of the compression chamber. The authors found that the use of liquid piston decreased the energy losses by 19%. The liquid piston and the reciprocating piston machines exhibited the overall efficiency of 83% and 70% respectively. The liquid

piston engine demonstrated significant improvements in the total compression efficiency in comparison to a conventional reciprocating piston engine.

2.6 Conclusions based on literature review

The cooling systems driven by solar energy are an attractive option because the cooling effect is provided in regions where the solar energy is abundant. The vast majority of solar cooling techniques use environmentally harmless working fluids. Using such systems is an innovative, promising way to alleviate the rise in the energy consumption caused by the excessive use of conventional vapour compression systems, particularly in the summer time.

In this Chapter an extensive review of existing technologies was performed and their operational principle, design and components, advantages and drawbacks were described. The literature review conducted shows that a number of solar cooling technologies have a great potential because of their environmental advantages and energy savings. Generally, studies performed on solar thermal cooling systems demonstrate sufficient potential exists to meet cooling loads in a number of regions around the world. For instance, many such systems employed in different climatic areas of Europe demonstrated significant energy savings between 29 and 55% for adsorption cycles and between 25 to 52 % for absorption systems. It was shown that absorption cycles were more efficient than adsorption cycles but the latter need lower heat source temperatures ranging from 60 to 90^{o}C. In addition, in the adsorption systems, there are no moving parts and consequently they have lower maintenance costs. In desiccant cooling systems their main features are the good humidity control and the possibility to be readily integrated with heating and ventilation systems. Thermo-mechanical technologies, especially Rankine and Stirling cycle based ones, have

high capital and maintenance costs and therefore, these are not appropriate for low cooling capacity applications.

The operating costs are low for ejector cooling systems and these can operate at low heat source temperatures but their performance substantially dependence on the ambient temperature.

The coefficient of performance for the solar thermal cooling technologies in general needs to be enhanced in order to compete with the conventional vapour compression cycles. This enhancement can be achieved by further R & D activities and design optimisation.

In this PhD research, the task is to experimentally and numerically investigate the performance of a novel solar cooling system with a fluid piston converter. The main aim of this research is to develop an accurate mathematical model of this novel system, perform tests on the laboratory prototype to acquire experimental data on its performance and validate the mathematical model. The developed and validated mathematical model then can be used for the determination of the rational design parameters of the novel solar cooling system.

2.7 Summary

In this Chapter, the review was focused on existing solar thermal cooling technologies. The operational principles of a number of systems, their design and components, advantages and shortcomings together recent advances made in research on solar cooling technologies were described. Table 2.3 summarises the main features of the different systems considered in this Chapter.

Table 2.3 Specific features of different solar cooling systems

No.	Solar Cooling System	Specific features of the system
1	Solar absorption cooling systems	• It is possible to produce a cooling effect for applications in the range between -60 and 5 ˚C [13]. • Can be classified as single, half and double effect systems [13]. • Single effect absorption systems need a minimum temperature of heat source at 100 °C and have coefficient of performance (COP) of 0.75 [22, 30]. • Half effect absorption systems need a heat source at temperature between 55 and 75 °C and have COP of 0.36 [23-25]. • Double effect systems require a relatively high generation temperature, namely higher than 130 ˚C [27] with a COP of 1.4 [30]. • Very high heat source temperature (above 200 ˚C) leads to intense corrosion [48].
2	Solar adsorption cooling systems	• Adsorption systems have a wide range of the heat source temperature varying between 50 and 500 ˚C without and work without corrosion problems [48]. • Suitable for operation in strong vibration conditions such as present in fishing boats or locomotives [54]. • The adsorption cooling systems need to maintain in the design high vacuum, have large volumes and weight compared to traditional refrigeration systems [55]. • The COP is low for the adsorption systems (0.4) compared to absorption systems for the same operational conditions [55].
3	Solar desiccant cooling systems	• It is possible to control the humidity of the cooling space which is needed in hospitals to decrease the risk of infection [89]. • CO2 emission reduction of 13% compared to the vapour compression air conditioning [88]. • Electricity saving is up to 24% in hot and humid climatic conditions [93] • The coefficient of performance is about 0.75 [8].
4	Goswami cycle	• Generates power output and cooling effect [120]. • Regeneration temperature is 130 ˚C with an efficiency of 23.5% [124]
5	Stirling cycle	• Stirling engine has high efficiency at low capacity [135]. • Stirling cycles are able to generate both power and cold [136]. • The main drawback is quite complex design [12]. • It needs high-quality heat at temperatures between 600 and 700 ˚C [12].
6	Solar ejector refrigeration	• The construction of the solar ejector refrigeration system is simple [140]. • No moving parts in these systems which reduces the need for

		the maintenance [140]. • The operation and installation costs of these systems are low compared to other solar cooling types [141]. • The COP of these systems is very low at about 0.3 [141].

Chapter 3 Mathematical Modelling of the Cooling Part of the System

This Chapter describes the physical model of a dynamic solar cooling unit with a liquid piston converter and its thermodynamic mathematical model. This mathematical model is used for numerical simulations of the operation of the unit and theoretical results, describing the working process of the unit, are presented and discussed.

3.1 Physical Model

Figure 3.1 shows the general schematic diagram of the dynamic solar cooling system analysed in this study. The solar cooling system utilises the solar energy collected by the solar collector. This energy is used to drive a fluid piston heat engine. The engines output work is used to drive a reverse heat machine to produce the needed cooling effect.

The physical model of the cooling part consists of three main components namely, the cylinder with the liquid piston, cooler and cooling space. The liquid piston engine, which is driven by the heat generated in the solar collector, works as an actuator to generate fluctuations of pressure inside the closed system. The temperature in every compartment will change as a function of this oscillation in the pressure. When the temperature is high, heat is rejected in the cooler by using the counter flow concentric pipe heat exchanger. The cooling fluid is water with temperature of 20˚C. In the last compartment, namely cooling space, the temperature is lowest in the system to produce the cooling effect.

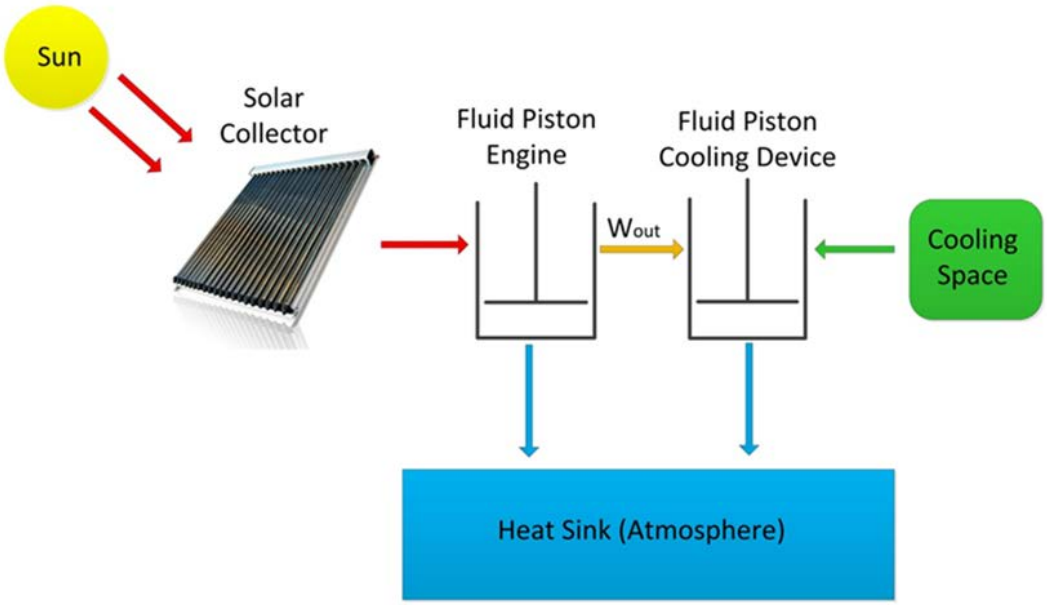

Figure 3.1 General schematic diagram of the dynamic solar cooling system

3.2 Mathematical Model

In order to derive the mathematical model of the operation, the proposed scheme is divided into three separate control volumes, namely: the liquid piston cooling device, cooler and cooling space, see Figure 3.2.

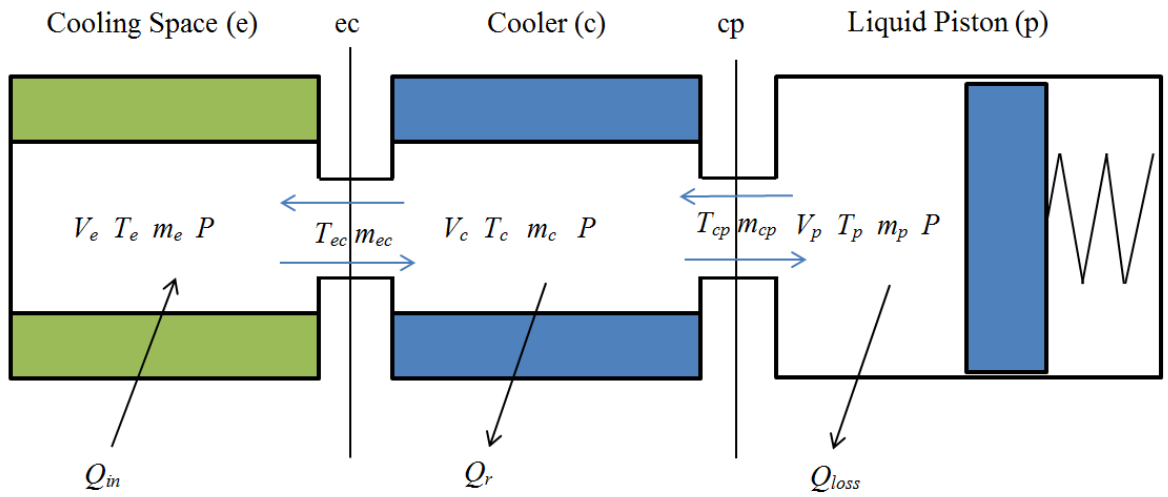

Figure 3.2 Schematic diagram of dynamic solar desalination unit

In this diagram, indexes p, c and e indicate the above three control volumes, respectively, and indexes cp and ec are used to denote two interfaces between the corresponding control volumes. The working fluid in all the system is air only, which is considered as an ideal gas. The liquid piston cooling device is presented as a mass-spring oscillating system with a rigid piston and a dumper. Using such the calculation scheme, the lumped parameter mathematical model of the system can be presented as a system of energy and the mass conservation equations written for each control volume in the form of ordinary differential equations. By solving these equations, information on the cyclic variations of the pressure inside the system and the temperatures in each control volumes can be calculated. During calculations, the value of temperatures T_{ec} and T_{cp} depend on the direction of the flow across control surfaces ec and cp and equal to the temperature in the corresponding adjacent upstream control volume. The temperature in the cylinder of the liquid piston cooling device T_p varies as a result of expansion and compression of this control volume and the flow of air passing

through the cylinder's control surface. The general form of the energy conservation equation for unsteady flow closed control volume could be written as [169]:

$$\dot{Q} + (C_p \dot{m} T)_{in} - (C_p \dot{m} T)_{out} = P\frac{dV}{dt} + C_v \frac{d}{dt}(mT) \tag{3.1}$$

where Cp and Cv are the specific heat capacities at the constant pressure and constant volume, respectively, T is the temperature, P is pressure, V is the volume, M is the mass of air, $\dot{m}$ is the mass flow rate into or out the control volume. The specific heats C_p, C_v can be calculated by using the universal gas constant R and isentropic index γ [5]:

$$\left.\begin{aligned} C_p &= \frac{R\gamma}{\gamma - 1} \\ C_v &= \frac{R}{\gamma - 1} \end{aligned}\right\} \tag{3.2}$$

As mentioned above that the air in the system is assumed to be an ideal gas and the equation of the state can be used for the gas in each control volume as follows:

$$PV = mRT \tag{3.3}$$

3.2.1 The control volume of air in the cylinder of the liquid piston cooling device

By applying the energy equation (3.1) for the liquid piston cooling device by taking into account the heat loss from or into this control volume, the following equation can be written:

$$\frac{V_p}{\gamma - 1}\frac{dp}{dt} = \dot{m}_{cp} c_p T_{cp} - \frac{\gamma}{\gamma - 1} p \frac{dV_p}{dt} + \dot{Q}_{losses} \tag{3.4}$$

where T_{cp} is the temperature at the control surface between the liquid piston cylinder and the cooler. This temperature can be defined as:

$$T_{cp} = \begin{cases} T_c\,, & \dot{m}_{cp} > 0 \\ T_p, & \dot{m}_{cp} < 0 \end{cases} \tag{3.5}$$

The input value in calculations is the displacement of the piston, which is denoted as X and can be expressed as:

$$X = Am\ cos(\omega t + Ph) + X_0 \tag{3.6}$$

$$\omega = 2\pi f \tag{3.7}$$

where ω is the angular velocity, f is the frequency, Ph is the phase angle in the displacement of the piston (which generally can be assumed to be $\frac{\pi}{2}$) , Am is the water level amplitude and finally X_0 is the initial value of the piston position.

The volume of the air in the cylinder of the liquid piston can be calculated as

$$V_p = X * A_1 \tag{3.8}$$

where A_1 is the liquid piston cylinder's cross-sectional area.

3.2.2 The control volume of cooler

The cooler is similar to double pipe heat exchanger which is used to cool air in the inner pipe by means of circulation of the cooling water at 20 ˚C in the outer pipe. The energy equation for the air in the cooler may be defined as:

$$\frac{V_c}{\gamma - 1}\frac{dp}{dt} = -\dot{m}_{cp}c_pT_{cp} + \dot{m}_{ec}c_pT_{ec} - Q_r \tag{3.9}$$

where ec denotes the control surface between the cooler and cooling space, Q_r is the heat rejected in the cooler. The heat rejected from air to the water jacket in the cooler can be calculated by using effectiveness-NTU (Number of Transfer Units) method described in [170]:

$$\dot{Q}_r = \varepsilon\dot{m}_{cp}C_p\left(T_{ci} - T_{cp}\right) \tag{3.10}$$

where T_{ci} is the temperature of inlet cooling water and ε is the cooler effectiveness can be calculated for the counter flow heat exchangers as [170]:

$$\varepsilon = \frac{1 - exp[-NTU(1-C)]}{1 - C * exp[-NTU(1-C)]} \tag{3.11}$$

In equation (3.11) the values of C and NTU are defined as follows:

$$C = \dot{m}_{cp} Cp_{air} / \dot{m}_{cl} Cp_{water} \tag{3.12}$$

$$NTU = \frac{UA_c}{\dot{m}_{cp} Cp_{air}} \tag{3.13}$$

In the above equation, U is the overall heat transfer coefficient and its value is taken to be constant at 230 W/m^2 K [9].

3.2.3 The control volume of cooling space

The last chamber in the system is the cooling space in which the heat is transferred between the system and the surrounding. The energy equation for the cooling space is:

$$\frac{V_e}{\gamma - 1}\frac{dp}{dt} = -\dot{m}_{ec} c_p T_{ec} + Q_{in} \tag{3.14}$$

To obtain the pressure variation in the system, the equations (3.4), (3.9) and (3.14) are added to produce the following equation:

$$\frac{V_t}{\gamma - 1}\frac{dp}{dt} = -\dot{Q}_r - \frac{\gamma}{\gamma - 1} p \frac{dV_p}{dt} + \dot{Q}_{loss} + Q_{in} \tag{3.15}$$

Here V_t is the total air volume in all three compartments:

$$V_t = V_p + V_c + V_e \tag{3.16}$$

By applying the equation of state for ideal gas, the temperatures of air in the cylinder of the liquid piston, cooler and cooling space can be expressed as

$$T_p = \frac{PV_p}{R\ m_p} \tag{3.17}$$

$$T_c = \frac{PV_c}{Rm_c} \tag{3.18}$$

$$T_e = \frac{PV_e}{Rm_e} \tag{3.19}$$

Regarding the masses of air in the system, the total mass in the whole system is constant because the system is closed and it is calculated as follows [171]:

$$m_t = m_p + m_c + m_e \tag{3.20}$$

The derivative of equation (3.20) gives the relation between masses passes through the control surfaces;

$$\frac{dm_p}{dt} + \frac{dm_c}{dt} + \frac{dm_e}{dt} = 0 \tag{3.21}$$

Physically, in equation (3.21), the terms $\frac{dm_p}{dt}$, $\frac{dm_c}{dt}$ and $\frac{dm_e}{dt}$ represent the change in the masses of air in the cylinder, cooler and cooling space, respectively. These terms in equation (3.21) can be written as:

$$\left.\begin{aligned} \frac{dm_p}{dt} &= \dot{m}_{cp} \\ \frac{dm_e}{dt} &= -\dot{m}_{ec} \end{aligned}\right\} \tag{3.22}$$

Also, for the air mass in the cooler

$$m_c = m_c^i + \frac{dm_c}{dt} * dt \tag{3.23}$$

where m_c^i is the initial value of air mass in the cooler which is calculated from the previous time step and dt represents the time step in calculations.

3.3 Matlab/Simulink Model

The equations of the above mathematical model of the dynamic solar cooling system were solved by using Simulink which works in the Matlab environment. The Simulink model was

built as a closed loop as shown in Figure 3.3. The model consists of four main sub-system blocks. The first block simulates the liquid piston cooling device; in this block the input signal is the piston's displacement (X) which is used to generate the volume of the air in the cylinder, so the system pressure can be calculated. Thereafter, the mass and temperature of air in the cylinder can be calculated, see Figure 3.4.

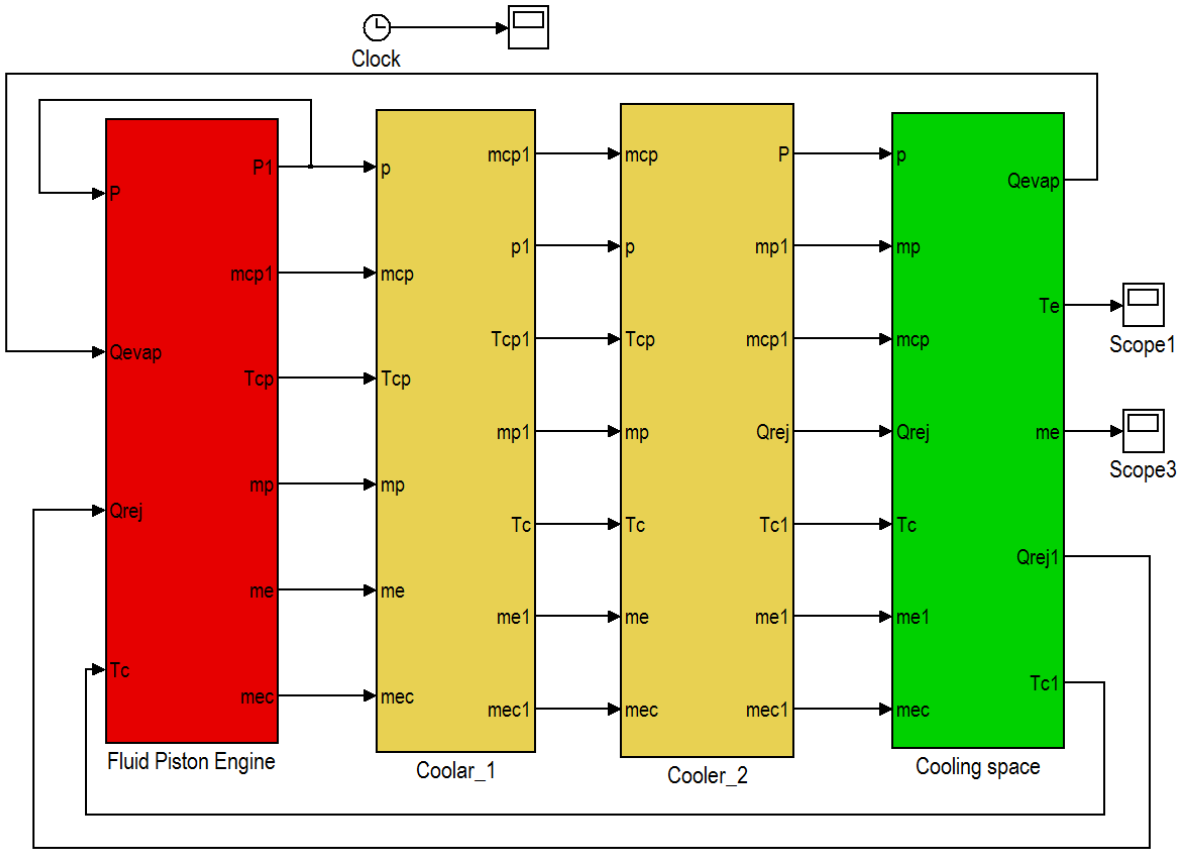

Figure 3.3 The Simulink model of the dynamic solar cooling system

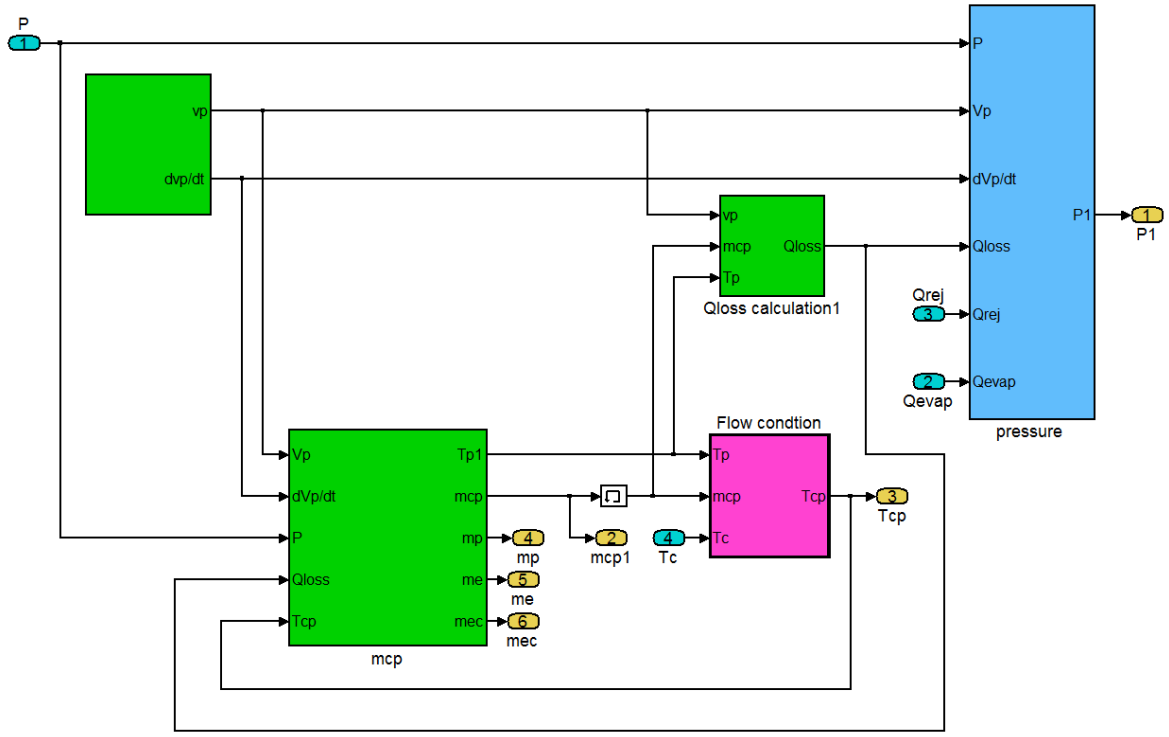

Figure 3.4 The Simulink model of the liquid piston cooling device

The Figures 3.5 shows the second main block which is used for the first part of the cooler's calculations. In this block, the mass and temperature of the air in the cooler are calculated.

Figure 3.6 shows the simulation block used for the part of the cooler calculations in which the heat rejected from the air to the coolant (water) is defined by using the NTU method.

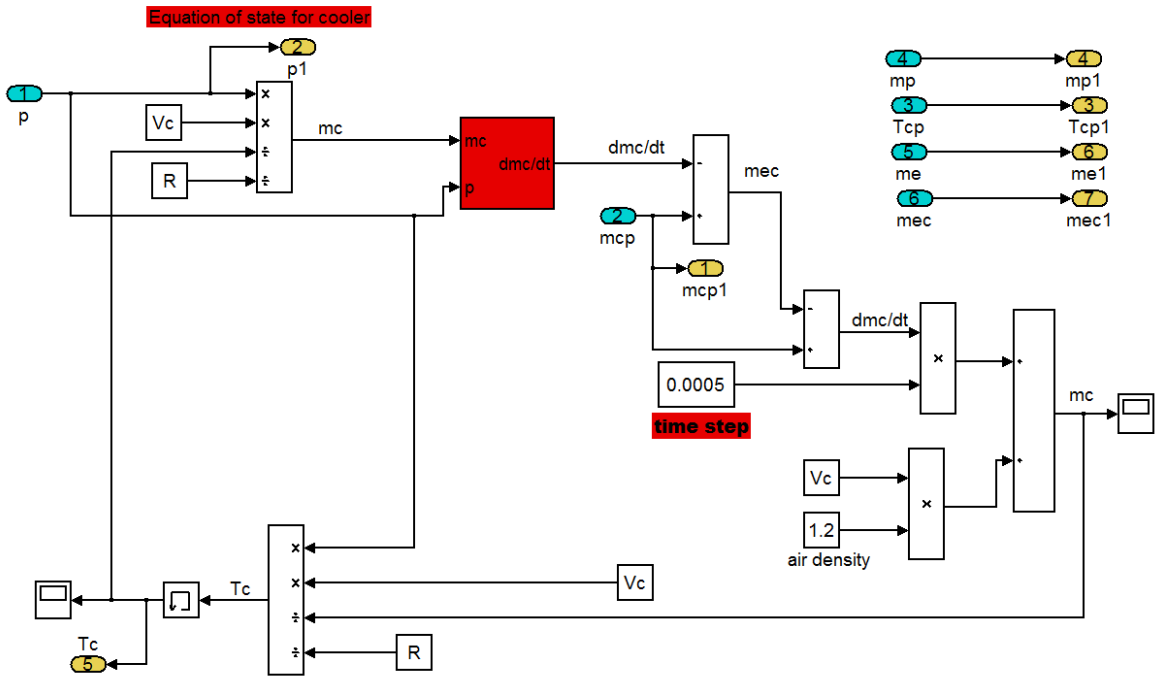

Figure 3.5 The first block of the Simulink model of the cooler

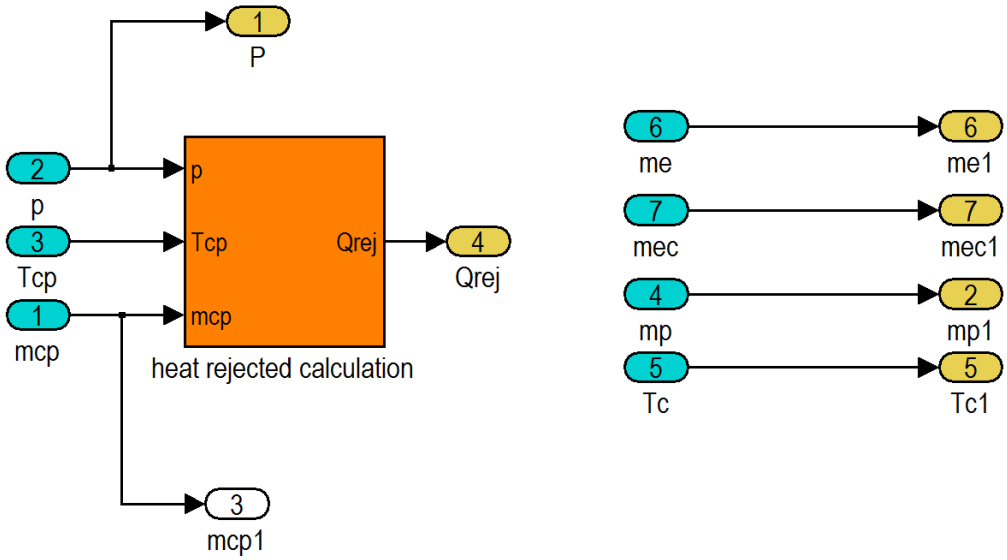

Figure 3.6 The first block of the Simulink model of the cooler

The fourth main block simulates the cooling space and used to determine in which the mass and temperature of the air in the cooling space, see Figure 3.7.

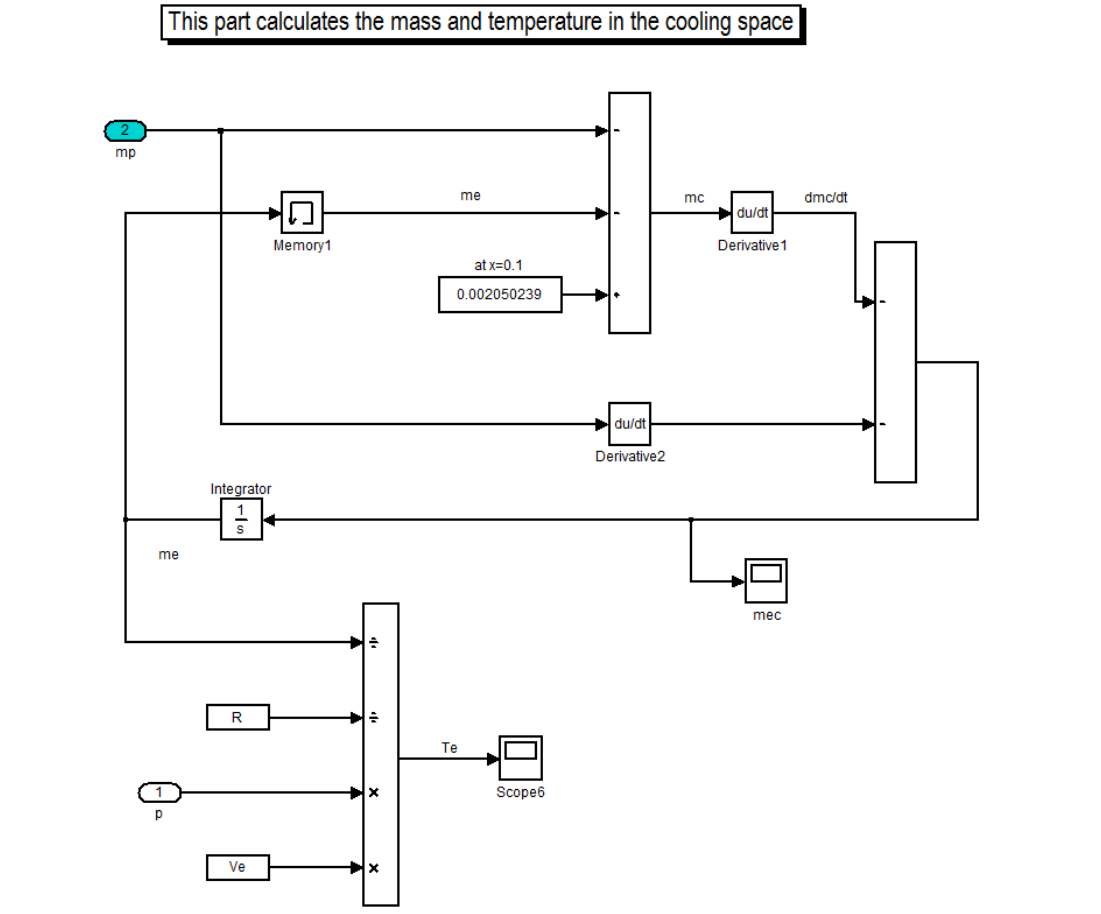

Figure 3.7 Simulink model of the cooling space

3.4 Discussion of numerical results

The theoretical simulations of the proposed solar dynamic cooling system were carried out by using the above described Simulink system. In the simulations, the displacement in the water level was assumed to be an input data to evaluate the rest of variables such as air pressure, temperatures and masses. The physical dimensions of the piston cylinder, cooler and cooling space were the same as of the prototype on the test rig in the laboratory.

3.4.1 The water level in the fluid piston engine

The displacement of the water level in the liquid piston cooling device as a function of the angle degree for one operating cycle is illustrated in Figure 3.8. The horizontal coordinate units in Figures 3.8 to 3.16 are shown degrees, in analogy with conventional engines with a shaft, completing the full rotation (one cycle) in 360 degrees. It can be seen that the position of the piston from the top of cylinder fluctuates between 0.15 and 0.05 m where 0.05 m is the initial position of the piston from the top of the cylinder. The stroke of the piston is 0.1 m.

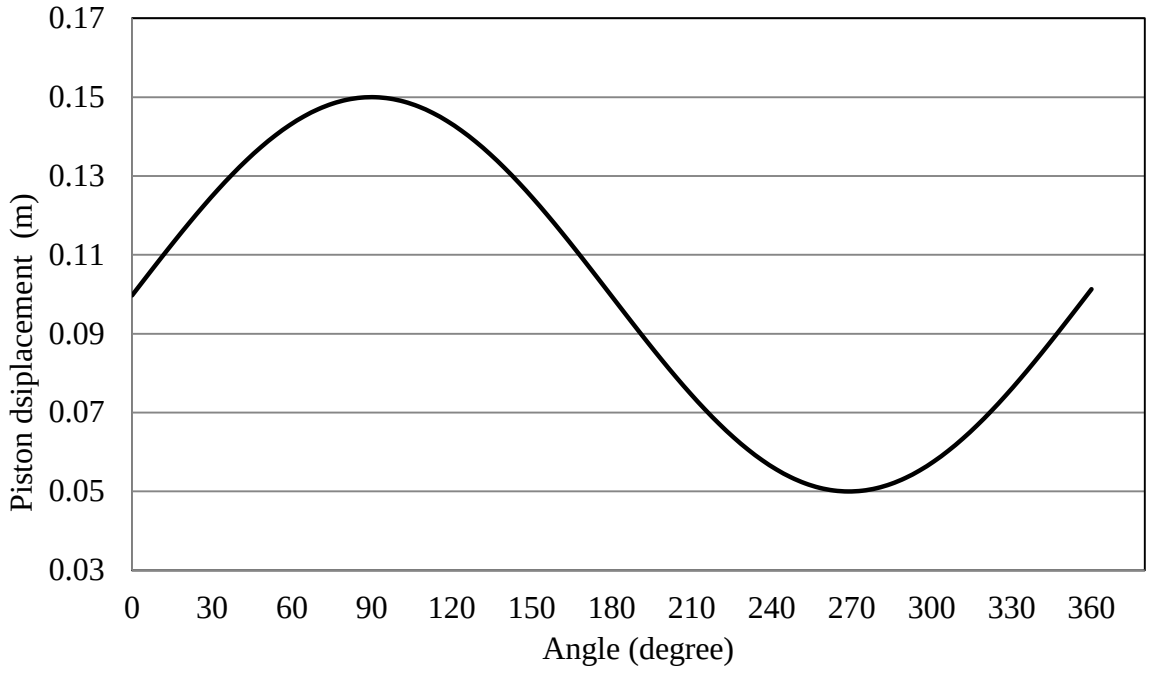

Figure 3.8 Amplitude of oscillations of the water level in liquid piston cooling device

3.4.2 Volume and mass of the air in the cylinder of the piston

As a result of the change in the water level in the liquid piston cooling device its volume can be calculated, see Figure 3.9. The volume of the cylinder changes between $8.5x10^{-4}$ m^3. And 2.84 $x10^{-4}$ m^3. The amount of the air mass in the cylinder follows the same trend as

demonstrated in Figure 3.10. This value varies over the cycle between 9.8 $x10^{-4}$ and $3.5x10^{-4}$ kg.

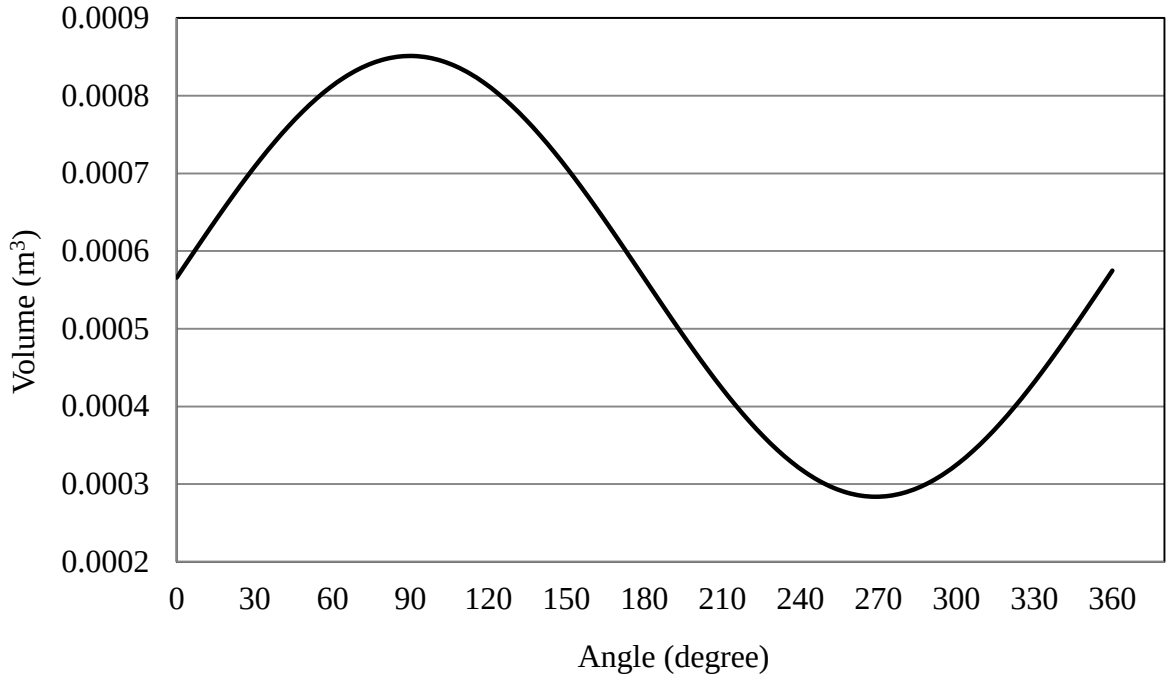

Figure 3.9 The volume of the air in the cylinder

3.4.3 Variation in the system pressure

The calculated variation of the pressure in the system is illustrated in Figure 3.11. It changes between 0.958 and 1.067 bar.

3.4.4 Variation in the air temperature in the cylinder

The variation in the air temperature in the cylinder is illustrated in Figure 3.12. It varies between 290 and 304 K. Unlike previous results, the shape of the temperature variations differs that of the harmonic function and this is results of mass exchange with adjustment control volume.

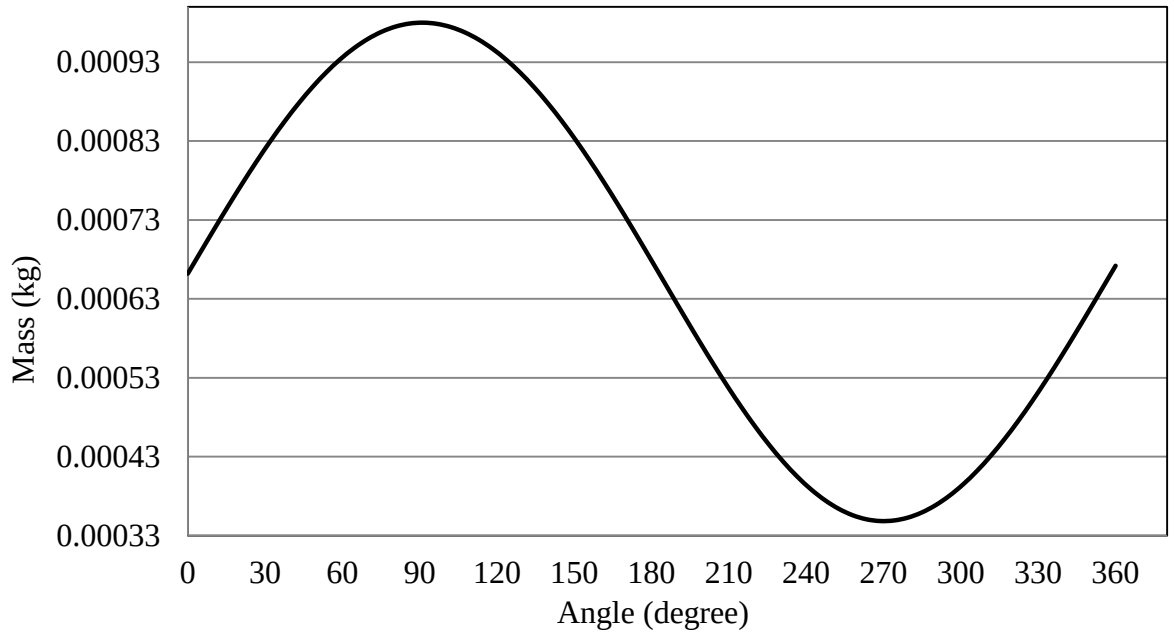

Figure 3.10 The mass of the air in the cylinder

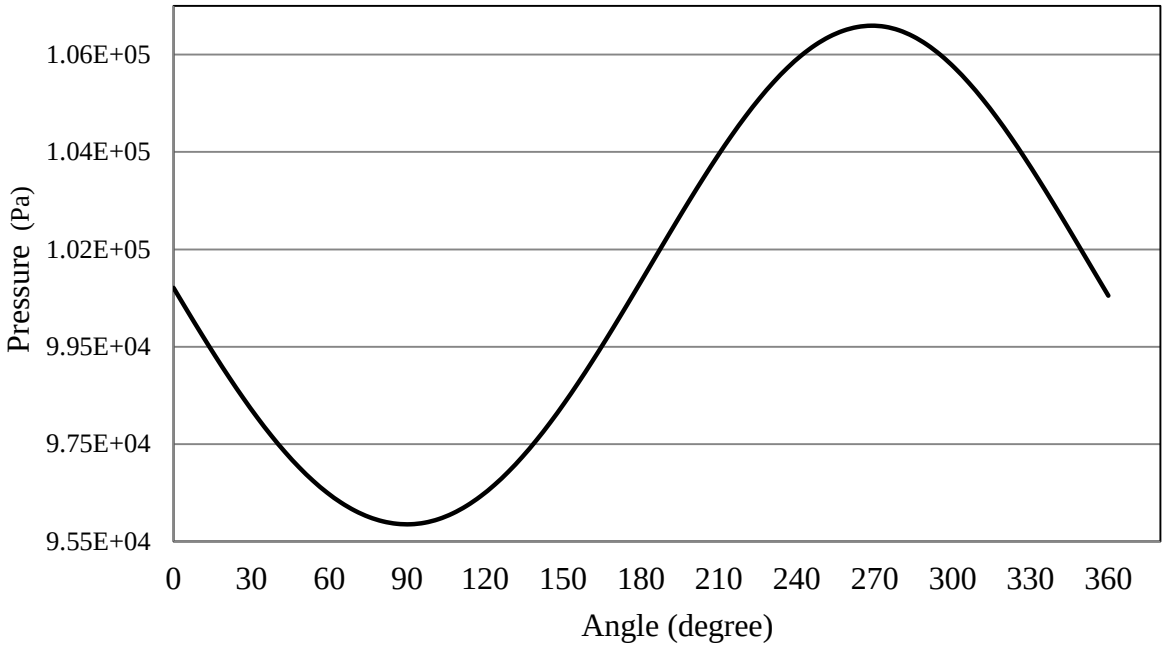

Figure 3.11 The pressure variation in the system

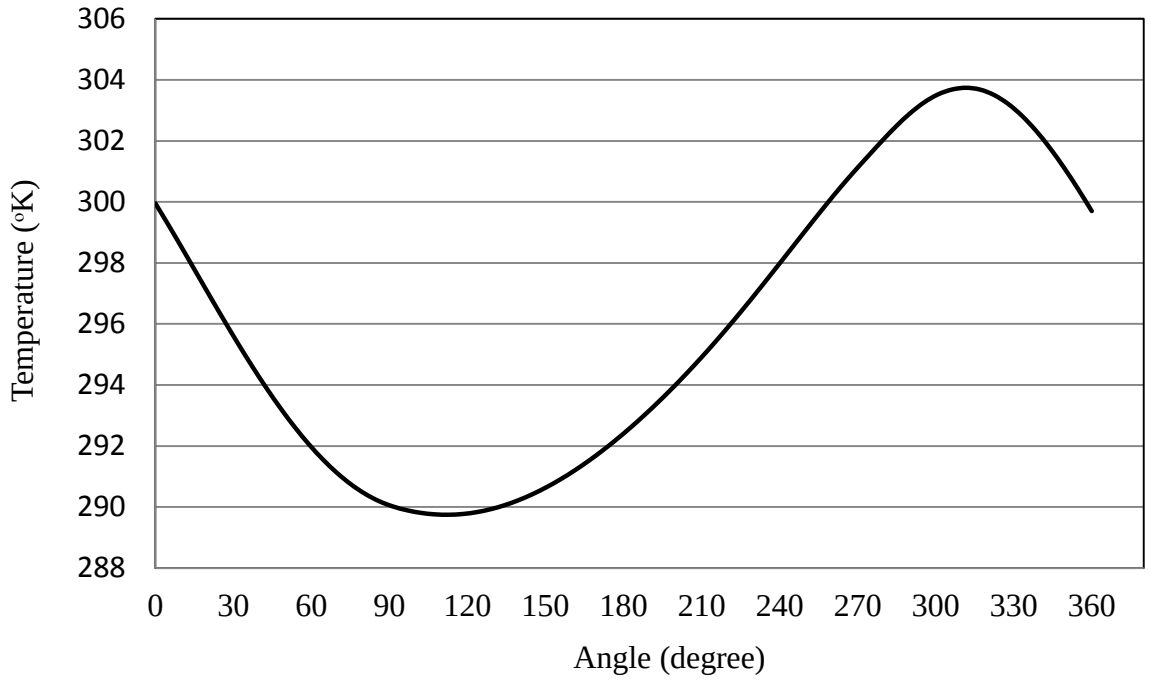

Figure 3.12 Air temperature in the cylinder

3.4.5 Variation in air mass and temperature in the cooler

Figure 3.13 shows that the mass of the air in the cooler varies between starts the cycle with a certain value of 1.695×10^{-4} and 1.697×10^{-4} kg. There is approximately 90^0 lag in compared to the mass variation curve in the cylinder, which is also a result of heat transfer and mass exchange with adjacent control volumes.

As shown in Figure 3.14 for the air temperature in the cooler oscillates between the values of 308 K and 278 K demonstrating the presence of the cooling effect in the system (temperature of the cooling water is 293 K).

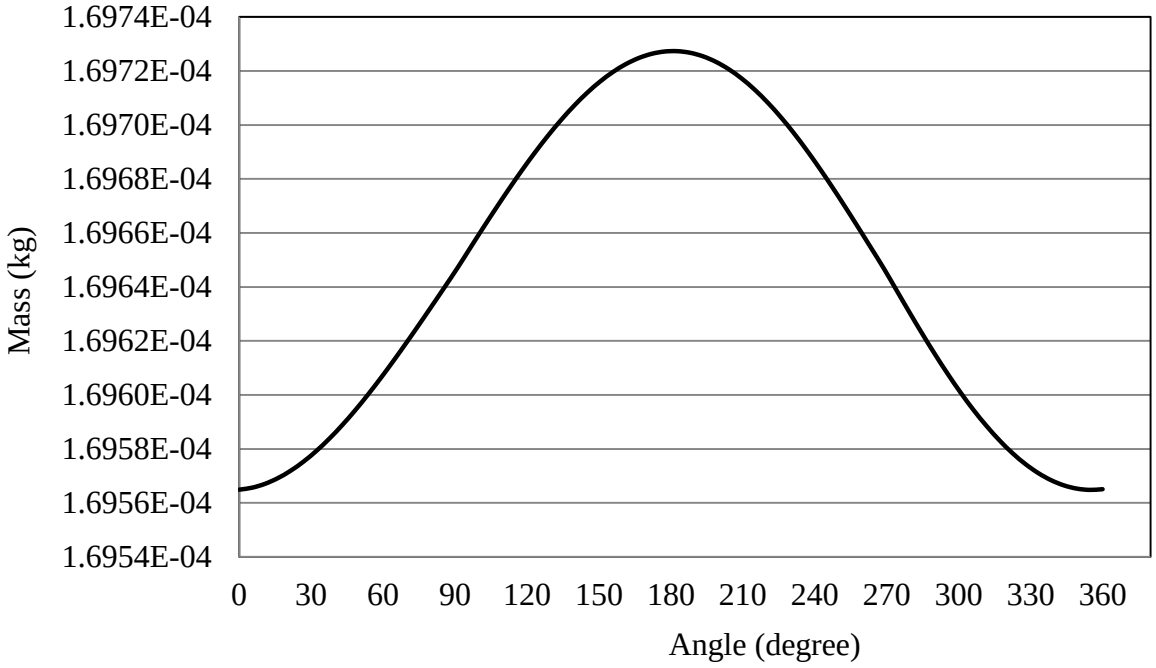

Figure 3.13 Variation of mass of air in the cooler

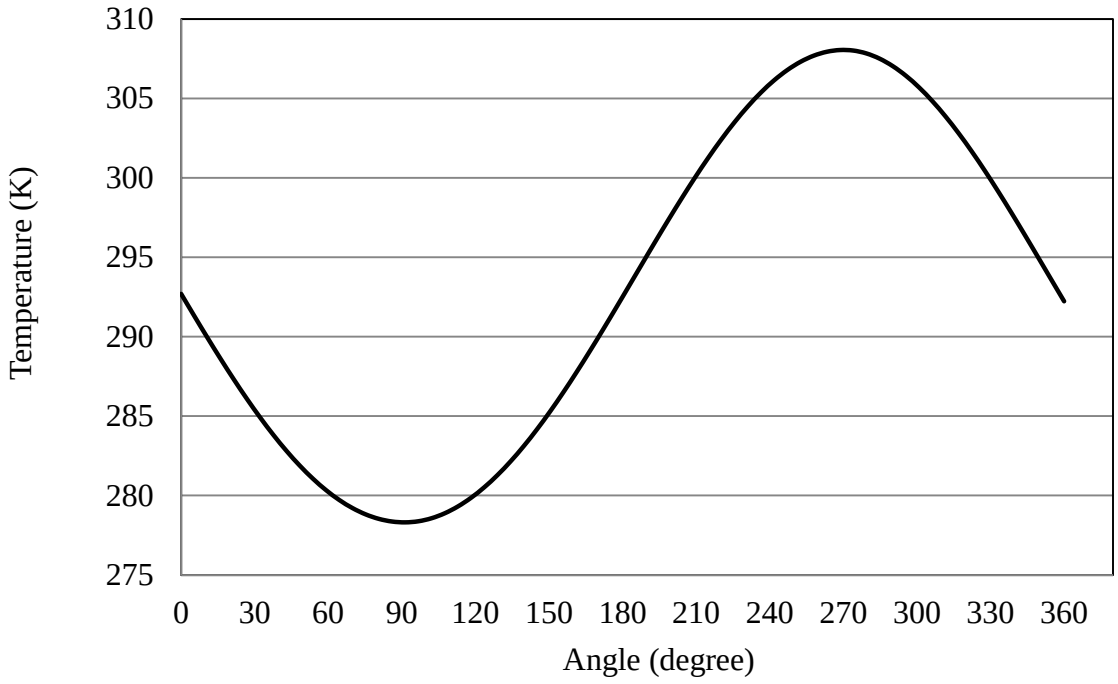

Figure 3.14 Air temperature in the cooler

3.4.6 Variation in the mass and temperature of air in the cooling space

Variations in the mass and temperature of the air in the cooling space are shown in Figure 3.15 and Figure 3.16, respectively. The air mass during the cycle changes from 1.1992 x 10^{-3} to 1.2008 x 10^{-3} kg and the air temperature fluctuates between 278 K and 308 K. The pressure effect and that of the air mass transfer on the variation of the temperatures of air in the cooler and cooling space are dominant in the obtained results since the volumes of the cooler and cooling space are constant.

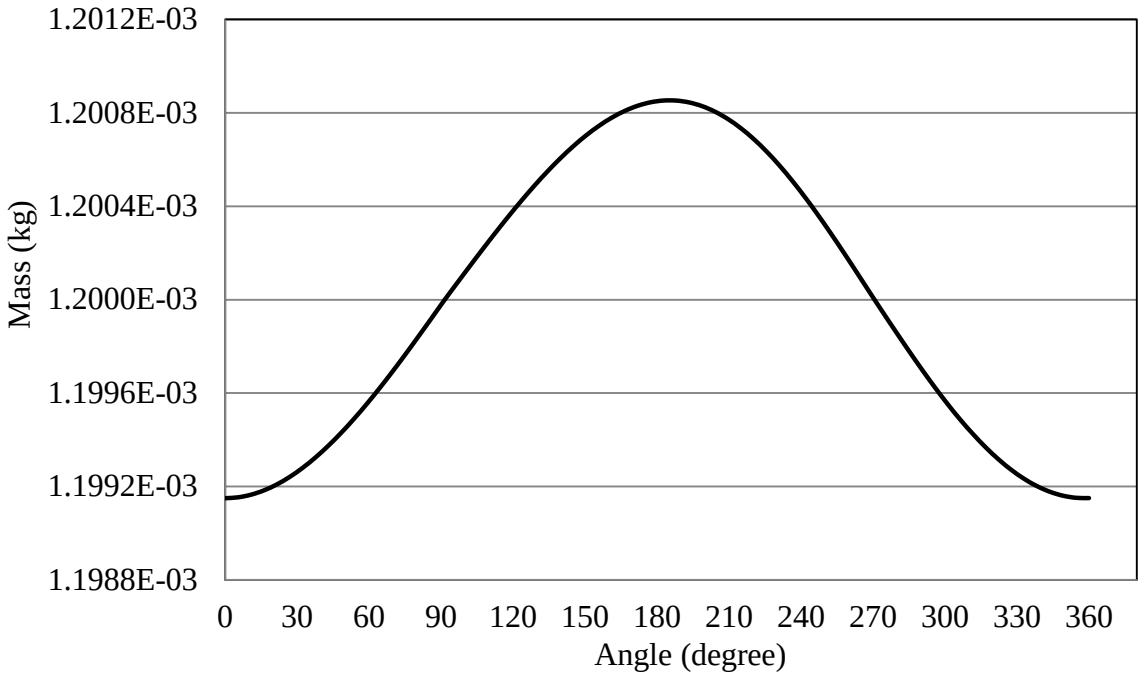

Figure 3.15 Variation of the air mass in the cooling space

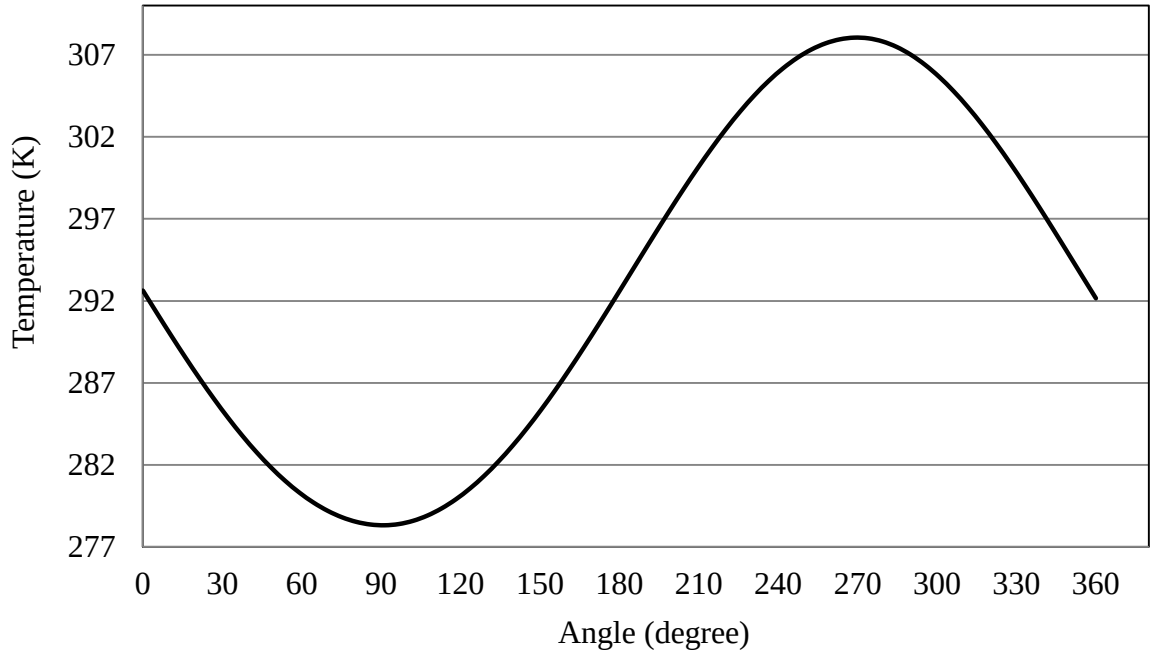

Figure 3.16 Variation in air temperature in the cooling space

3.5 Summary

In this chapter, a theoretical study of the dynamic solar cooling system based on the liquid piston converter was carried out. The calculation scheme presents the cooling system as a combimation of three control volumes with the governing equations of mass and energy conservation for each volume. This set of equations of the mathematical model is solved in the MATLAB/Simulink environment. The typical variations of the air temperatures in the cylinder, cooler and cooling space are presented. Also, an example of the change in the air pressure in the whole system over the cycle is shown. The numerical results obtained show that the cooling effect can be obtained in the cooling space using such systems powered by solar energy.

Chapter 4 Experimental Study of the Dynamic Solar Cooling System

The theoretical simulation model of the cooling part of the whole dynamic solar cooling system, described in Chapter 3, needs to be evaluated by comparing theoretically obtained results to experimental data. Operational principles of the systems for solar water pumping and dynamic water desalination were developed by Prof. K Mahkamov at Northumbria University. These systems have been built based on the liquid piston converter, which has a simple design and made of low cost materials. In the water pump and desalination systems, the liquid piston converter works as an engine driven by solar thermal energy accumulated by flat- plate or evacuated tube collectors. In this part of PhD study the test rig was assembled to test the dynamic solar cooling system which consisted of the liquid piston engine coupled with a cooling unit to produce a cooling effect. This Chapter describes tests on three different configurations of the dynamic solar cooling system. Additionally, the main components of all experimental set ups and the operational principles of all three systems are described. Additionally, the Chapter includes description of all sensors and data acquisition system which were used to monitor and record experimental data. Finally, the procedures of the experiments are presented and the experimental data obtained is analysed.

4.1 Experimental Test Rig

Each of the three tested experimental systems consist of two parts, namely the engine part which absorbs the solar energy and produces work, and cooling part which is driven by the engine part to generate a cooling effect in the cooling space.

4.1.1 The first configuration

The first tested configuration of the solar cooling system, has a liquid piston engine and a liquid piston cooling device, as shown in Figure 4.1 and 4.2. The liquid piston cooling device is made as a U-shaped pipe with a height of 500 mm.

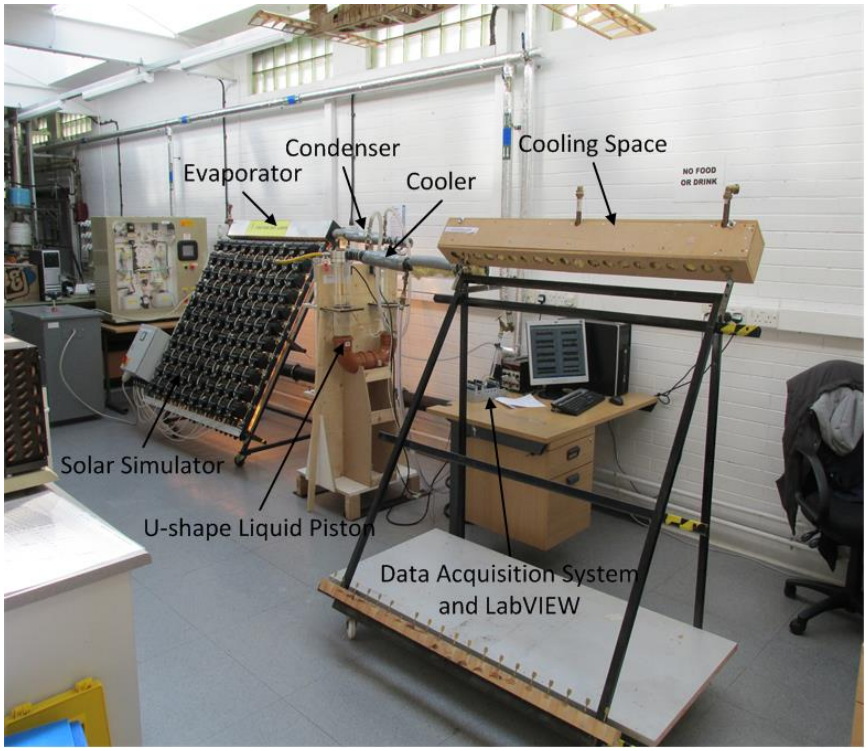

Figure 4.1 The test rig of the first configuration

4.1.1.1 The engine part

The engine part has five main components, namely solar radiation simulator, heat pipe evacuated tube solar collector, evaporator, double-pipe counter-flow condenser and liquid piston engine, see Figure 4.3.

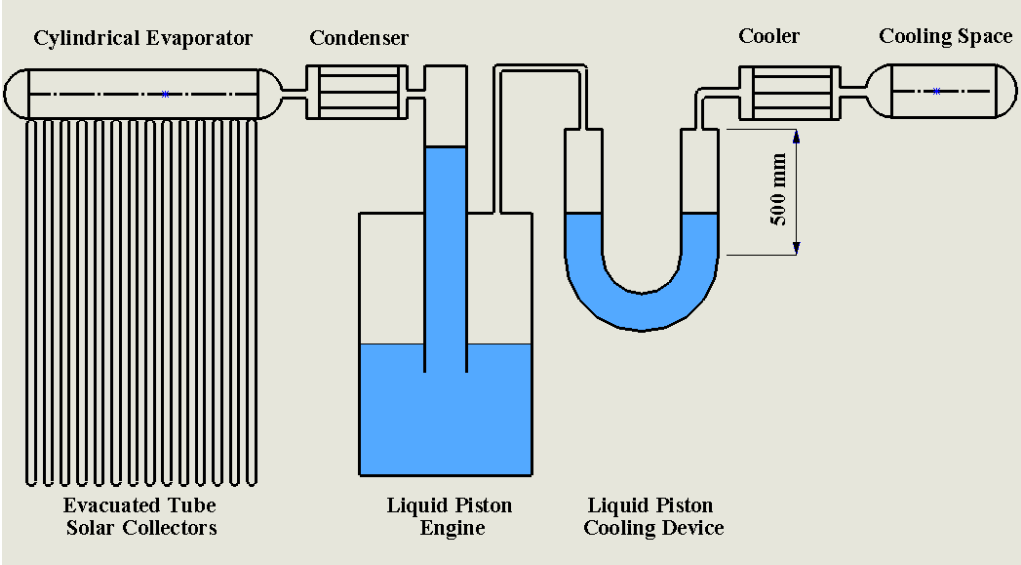

Figure 4.2 Schematic diagram of the first configuration

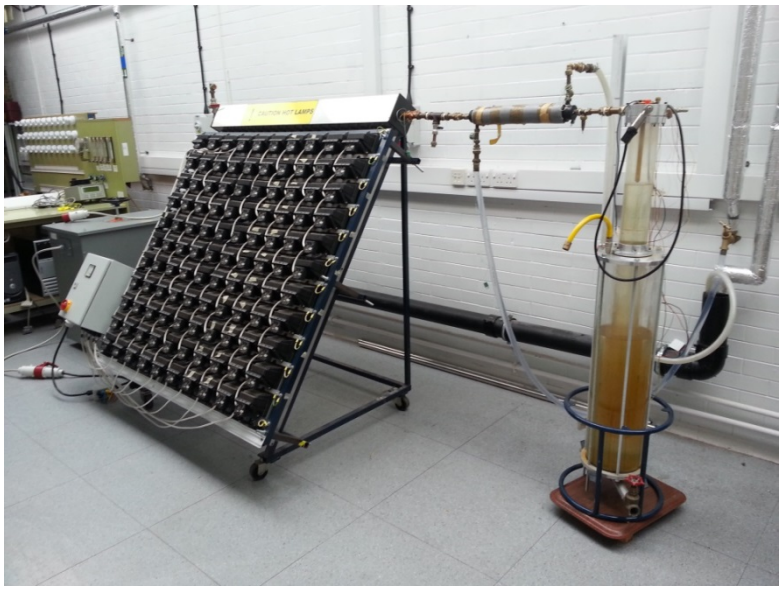

Figure 4.3 The engine part

4.1.1.1.1 Solar radiation simulator

The solar radiation source is simulated in the laboratory using an array of floodlight lamps, connected to variable voltage three phase transformer [172]. The simulator consists of 10×11

tungsten halogen floodlight lamps with a maximum electrical power of 150 W/lamp. This set of lamps is mounted on a steel frame so that their irradiation is perpendicular to the surface of the evacuated tube solar collector, see Figure 4.4. The lamps in the solar radiation simulator are divided into three groups and each group is connected to one of three phases of the variable voltage transformer. It is possible to vary the voltage from 0 to 240 V in each phase.

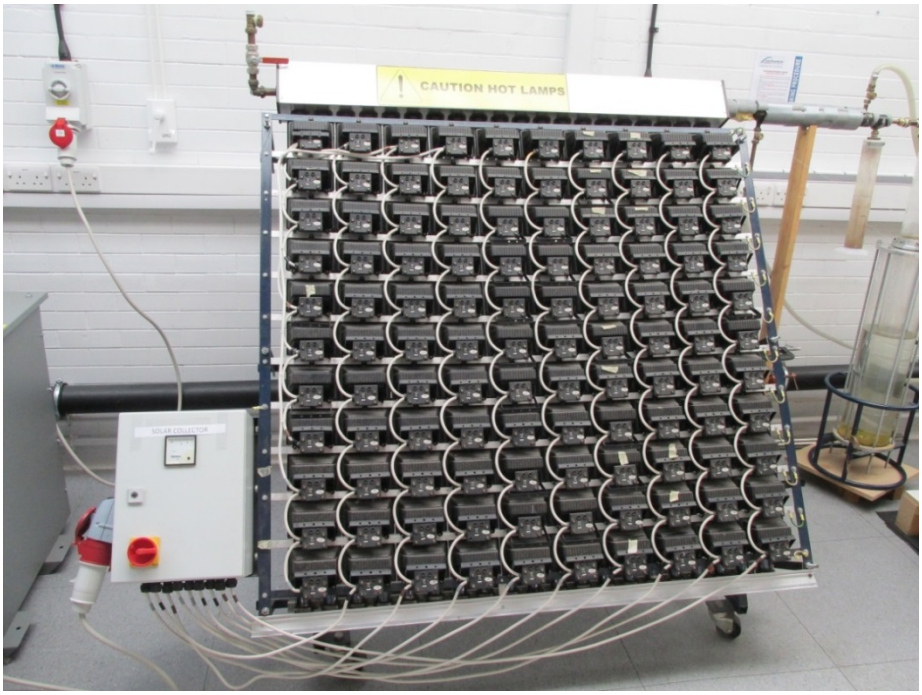

Figure 4.4 Solar radiation simulator

4.1.1.1.2 Evacuated tube solar collector

Twenty evacuated tube solar pipes are installed on the frame directly beneath of the solar simulator to transfer the produced heat to the water in the evaporator, see Figure 4.5. The evacuated tube solar collector was chosen to be used in tests because of its higher efficiency at a working temperature above 80 ˚C, compared to other types [173], due to the vacuum

insulation of the absorber element and the highly selective surface coating [174]. The condensing side of the heat pipes of the evacuated tubes (the top side) is inserted into the evaporator through the cylindrical ports as shown in Figure 4.6. Each heat pipe is inside the evacuated glass tube. In normal conditions, the solar radiation heats up the external surface of the heat pipe in the vaporization zone. The working fluid inside the pipe is vapourised and moves under the effect of the density difference to the condensing zone at the top, where the heat is transferred to the water in the evaporator. The working fluid inside the heat pipe is then condensed and returned to the vaporization zone [175]. The detailed specifications of the evacuated solar pipes used in this test rig are presented in Table 4.1.

Figure 4.5 Evacuated tube solar collectors

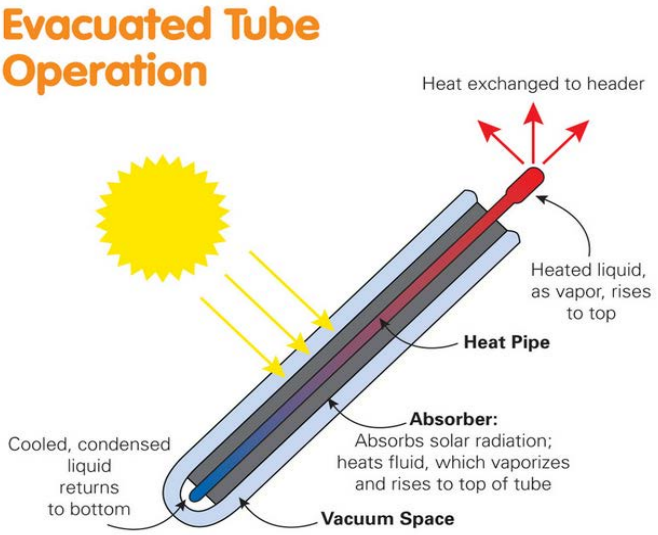

Figure 4.6 Schematic diagram of evacuated tube solar collector [176]

Table 4.1 The evacuated tube solar collectors' specification

Parameter	**Description**
Collector Type	Evacuated-tube with heat pipe
Number of tubes	20 tubes
Tube Length	1.74 m
Outer Tube Diameter	0.047 m
Collector Area	2.250 m^2
Absorber Area	1.80 m^2
Dimensions L×W×H	1760×1500×130 (mm)
Weight	55 kg
Maximum Operating Temperature	190 ˚C
Stagnation Temperature	247 ˚C

4.1.1.1.3 Evaporator

A copper manifold pipe is used an the evaporator. The dimensions of the evaporator are 150 cm in length and 6 cm in the diameter. It can be seen in Figure 4.7 that the evaporator has

twenty cylindrical ports built in and the axes of these ports are normal to the main axis of the evaporator. The aim of inserting these ports into the evaporator is to house the condenser side of the evacuated tube solar pipes, permitting the solar energy to be absorbed from the solar simulator and then transferred to water in the evaporator as a result of the direct contact between the ports and evacuated tube pipes. With such the arrangement the evaporator is sealed and watertight.

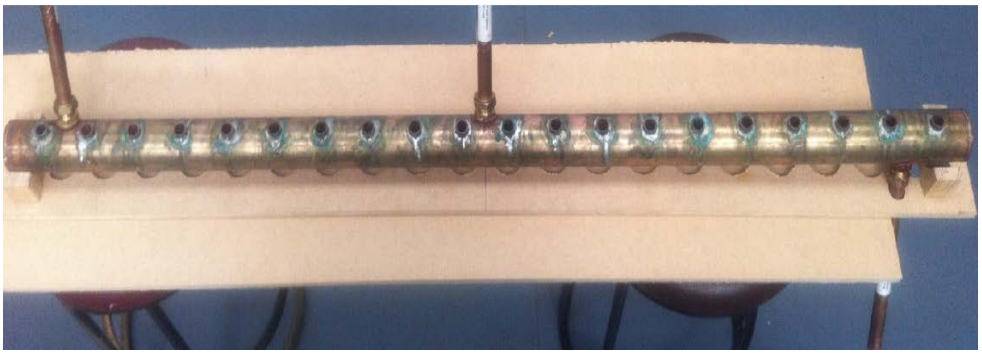

Figure 4.7 The evaporator

To reduce the contact thermal resistance between the surfaces of ports and heat pipes, a special metallic glue is used between them and this glue has a high thermal conductivity. To reduce the heat losses from the evaporator to the surroundings, the evaporator is wrapped by a glass wool and then placed into a wooden box.

4.1.1.1.4 Condenser

The condenser used in this study is a counter flow double pipe heat exchanger as shown in Figure 4.8. The cooling water flows between two concentric pipes. The diameter of the inner pipe is 15 mm the diameter of the external pipe is 50 mm works.

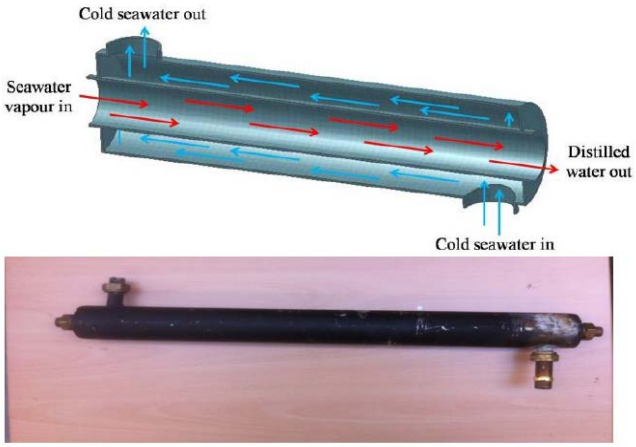

Figure 4.8 The condenser of the dynamic desalination unit

4.1.1.1.5 Fluid piston engine

The liquid piston engine is made of plastic pipes [165] and runs at the pressure close to the atmospheric at a relatively low frequency of about 3 Hz. In this study, the main function of the liquid piston engine is to convert the heat energy collected by the evacuated tubes into oscillations of a water column in the cylinder. The material of the pipes used in the engine is Polymethyl-Methacrylate which is known as clear acrylic tubes [177]. The engine is made of two vertical pipes installed concentrically. The combination of these acrylic pipes, which form the cylinder itself and then bouncing space, is closed at the top, middle section and bottom with the aluminium flanges as shown in Figure 4.9. The upper aluminium flange is designed to house the pressure sensor, water level sensor and thermocouple. The upper and middle flanges also house ports to allow connection of the engine to other units. The concept of the operation process of the liquid piston engine is described in Chapter 3.

4.1.1.2 The cooling part

The cooling part is a combination of three main components, including U-shape tube fluid piston machine, double-pipe counter-flow cooler and the cooling space, see Figure 4.10. It can be seen that the cooling part is a “thermodynamic” reverse of the engine part. The fluid piston machine is driven by the energy provided by the fluid piston engine, described above.

4.1.1.2.1 Fluid piston cooling device

The fluid piston cooling device is designed to have the U-shape, see Figure 4.11. The U-shaped tube is made from two clear acrylic tubes with aluminium flanges on the top of both sides and connected to each other at the bottom using two PVC elbows. The height of acrylic pipes is 500 mm. The design of aluminium flanges is shown in Figure 4.12 and can house pressure and temperature sensors together with water level sensor.

Figure 4.9 The liquid piston engine

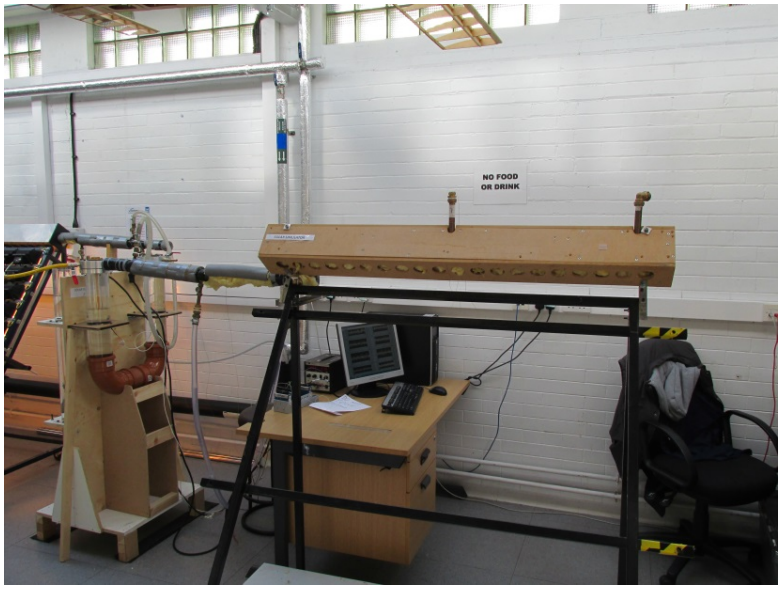

Figure 4.10 The cooling part

Figure 4.11 The liquid piston cooling device of 500 mm long

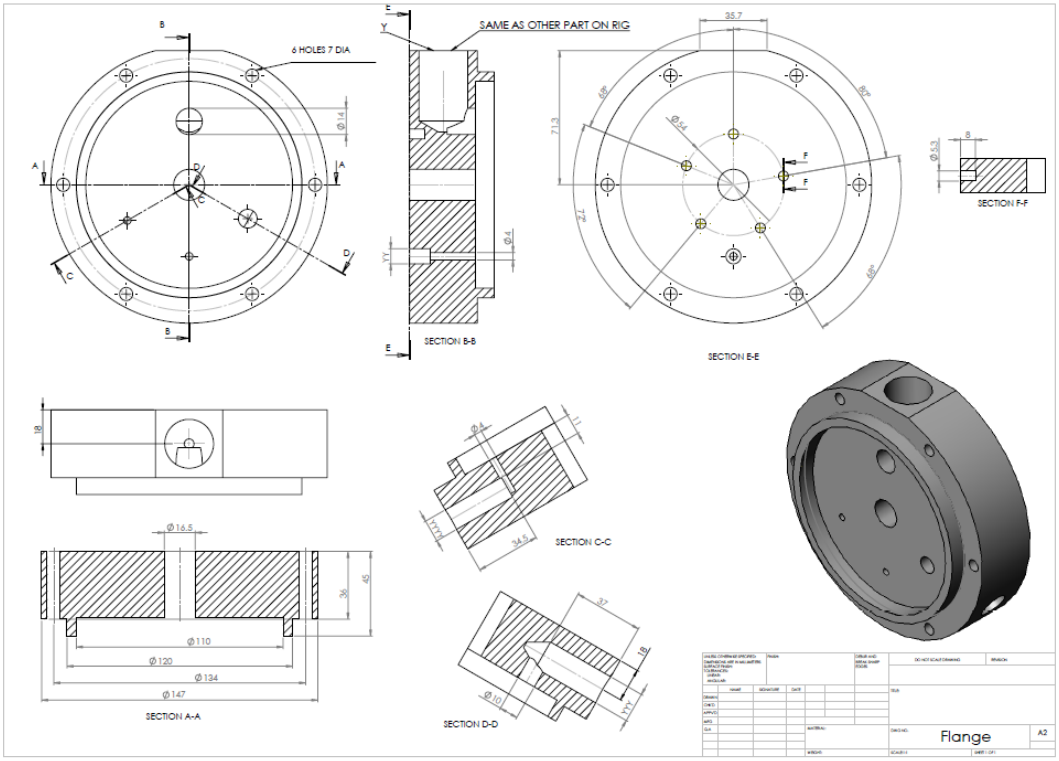

Figure 4.12 Aluminium flange for sealing the cylinder and housing sensors

4.1.1.2.2 Cooler

The cooler used in the prototype is a counter flow double pipe heat exchanger which has the same design and dimensions as the condenser on the “engine” part, see Figure 4.8. The cooler in the cooling part functions as the heat sink in the cooling cycle. It uses water as a coolant to absorb the heat rejected from the air during compression phase of the cycle.

4.1.1.2.3 Cooling space

Next to the cooler there is the cooling space in which the cooling effect takes place. The cooling space is a confined copper pipe manifold which has the same design and dimensions as the evaporator on the “engine’s” side , see Figure 4.7. The cooling space is insulated in

the same way – it is wrapped into glass wool before and placed in the wooden box, see Figure 4.13.

Figure 4.13 The cooling space

4.1.2 The second configuration

As the first configuration of the cooling system, the second one consists of the "engine" part and cooling part. The difference is that the liquid piston cooling device has pipes with height of 1000 mm. Figures 4.14 and 4.15 show the laboratory prototype and the schematic diagram of the second configuration. With the exception of this difference, the rest components of both configurations are identical.

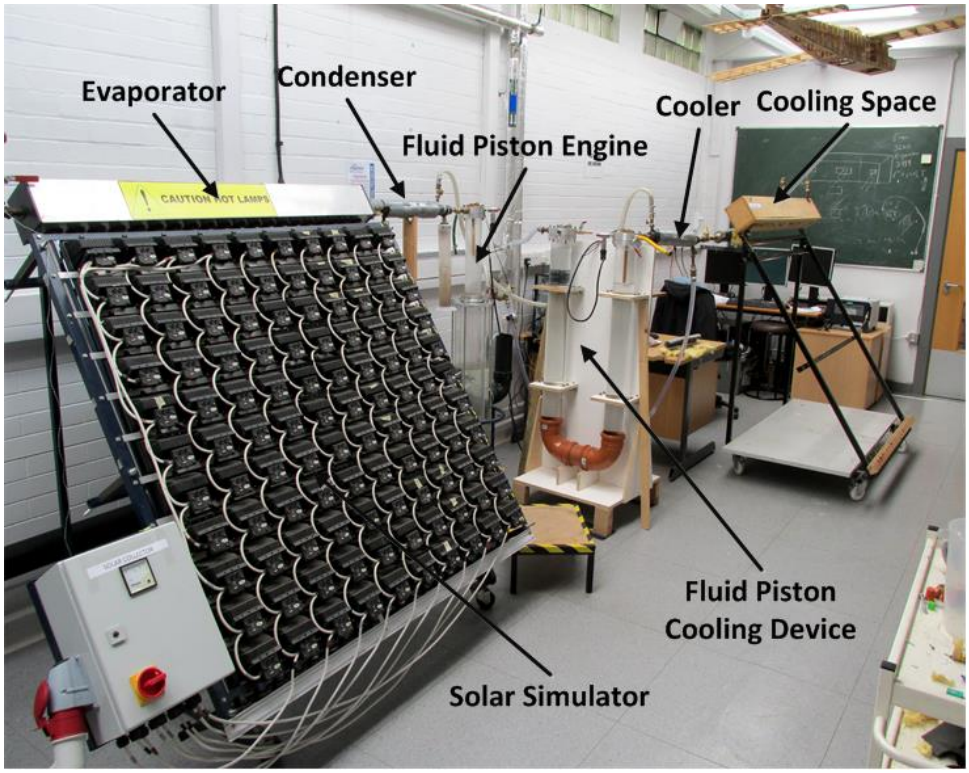

Figure 4.14 The test rig with the second configuration of the system

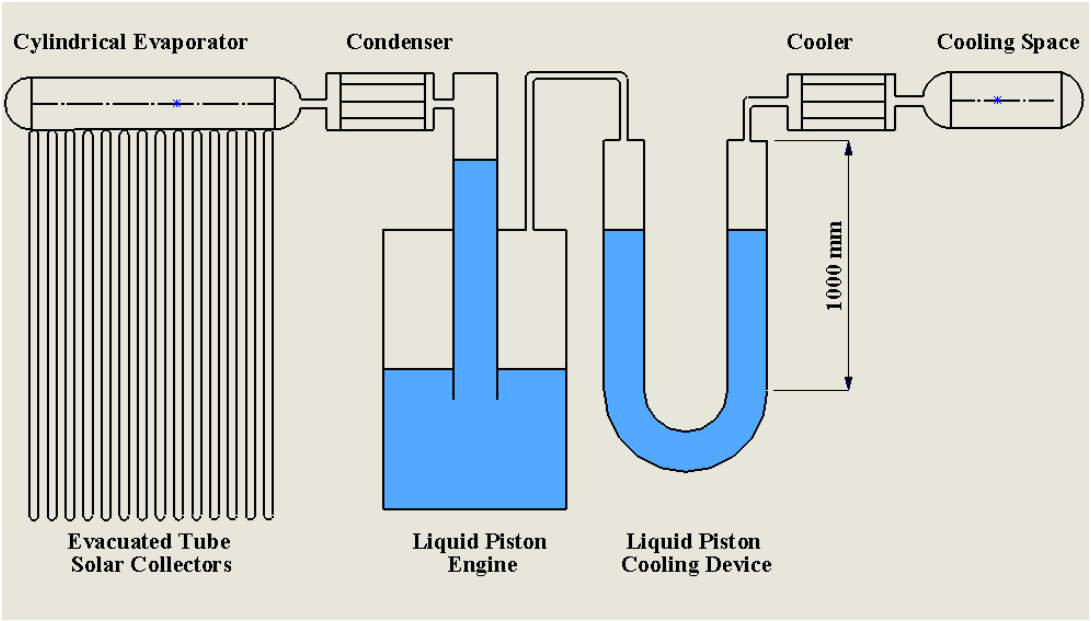

Figure 4.15 Schematic diagram of the second configuration

It can be seen in Figure 4.15 that there is a gas connection between the fluid piston engine and fluid piston cooling machine and oscillations of the water column in the latter are caused by variations of the pressure generated in the engine. The length of the U-shaped tube is a very important factor to have the optimum tuning between the pressure change amplitude in the cylinder and the mass of water in the fluid piston in the engine or cooling machine. Therefore, to obtain additional experimental information on rational combination of these two parameters these two different (the heights of 500 and 1000 mm) cases were tested. Figure 4.16 illustrates the fluid piston cooling device used in the second configuration.

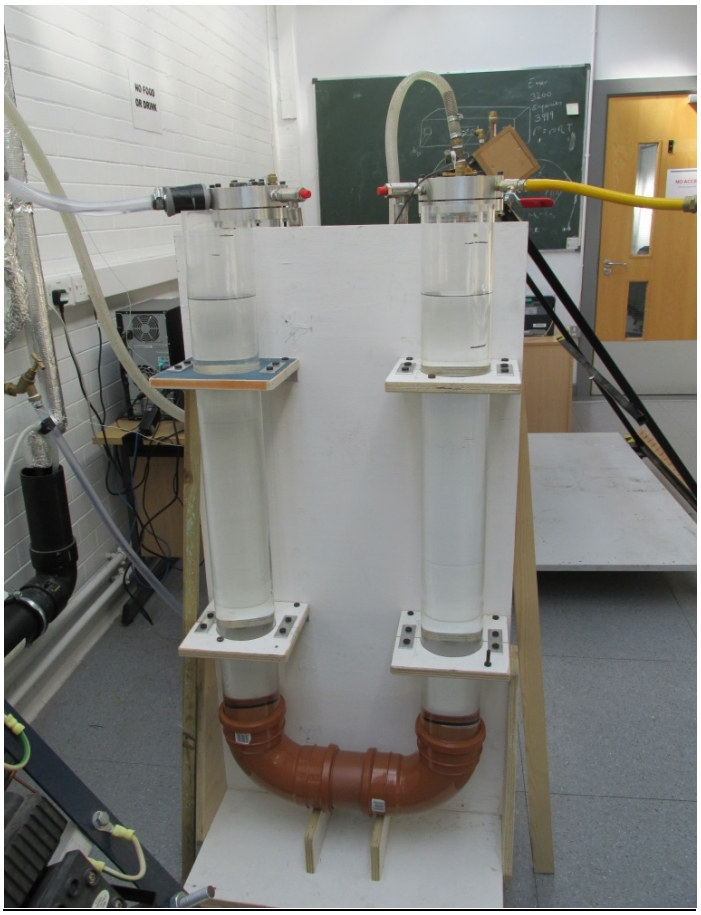

Figure 4.16 The fluid piston cooling device with pipes of 1000 mm long

4.1.3 The third configuration

In this configuration the U-shaped pipe was used as both the liquid piston engine (the first column) and the liquid piston cooling machine (the second column). The use of completely two different machine arrangements in the first and second configuration leads and gas connection between them results losses of the "driving" power of the engine part. This third configuration of the whole system is shown in Figures 4.17 and 4.18. In this case, the identical set of temperature and pressure sensors are installed on both flanges of pipes as illustrated in Figure 4.19.

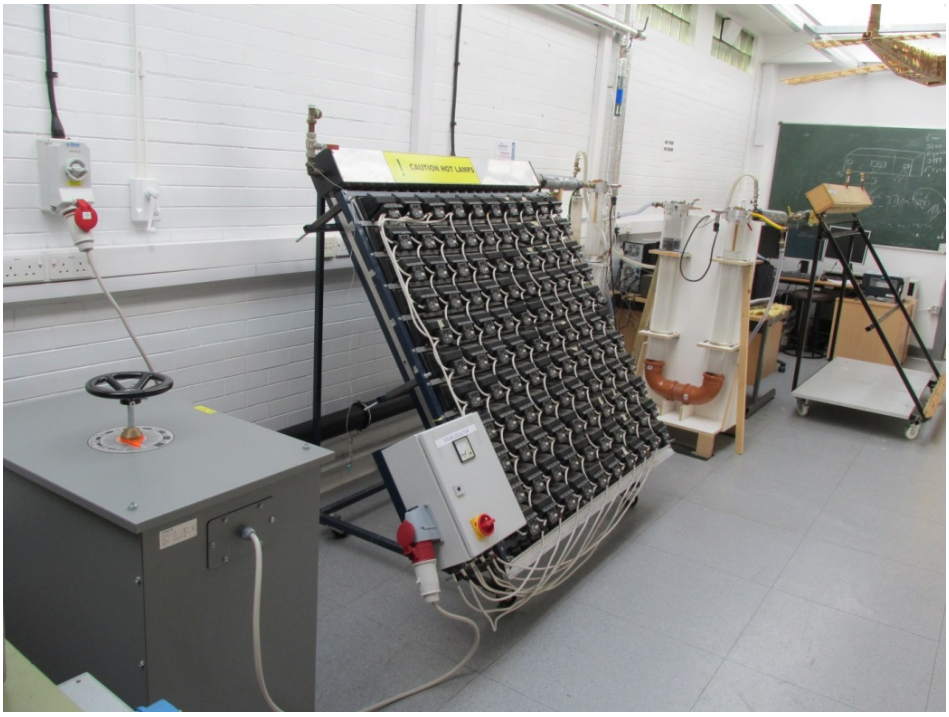

Figure 4.17 The test rig of the third configuration

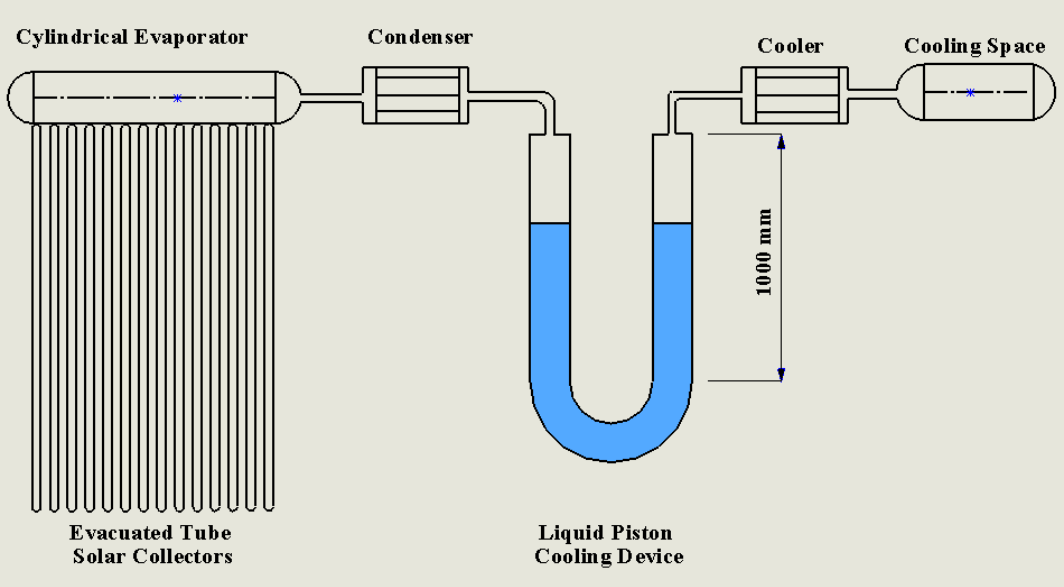

Figure 4.18 Schematic diagram of the third configuration

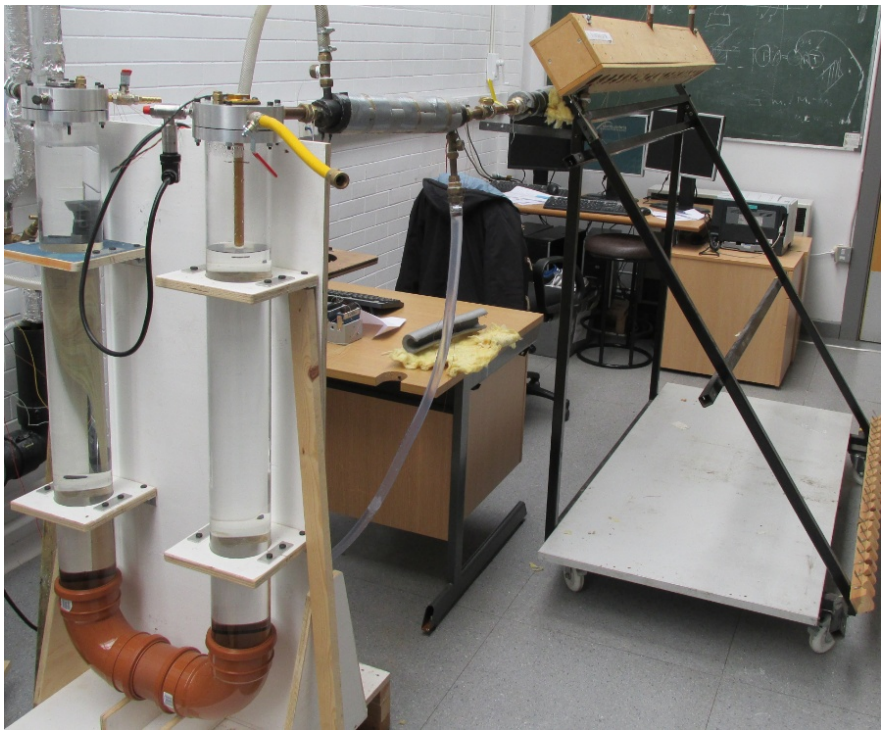

Figure 4.19 Cooling part of the third configuration

4.2 Data Measuring and Collection

In the describe above laboratory prototypes, several sensors were used to monitor and record working parameters of the engine's and cooling part cycles see Figure 4.20. The parameters needed to be monitored are amplitudes of the water level in both liquid piston machines, air pressures and temperatures in components of both sides of the test rig.

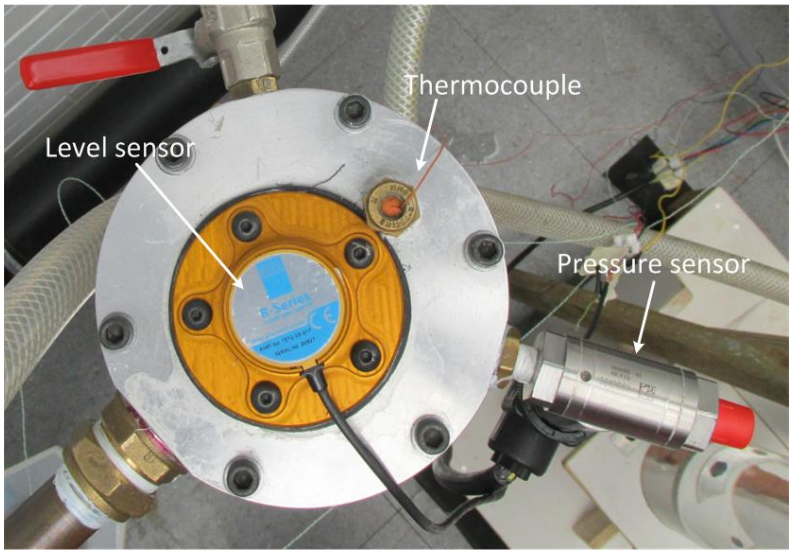

Figure 4.20 Sensors mounted on the flange at the top of liquid piston

The amplitudes of the water level in the liquid piston engine and liquid piston cooling machine were measured using an aluminium R-series liquid level sensor [178]. The level sensor is shown in Figure 4.21 and has the SAE 5-bolt flange mount with fully-integrated electronics. The sensor has a bar with a diameter of 16 mm and 24 cm long. It is factory calibrated device with a sampling rate of 80 Hz.

Figure 4.21 Aluminium R-series liquid level sensor

The change in the air temperature in the system is measured using three T-type thermocouples. One of these thermocouples is embedded into the flange at the top of the interior cylinder of the liquid piston engine. In addition, to monitor changes in air temperatures on the cooling part of the system, two similar thermocouples are inserted into the cylinder of the cooling machine and in the cooling space Thermocouples used are PFA-insulated, 2 m long and with the thickness of wires of 0.08 mm [179], see Figure 4.22. Because the fluctuations of the air temperature over the cycle has the same frequency as the cycle (about 3 Hz) then the use of such the thin thermocouple can reflect the tendency in the change of the temparture but this will not be suffcient to record instanteneous tempetaure variations over the cycle due to their thermal mass/inertia. The amplitude of the temperature change recorded by these thermocouples will be reduced compared to real process and also there will be phase lag in the temperature recording. The formation of the water film on the thermocouple surface in the wet environment introduces additional errors in readings.

For measuring the temperatures of cooling water in the inlet and outlet of the cooler and condenser, four K-type thermocouples were used with the diameter of 0.2 mm as shown in Figure 4.23.

Figure 4.22 T-type thermocouple

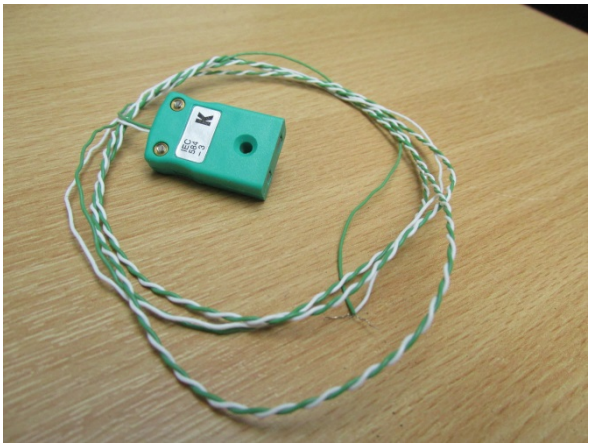

Figure 4.23 K-type thermocouple

The variation in the pressure in the system is measured by means of two UNIK 5000 instantaneous pressure sensors made by DRUCK Ltd, see Figure 4.24. The sensors are installed at the top of corresponding flanges of the fluid piston machines. These Druck PMP 5073-TB-A3-CC-H1-PG are differential bi-directional gauge pressure transducers with a -4 bar to + 4 bar [180]. The pressure sensors have an accuracy range of ±0.04% and the frequency response up to 5 kHz at the temperature range from -20 up to 80 ˚C, which is within the temperature range in the system. The calibration of this sensor is made by the manufacturer.

Figure 4.24 Pressure sensor

The radiation from floodlights lamps was measured and calibrated using a PMA 2200 photometer, shown in Figure 4.25. This photometer measures the full spectrum of radiation from ultraviolet to visible and infrared waves with a sampling rate of 3 Hz. The photometer was calibrated by the supplier and has an accuracy of 0.2% over the full range of measurements [181].

Figure 4.25 Photometer PMA 2200

4.3 Data Acquisition System

The data acquisition system was assembled from modules supplied by National Instruments and connected to sensors in order to record experimental data on the parameters in the cycles. Figure 4.26 illustrates the schematic of connections of components of the data acquisition system. LabVIEW software was used in conjunction with the above data acquisition system. The system consists of two types of modules, namely NI-9213 module with 16 “slow” channels and the 4 “fast” channel simultaneous analogue NI-9222 module. These modules were mounted on the 8-slot USB chassis of the NI cDAQ-9178 model connected to a PC with LabVIEW software.

The thermocouples measuring the temperature of the cooling water in the condenser and cooler and that used for measuring air temperatures were connected to a separate NI 9213 modules. The NI 9213 module has a built-in cold-junction compensation with the accuracy of measurements at 0.02 ˚C. The high-speed mode was chosen to operate for this module with a sampling rate of 1200 Hz in aggregate which results in every channel sampling rate 75 Hz if the module was connected to 16 thermocouples [182]. To increase the sampling rate value for each deployed thermocouple two NI 9213 modules were used with one of them being connected to 3 thermocouples measuring the temperature of the air. The second module was connected to 4 thermocouples measuring the temperature of cooling water in the inlets and outlets of the condenser and cooler.

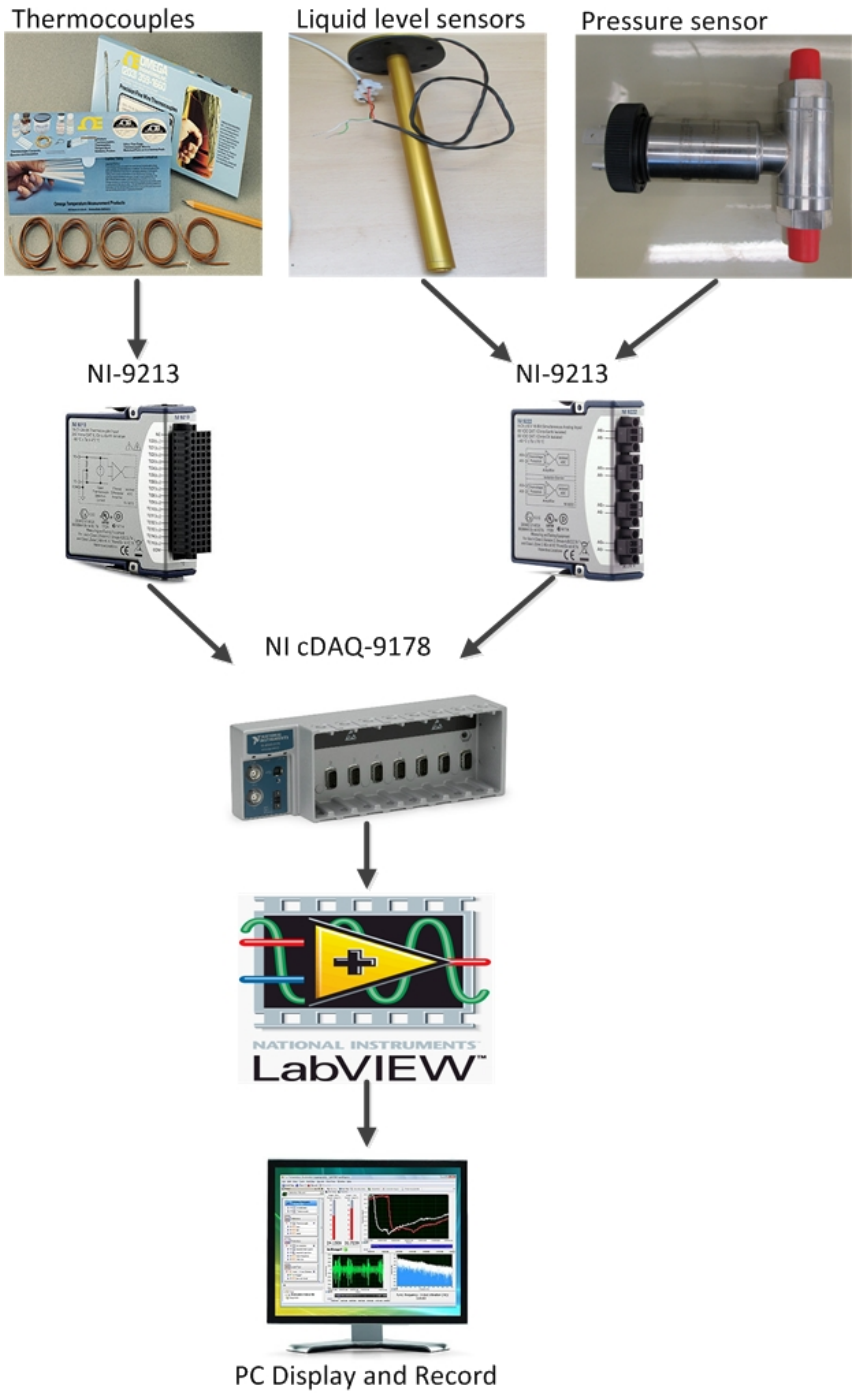

Figure 4.26 The arrangement used in the data acquisition system

The high-speed 4-channels NI 9222 module has a channel-to-channel isolation with enhanced sampling rate and accuracy [183]. These four fast channels were used for two pressure

transducers and two liquid level sensors. Each channel in this module has a sampling rate of 500 KHz with an accuracy of ±0.2% of the measuring value.

The all above modules were mounted on the 8-slot NI-cDAQ-9178 USB chassis which has a built-in timing controller for synchronizing operation of modules and sampling process. The cDAQ chassis is connected to a PC through a USB cable [184].

For experiment controlling, visualisation of signals and data saving a computer program in LabVIEW was developed [185], Figure 4.27. Example of results visualisation in LabView is shown in Figure 4.28.

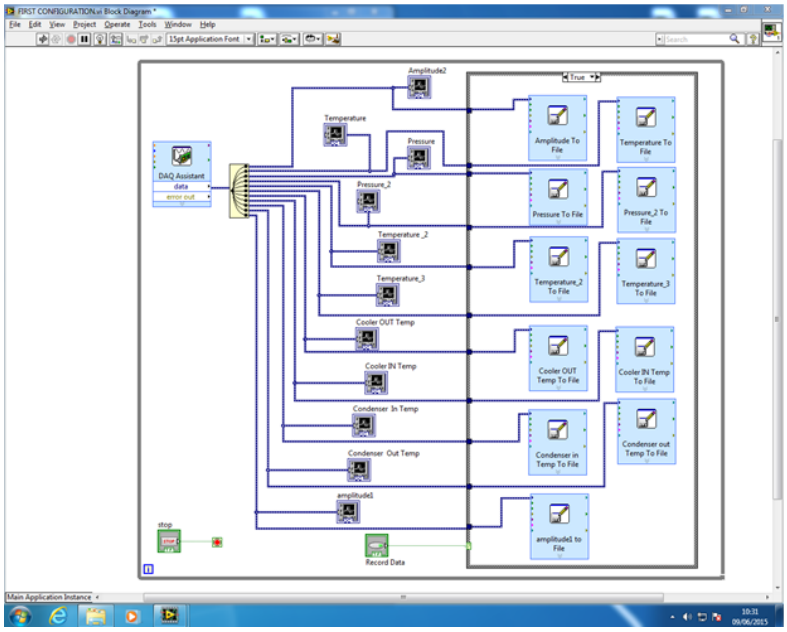

Figure 4.27 LabVIEW block diagram panel

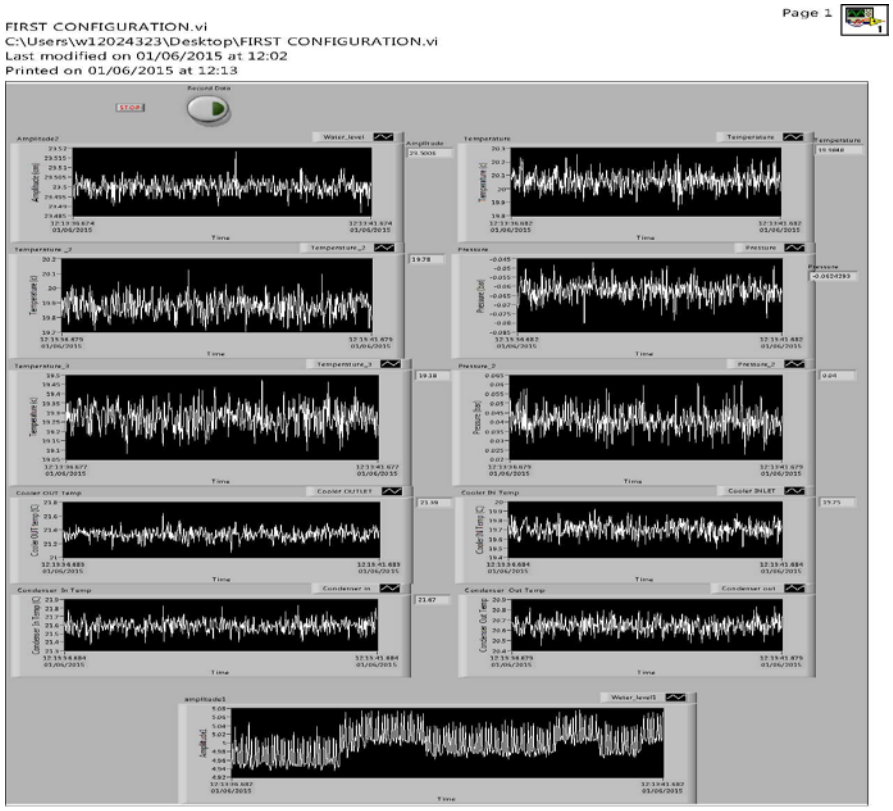

Figure 4.28 LabVIEW results visualisation panel

4.4 Experimental Procedure

Before conducting experiments on the solar cooling system, the solar radiation simulator had to be calibrated to simulate the solar irradiance daily variation in a typical summer in Benghazi, Libya, see Figure 4.29.

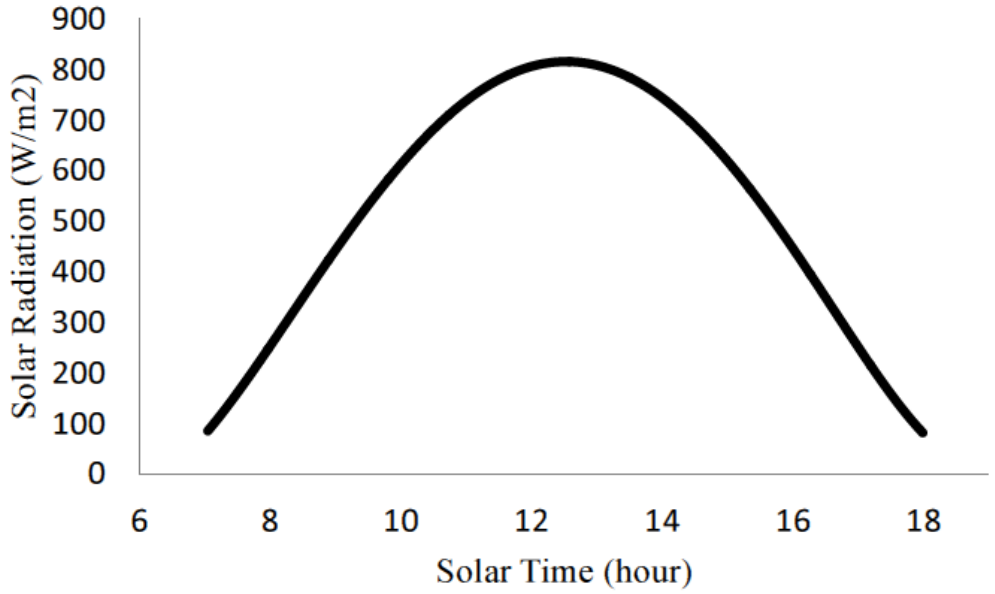

Figure 4.29 The total solar radiation in a typical summer day in Benghazi city, Libya [9]

The calibration operation was aiming to quantify the average radiation delivered by the halogen lamps at different values of the voltage controlled by the 3-phase transformer. Because the radiation generated from the lamps is high at the centre of the simulator, compared to that on its periphery, the whole simulator's area was split into a grid as shown in Figure 4.30. The area was split into 11 rows and 10 columns. The photometer PMA 2200 was used to for calibration of the simulator.

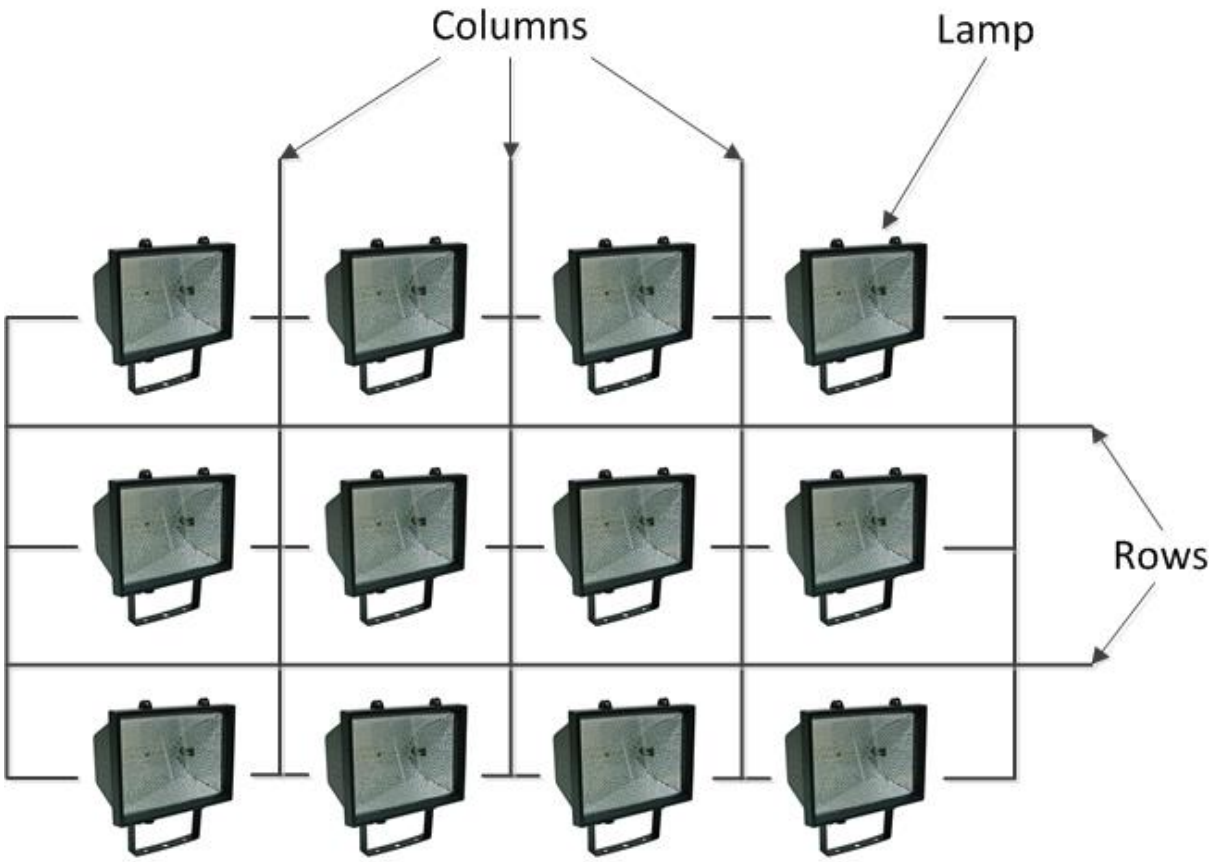

Figure 4.30 A part of solar simulator

The measurements of radiation were done in a two-step procedure. Firstly, the average quantity of the radiation in the central area of each lamp was measured and then multiplied by the total area of lamps. Secondly, the average quantity of the radiation in the area between lamps was measured following the same procedure. Those two values of irradiation were added in order to find the total amount of irradiation generated by the lamps. Finally, to calculate the average irradiation generated from the solar simulator, the total amount of irradiation generated by the floodlights was divided by the total area of the simulator. The relation between the average solar radiation and transformer voltage percentage is shown in Figure 4.31.

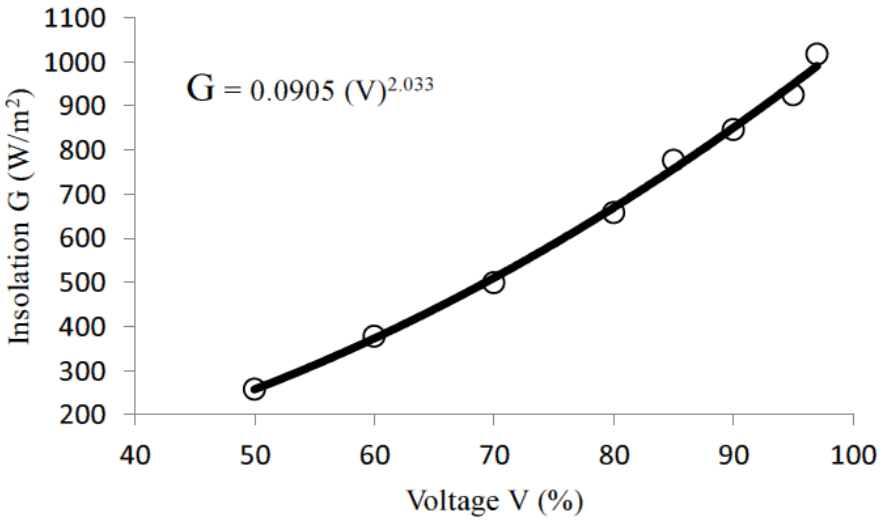

Figure 4.31 Average irradiation versus transformer voltage

After assembling the whole system components together, the pressure in the system was raised to 1.5 bars gauge and then all the fittings and the pipe joints were checked by using a gas leakage detector to ensure that the system is hermetic and there was no pressure drop. To reduce the heat losses, the system was thermally insulated by wrapping the connection pipes and heat exchangers with a low conductivity mineral wool.

The dynamic solar cooling unit was tested experimentally for the irradiation level of 700 W/m^2 which corresponds to transformer voltage of 82%. The test procedure starts with filling the evaporator with a half-litre of water and setting the certain mass flow rate of cooling water in the cool the cooler and condenser. Then, the solar simulator is switched on and the three phase transformer regulator is set in the position to achieve the required level of irradiation according to the calibration curve. It takes about 90 minutes to reach the steady state condition of operation of the cooling unit after which the measurements are taken and recorded. The procedure for a certain level of irradiation was repeated several to eliminate any human errors in measurements

4.5 Discussion of experimental results

The experimental investigations were conducted for all three proposed configurations. For the first and second configurations, the experimental findings on the water level amplitude in the engine cylinder, the air pressure and temperature of the engine cylinder, the water level amplitude in the cooling machine cylinder, the air pressure and temperature in the cooling cylinder and the air temperature in the cooling space were recorded. For the third configuration the water level in the engine cylinder only was measured since this was identical to that in the cooling device cylinder, taking into account that displacements are in counter phase. The other measured parameters were the same as for the first and second configurations.

4.5.1 Experimental results for the first configuration

The oscillation of the water level in the cylinder of the engine over a single cycle is shown in Figure 4.32. It can be seen that the maximum value of the displacement is 13 cm whilst the minimum value is 9 cm. The frequency of the engine operation is about 3 Hz. The increase in the displacement of the water level in the cylinder results in an increase in the volume of air in the cylinder and consequently an increase in the total air volume of the engine part of the system. In Figure 4.33, the variation of the air pressure in the engine part over the cycle is presented. The pressure in the engine fluctuates between 104500 Pa (the maximum, when the total air volume is minimum) and 100700 Pa (the minimum, when the total air volume is maximum). Figure 4.34 and Figure 4.35 show oscillations of the water level in the cooling cylinder and the air pressure in the cooling part. The air temperature variation in the cooling space of the first configuration of the system is illustrated in Figure 4.36.

The water level in the cylinder of the cooling machine oscillates between 18 and 12 cm with a stroke of water column being 6 cm. The air pressure in the cooling part of the system fluctuates between 106000 and 98000 Pa.

It was observed during experiments that at frequencies higher than 3 Hz there were distortions of the fluid surface during fluid piston oscillations. Such splashes resulted in losses of kinetic energy of fluid piston oscillations, reducing effective power output of the engine, see Figure 4.37. Fluid piston oscillations with frequencies below 3 Hz were smooth, see Figure 4.38. The main reason for such behaviour was considered to be is that the mass of the water in the liquid piston was not sufficient to have necessary movement inertia.

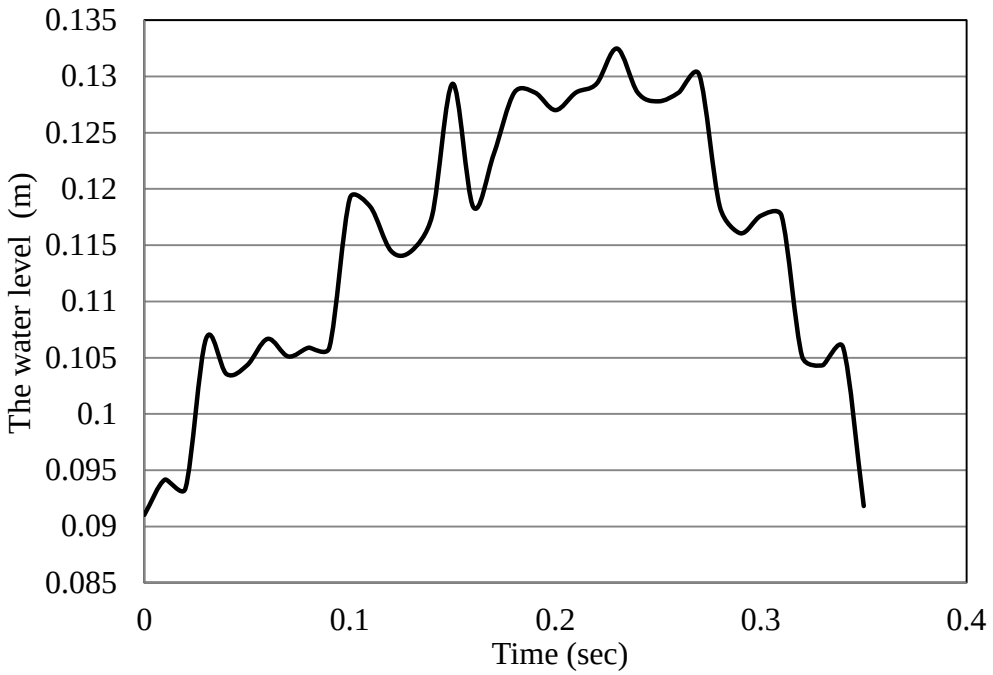

Figure 4.32 The water level oscillations in the cylinder of the engine

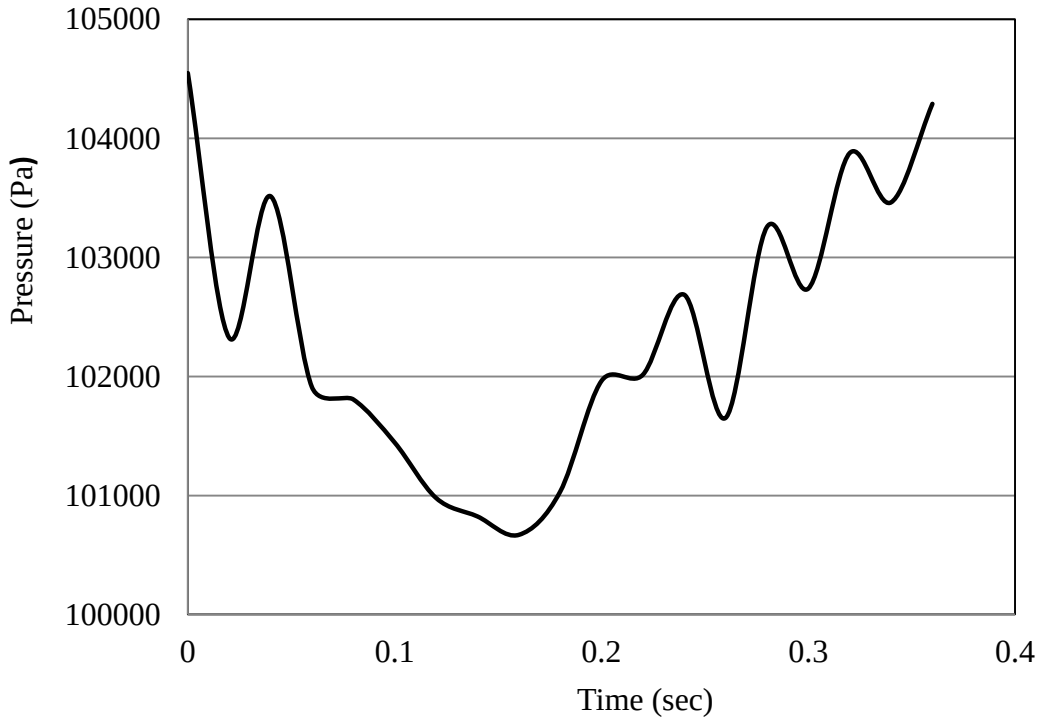

Figure 4.33 The air pressure in the engine part

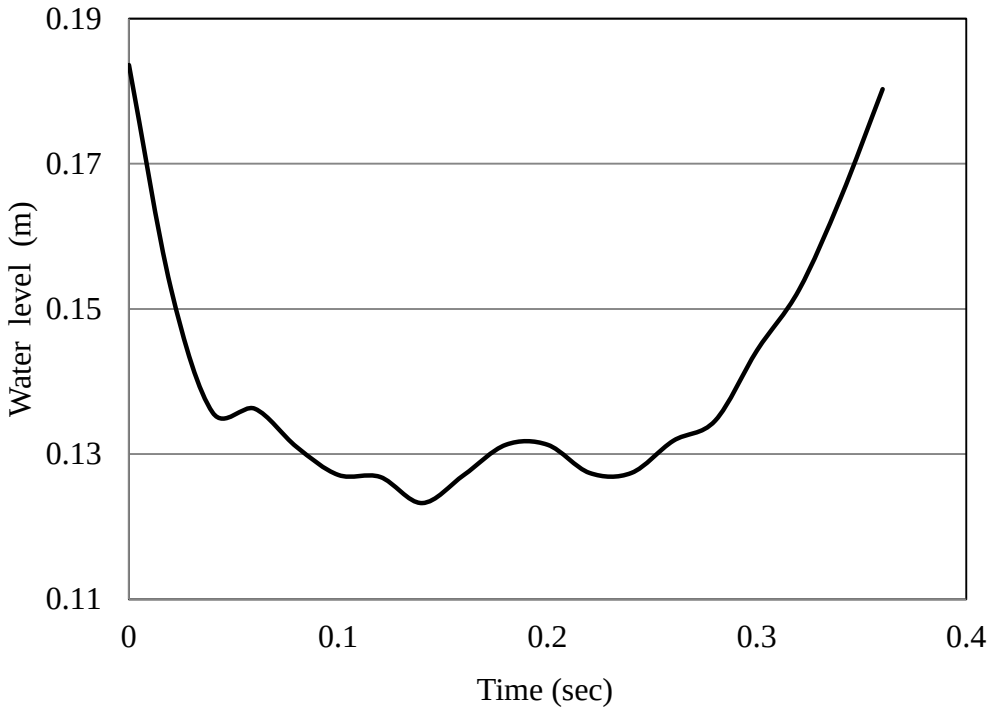

Figure 4.34 The water level in the cylinder of the cooling machine

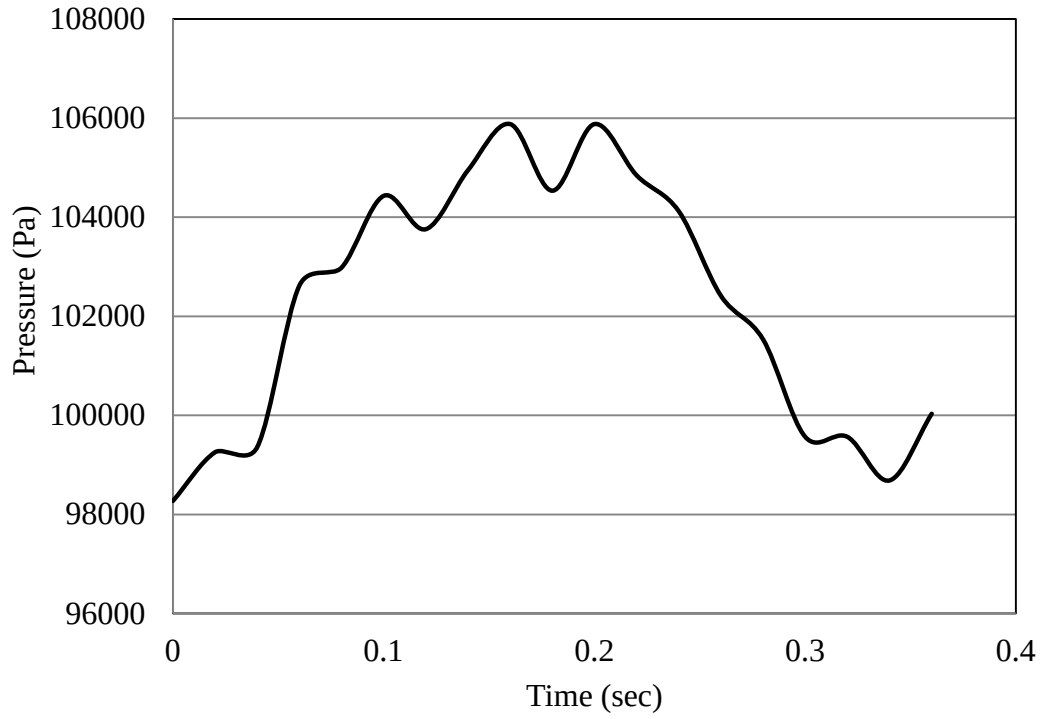

Figure 4.35 The air pressure in the cooling part

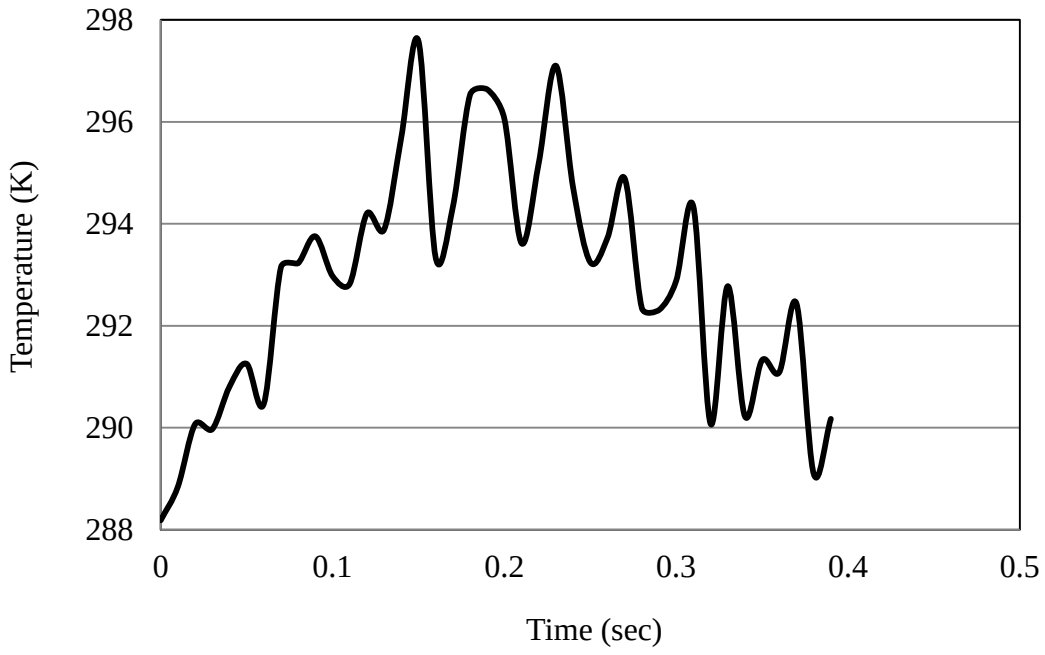

Figure 4.36 The air temperature variation in the cooling space of the first configuration of the system

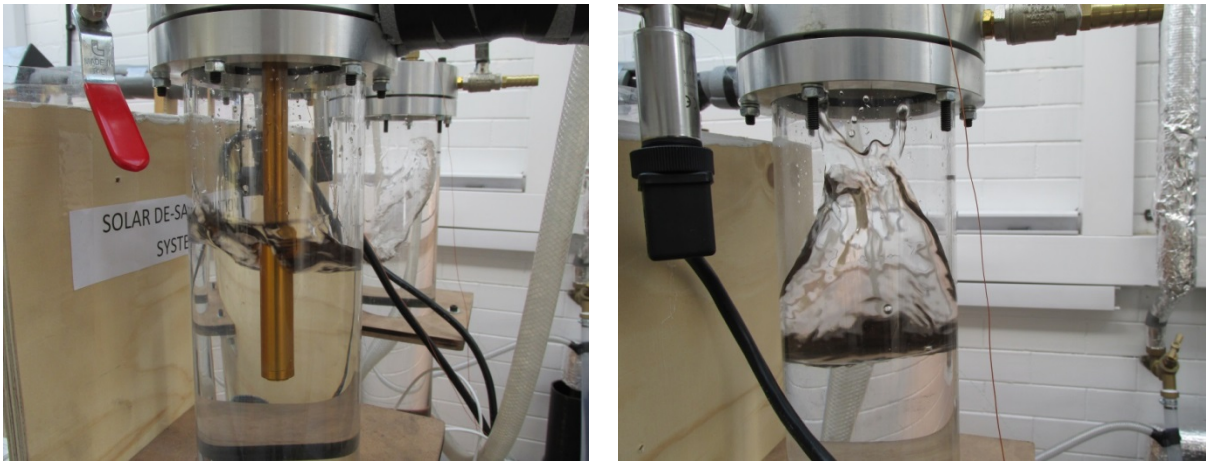

Figure 4.37 The liquid surface distortion during the liquid piston movement

Figure 4.38 The smooth oscillations of liquid piston

4.5.2 Experimental results for the second configuration

Figures 4.39 to 4.43 show experimental results obtain for the second configuration of the system. The variation in the water level in the engine cylinder over the cycle is shown in Figure 4.39. The fluid piston oscillates with a frequency of 2.5 Hz. The minimum value of water level is 9 cm, with the maximum level being 13.5 cm, with piston's stroke being 4.5

cm. The air pressure in the engine part varies between 92700 Pa and 104900 Pa, as shown in Figure 4.40.

On the cooling side of the system, the water level in the liquid piston cooling machine varies between 8.8 cm and 12 cm, with the stroke of the piston being 3.2 cm, see Figure 4.41. This change in the water level in the cooling machine cylinder generates an oscillation in the air pressure between 97700 Pa and 102000 Pa, as illustrated in Figure 4.42. Figure 4.43 shows the experimental results on the air temperature variation in the cooling space of the second configuration of the system.

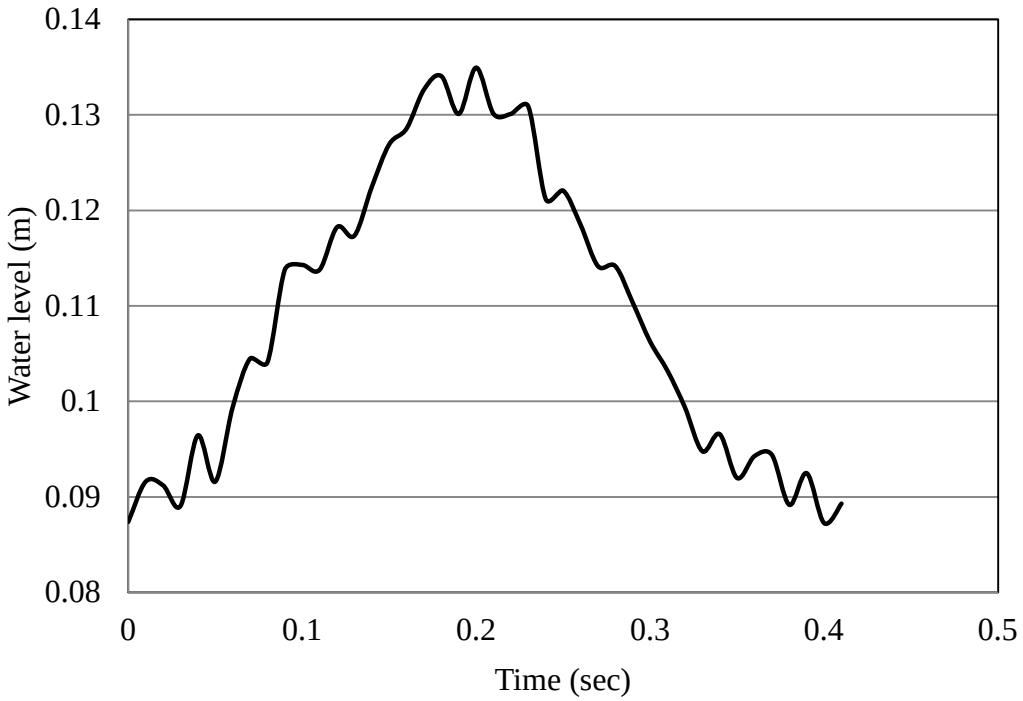

Figure 4.39 The variation of water level in the cylinder of the engine

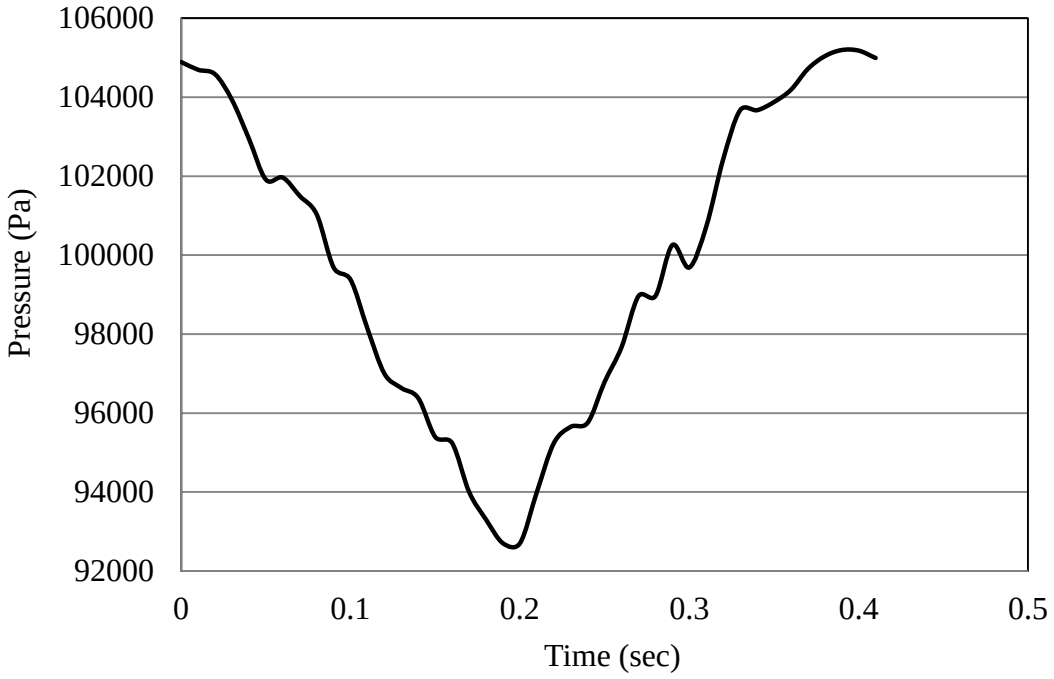

Figure 4.40 The air pressure in the engine part

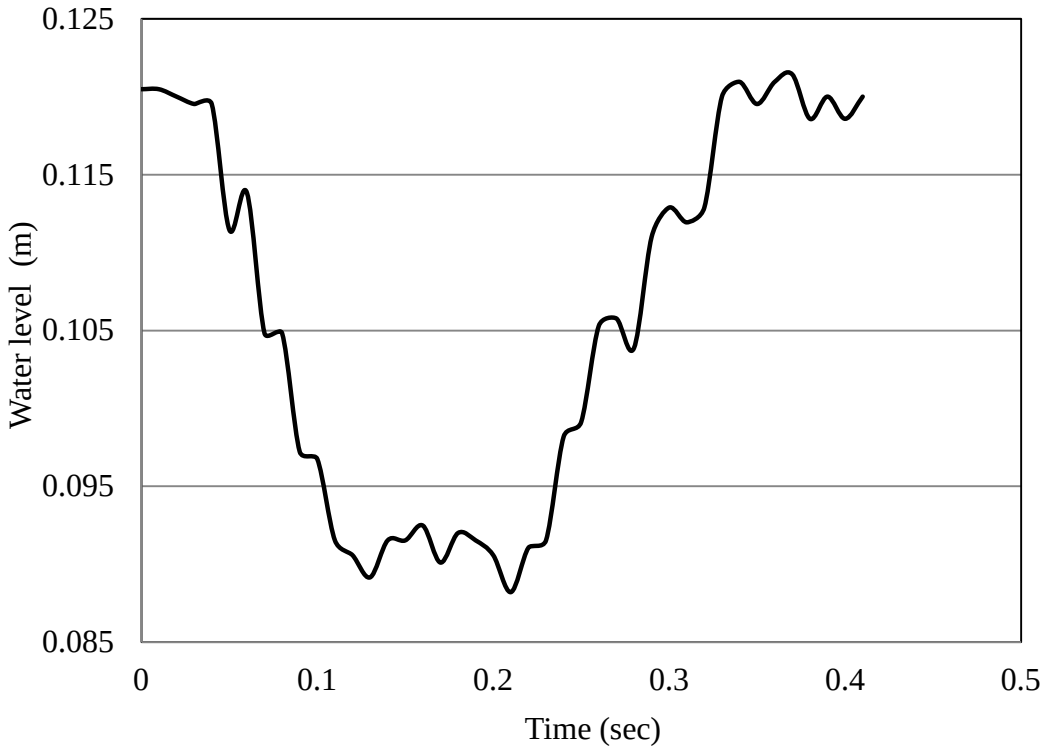

Figure 4.41 The water level in the cylinder of the cooling machine

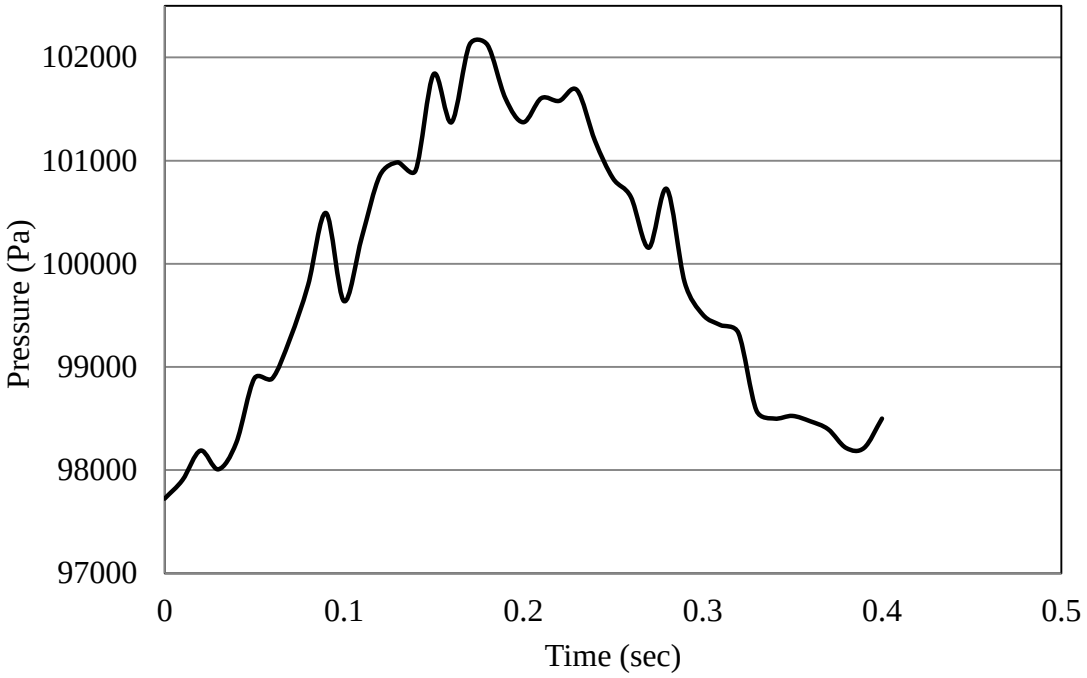

Figure 4.42 The air pressure in the cooling part

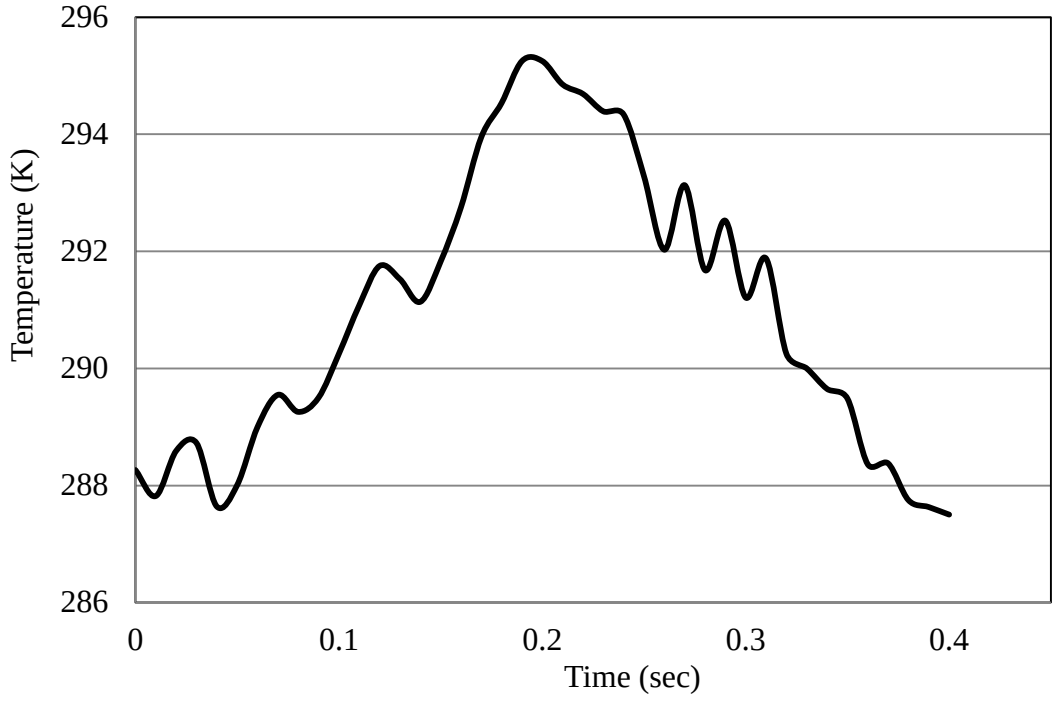

Figure 4.43 The air temperature variation in the cooling space of the second configuration of the system

4.5.3 Experimental results for the third configuration

As mentioned previously, the third configuration differs from the first and second configurations in that it does not have a separate liquid piston engine and cooling machine, but instead the water columns in the U-tube work as pistons for the above machines. Accordingly, the water level is recorded only in one water column and this is identical to the water level variation in another column of the U-tube pipe (in counter phase). The experimental results for such configuration are shown in Figures 4.44 to 4.47. The water level sensor has been installed in the U-tube on the cooling part and oscillations of the water level are illustrated in Figure 4.44. The frequency of oscillations is 3 Hz. The minimum value of the water level is 1 cm and the maximum value is 3.5 cm. The variation in the air pressure in the engine part is shown in Figure 4.45, and it varies between 104800 Pa and 107750 Pa. Figure 4.46 shows the air pressure variation in the cooling part it occurs between 99500 and 101700 Pa. The variation in the air temperature in the cooing space of the third configuration of the system is illustrated in Figure 4.47.

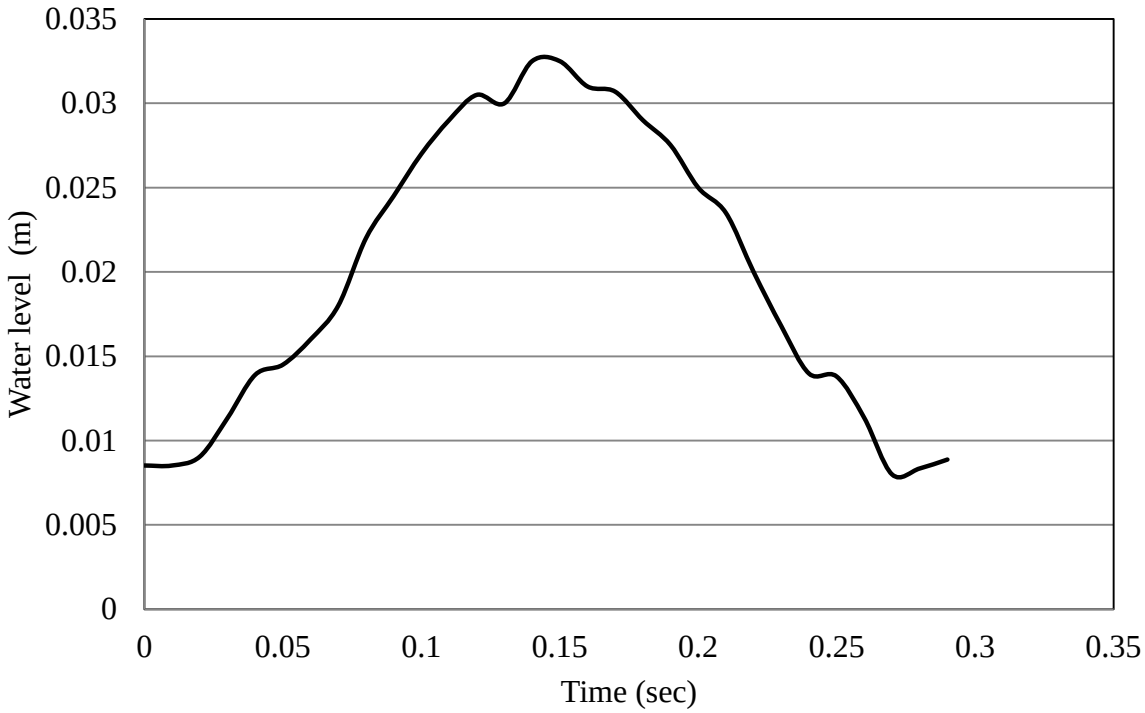

Figure 4.44 The amplitude of the water level in the cylinder of the cooling device

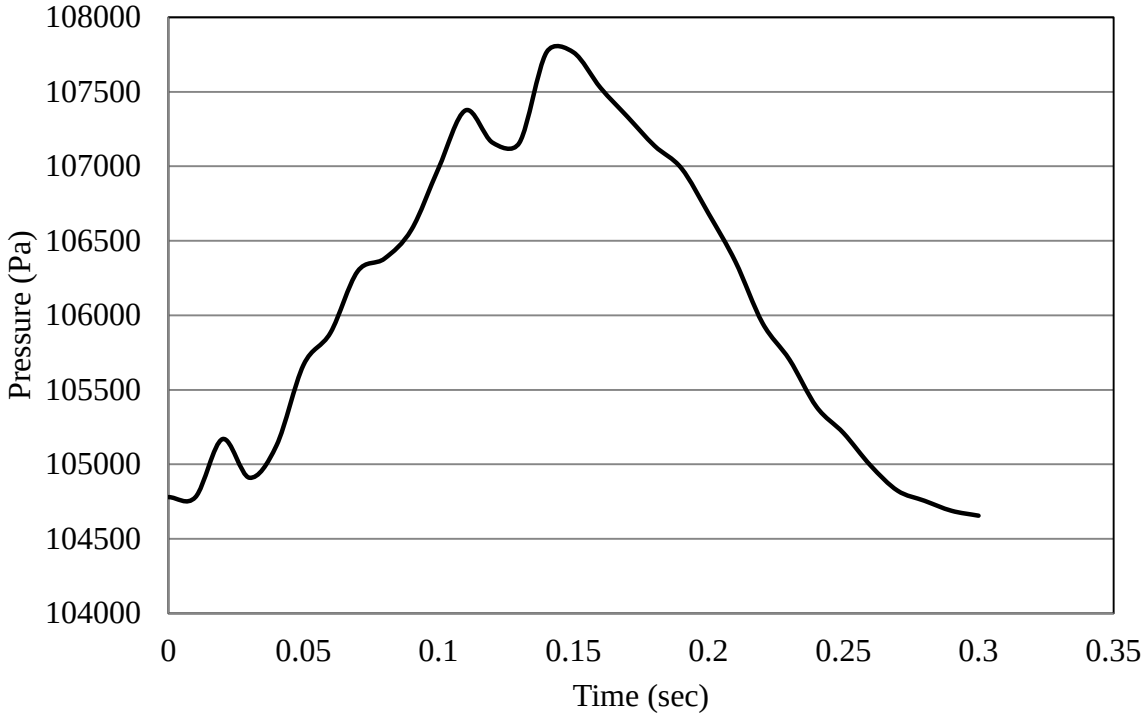

Figure 4.45 The air pressure in the engine part

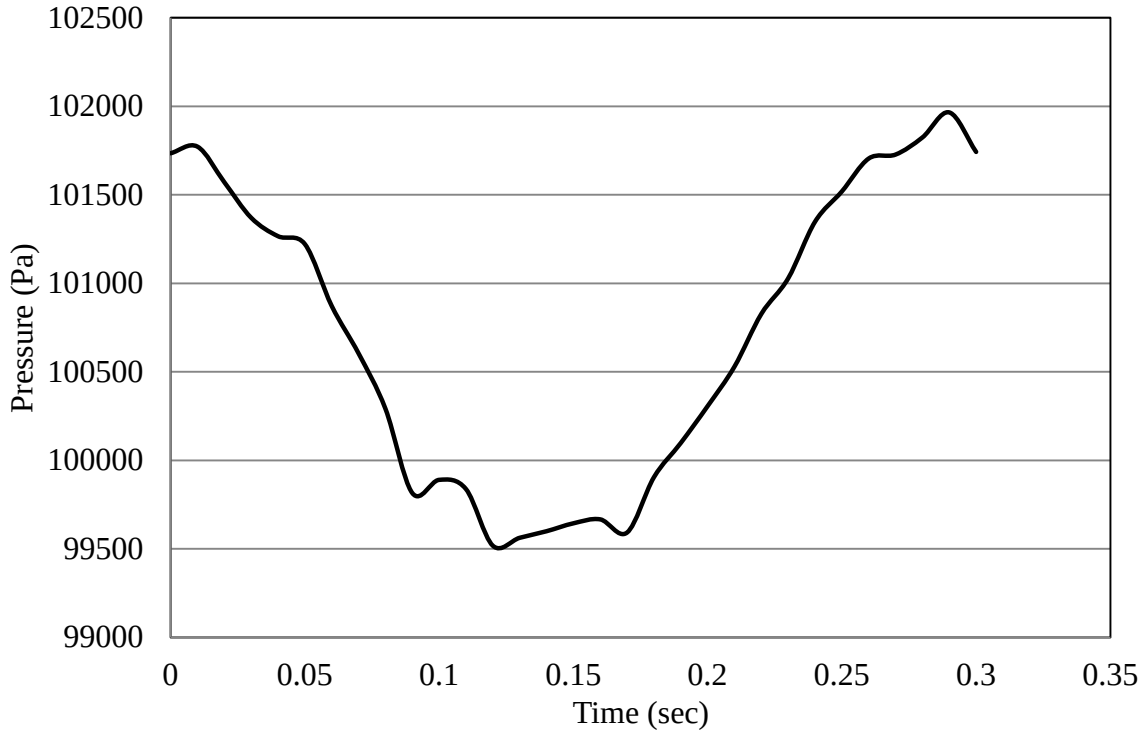

Figure 4.46 The air pressure in the cooling part

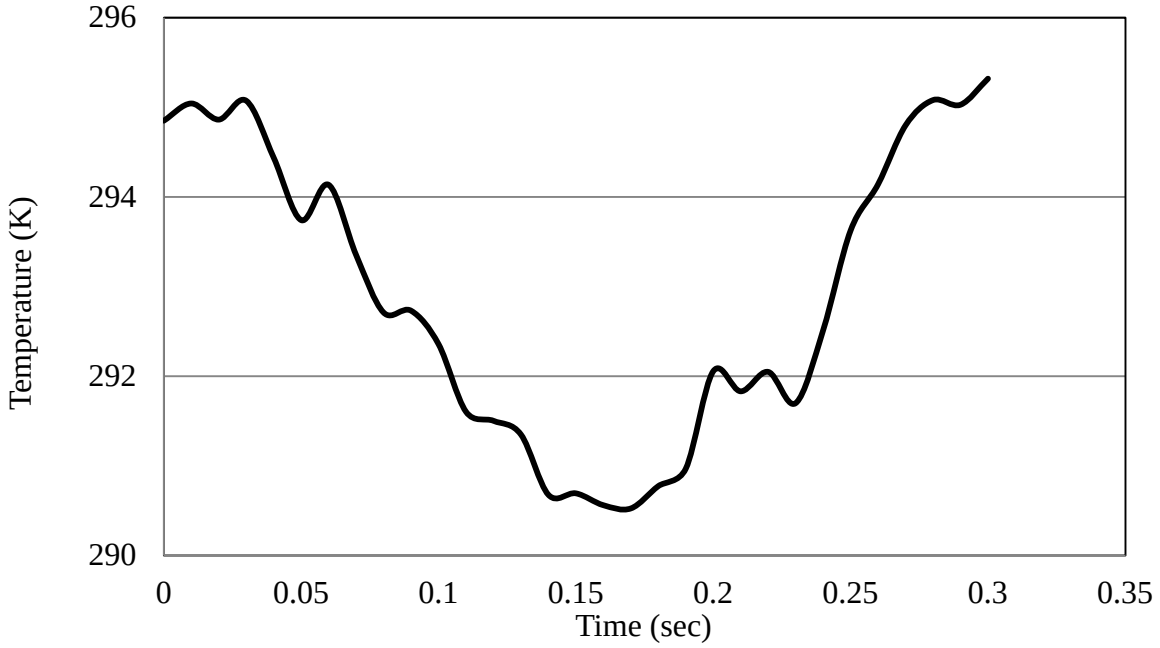

Figure 4.47 The air temperature variation in the cooling space of the third configuration of the system

4.6 Summary

In this chapter, three different configurations of dynamic solar cooling system prototypes have been introduced and tested experimentally. The test rig was for performing experiments was described together with three configurations of the system and instrumentation used for measurements. Examples of obtained experimental results on oscillations of water columns and variation of air pressure inside the engine and cooling parts are presented and discussed. The results showed that the oscillations of the liquid piston in the first configuration are less stable than in the second and third configurations.

Chapter 5 Development and Validation of the Whole System Mathematical Model

In Chapter 3, the mathematical model of the cooling part of the whole system was presented with the equation of the prescribed motion of the fluid piston in the cooling machine being used as an input parameter. In this Chapter the mathematical model of the whole system is described, consisting of equations describing the simultaneous and interconnected operations of the engine part and cooling part of the whole dynamic solar cooling system. Theoretical results obtained for operation of the whole system are validated using obtained expememntal data.

5.1 Development of simulation model

The Simulink model of the cooling part presented in Chapter 3 will be further developed for the second and the third configurations of the whole system. The first configuration of the system is not modelled due to the inferior performance of such system compared to others.

5.1.1 Mathematical Model of the Second Configuration System

Figure 5.1 shows the general schematic of the whole second configuration system containing both the engine and cooling parts. The engine part was previously simulated by Mahkamov and Belgasim[9, 167]. In the mathematical model the solar irradiance value will be used as the input and this value was assumed to be 700 W/m^2. Such the value of irradiance is the mean solar irradiation in a typical summer day in Benghazi city, Libya.

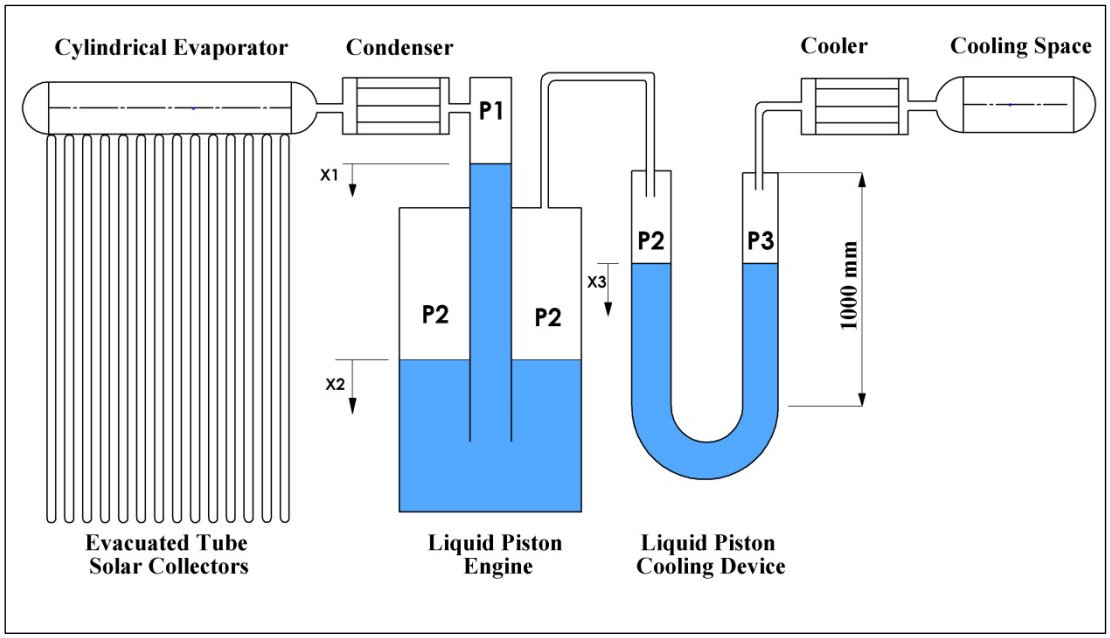

Figure 5.1 The second configuration of the solar cooling system

The operation of the whole plant can be described as follows. The system receives the heat through absorption of irradiation by the evacuated tube solar collector and transferring this heat to the water and air in the cylindrical evaporator. The water evaporates in the evaporator and this togeteher with heating up of air results in the pressure rise in the engine part. The evaporated steam then is condensed in the condenser and is eliminated from the cycle. The rise in the pressure results in the power stroke of the liquid piston and its returned to the initial position due to potential energy accumulated by the external water column in the engine part. The engine has a gas connection with the water column in the U-shaped pipe and pressure oscillations in the bouncing space of the engine part cause oscillations of the liquid piston in the U-shaped pipe. This oscillation of the liquid piston in the U-shape pipe drives the cooling cycle. The entire system works as a dynamic thermal oscillation system.

5.1.1.1 Description of the Mathematical Model for the second configuration system

5.1.1.1.1 The engine part

In the mathematical the engine part is divided into three control volumes, including an evaporator, condenser and liquid piston cylinder as shown in Figure 5.2. In this schematic indexes e, c and p correspond to the above three control volumes, respectively, whilst the two control surfaces between the three control volumes are denoted as ec and cp. The evaporator has a volume of two litres but it is normally half filled by water and the rest is occupied by air. The generation of saturation steam is a continuous process in the evaporator, therefore, in this control volume, and the working fluid in the model is assumed to be just the generated steam. In the control volume of the condenser, the working fluid consists of the mixture of the steam coming out from the evaporator and air. In the liquid piston engine, the working fluid is assumed to be only air because all the steam passing through the condenser is considered to be converted to the liquid water and collected in the water trap. Air and steam in the system are assumed to behave as an ideal gases. The fluid piston engine is considered as a mass-spring oscillating system with a rigid piston and a dumper. The displacement of the piston can be described by the Newton's second low with forces action on a rigid body with some mass due to pressure in the cycle, pressure in the bouncing space (spring) and in the damping device. By using such the calculation scheme, the lumped parameter mathematical model of the system can be described as a system of energy and the mass conservation equations, written for each control volume in the form of ordinary differential equations. By solving these equations, the information on the cyclic change of the air pressure in the system and air temperatures in each control volume can be found.

In the modelling process, the temperature in the evaporation space *Te* is assumed to be equal to the saturation temperature depending on the instantaneous pressure value in the system. Temperatures Tec and Tcp depend on the direction of the air flow.

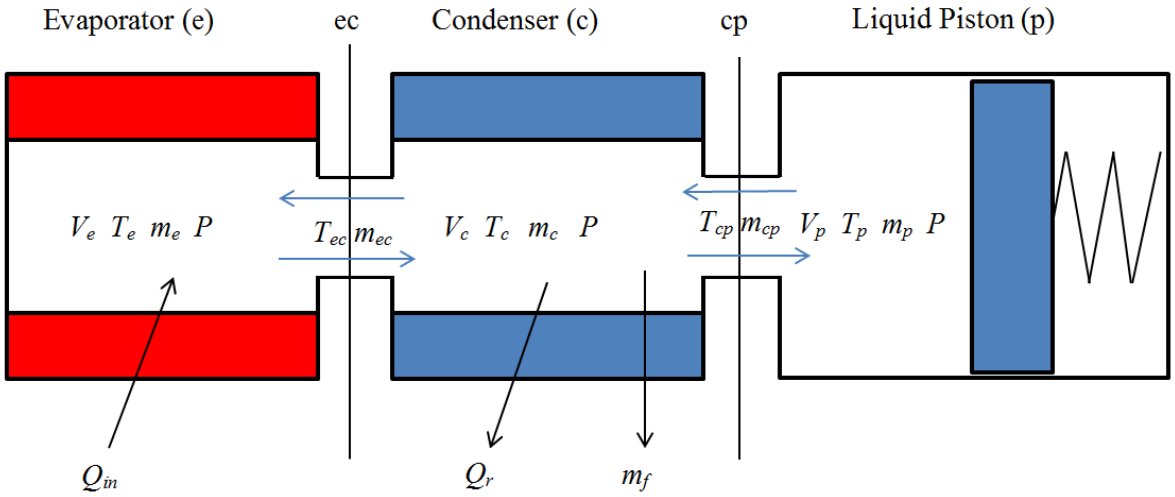

Figure 5.2 The calculation scheme of the engine part

The general form of energy conservation equation for a control volume could be written as [169]:

$$\dot{Q} + (C_p \dot{m} T)_{in} - (C_p \dot{m} T)_{out} = P\frac{dV}{dt} + C_v \frac{d}{dt}(mT) \tag{5.1}$$

5.1.1.1.1.1 Control volume of the evaporator

The space of the evaporator contains two different fluids, namely water and a mixture of steam and air. Therefore, the entire volume of the evaporator has been divided into two control volumes as shown in Figure 5.3.

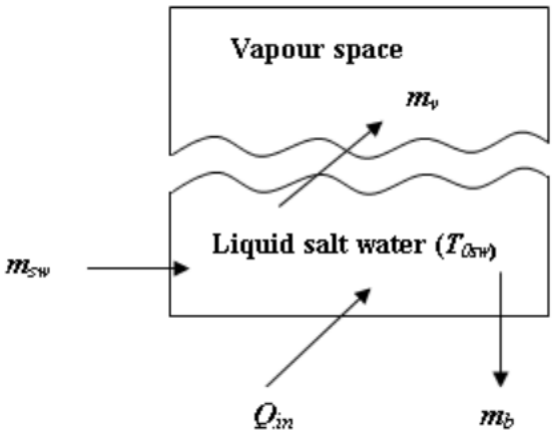

Figure 5.3 The control volume of the evaporator

Application of the energy equation (5.1) for the vapour space of the evaporator leads to the following equation:

$$\frac{V_e}{\gamma_v - 1}\frac{dP_1}{dt} = \dot{m}_v h_g - \dot{m}_{ec} h_g \tag{5.2}$$

where $\dot{m}_v$ is the vapour mass production rate inside the evaporator, $\dot{m}_{ec}$ is the vapour mass flow rate from the evaporator to the condenser, h_g is the enthalpy of the vapour, γ_v is isentropic index of vapour and P_1 is the vapour pressure in the engine part.

The mass balance equation for the vapour space is:

$$\frac{dM_e}{dt} = m_v - m_{ec} \tag{5.3}$$

In this equation m_v can be obtained from the energy equation of the liquid saline water in the evaporator:

$$m_v\left[h_{fg} - C_{psw}(T_{0sw} - T_{sat})\right] = Q_{in} \tag{5.4}$$

Here T_{0sw} is the boiling point of the saline water, which is assumed to be constant during the operation of the system. $T_{0sw} = 103$ °C.

5.1.1.1.1.2 Control volume of the condenser

For the control volume of the condenser, the energy equation takes the following form:

$$\frac{V_c}{\gamma - 1}\frac{dP_1}{dt} = \dot{m}_{ec}h_g - \dot{m}_f h_f - \left(\dot{m}_{cp}C_p T_{cp}\right)_v - \left(\dot{m}_{cp}C_p T_{cp}\right)_a - \dot{Q}_r \quad (5.5)$$

where $\dot{m}_f$ and h_f are the mass and enthalpy of the freshwater condensed, $\dot{Q}_r$ is the heat rejected from the working fluid in the condenser, Cp_v and Cp_a are the heat capacity of the water vapour and air, respectively, and the temperature of the working fluid in the condenser is T_c which is equal to saturation temperature.

The temperature of the control surface T_{cp} depends on the direction of the flow between the two control volumes and is:

$$T_{cp} = \begin{cases} T_c\,, & \dot{m}_{cp} > 0 \\ T_p, & \dot{m}_{cp} < 0 \end{cases} \quad (5.6)$$

The heat exchanged in the condenser, which is the concentric double pipe counter flow heat exchanger, is calculated by using the effectiveness-NTU method described in [170]:

$$\dot{Q}_r = \varepsilon \dot{m}_{cool} C_{pcool}(T_{sat} - T_{ci}) \quad (5.7)$$

In this equation ε is the heat exchanger effectiveness, $\dot{m}_{cool}$ and C_{pcool} are mass flow rate and heat capacity of cooling water in the water jacket, respectively, and T_{ci} is the inlet temperature of the cooling water.

$$NTU = \frac{UA_c}{\dot{m}_{cool}C_{pcool}} \quad (5.8)$$

where A_c denotes the contact surface area between the two fluids, and U is the overall heat transfer coefficient which is

$$U = \frac{h_o h_i}{h_o + h_i} \tag{5.9}$$

Here the outer and inner heat transfer coefficients h_o , h_i are the convective heat transfer coefficients on the condensation and water jacket sides, respectively.

$$h_i = 0.555 \left[\frac{g\rho_l(\rho_l - \rho_v)k_l^3 h'_{fg}}{\mu_l(T_{sat} - T_s)D} \right]^{1/4} \tag{5.10}$$

The term h'_{fg} denotes the modified value of the condensation heat:

$$h'_{fg} = h_{fg} + \frac{3}{8} C_{p,l}(T_{sat} - T_s) \tag{5.11}$$

The outer convective heat transfer coefficient h_o is usually determined as a function of Nusselt number *Nu* found from a heat transfer correlation [186]. This correlation is a function of the flow regime which depends on Reynolds number *Re* and Prandtl number *Pr*.

5.1.1.1.1.3 Control volume of the cylinder of the liquid piston engine converter

The energy equations for the cylinder of the liquid piston engine can be written as:

$$\frac{V_p}{\gamma - 1}\frac{dP_1}{dt} = \left(\dot{m}_{cp} C_p T_{cp}\right)_v + \left(\dot{m}_{cp} C_p T_{cp}\right)_a - \frac{\gamma}{\gamma - 1} P \frac{dV_p}{dt} - \dot{Q}_{loss} \tag{5.12}$$

where V_p is the volume of the cylinder, $\dot{Q}_{loss}$ is the heat exchanges between the cylinder and the surrounding.

To obtain the pressure variation inside the engine part, the equations (5.2), (5.5) and (5.12) are added and rearranged as

$$\frac{dP_1}{dt} = \frac{\gamma - 1}{V_t} \left[\dot{m}_v h_g - \dot{m}_f h_f - \frac{\gamma}{\gamma - 1} P \frac{dV_p}{dt} - \dot{Q}_r - \dot{Q}_{loss} \right] \tag{5.13}$$

where V_t is the total volume of the engine part:

$$V_t = V_e + V_C + V_p \tag{5.14}$$

As highlighted above, it was assumed that the whole amount of the steam is completely converted to liquid and no water enters the liquid piston cylinder.

5.1.1.1.1.4 Displacement of the liquid columns of the engine and cooling part

The relationship between water levels in the liquid piston engine during expansion and compression strokes are illustrated in Figure 5.4.

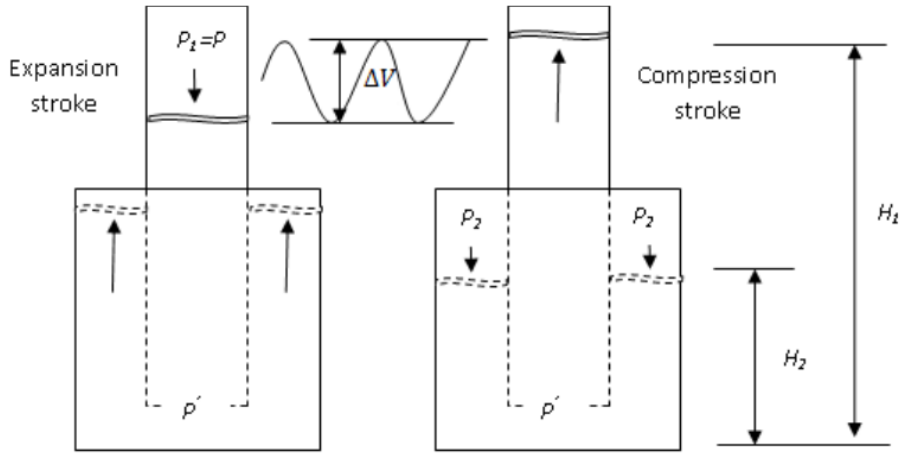

Figure 5.4 Fluid piston engine operation

In the engine, the equation of motion of the liquid piston can be written as

$$M_{lp1}\ddot{x_1} + C_1\dot{x_1} + (K_1A + 2A_1\rho g)x_1 = \Sigma pressure\ forces \quad (5.15)$$

where M_{lp1} is the mass of the liquid piston; K_1 and C_1 are the spring stiffness and damping coefficient, respectively, A_1 is the cross-sectional area of the cylinder; and x_1 is the displacement of the liquid column.

The pressure forces can be expressed as

$$\Sigma pressure\ forces = [P_1 + [(H_1 - H_2) - (1 + A)X_1]\rho g]A_1 \quad (5.16)$$

Here $A = \frac{A_1}{A_2}$, and $(H_1 - H_2)$ is the difference between the height of the water columns. The spring stiffness can be calculated as [165]:

$$K_1 = \frac{\gamma P_2 A_2^2}{(V_2 + V_3)} \tag{5.17}$$

where γ is isentropic index of vapour; A_2 and P_2 are the cross sectional area and the air pressure in the external cylinder, respectively. Also, the term $(V_2 + V_3)$ is the total volume of air in the external cylinder of the liquid piston engine and in the left branch of the liquid piston cooling device.

Accordingly, the displacement of the liquid piston cooling machine can be defined as:

$$M_{lp2}\ddot{x_3} + C_2\dot{x_3} + (K_2 + 2A_3\rho g)x_3 = (P_2 - P_3)A_3 \tag{5.18}$$

Here in the liquid piston cooling machine M_{lp2} is the mass of the water, x_3 is the displacement of the liquid column, A_3 is the cross sectional area, K_2 and C_2 are the spring stiffness and the damping coefficient, P_3 is the air pressure in the cooling part.

The spring stiffness in the cooling part can be written as

$$K_2 = \frac{\gamma P_3 A_3^2}{V_3} \tag{5.19}$$

5.1.1.1.2 The cooling part

The cooling part of the system is described schematically in Figure 5.5. From the figure, it can be seen that the cooling part is a reverse thermodynamic machine of the engine part. It consists of three control volumes, namely liquid piston cooling machine, cooler and cooling space. The pressure or piston oscillations generated in the engine part will drive the liquid piston of the cooling machine leading to variations in the air pressure and temperatures in the volumes of the cooling part. The cooler absorbs heat generated during the compassion of the air resulting in the production of the cooling effect in the cooling space.

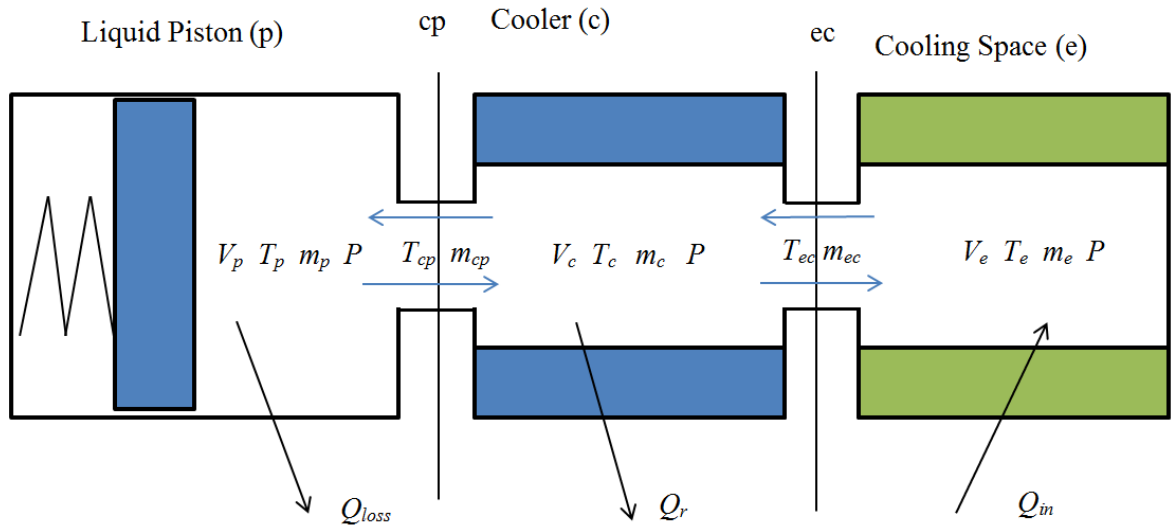

Figure 5.5 The calculation scheme of the cooling part

5.1.1.1.2.1 Control volume of the cylinder in the liquid piston cooling machine

By applying the general form of the energy equation (5.1), the energy equation for the cylinder is

$$\frac{V_p}{\gamma-1}\frac{dP_3}{dt} = \dot{m}_{cp}c_pT_{cp} - \frac{\gamma}{\gamma-1}P\frac{dV_p}{dt} + \dot{Q}_{losses} \tag{5.20}$$

Equation (5.20) is used to calculate the mass flow of air $\dot{m}_{cp}$ between the cylinder and the cooler. The temperature T_{cp} depends on the direction of the mass $\dot{m}_{cp}$:

$$T_{cp} = \begin{cases} T_c, & \dot{m}_{cp} > 0 \\ T_p, & \dot{m}_{cp} < 0 \end{cases} \tag{5.21}$$

5.1.1.1.2.2 Control volume of the cooler

The geometry and dimensions of the cooler are identical to that of the condenser in the engine part. The energy equation for the cooler can be written as

$$\frac{V_c}{\gamma-1}\frac{dP_3}{dt} = -\dot{m}_{cp}c_pT_{cp} + \dot{m}_{ec}c_pT_{ec} - \dot{Q}_r \tag{5.22}$$

The effectiveness-NTU method is used in order to calculate the heat rejected in the cooler [170]:

$$\dot{Q}_r = \varepsilon \dot{m}_{cp} C_p \left(T_{ci} - T_{cp}\right) \tag{5.23}$$

where the effectiveness ε is calculated from the formula

$$\varepsilon = \frac{1 - exp[-NTU(1-C)]}{1 - C * exp[-NTU(1-C)]} \tag{5.24}$$

In this equation:

$$C = \dot{m}_{cp} Cp_{air} / \dot{m}_{cl} Cp_{water} \tag{5.25}$$

$$NTU = \frac{UA_c}{\dot{m}_{cp} Cp_{air}} \tag{5.26}$$

5.1.1.1.2.3 Control volume of the cooling space

The cooling space has the same geometry and dimensions as that of the evaporator. For the control volume of the cooling part the energy equation is

$$\frac{\mathrm{V_e}}{\gamma - 1}\frac{\mathrm{dp}}{\mathrm{dt}} = -\dot{\mathrm{m}}_{\mathrm{ec}} \mathrm{c_p} \mathrm{T_{ec}} + \dot{Q}_{CS} \tag{5.27}$$

The air pressure in the cooling part of the system can be calculated by adding and rearranging the energy equations for the cylinder of the liquid piston cooling machine, the cooler and the cooling space:

$$\frac{\mathrm{V_t}}{\gamma - 1}\frac{\mathrm{dp}}{\mathrm{dt}} = -\frac{\gamma}{\gamma - 1}\mathrm{p}\frac{\mathrm{dV_p}}{\mathrm{dt}} + \dot{Q}_{losses} - \dot{Q}_r + \dot{Q}_{cs} \tag{5.28}$$

where V_t is the total air volume confined in the cooling space:

$$V_t = V_p + V_c + V_e \tag{5.29}$$

The temperature in each control volume can be calculated from the equation of state for the ideal gas:

$$T_p = \frac{PV_p}{R\ m_p} \tag{5.30}$$

$$T_c = \frac{PV_c}{Rm_c} \tag{5.31}$$

$$T_e = \frac{PV_e}{Rm_e} \tag{5.32}$$

The total mass of the air in the cooling part is a constant:

$$m_t = m_p + m_c + m_e \tag{5.33}$$

The exchanged masses between the control volumes are found as [171]:

$$\frac{dm_p}{dt} + \frac{dm_c}{dt} + \frac{dm_e}{dt} = 0 \tag{5.34}$$

Here the term $\frac{\mathrm{dm_p}}{\mathrm{dt}}$ and the term $\frac{\mathrm{dm_e}}{\mathrm{dt}}$ are defined as:

$$\left.\begin{aligned} \frac{dm_p}{dt} &= \dot{m}_{cp} \\ \frac{dm_e}{dt} &= -\dot{m}_{ec} \end{aligned}\right\} \tag{5.35}$$

Finally, the mass of air in the cooler can be calculated as

$$m_c = m_c^i + \frac{dm_c}{dt} * dt \tag{5.36}$$

where m_c^i is the mass of the air before the variation in the pressure and dt represents the time step in numerical integration of equations .

5.1.2 Description of the Mathematical Model of the third configuration of the system

The schematic of the third configuration of the system is shown in Figure 5.6. The only difference in this mathematical model, compared to the previous one is the displacement of the liquid piston, which is common for both engine and cooling parts.

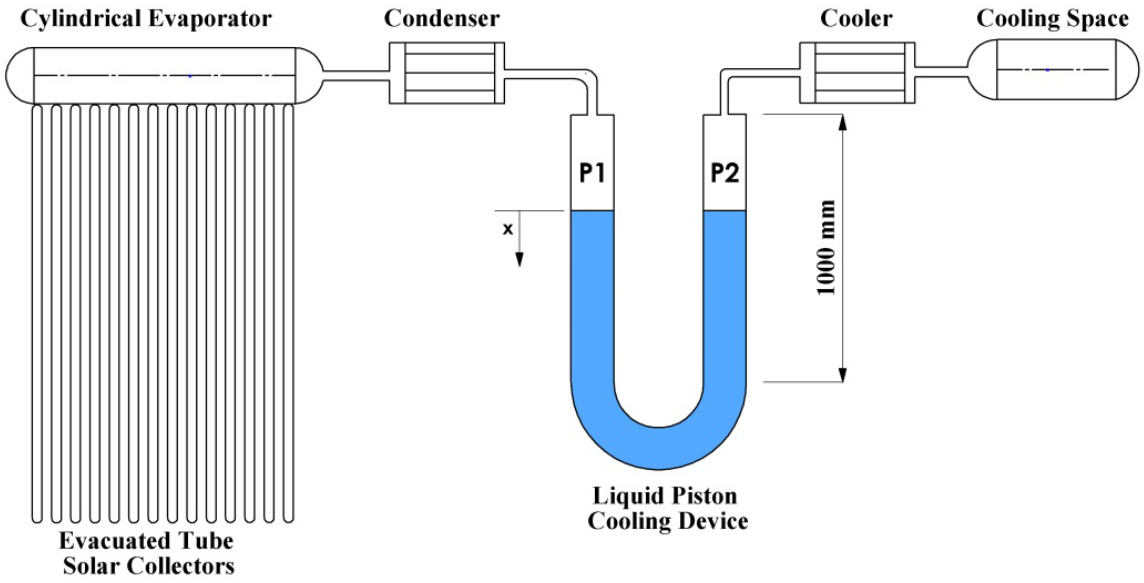

Figure 5.6 The third configuration of the solar cooling system

The displacement of the water level can be written as

$$M_{lp2}\ddot{x} + C_2\dot{x} + (K_2 + 2A_3\rho g)x = (P_1 - P_3)A_3 \tag{5.37}$$

where $\dot{x}$ is the displacement of the water level in the liquid piston cooling device. And the spring stiffness K_2can in the cooling part be calculated from the formula:

$$K_2 = \frac{\gamma P_3 A_3^2}{V_3} \tag{5.38}$$

5.2 Matlab/Simulink Developed Model

The equations described in the previous section were solved to simulate the operation of second and third configurations of the dynamic solar cooling system. The displacement of the water level of the liquid piston engine is considered as an input for the calculations of the cooling part. The equations of the mathematical models were solved using Simulink/Matlab environment.

Figures 5.7 and 5.8 show the Simulink model's interface for the second and third configurations of the system. It can be seen from these figures that the system is divided into separate blocks to simulate the whole cooling system. The solar radiation is input data an the value of 700 W/m^2 was used in simulations. The three first blocks simulate the engine part whilst the remaining four blocks simulate the cooling part. The results on pressure, temperature and volume variations are displayed and recorded by using scope blocks.

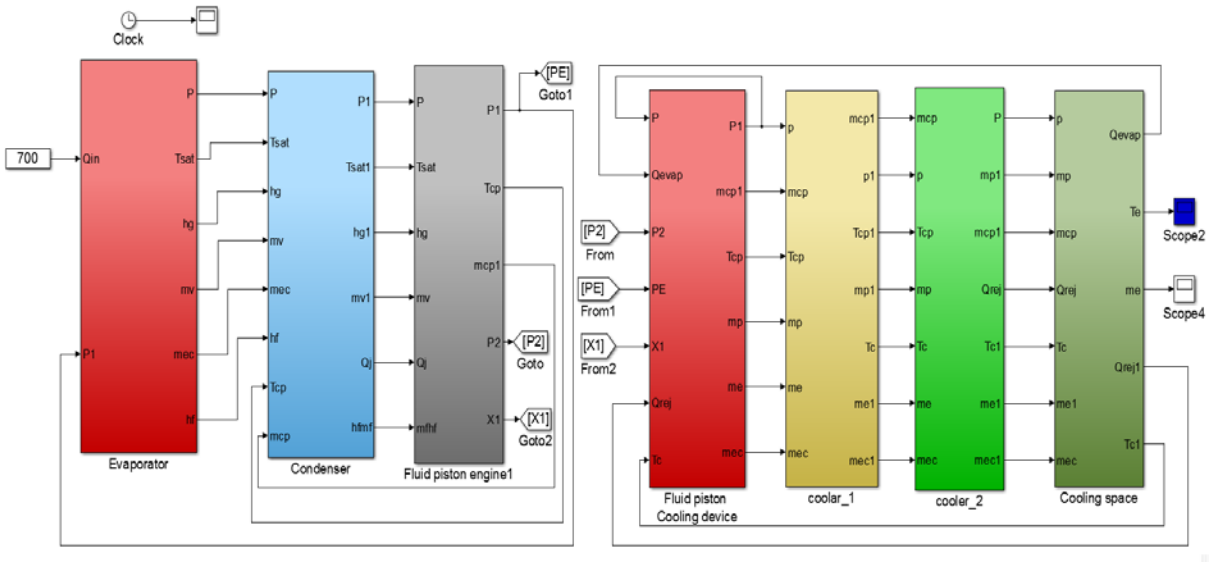

Figure 5.7 The Simulink model for the second configuration

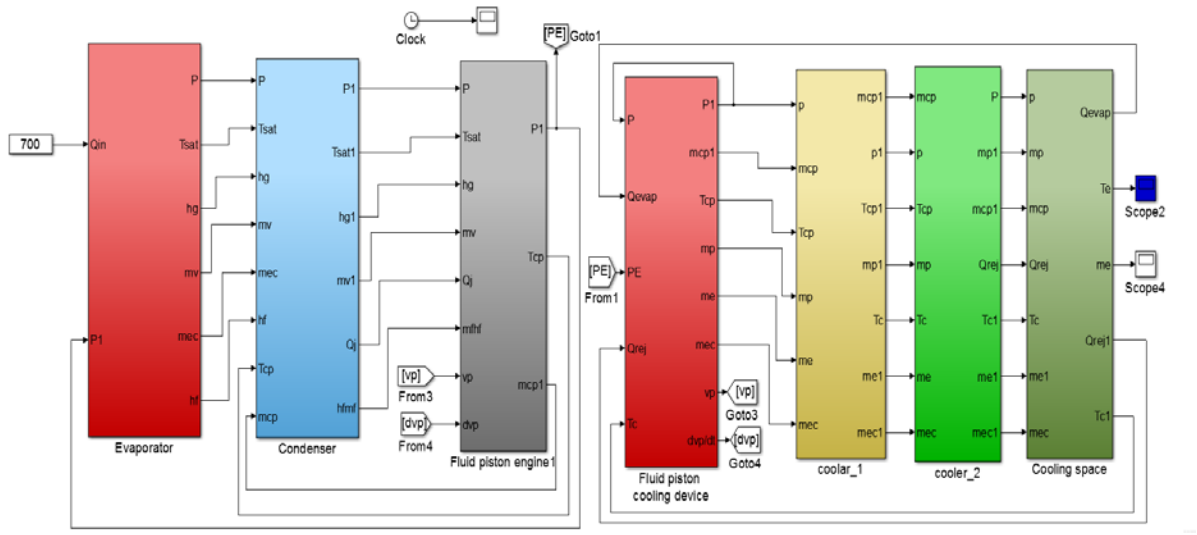

Figure 5.8 The Simulink model for the third configuration

5.3 Validation of Theoretical Results

The validation of the theoretical results is presented in this section. This is done by comparing the theoretical results obtained using the developed mathematical models to the experimental results obtained on the prototype in the laboratory. The comparison is performed in terms of water level displacements in the engine's and cooling machine's cylinders, pressures in the engine and cooling parts, air temperatures in the engine cylinder, cooling machine cylinder and in the cooling space. In the theoretical models, the design and working process parameters such as dimensions of the different components of the prototype, the dead volumes of the cylinders and the flowrates and inlet temepratures of the cooling water in the condenser and cooler were used the same as during the experiments.

5.3.1 Validation of theoretical results obtained for the second configuration

For the second configuration, Figure 5.9 shows a comparison between theoretical and experimental results on oscillations of the liquid piston in the engine over a period of one

cycle. It can be seen that both the theoretical and experimental results have the same frequency of 2.5 Hz. The maximum absolute value of the relative deviation between the two curves is 18.24% whilst the minimum relative deviation is 0.15%. The relative deviation is calculated according to the formula

$$deviation = \left|\frac{E - T}{E}\right| \tag{5.39}$$

For calculating the deviation in the temperature the following equation is used:

$$deviation\ (temp.) = 1 - \left|\frac{\Delta E}{\Delta T}\right| \tag{5.40}$$

where E is the experimental result and T is the corresponding theoretical result.

This deviation between the theoretical and experimental results caused by three main reasons including accounting for the heat losses in the prototype, low sampling rate of the level sensor and assumptions made in the model (such as that the air behaves as an ideal gas etc.). Although the experimental system is well insulated, there are still heat losses in the joints, adapters for installation of measuring sensors and from the aluminium flanges mounted on the top of the liquid pistons. This effect of the heat losses is neglected in the numerical model. The level sensor used in this study is the state-of-the-art with a sampling rate of 80 samples per second, but it still low value taking into account that the frequency of the liquid piston oscillations is about 3 Hz which means that every cycle only about 25 readings of the water level are taken during the cycle. The comparison between theoretical and experimental amplitudes of the water level in the cooling machine is demonstrated in Figure 5.10. In this figure, the maximum relative deviation is 21.5% while the minimum relative deviation is 0.08%. In Figures 5.9 and 5.10 it can be seen that the amplitude of the oscillations of the liquid piston in the engine is 7 cm while the amplitude of the water level oscillations in the cooling machine is 4 cm. This is because the diameters of the inner

diameter of the liquid piston engine and cooling machine are 8.5 cm and 10 cm respectively. Additionally, this reduction in the amplitude is a result of friction losses between the moving water column and the walls of cylinders.

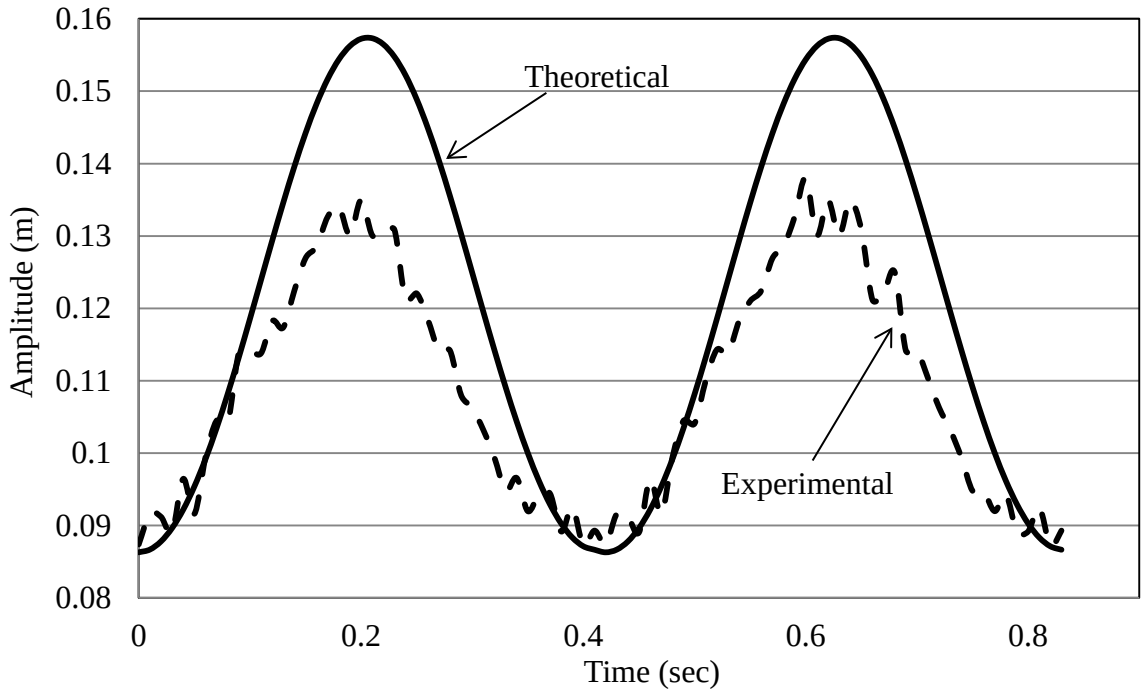

Figure 5.9 Comparison between theoretical and experimental amplitudes of the liquid piston engine

Figures 5.11 and 5.12 illustrate the variation in the operating pressure in the engine and cooling machine, respectively. The operating pressure in the engine varies between 104700 Pa and 92040 Pa. The pressure in the cooling part changes from 102230 Pa to 98835 Pa. The theoretical and experimental results on the pressure variations in the engine and cooling parts are in a very good agreement. The maximum relative deviation in results for the engine part is 3.07% and for the cooling part this value is 1.15%.

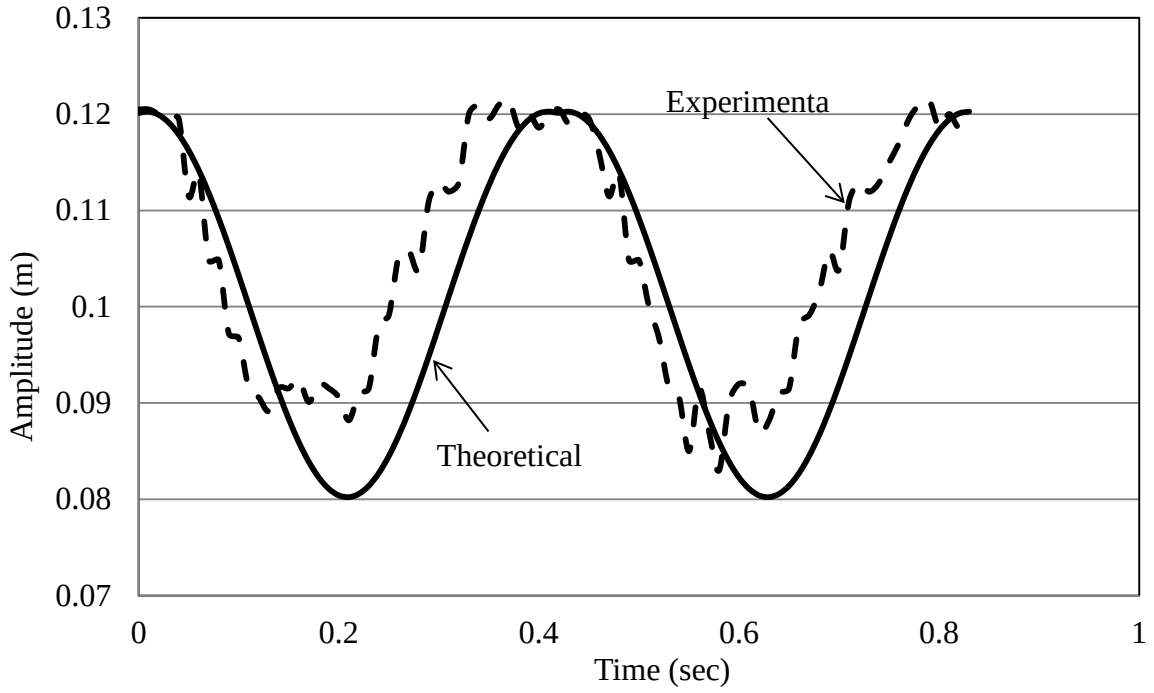

Figure 5.10 Comparison between theoretical and experimental amplitudes of the liquid piston of cooling machine

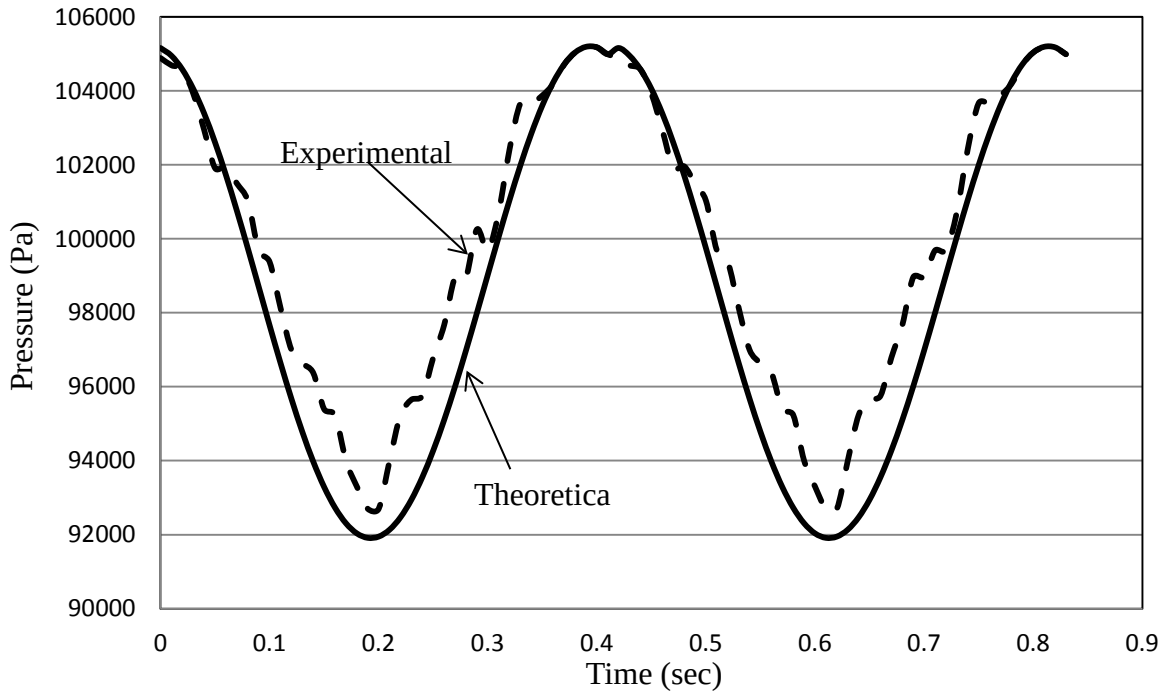

Figure 5.11 Comparison between theoretical and experimental pressure in the engine part

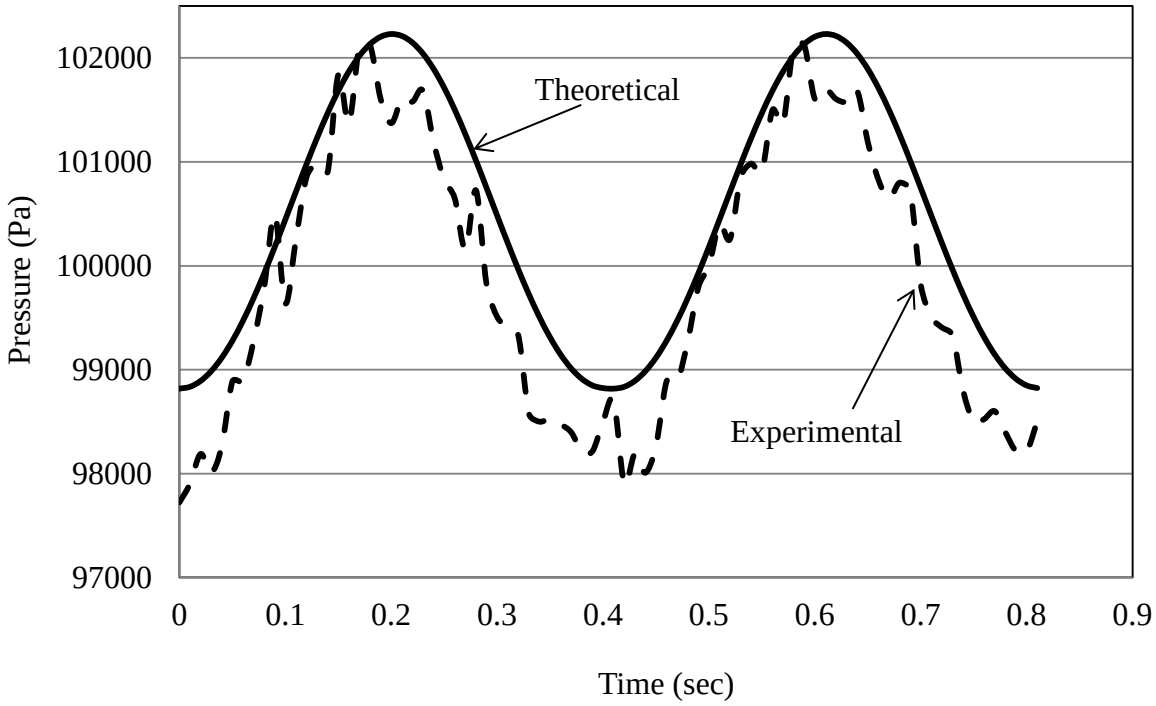

Figure 5.12 Comparison between theoretical and experimental pressure in the cooling part

The experimental and theoretical results on the temperature variation in the engine cylinder, in the cooling machine's cylinder and in the cooling space are shown in Figures 5.13, 5.14 and 5.15, respectively. The temperature in Figure 5.13 fluctuates between 358 K and 347 in numerical simulations and between 358 K and 350 K in the experiments the maximum deviation between these two curves is 27.2%. The deviation in this case is caused by the thermal inertia of the thermocouple, low sampling rate at 100 Hz and formation of the liquid film on the surface of the thermocouple. Consequently, the thermocouple is not able to record accurately the amplitude of the temperature oscillation in the cylinder and its phase angle. These fine thermocouples were used since hot wire sensor deployment was restricted by the wetness level in cylinders [187, 188]. In Figure 5.14, the comparison between theoretical and experimental results on the temperatures in the cylinder of the cooling machine is shown. The temperature varies between 294.3 and 290.8 K and the maximum

deviation between these two curves is 6.45%. Figure 5.15 shows the comparison between the theoretical and experimental results on the air temperatures variation in the cooling space. In this case the theoretical temperature varies between 296.8 and 287 K whilst the experimental temperature changes between 295 and 288 K. The maximum deviation between experimental and theoretical curves is 22.6%. It can be seen that the deviations between curves in Figure 5.14 and Figure 5.15 are lower than that in Figure 5.13 and this is because there is less or no formation of the liquid film on the surface of the thermocouple in the cylinder of the cooling machine and in the cooling space. Overall, both theoretical and experimental average temperatures in the cooling space are below than the inlet cooling water temperature in the cooler (about 293 K) and this demonstrate the production of the cooling effect in the system.

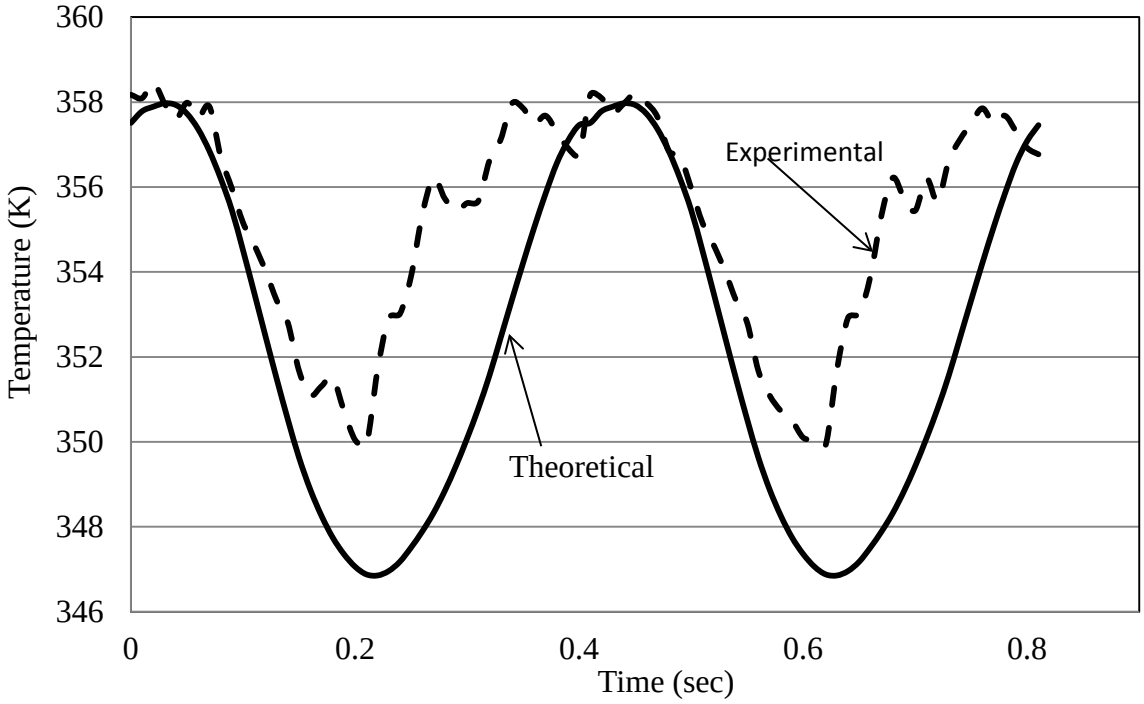

Figure 5.13 Comparison between theoretical and experimental results on the temperature in engine cylinder

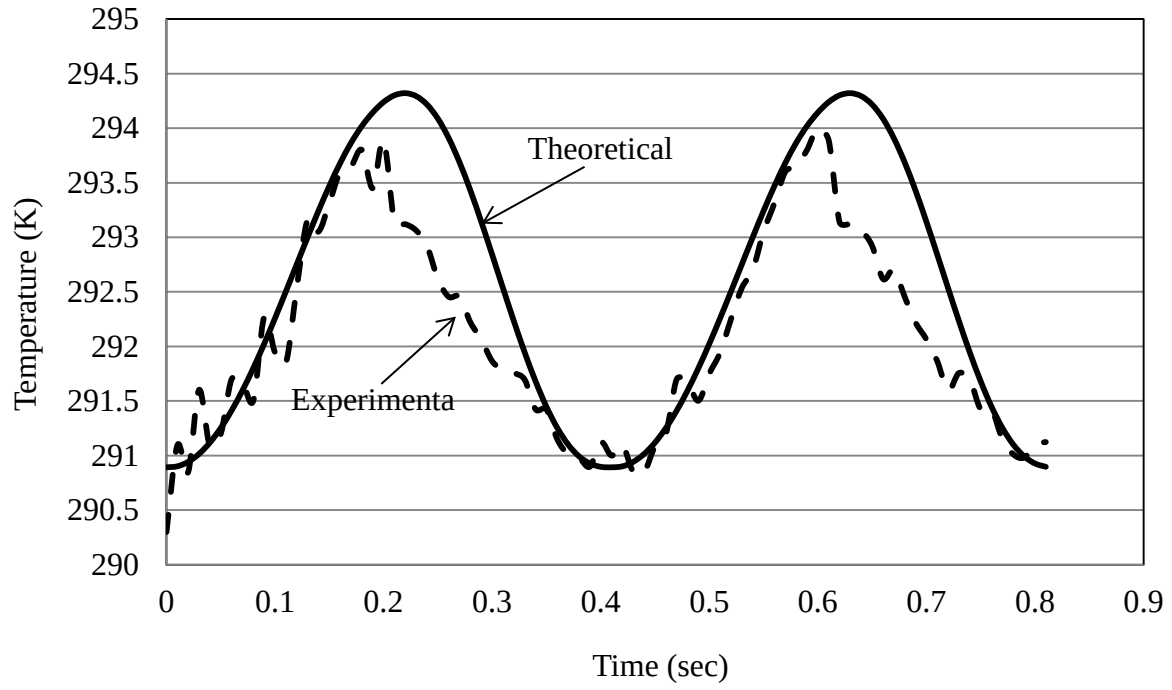

Figure 5.14 Comparison between theoretical and experimental temperature in the cylinder of the cooling machine

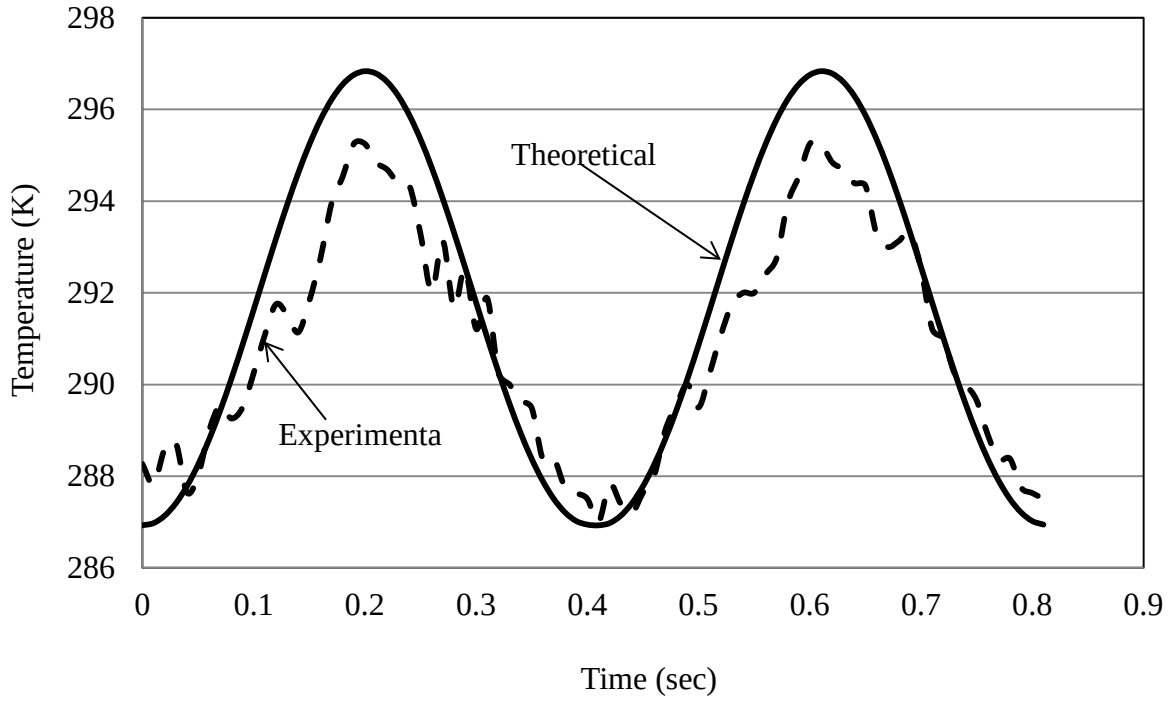

Figure 5.15 Comparison between theoretical and experimental temperature in cooling space

5.3.2 Validation of theoretical results obtained for third configuration

Figures 5.16 to 5.21 show the comparison between the experimental and theoretical results obtained for the third configuration of the system. A comparison between the theoretical and experimental results on the water level oscillations is demonstrated in Figure 5.16. It can be seen from the figure that the water level fluctuates with a stroke of about 2.5 cm and the maximum relative deviation in results is 27.02%. The stroke of the piston in this configuration is less than in the second configuration. On the other hand, the frequency in this configuration is 3 Hz which is 20% rise than in the second configuration. Experimental and theoretical results on the variation in the cyclic pressure in the engine part are shown in Figure 5.17, It can be seen that the maximum pressure value is 107800 Pa and the minimum pressure value is 104800 Pa. The maximum relative deviation between the experimental and theoretical results in this case is 0.48%. Figure 5.18 illustrates a validation of the numerical model in terms of pressure variation in the cooling part. Both theoretical and experimental curves oscillate between 102000 and 99500 Pa and the maximum relative deviation is 0.37%. Figures 5.19 to 5.21 show the comparison between the experimental and theoretical results on the temperature variations in the system. Figure 5.19 presents comparison of the theoretical and experimental temperature values in the engine cylinder. Theoretically, the maximum value of the temperature is 356 K. In the experimental results this value is 362 K and the maximum deviation between experimental and theoretical results is 37.5%.The minimum temperature in both experimental and theoretical results is 257 K. Again, the reasons for this difference in results are the thermal inertia of the thermocouple and formation of the condensation film on its surface. Figure 5.20 displays theoretical and experimental temperature variations in the cooling machine cylinder. The temperature varies between

297.2 and 291.3 K with a maximum deviation between these two curves is 22.7%. Figure 5.21 shows the temperature change in the cooling space which varies between 295 and 289.2 K with the maximum deviation is 13.4%.

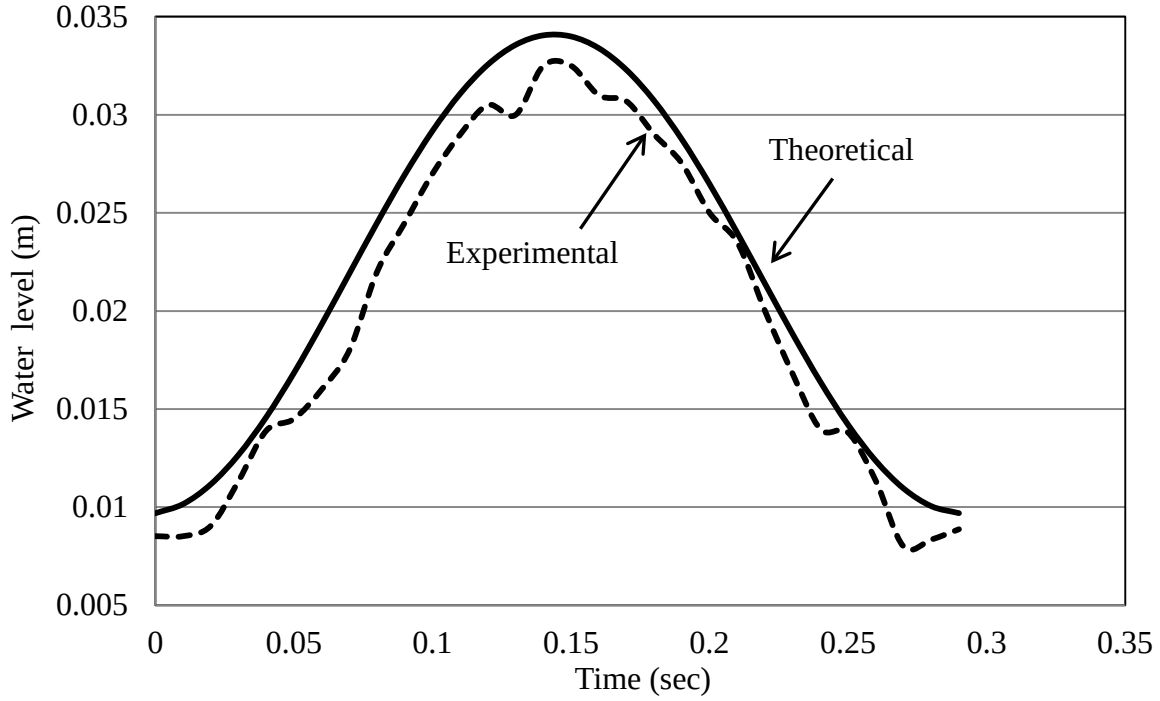

Figure 5.16 Comparison between theoretical and experimental amplitudes of the liquid piston

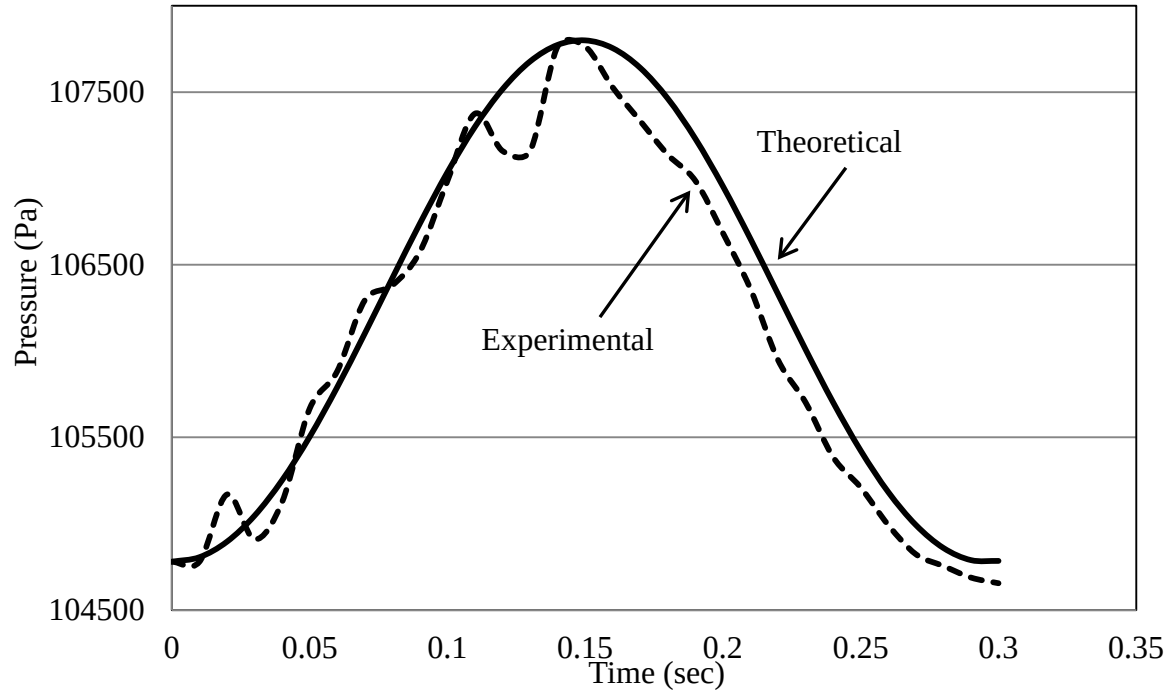

Figure 5.17 Comparison between theoretical and experimental pressure variation in the engine part

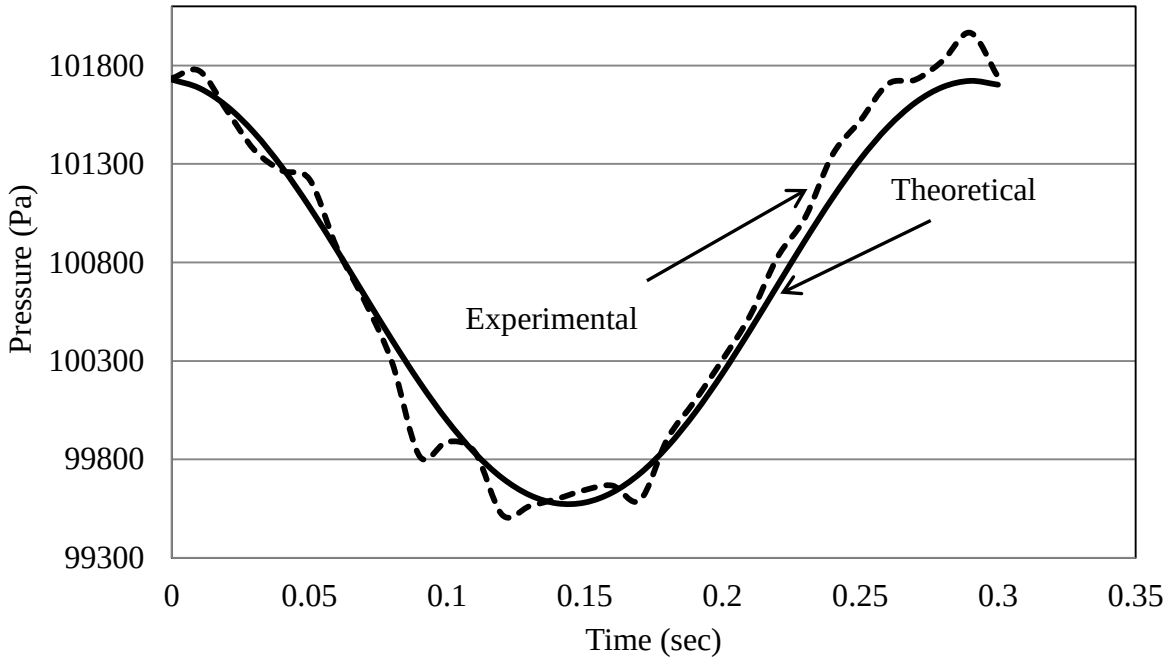

Figure 5.18 Comparison between theoretical and experimental pressure in the cooling part

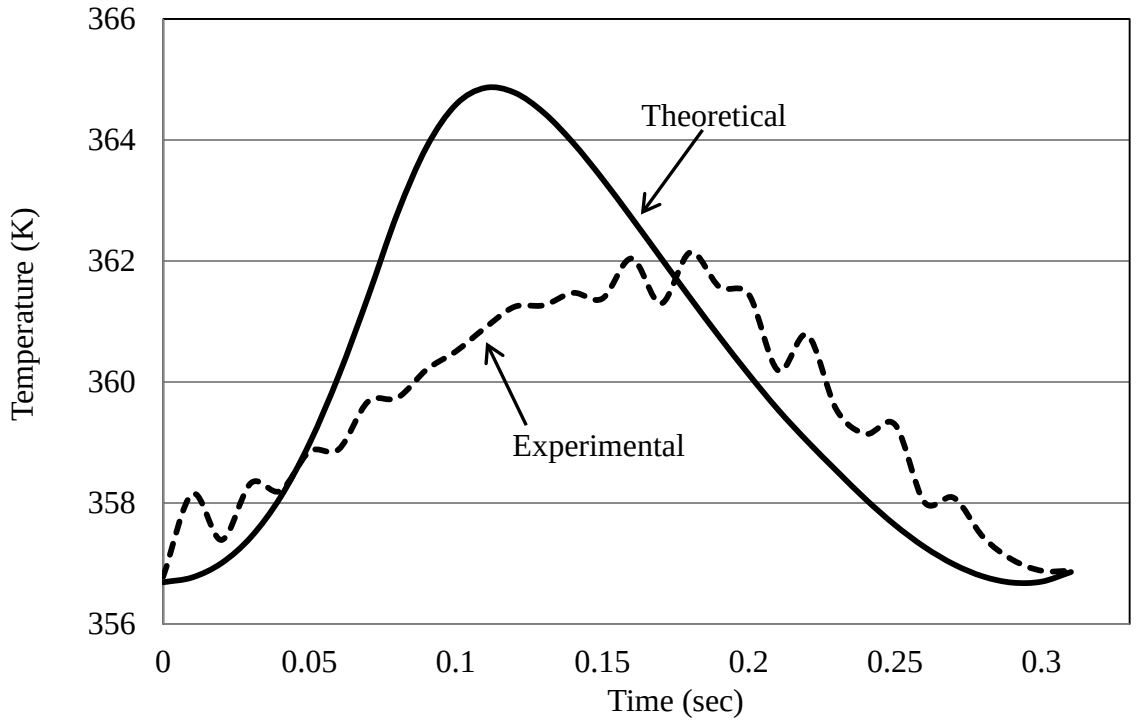

Figure 5.19 Comparison between theoretical and experimental engine cylinder temperature

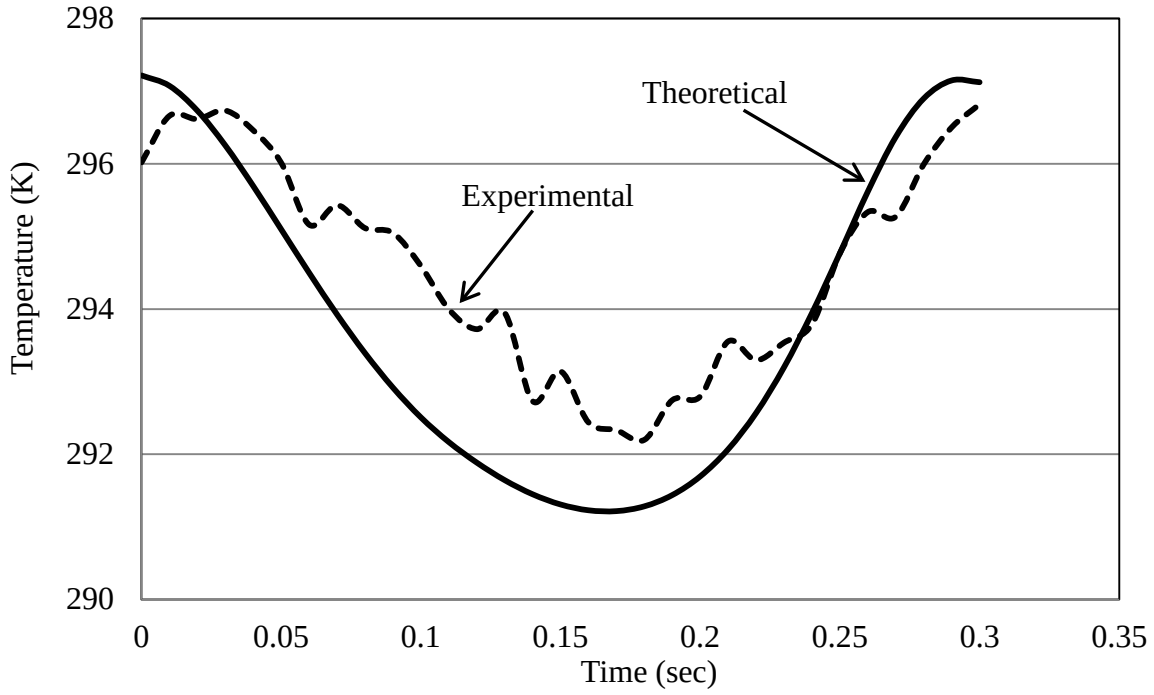

Figure 5.20 Comparison between theoretical and experimental cooling machine cylinder temperature

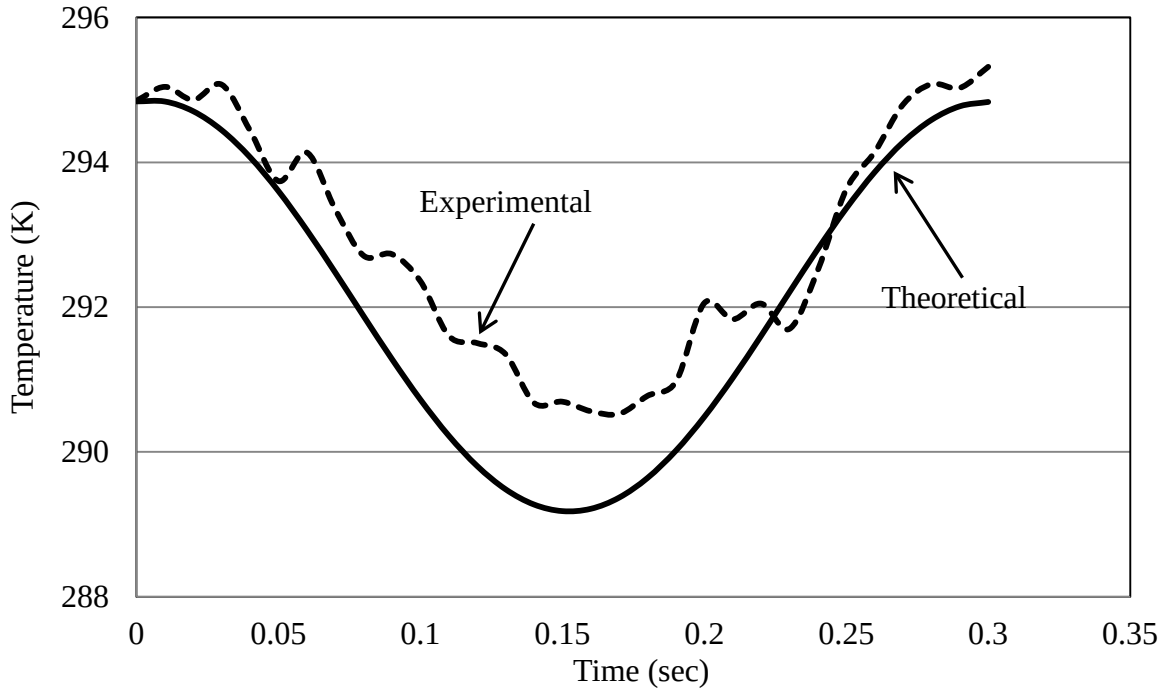

Figure 5.21 Comparison between theoretical and experimental cooling space temperature

In this case too both theoretical and experimental average temperatures in the cooling space are below than the inlet cooling water temperature in the cooler (about 293 K) and this demonstrate the production of the cooling effect in the system.

5.4 Summary

In this Chapter, the mathematical models were developed for the whole system, including both engine and cooling parts. The equations of mathematical models were solved in the Matlab/Simulink environment and obtained theoretical results were compared to that obtained in experiments. The investigation involved comparisons of the water level displacement in the engine cylinder and cooling device cylinder, the pressure in the engine part, the pressure in the cooling part, the air temperature in the engine cylinder, the air temperature in the cooling device cylinder and the air temperature of the cooling space. For the water level cylinders, the maximum relative deviation ranges between 18% and 27% for

the engine and cooling parts, respectively. The maximum relative deviation for pressure curves is between 3 and 1%. Overall, the accuracy of the developed mathematical models in prediction of the performance of the whole system is sufficient for caring out engineering calculations.

Chapter 6 Parametric Analysis of the Dynamic Solar Cooling System for Designing Purpose

This Chapter presents results of the detailed parametric analysis conducted on the third configuration of the dynamic solar cooling system. The effects of the heat input in the evaporator from the solar collector, cooling water temperature and cooling water flow rate on the performance of the unit are defined.

6.1 Introduction

Several operational parameters in the system affect the performance of the dynamic solar cooling unit. The design parametric analysis for the engine part was already conducted in [9] and this included the diameter of the cylinder of the liquid piston engine, the dead volume of the cylinder and the condenser length. Therefore, the focus in this Chapter is on the operational parameters, namely the heat input to the evaporator from the solar collector, cooling water temperature and cooling water flow rate. In previous investigations the constant values of the heat input to the system at 700 W, the cooling water temperature at 20 ^{o}C and the cooling water flow rate at 270 kg/hour were used in both numerical simulations and experiments. The theoretical parametric analysis was carried out using the developed mathematical model and by variation of above operational parameters.

6.2 The effect of the heat input to the evaporator

Figures 6.1- 6.5 show the effect of the heat input to the evaporator on the amplitude of the water level oscillations in the piston cylinder, the pressure in the engine part, the pressure in the cooling part, the air temperature in the cylinder of the cooling machine and the air temperature in the cooling space. The heat input to the evaporator directly influences the performance of the liquid engine in terms of its cooling capacity. The heat input to the system used for simulations was equal to 700, 800 and 900 W while the cooling water temperature was kept at 20 ^{0}C and the cooling water flow rate was fixed at 270 kg/hr. Figure 6.1 demonstrates that the amplitude of the water level remained approximately at the same value of 2.3 cm for the heat input values of 700 and 800 W. However at the heat input value of 900 W the amplitude increased to 2.8 cm. The frequency of the liquid piston oscillations decreased from 3 Hz at 700 W heat input to 2.8 Hz at 800 W heat input and to 2.3 Hz when the heat input was 900 W.

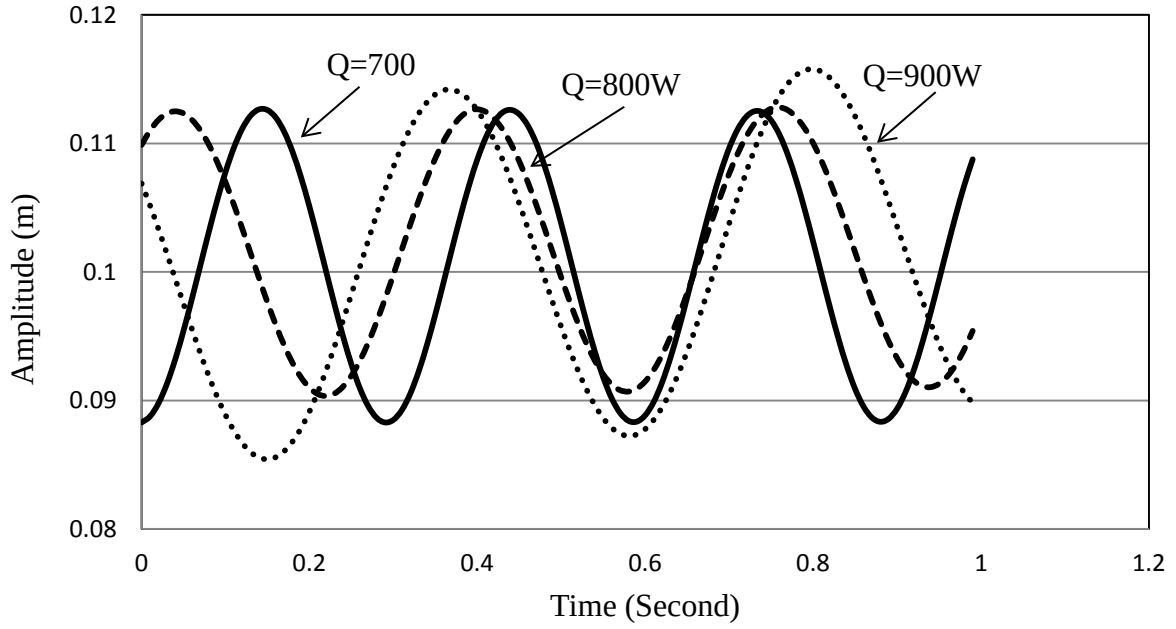

Figure 6.1 The effect of the heat input on the water level oscillations amplitude and frequency

The pressure variations in the engine and cooling parts are demonstrated in Figures 6.2 and 6.3. In these figures, it can be seen that the engine pressure increases with the increase in the heat input to the evaporator whist the pressure in the cooling part decreases. The values of the heat input to the evaporator of 700 W, 800 W and 900 W lead to average values of the engine pressure at 106410 Pa, 141080 Pa and 167560 Pa and average values of the cooling part pressure were 100670 Pa, 99870 Pa and 97420 Pa, respectively.

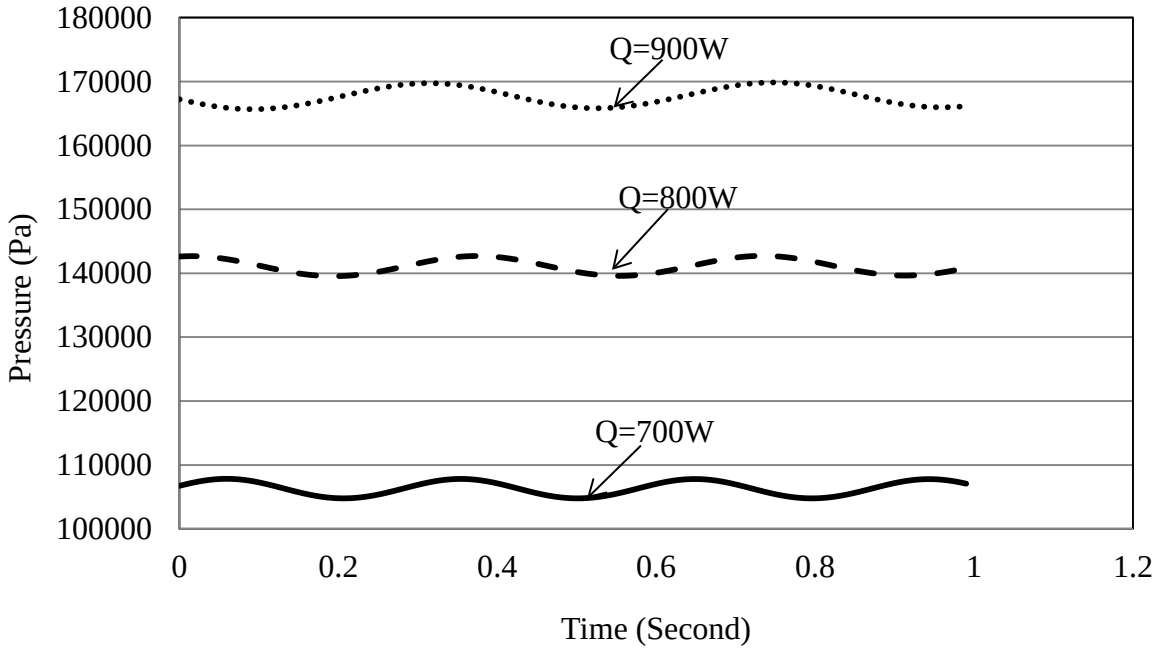

Figure 6.2 The effect of the heat input on the engine part pressure

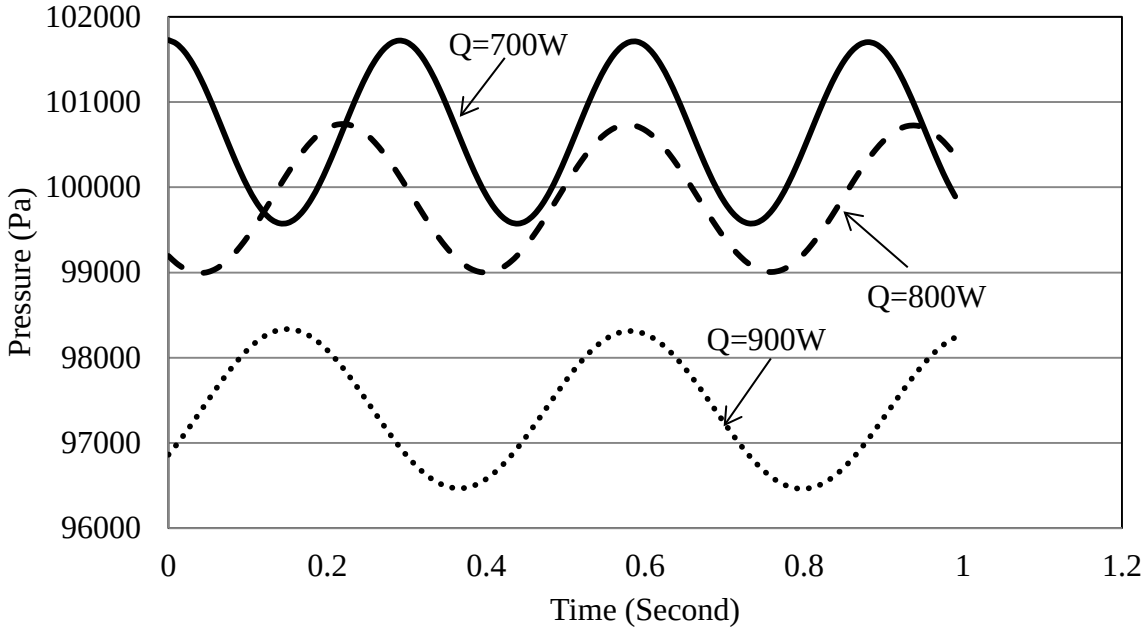

Figure 6.3 The effect of the heat input on the cooling part pressure

The effect of the heat input to the evaporator on the air temperature in the cooling cylinder is shown in Figure 6.4. The increase in the heat input causes a decrease in the air temperature in

the cooling cylinder which occurs as a result of the decrease in the cooling part pressure. The average values of the temperature of air in the cooling cylinder are 293.8 K for the heat input of 700 W. This value decreases to 291 K when the heat input is 800 W and becomes 289 K when the heat input is 900 W. The same trend can be seen in Figure 6.5 which shows the effect of the heat input on the temperature in the cooling space. The figure demonstrates that the temperature of the cooling space decreases with the increase in the heat input to produce an increasing cooling effect in the cooling space. The average temperature of the air in the cooling space decreases from 291.8 K at the heat input value of 700 W to 289.7 K at the heat input of 800 W. In the case of the heat input at 900 W, the air temperature in the cooling space lowers to 282 K.

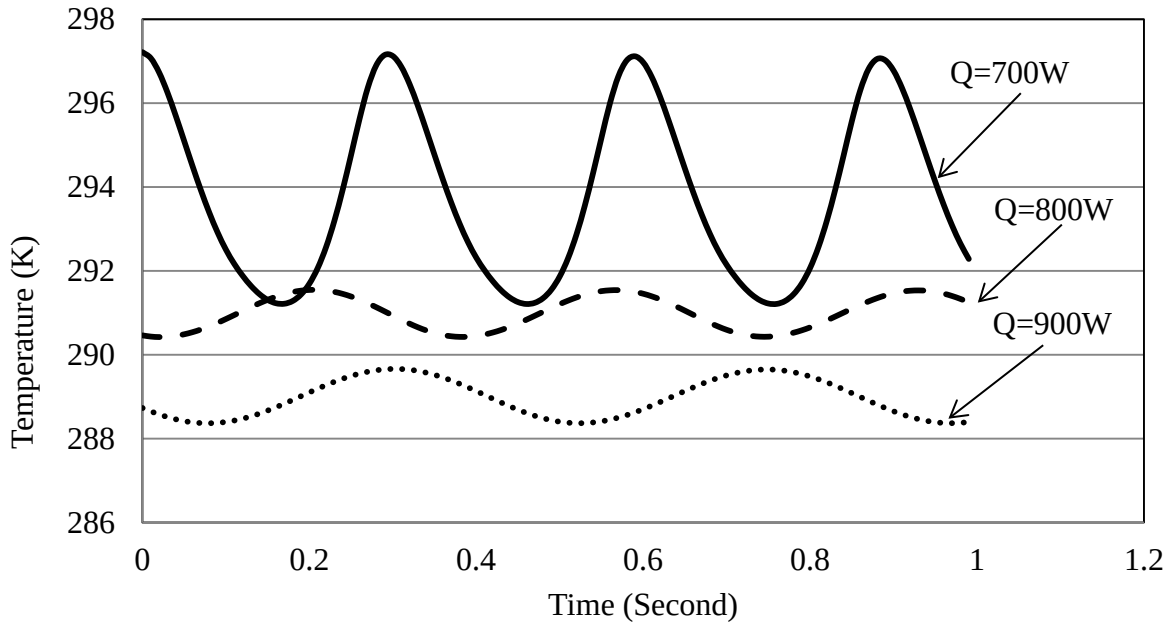

Figure 6.4 The effect of the heat input on the air temperature in the cooling cylinder

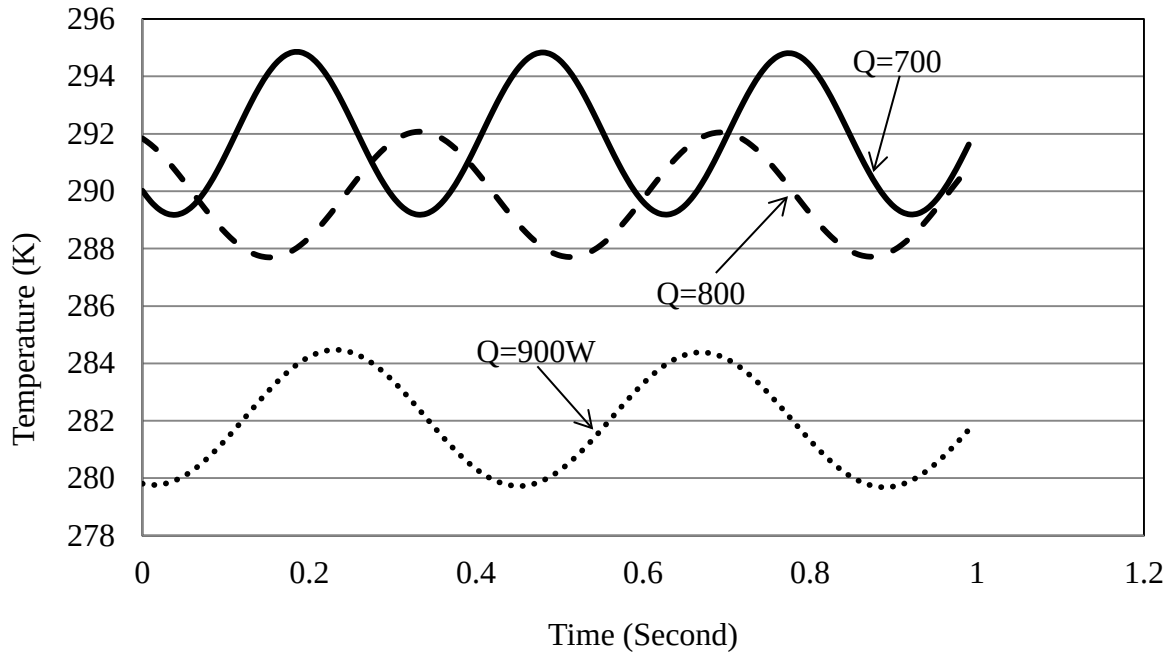

Figure 6.5 The effect of the heat input on the air temperature in the cooling space

6.3 The effect of the cooling water temperature

The cooling water temperature in the cooler affects the heat rejected from the cycle in the cooling part, which consequently changes the performance of the cooling unit. In this section, the effect of the cooling water temperature is investigated and three value of this temperature were considered, namely 20, 15 and 10 ^{o}C. The temperature of the cooling water in the condenser, which is the heat sink in the engine part, was kept at the constant level at 20 ^{o}C. Figures 6.6- 6.10 show the influence of this parameter on the amplitude of the water level oscillations in the cylinder, the pressure in the engine part, the pressure in the cooling part, the air temperature in the cylinder of the cooling part and on the air temperature in the cooling space. The values of the heat input to the evaporator and the cooling water flow rate were kept constant at 700 W and 270 kg/hr.

The effect of the cooling water temperature on the amplitude of the water level oscillation in the cylinder is shown in Figure 6.6. It can be seen that the amplitude of the water level oscillations has the same value of 2.5 cm and the same frequency of 3.3 Hz for all the three cooling water temperature in the cooler. This is because the cooling water temperature in the condenser is kept constant.

The effect of the cooling water temperature on the engine pressure is demonstrated in Figure 6.7. The engine pressure decreases with the decrease in the cooling water temperature in the cooler. The figure demonstrates that the average values of the engine pressure are 106410, 106100 and 105770 Pa when the cooling water temperature is 20, 15 and 10 °C, respectively.

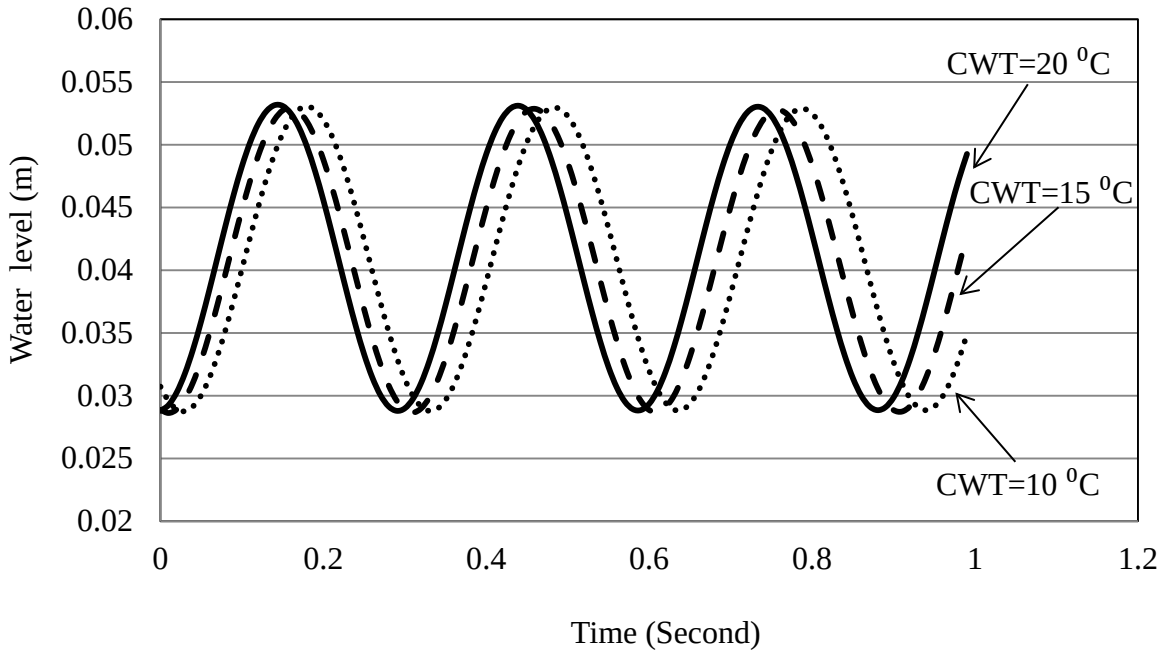

Figure 6.6 The effect of the cooling water temperature in the cooler on the liquid piston amplitude in the engine

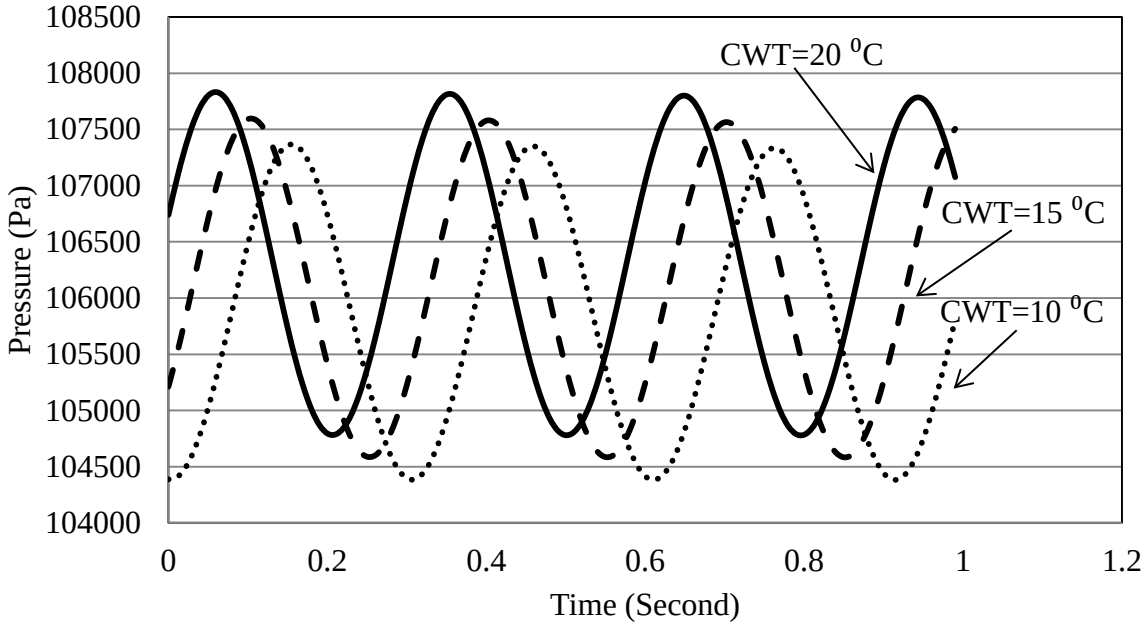

Figure 6.7 The effect of the cooling water temperature on the engine pressure

The cooling water temperature has the same influence on the pressure of air in the cooling part as shown in Figure 6.8. The cooling part pressure decreases with the reduction of the cooling water temperature. The average value of the pressure in the cooling part is 100670 Pa for the cooling water temperature of 20 ^{o}C. When the cooling water temperature is 15 ^{o}C, the average value of the pressure in the cooling part is 99080 Pa. For the cooling water temperature of 10 ^{o}C, the cooling part pressure fluctuates around 97470 Pa.

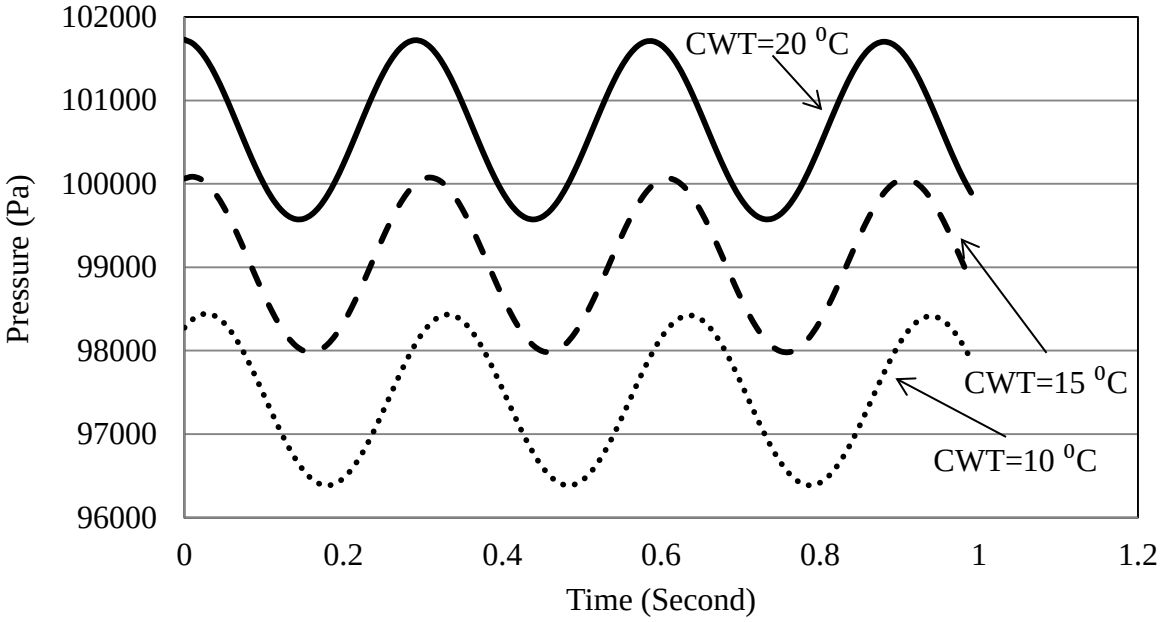

Figure 6.8 The effect of the cooling water temperature on the cooling part pressure

Figure 6.9 shows the effect of the cooling water temperature in the cooler on the air temperature variation in the cooling machine cylinder. In this figure it can be seen that the air temperature in the cooling machine cylinder reduces with the reduction in the cooling water temperature. When the cooling water temperature is 20, 15 and 10 ^{o}C, the average values of the air temperature in the cooling machine cylinder is found to be 293.8, 288.8 and 284.6 K respectively.

Figure 6.10 shows the effect of the cooling water temperature in the cooler on the air temperature variation in the cooling space. With lowering the cooling water temperature, the air temperature in the cooling space is decreased. It was found that the average air temperatures in the cooling space were 291.8, 287.4 and 282.6 K for the cooling water temperature of 20, 15 and 10 ^{o}C.

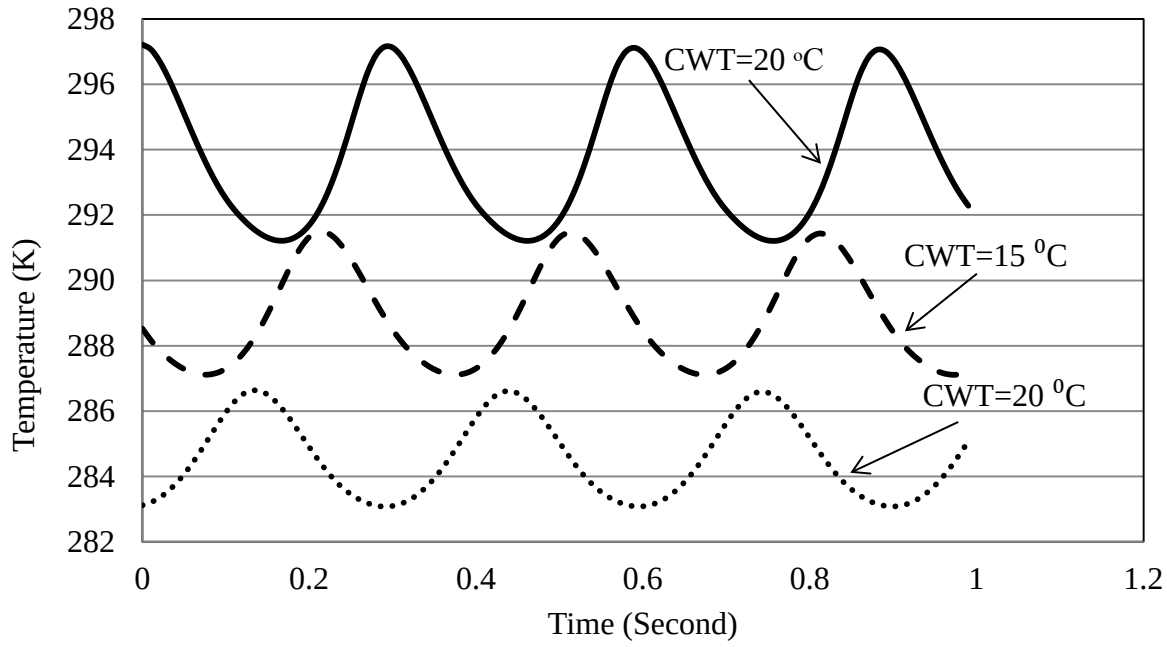

Figure 6.9 The effect of the cooling water temperature on the air temperature in the cooling machine cylinder

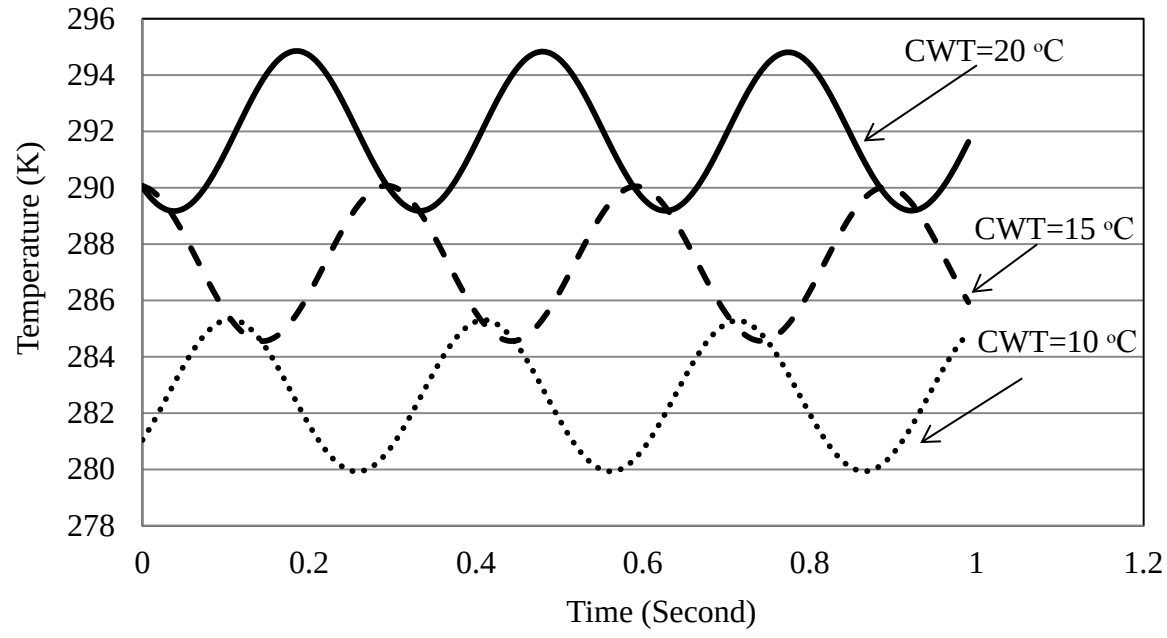

Figure 6.10 The effect of the cooling water temperature on the air temperature in cooling space

6.4 The effect of the cooling water flow rate

Since the condenser on the engine part and cooler on the cooling part are connected to each other in series then the flow rate in both these heat exchangers is the same. The cooling water flow rate (CFR) directly affects the amount of the heat rejected to the surroundings in both the condenser and cooler. The effect of the cooling water flow rate on the water level oscillations in the engine's cylinder, engine pressure, cooling part pressure, air temperature in the cooling machine cylinder and on the air temperature in the cooling space were investigated in this section. In the theoretical model, the cooling water flow rate was set to 180, 220 and 270 kg/hr. The heat input to the evaporator and the cooling water temperature were kept at 700 W and 20 ^{o}C, respectively.

Figure 6.11 shows the effect of the cooling water flow rate on the amplitude and frequency of the water level oscillations in the engine cylinder. It can be seen that the amplitude of the water level oscillations decrease from 2.9 cm at the cooling water flow rate of 180 kg/hr to 2.2 cm at the flow rate of 220 kg/hr. Finally, the amplitude increases to 2.4 cm at the cooling water flow rate of 270 kg/hr.

The effect of the cooling water flow rate on the engine pressure is illustrated in Figure 6.12 which shows that the engine pressure decreases with the increase in the cooling water flow rate. The average amount of the engine pressure decreases from 139390 Pa for the cooling water flow rate of 180 kg/hr to 123100 Pa for the flow rate of 220 kg/hr. The average pressure is 106410 Pa for the cooling water flow rate is 270 kg/hr.

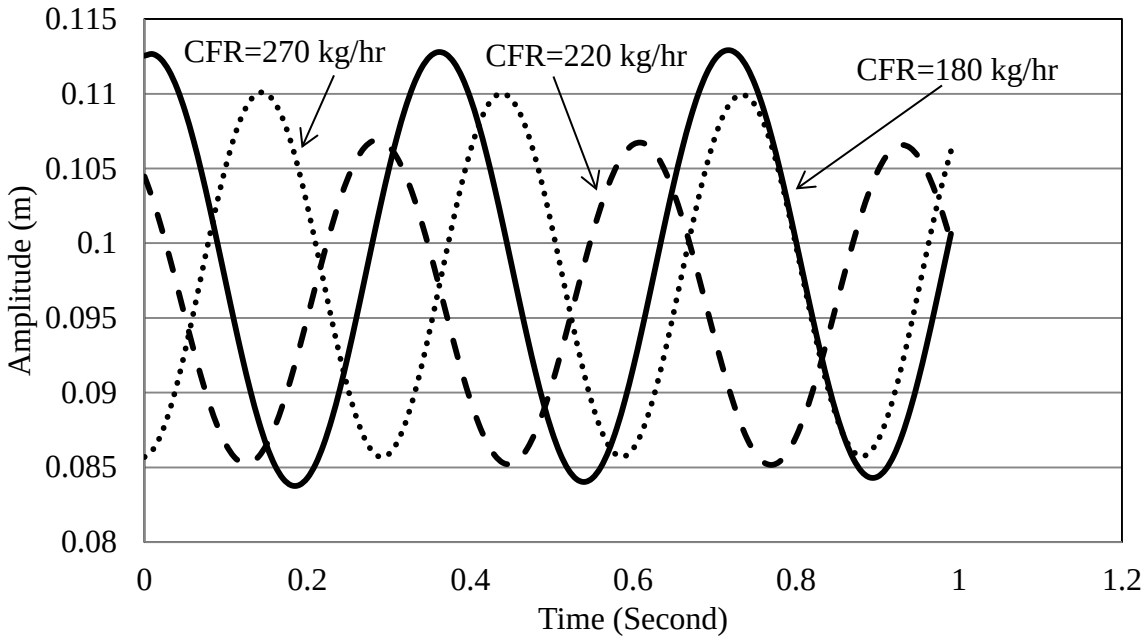

Figure 6.11 The effect of the cooling water flow rate on the water level oscillation amplitude in the engine

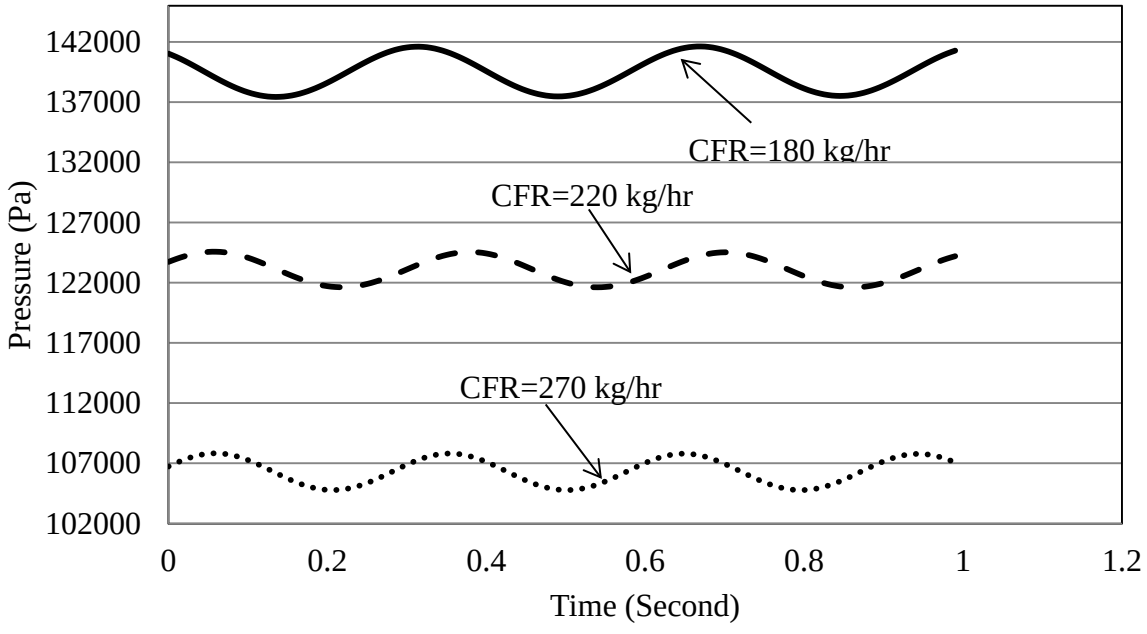

Figure 6.12 The effect of the cooling water flow rate on the engine pressure

Figure 6.13 shows that the cooling part pressure increases from an average value of 100160 Pa for the cooling water flow rate of 180 kg/hr to 100600 Pa for the flow rate of 220 kg/hr and to 100670 Pa at the flow rate of 270 kg/hr. This increase in the cooling part pressure leads to an increase in the average value of the air temperature in the cooling cylinder, as shown in Figure 6.14. The average air temperatures in the cooling machine cylinder is 291.4, 292.4 and 293.8 K at flow rates of 180, 220 and 270 kg/hr, respectively.

Figure 6.15 shows the effect of cooling water flow rate on the air temperature in the cooling space. By calculating the average value of the air temperatures in the cooling space for the three flow rates it was found that the air temperature increases with the increase in the cooling water flow rate and is 290.7, 292 and 292.05 K.

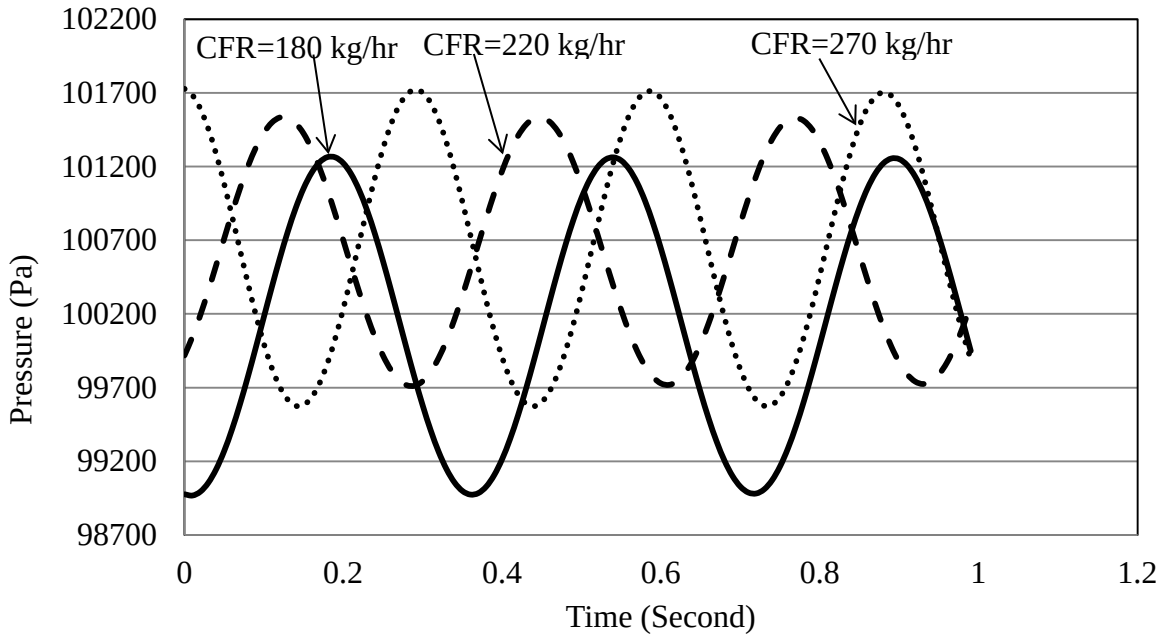

Figure 6.13 The effect of the cooling water flow rate on the cooling part pressure

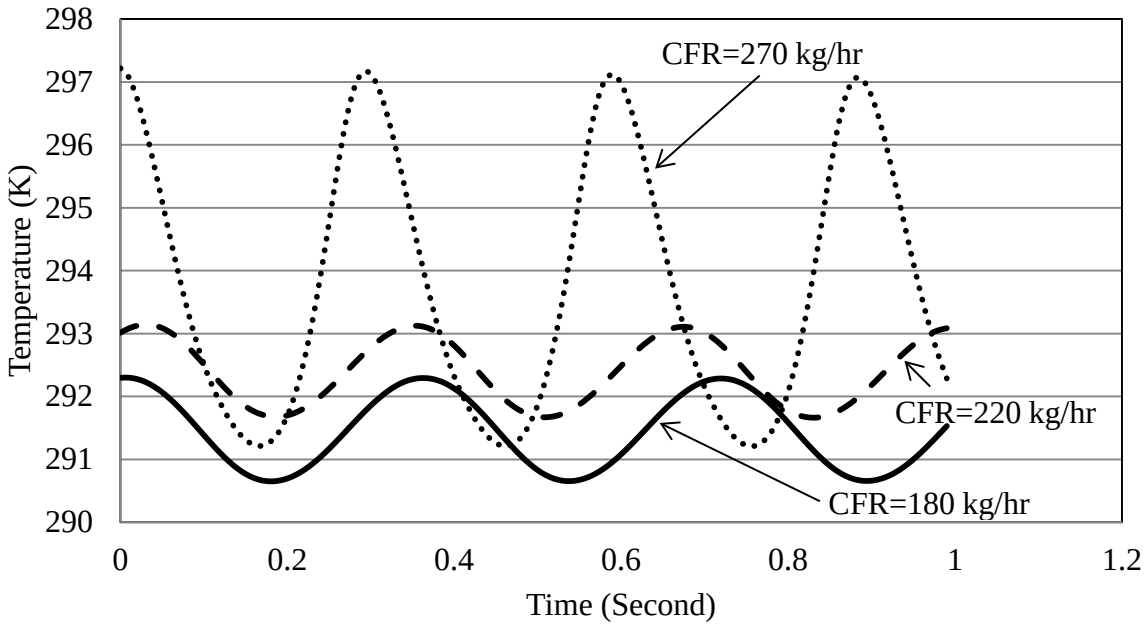

Figure 6.14 The effect of the cooling water flow rate on the temperature in the cooling machine cylinder

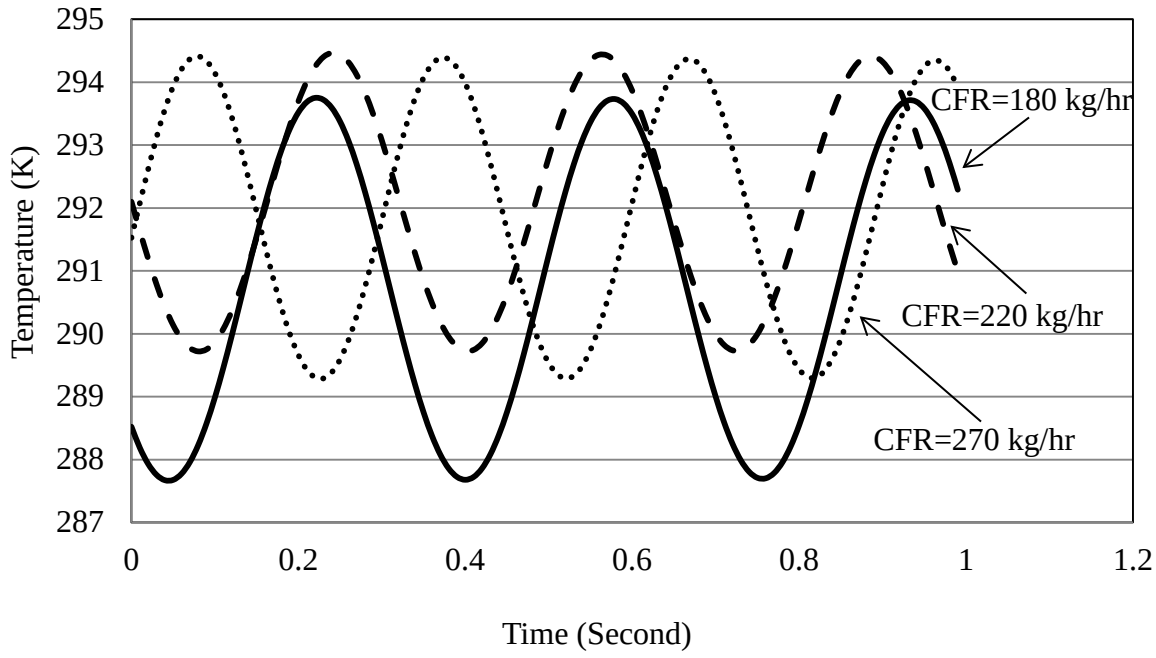

Figure 6.15 The effect of the cooling water flow rate on the temperature in cooling space

6.5 Summary

In this Chapter, the detailed parametric analysis for the third configuration of the dynamic solar cooling system was performed to determine the effect of the heat input to the evaporator, cooling water temperature and cooling water flow rate on the fluid piston amplitude, the pressure in the engine and cooling parts and the air temperatures in the cooling machine cylinder and cooling space. It can be concluded from this study that the increase of the heat input has the most profound positive influence on the system performance compared to effects of the cooling water temperature and its flow rate. It was shown that the raise in the heat input from 700 to 900 W in the laboratory prototype of the solar cooling system might reduce the air temperature in the cooler by 7 K. Therefore, one of the feasible ways to increase the cooling capacity of the system is to increase the absorbing surface of the solar collector.

Chapter 7 Conclusions and Recommendations for Future Work

7.1 Conclusions

1- The literature review demonstrates that the cooling systems driven by solar energy is an attractive option which in certain cases can replace the conventional fossil fuel or electricity driven vapour compression cooling systems, especially in regions with high solar irradiation.

2- The physical models of the three modifications of the dynamic solar cooling system based on a liquid piston converter were developed and experimentally tested to demonstrate their capacity to produce the cooling effect using solar energy.

3- The mathematical models of the solar cooling systems were developed and numerical simulations of the systems operation were performed in MATLAB/Simulink environment.

4- The numerical simulations demonstrated that in the built physical models the reduction in the air temperature in the cooling part of about 3 K can be achieved compared to the ambient temperature if the liquid piston amplitude is 10 cm.

5- In the experimental tests, all three configurations of the solar cooling system prototype were investigated. The first configuration with the height of the liquid piston in cooling machine equal to 500 mm has the frequency higher than 3 Hz which resulted in the distortion of the fluid surface during oscillations and this had a substantial negative effect on the cooling performance of the system.

6- Both the second and third configurations of the system demonstrated a stable operation during the tests with reduction in the air temperature in the cooling space being about 1 and 2 K, respectively, compared to the ambient temperature.

7- Comparison of theoretical and experimental results demonstrated that the developed mathematical models predict the operation of the solar cooling system with the accuracy acceptable for engineering calculations.

8- Using the experimentally validated mathematical models, the parametric analysis was performed to investigate the effect of several operational parameters on the system performance. These operational parameters included the heat input in the evaporator, the cooling water temperature and its flow rate. The heat input in the evaporator has the most profound effect on the system performance. It was shown that the rise in the heat input from 700 to 900 W in the laboratory prototype of the solar cooling system might reduce the air temperature in the cooler by 7 K .

7.2 Recommendations for future work

The theoretical models of the solar cooling systems developed in this thesis can be efficiently used for the prediction of their performance. Nevertheless, the developed mathematical models can be further rectified for a more accurate predictions. The laboratory prototype of the solar cooling system also can be further modified to work more efficiently and to have higher cooling capacity. Recommendations for the further investigations are as follows:

1- In this study the air was used as a working fluid. It is recommended to test different gases with superior thermos-physical properties, such as hydrogen or helium, to improve the system performance.

2- In the engine and cooling machine, water was used as the liquid piston. Other, more volatile, liquids could be tested instead of water which can improve the performance of the system due to increased evaporation rate.

3- The mathematical model can be further developed by including the exergy analysis of the system which enables improving the design of separate components of the system.

4- The mathematical model of the system should be coupled to the optimization code to determine its optimal design parameters.

5- More advanced sensors which have the higher sampling rates and accuracy should be used in the experimental work, especially for the measuring liquid piston oscillations and the temperature measurements.

6- The economical feasibility studies of the dynamic solar cooling system should be carried out to determine its competitiveness level compared to other types of solar cooling systems.

References

[1] J. L. Seitz and K. A. Hite, *Global Issues: An Introduction, 4th Edition*, 4th edition ed. Malden, USA: Blackwell, 2012.

[2] H. Z. Hassan, A. A. Mohamad, and R. Bennacer, "Simulation of an adsorption solar cooling system," *Energy*, vol. 36, pp. 530-537, 2011.

[3] M. Beerepoot, "Technology Roadmap Solar Heating and Cooling," *International Energy Agency, Paris, France*, 2012.

[4] S. LANGDON-ARMS, M. GSCHWENDTNER, and M. NEUMAIER, "Performance of Heat-powered Unconstrained 4 Cylinder Double-acting Alpha-type Liquid Piston Stirling Cooler," presented at the The 16th International Stirling Engine ISEC, Bilbao, Spain, 2014.

[5] F. Muhammad-Sukki, A. B. Munir, R. Ramirez-Iniguez, S. H. Abu-Bakar, S. H. Mohd Yasin, S. G. McMeekin, *et al.*, "Solar photovoltaic in Malaysia: The way forward," *Renewable and Sustainable Energy Reviews*, vol. 16, pp. 5232-5244, 2012.

[6] Y. Fan, L. Luo, and B. Souyri, "Review of solar sorption refrigeration technologies: Development and applications," *Renewable and Sustainable Energy Reviews*, vol. 11, pp. 1758-1775, 2007.

[7] J. A. Duffie and W. A. Bekman, *Solar Engineering of Thermal Processes*, 2nd edn ed. New York, USA: John Wiley &Sons, INC, 1980.

[8] B. Choudhury, B. B. Saha, P. K. Chatterjee, and J. P. Sarkar, "An overview of developments in adsorption refrigeration systems towards a sustainable way of cooling," *Applied Energy*, vol. 104, pp. 554-567, 2013.

[9] B. Belgasim, "Theoretical and experimental investigation of the dynamic solar water desalination unit," PhD, School of Engineering and Environment, Northumbria University Newcastle upon Tyne, UK, 2013.

[10] H. Z. Hassan and A. A. Mohamad, "A review on solar cold production through absorption technology," *Renewable and Sustainable Energy Reviews*, vol. 16, pp. 5331-5348, 2012.

[11] H.-M. Henning, "Solar assisted air conditioning of buildings – an overview," *Applied Thermal Engineering*, vol. 27, pp. 1734-1749, 2007.

[12] A. Allouhi, T. Kousksou, A. Jamil, P. Bruel, Y. Mourad, and Y. Zeraouli, "Solar driven cooling systems: An updated review," *Renewable and Sustainable Energy Reviews,* vol. 44, pp. 159-181, 2015.

[13] S. A. Masheiti, "A thermodynamic and economic simulation modelling study of utilizing low-temperature sources to power

absorption and organic Rankine cycles," PhD, School of Mechanical and Systems Engineering Newcastle University, UK, 2011.

[14] X. Q. Zhai, M. Qu, Y. Li, and R. Z. Wang, "A review for research and new design options of solar absorption cooling systems," *Renewable and Sustainable Energy Reviews,* vol. 15, pp. 4416-4423, 2011.

[15] A. Zohar, M. Jelinek, A. Levy, and I. Borde, "The influence of diffusion absorption refrigeration cycle configuration on the performance," *Applied Thermal Engineering,* vol. 27, pp. 2213-2219, 9// 2007.

[16] N. Nakahara, Y. Miyakawa, and M. Yamamoto, "Experimental study on house cooling and heating with solar energy using flat plate collector," *Solar Energy,* vol. 19, pp. 657-662, 1977.

[17] M. R. Yeung, P. K. Yuen, A. Dunn, and L. S. Cornish, "Performance of a solar-powered air conditioning system in Hong Kong," *Solar Energy,* vol. 48, pp. 309-319, // 1992.

[18] R. M. Lazzarin, P. Romagnoni, and L. Casasola, "Two years of operation of a large solar cooling plant," *International Journal of Refrigeration,* vol. 16, pp. 185-190, 1993/01/01 1993.

[19] C. Vereda, R. Ventas, A. Lecuona, and R. López, "Single-effect absorption refrigeration cycle boosted with an ejector-adiabatic absorber using a single solution pump," *International Journal of Refrigeration,* vol. 38, pp. 22-29, 2014.

[20] D. S. Kim and C. A. Infante Ferreira, "Analytic modelling of steady state single-effect absorption cycles," *International Journal of Refrigeration,* vol. 31, pp. 1012-1020, 2008.

[21] X. Yan, G. Chen, D. Hong, S. Lin, and L. Tang, "A novel absorption refrigeration cycle for heat sources with large temperature change," *Applied Thermal Engineering,* vol. 52, pp. 179-186, 2013.

[22] K. E. Herold, R. Radermacher, and S. A. Klein, *Absorption chillers and heat pumps*: CRC press, 1996.

[23] S. Arivazhagan, R. Saravanan, and S. Renganarayanan, "Experimental studies on HFC based two-stage half effect vapour absorption cooling system," *Applied Thermal Engineering,* vol. 26, pp. 1455-1462, 2006.

[24] P. Lin, R. Z. Wang, and Z. Z. Xia, "Numerical investigation of a two-stage air-cooled absorption refrigeration system for solar cooling: Cycle analysis and absorption cooling performances," *Renewable Energy,* vol. 36, pp. 1401-1412, 2011.

[25] D. Kim and C. Machielsen, "Evaluation of air-cooled solar absorption cooling systems," in *International Sorption Heat Pump Conference, Shanghai, China,* 2002.

[26] K. Sumathy, Z. Huang, and Z. Li, "Solar absorption cooling with low grade heat source—a strategy of development in South China," *Solar energy,* vol. 72, pp. 155-165, 2002.

[27] R. Gomri, "Investigation of the potential of application of single effect and multiple effect absorption cooling systems," *Energy Conversion and Management,* vol. 51, pp. 1629-1636, 2010.

[28] Y. Liu and R. Wang, "Performance prediction of a solar/gas driving double effect LiBr–H< sub> 2</sub> O absorption system," *Renewable Energy,* vol. 29, pp. 1677-1695, 2004.

[29] Y. Shin, J. A. Seo, H. W. Cho, S. C. Nam, and J. H. Jeong, "Simulation of dynamics and control of a double-effect LiBr–H2O absorption chiller," *Applied Thermal Engineering,* vol. 29, pp. 2718-2725, 2009.

[30] R. Gomri, "Second law comparison of single effect and double effect vapour absorption refrigeration systems," *Energy Conversion and Management,* vol. 50, pp. 1279-1287, 2009.

[31] Z. Y. Xu, R. Z. Wang, and Z. Z. Xia, "A novel variable effect LiBr-water absorption refrigeration cycle," *Energy,* vol. 60, pp. 457-463, 2013.

[32] M. Owen, "ASHRAE handbook—fundamentals (IP edition)," *American Society of Heating, Refrigerating and Air-Conditioning Engineers,* 2009.

[33] J. L. Rodríguez-Muñoz and J. M. Belman-Flores, "Review of diffusion–absorption refrigeration technologies," *Renewable and Sustainable Energy Reviews,* vol. 30, pp. 145-153, 2014.

[34] P. Srikhirin, S. Aphornratana, and S. Chungpaibulpatana, "A review of absorption refrigeration technologies," *Renewable and sustainable energy reviews,* vol. 5, pp. 343-372, 2001.

[35] D. S. Ayou, J. C. Bruno, R. Saravanan, and A. Coronas, "An overview of combined absorption power and cooling cycles," *Renewable and Sustainable Energy Reviews,* vol. 21, pp. 728-748, 2013.

[36] G. Moreno-Quintanar, W. Rivera, and R. Best, "Comparison of the experimental evaluation of a solar intermittent refrigeration system for ice production operating with the mixtures NH3/LiNO3 and NH3/LiNO3/H2O," *Renewable Energy,* vol. 38, pp. 62-68, 2012.

[37] K. A. Joudi and A. H. Lafta, "Simulation of a simple absorption refrigeration system," *Energy Conversion and Management,* vol. 42, pp. 1575-1605, 2001.

[38] M. Ortiz, H. Barsun, H. He, P. Vorobieff, and A. Mammoli, "Modeling of a solar-assisted HVAC system with thermal storage," *Energy and Buildings,* vol. 42, pp. 500-509, 2010.

[39] G. Evola, N. Le Pierrès, F. Boudehenn, and P. Papillon, "Proposal and validation of a model for the dynamic simulation of a solar-assisted single-stage LiBr/water absorption chiller," *International Journal of Refrigeration,* vol. 36, pp. 1015-1028, 2013.

[40] M. Laidi and S. Hanini, "Optimal solar COP prediction of a solar-assisted adsorption refrigeration system working with activated carbon/methanol as working pairs using direct and inverse artificial neural network," *International Journal of Refrigeration,* vol. 36, pp. 247-257, 2013.

[41] I. Sarbu and C. Sebarchievici, "Review of solar refrigeration and cooling systems," *Energy and Buildings,* vol. 67, pp. 286-297, 2013.

[42] R. E. Critoph and S. J. Metcalf, "Specific cooling power intensification limits in ammonia–carbon adsorption refrigeration systems," *Applied Thermal Engineering,* vol. 24, pp. 661-678, 2004.

[43] B. B. Saha, S. Koyama, J. B. Lee, K. Kuwahara, K. C. A. Alam, Y. Hamamoto, *et al.*, "Performance evaluation of a low-temperature waste heat driven multi-bed adsorption chiller," *International Journal of Multiphase Flow*, vol. 29, pp. 1249-1263, 2003.

[44] H. Chua, K. Ng, A. Malek, T. Kashiwagi, A. Akisawa, and B. Saha, "Modeling the performance of two-bed, sillica gel-water adsorption chillers," *International Journal of Refrigeration*, vol. 22, pp. 194-204, 1999.

[45] N. Srivastava and I. Eames, "A review of adsorbents and adsorbates in solid–vapour adsorption heat pump systems," *Applied Thermal Engineering*, vol. 18, pp. 707-714, 1998.

[46] O. Iloeje, A. Ndili, and S. Enibe, "Computer simulation of a CaCl< sub> 2</sub> solid-adsorption solar refrigerator," *Energy*, vol. 20, pp. 1141-1151, 1995.

[47] Y. Kato, M. Yamada, T. Kanie, and Y. Yoshizawa, "Calcium oxide/carbon dioxide reactivity in a packed bed reactor of a chemical heat pump for high-temperature gas reactors," *Nuclear engineering and design*, vol. 210, pp. 1-8, 2001.

[48] L. W. Wang, R. Z. Wang, and R. G. Oliveira, "A review on adsorption working pairs for refrigeration," *Renewable and Sustainable Energy Reviews*, vol. 13, pp. 518-534, 2009.

[49] H. Z. Hassan and A. A. Mohamad, "A review on solar-powered closed physisorption cooling systems," *Renewable and Sustainable Energy Reviews*, vol. 16, pp. 2516-2538, 2012.

[50] Y. Zhang, "Adsorption function," *Shanghai, China: Publishing House of Scientific and Technological Literature in Shanghai*, 1989.

[51] R. Gasser, "The chemical adsorption and catalysis of metal," *Beijing, China: Publishing House of Beijing University; 1991 [in Chinese]*, 1991.

[52] R. Bansal, "Goyal. M. Activated Carbon Adsorption," ed: Boca Raton: Dekker/CRC Press, 2005.

[53] H. Hassan, "A Solar Powered Adsorption Freezer: A Case Study for Egypt's Climate," *International Journal of Energy Engineering*, vol. 3, pp. 21-29, 2013.

[54] M. Ron, "A hydrogen heat pump as a bus air conditioner," *Journal of the Less Common Metals*, vol. 104, pp. 259-278, 1984.

[55] D. C. Wang, Y. H. Li, D. Li, Y. Z. Xia, and J. P. Zhang, "A review on adsorption refrigeration technology and adsorption deterioration in physical adsorption systems," *Renewable and Sustainable Energy Reviews,* vol. 14, pp. 344-353, 2010.

[56] E. Anyanwu and N. Ogueke, "Thermodynamic design procedure for solid adsorption solar refrigerator," *Renewable energy,* vol. 30, pp. 81-96, 2005.

[57] M. Mujahid Rafique, P. Gandhidasan, S. Rehman, and L. M. Al-Hadhrami, "A review on desiccant based evaporative cooling systems," *Renewable and Sustainable Energy Reviews,* vol. 45, pp. 145-159, 2015.

[58] K. Daou, R. Wang, and Z. Xia, "Desiccant cooling air conditioning: a review," *Renewable and Sustainable Energy Reviews,* vol. 10, pp. 55-77, 2006.

[59] V. Martin and D. Y. Goswami, "Effectiveness of Heat and Mass Transfer Processes in a Packed Bed Liquid Desiccant Dehumidifier/Regenerator," *HVAC&R Research,* vol. 6, pp. 21-39, 2000.

[60] G. Heidarinejad, M. Bozorgmehr, S. Delfani, and J. Esmaeelian, "Experimental investigation of two-stage indirect/direct evaporative cooling system in various climatic conditions," *Building and Environment,* vol. 44, pp. 2073-2079, 2009.

[61] K. A. Joudi and S. M. Mehdi, "Application of indirect evaporative cooling to variable domestic cooling load," *Energy Conversion and Management,* vol. 41, pp. 1931-1951, 11/1/ 2000.

[62] W. Y. Saman and S. Alizadeh, "An experimental study of a cross-flow type plate heat exchanger for dehumidification/cooling," *Solar Energy,* vol. 73, pp. 59-71, 7// 2002.

[63] W. Kessling, E. Laevemann, and M. Peltzer, "Energy storage in open cycle liquid desiccant cooling systems," *International Journal of Refrigeration,* vol. 21, pp. 150-156, 3// 1998.

[64] M. Shariaty-Niassar and N. Gilani, "An Investigation of Indirect Evaporative Coolers, IEC With Respect to Thermal Comfort Criteria," *Iranian Journal of Chemical Engineering,* vol. 6, p. 15, 2009.

[65] J. R. Camargo, C. D. Ebinuma, and J. L. Silveira, "Experimental performance of a direct evaporative cooler operating during summer in a Brazilian city," *International Journal of Refrigeration,* vol. 28, pp. 1124-1132, 2005.

[66] S. B. Riffat and J. Zhu, "Mathematical model of indirect evaporative cooler using porous ceramic and heat pipe," *Applied Thermal Engineering,* vol. 24, pp. 457-470, 2004.

[67] X. Zhao, J. M. Li, and S. B. Riffat, "Numerical study of a novel counter-flow heat and mass exchanger for dew point evaporative cooling," *Applied Thermal Engineering,* vol. 28, pp. 1942-1951, 2008.

[68] R. Davis, "Evaluation of advanced evaporative cooler technologies; Pacific Gas and Electric (PG&E) customer energy management emerging technologies program," *Report no,* pp. 491-04.7, 2004.

[69] M. M. Rafique, P. Gandhidasan, and H. M. S. Bahaidarah, "Liquid desiccant materials and dehumidifiers – A review," *Renewable and Sustainable Energy Reviews,* vol. 56, pp. 179-195, 2016.

[70] S. Jain, P. Dhar, and S. Kaushik, "Evaluation of solid-desiccant-based evaporative cooling cycles for typical hot and humid climates," *International journal of refrigeration,* vol. 18, pp. 287-296, 1995.

[71] P. Mavroudaki, C. Beggs, P. Sleigh, and S. Halliday, "The potential for solar powered single-stage desiccant cooling in southern Europe," *Applied Thermal Engineering,* vol. 22, pp. 1129-1140, 2002.

[72] S. Halliday, C. Beggs, and P. Sleigh, "The use of solar desiccant cooling in the UK: a feasibility study," *Applied Thermal Engineering,* vol. 22, pp. 1327-1338, 2002.

[73] S. Alizadeh and W. Y. Saman, "Modeling and performance of a forced flow solar collector/regenerator using liquid desiccant," *Solar Energy,* vol. 72, pp. 143-154, 2// 2002.

[74] S. Alizadeh and W. Y. Saman, "An experimental study of a forced flow solar collector/regenerator using liquid desiccant," *Solar Energy,* vol. 73, pp. 345-362, 11// 2002.

[75] Y. K. Yadav, "Vapour-compression and liquid-desiccant hybrid solar space-conditioning system for energy conservation," *Renewable Energy,* vol. 6, pp. 719-723, 10// 1995.

[76] Y. J. Dai, R. Z. Wang, H. F. Zhang, and J. D. Yu, "Use of liquid desiccant cooling to improve the performance of vapor compression air conditioning," *Applied Thermal Engineering,* vol. 21, pp. 1185-1202, 8// 2001.

[77] P. Mazzei, F. Minichiello, and D. Palma, "Desiccant HVAC systems for commercial buildings," *Applied Thermal Engineering,* vol. 22, pp. 545-560, 4// 2002.

[78] S. Techajunta, S. Chirarattananon, and R. H. B. Exell, "Experiments in a solar simulator on solid desiccant regeneration and air dehumidification for air conditioning in a tropical humid climate," *Renewable Energy,* vol. 17, pp. 549-568, 8/1/ 1999.

[79] C. X. Jia, Y. J. Dai, J. Y. Wu, and R. Z. Wang, "Experimental comparison of two honeycombed desiccant wheels fabricated with silica gel and composite desiccant material," *Energy Conversion and Management,* vol. 47, pp. 2523-2534, 9// 2006.

[80] M. Sultan, I. I. El-Sharkawy, T. Miyazaki, B. B. Saha, and S. Koyama, "An overview of solid desiccant dehumidification and air conditioning systems," *Renewable and Sustainable Energy Reviews,* vol. 46, pp. 16-29, 2015.

[81] W. A. Belding, M. P. Delmas, and W. D. Holeman, "Desiccant aging and its effects on desiccant cooling system performance," *Applied Thermal Engineering,* vol. 16, pp. 447-459, 1996.

[82] H. M. Factor and G. Grossman, "A packed bed dehumidifier/regenerator for solar air conditioning with liquid desiccants," *Solar Energy,* vol. 24, pp. 541-550, 1980/01/01 1980.

[83] G. R. Thorpe, "The modelling and potential applications of a simple solar regenerated grain cooling device," *Postharvest Biology and Technology,* vol. 13, pp. 151-168, 4// 1998.

[84] Y. J. Dai, R. Z. Wang, and Y. X. Xu, "Study of a solar powered solid adsorption–desiccant cooling system used for grain storage," *Renewable Energy,* vol. 25, pp. 417-430, 3// 2002.

[85] K. Nagaya, T. Senbongi, Y. Li, J. Zheng, and I. Murakami, "High energy efficiency desiccant assisted automobile air-conditioner and its temperature and humidity control system," *Applied Thermal Engineering,* vol. 26, pp. 1545-1551, 10// 2006.

[86] G. Heidarinejad, M. Heidarinejad, S. Delfani, and J. Esmaeelian, "Feasibility of using various kinds of cooling systems in a multi-climates country," *Energy and Buildings,* vol. 40, pp. 1946-1953, // 2008.

[87] T. S. Ge, Y. Li, Y. J. Dai, and R. Z. Wang, "Performance investigation on a novel two-stage solar driven rotary desiccant cooling system using composite desiccant materials," *Solar Energy,* vol. 84, pp. 157-159, 2// 2010.

[88] B. O. Bolaji and Z. Huan, "Ozone depletion and global warming: Case for the use of natural refrigerant – a review," *Renewable and Sustainable Energy Reviews,* vol. 18, pp. 49-54, 2// 2013.

[89] T. Sookchaiya, V. Monyakul, and S. Thepa, "Assessment of the thermal environment effects on human comfort and health for the development of novel air conditioning system in tropical regions," *Energy and Buildings,* vol. 42, pp. 1692-1702, 10// 2010.

[90] J. Jeong, S. Yamaguchi, K. Saito, and S. Kawai, "Performance analysis of four-partition desiccant wheel and hybrid dehumidification air-conditioning system," *International Journal of Refrigeration,* vol. 33, pp. 496-509, 5// 2010.

[91] G. Panaras, E. Mathioulakis, and V. Belessiotis, "Achievable working range for solid all-desiccant air-conditioning systems under specific space comfort requirements," *Energy and Buildings,* vol. 39, pp. 1055-1060, 9// 2007.

[92] S. H. Lee and W. L. Lee, "Site verification and modeling of desiccant-based system as an alternative to conventional air-conditioning systems for wet markets," *Energy,* vol. 55, pp. 1076-1083, 6/15/ 2013.

[93] J. Hirunlabh, R. Charoenwat, J. Khedari, and S. Teekasap, "Feasibility study of desiccant air-conditioning system in Thailand," *Building and Environment,* vol. 42, pp. 572-577, 2// 2007.

[94] E. Hürdoğan, O. Büyükalaca, T. Yılmaz, A. Hepbasli, and İ. Uçkan, "Investigation of solar energy utilization in a novel desiccant based air conditioning system," *Energy and Buildings,* vol. 55, pp. 757-764, 12// 2012.

[95] M. Sultan, T. Miyazaki, B. B. Saha, and S. Koyama, "Steady-state investigation of water vapor adsorption for thermally driven adsorption based greenhouse air-conditioning system," *Renewable Energy,* vol. 86, pp. 785-795, 2// 2016.

[96] Z. Guojie, Z. Chaoyu, Y. Guanghai, and C. Wu, "Development of a New Marine Rotary Desiccant Airconditioning System and its Energy Consumption Analysis," *Energy Procedia,* vol. 16, Part B, pp. 1095-1101, // 2012.

[97] F. Ascione, L. Bellia, and A. Capozzoli, "A coupled numerical approach on museum air conditioning: Energy and fluid-dynamic analysis," *Applied Energy,* vol. 103, pp. 416-427, 2013.

[98] T. S. Ge, Y. J. Dai, and R. Z. Wang, "Review on solar powered rotary desiccant wheel cooling system," *Renewable and Sustainable Energy Reviews,* vol. 39, pp. 476-497, 2014.

[99] A. Preisler and M. Brychta, "High Potential of Full Year Operation with Solar Driven Desiccant Evaporative Cooling Systems," *Energy Procedia,* vol. 30, pp. 668-675, // 2012.

[100] K. A. Joudi and N. S. Dhaidan, "Application of solar assisted heating and desiccant cooling systems for a domestic building," *Energy Conversion and Management,* vol. 42, pp. 995-1022, 5// 2001.

[101] Z. Guidara, M. Elleuch, and H. Ben Bacha, "New solid desiccant solar air conditioning unit in Tunisia: Design and simulation study," *Applied Thermal Engineering,* vol. 58, pp. 656-663, 9// 2013.

[102] P. Bourdoukan, E. Wurtz, and P. Joubert, "Experimental investigation of a solar desiccant cooling installation," *Solar Energy,* vol. 83, pp. 2059-2073, 11// 2009.

[103] I. L. Maclaine-Cross and P. J. Banks, "Coupled heat and mass transfer in regenerators—prediction using an analogy with heat transfer," *International Journal of Heat and Mass Transfer,* vol. 15, pp. 1225-1242, 1972/06/01 1972.

[104] P. Stabat and D. Marchio, "Heat-and-mass transfers modelled for rotary desiccant dehumidifiers," *Applied Energy,* vol. 85, pp. 128-142, 2// 2008.

[105] P. Bourdoukan, E. Wurtz, P. Joubert, and M. Spérandio, "Potential of solar heat pipe vacuum collectors in the desiccant cooling process: Modelling and experimental results," *Solar Energy,* vol. 82, pp. 1209-1219, 12// 2008.

[106] T. S. Ge, Y. Li, R. Z. Wang, and Y. J. Dai, "Experimental study on a two-stage rotary desiccant cooling system," *International Journal of Refrigeration,* vol. 32, pp. 498-508, 5// 2009.

[107] T. S. Ge, Y. J. Dai, R. Z. Wang, and Y. Li, "Experimental investigation on a one-rotor two-stage rotary desiccant cooling system," *Energy,* vol. 33, pp. 1807-1815, 12// 2008.

[108] T. S. Ge, F. Ziegler, R. Z. Wang, and H. Wang, "Performance comparison between a solar driven rotary desiccant cooling system and conventional vapor compression system (performance study of desiccant cooling)," *Applied Thermal Engineering,* vol. 30, pp. 724-731, 5// 2010.

[109] M. Pouraghaie, K. Atashkari, S. M. Besarati, and N. Nariman-zadeh, "Thermodynamic performance optimization of a combined power/cooling cycle," *Energy Conversion and Management,* vol. 51, pp. 204-211, 2010.

[110] J. D. Maloney Jr and R. C. Robertson, "Thermodynamic study of ammonia-water heat power cycles," DTIC Document1953.

[111] M. Liu and N. Zhang, "Proposal and analysis of a novel ammonia–water cycle for power and refrigeration cogeneration," *Energy,* vol. 32, pp. 961-970, 2007.

[112] A. Kalina, "Combined cycle and waste heat recovery power systems based on a novel thermodynamic energy cycle utilizing low-temperature heat for power generation," *Am. Soc. Mech. Eng.,(Pap.);(United States),* vol. 83, 1983.

[113] A. I. Kalina, "Combined-cycle system with novel bottoming cycle," *Journal of engineering for gas turbines and power,* vol. 106, pp. 737-742, 1984.

[114] H. Saffari, S. Sadeghi, M. Khoshzat, and P. Mehregan, "Thermodynamic analysis and optimization of a geothermal Kalina cycle system using Artificial Bee Colony algorithm," *Renewable Energy,* vol. 89, pp. 154-167, 2016.

[115] D. V. Singh and E. Pedersen, "A review of waste heat recovery technologies for maritime applications," *Energy Conversion and Management,* vol. 111, pp. 315-328, 2016.

[116] D. W. Wu and R. Z. Wang, "Combined cooling, heating and power: A review," *Progress in Energy and Combustion Science,* vol. 32, pp. 459-495, 2006.

[117] J. Xu, J. Sui, B. Li, and M. Yang, "Research, development and the prospect of combined cooling, heating, and power systems," *Energy,* vol. 35, pp. 4361-4367, 2010.

[118] D. Goswami, "Solar thermal power: status of technologies and opportunities for research," in *Proceedings of Proceedings of the 2nd ISHMT-ASME Heat and Mass Transaction Conference*, 1995, pp. 57-60.

[119] D. Yogi Goswami, "Solar thermal power technology: present status and ideas for the future," *Energy Sources,* vol. 20, pp. 137-145, 1998.

[120] D. Y. Goswami and F. Xu, "Analysis of a new thermodynamic cycle for combined power and cooling using low and mid temperature solar collectors," *Journal of Solar Energy Engineering,* vol. 121, pp. 91-97, 1999.

[121] S. Lu and D. Y. Goswami, "Optimization of a novel combined power/refrigeration thermodynamic cycle," in *ASME Solar 2002: International Solar Energy Conference*, 2002, pp. 75-82.

[122] S. Lu and D. Y. Goswami, "Theoretical analysis of ammonia-based combined power/refrigeration cycle at low refrigeration temperatures," in *ASME Solar 2002: International Solar Energy Conference*, 2002, pp. 117-125.

[123] C. Martin and D. Y. Goswami, "Effectiveness of cooling production with a combined power and cooling thermodynamic cycle," *Applied Thermal Engineering,* vol. 26, pp. 576-582, 2006.

[124] F. Xu, D. Y. Goswami, and S. S. Bhagwat, "A combined power/cooling cycle," *Energy,* vol. 25, pp. 233-246, 2000.

[125] F. Xu and D. Y. Goswami, "Thermodynamic properties of ammonia–water mixtures for power-cycle applications," *Energy,* vol. 24, pp. 525-536, 1999.

[126] A. A. Hasan, D. Y. Goswami, and S. Vijayaraghavan, "First and second law analysis of a new power and refrigeration thermodynamic cycle using a solar heat source," *Solar Energy,* vol. 73, pp. 385-393, 2002.

[127] A. Vidal, R. Best, R. Rivero, and J. Cervantes, "Analysis of a combined power and refrigeration cycle by the exergy method," *Energy,* vol. 31, pp. 3401-3414, 2006.

[128] S. Vijayaraghavan and D. Y. Goswami, "On evaluating efficiency of a combined power and cooling cycle," in *ASME 2002 International Mechanical Engineering Congress and Exposition*, 2002, pp. 287-295.

[129] S. Vijayaraghavan and D. Y. Goswami, "A combined power and cooling cycle modified to improve resource utilization efficiency using a distillation stage," *Energy,* vol. 31, pp. 1177-1196, 2006.

[130] S. M. Sadrameli and D. Y. Goswami, "Optimum operating conditions for a combined power and cooling thermodynamic cycle," *Applied Energy,* vol. 84, pp. 254-265, 2007.

[131] G. Tamm, D. Y. Goswami, S. Lu, and A. A. Hasan, "Theoretical and experimental investigation of an ammonia–water power and refrigeration thermodynamic cycle," *Solar Energy,* vol. 76, pp. 217-228, 2004.

[132] D. Goswami, G. Tamm, and S. Vijayaraghavana, "A new combined power and cooling cycle for low temperature heat sources," presented at the International Joint Power Generation Conference Atlanta, Georgia, USA, 2003.

[133] S. Vijayaraghavan and D. Goswami, "Organic working fluids for a combined power and cooling cycle," *Journal of energy resources technology,* vol. 127, pp. 125-130, 2005.

[134] G. Demirkaya, R. Vasquez Padilla, D. Y. Goswami, E. Stefanakos, and M. M. Rahman, "Analysis of a combined power and cooling cycle for low-grade heat sources," *International Journal of Energy Research,* vol. 35, pp. 1145-1157, 2011.

[135] B. Kongtragool and S. Wongwises, "A review of solar-powered Stirling engines and low temperature differential Stirling engines," *Renewable and Sustainable Energy Reviews,* vol. 7, pp. 131-154, 4// 2003.

[136] J. R. Senft, "Ringbom Stirling Engines Oxford University Press," *New York,* vol. 3, 1993.

[137] J. Chen, Z. Yan, L. Chen, and B. Andresen, "Efficiency bound of a solar-driven Stirling heat engine system," *International journal of energy research,* vol. 22, pp. 805-812, 1998.

[138] S. Le'an, Z. Yuanyang, L. Liansheng, and S. Pengcheng, "Performance of a prototype Stirling domestic refrigerator," *Applied Thermal Engineering,* vol. 29, pp. 210-215, 2009.

[139] K. Chunnanond and S. Aphornratana, "Ejectors: applications in refrigeration technology," *Renewable and Sustainable Energy Reviews,* vol. 8, pp. 129-155, 2004.

[140] M. Zeyghami, D. Y. Goswami, and E. Stefanakos, "A review of solar thermo-mechanical refrigeration and cooling methods," *Renewable and Sustainable Energy Reviews,* vol. 51, pp. 1428-1445, 2015.

[141] K. Cizungu, A. Mani, and M. Groll, "Performance comparison of vapour jet refrigeration system with environment friendly working fluids," *Applied Thermal Engineering,* vol. 21, pp. 585-598, 4// 2001.

[142] J. M. Abdulateef, K. Sopian, M. A. Alghoul, and M. Y. Sulaiman, "Review on solar-driven ejector refrigeration technologies," *Renewable and Sustainable Energy Reviews,* vol. 13, pp. 1338-1349, 2009.

[143] M. Sokolov and D. Hershgal, "Optimal coupling and feasibility of a solar-powered year-round ejector air conditioner," *Solar Energy,* vol. 50, pp. 507-516, 1993/06/01 1993.

[144] S. S. Murthy, R. Balasubramanian, and M. V. K. Murthy, "Experiments on vapour jet refrigeration system suitable for solar energy applications," *Renewable Energy,* vol. 1, pp. 757-768, 1991/01/01 1991.

[145] D.-W. Sun, "Comparative study of the performance of an ejector refrigeration cycle operating with various refrigerants," *Energy Conversion and Management,* vol. 40, pp. 873-884, 5// 1999.

[146] W. Pridasawas and P. Lundqvist, "Natural working fluids for a solar-driven ejector refrigeration system," 2003.

[147] J. Wolpert, S. Riffat, and S. Redshaw, "Prototype for a novel solar powered ejector air conditioning system in Mazunte Mexico," in *Proceeding of the international solar energy congress,* 2003.

[148] X. Chen, S. Omer, M. Worall, and S. Riffat, "Recent developments in ejector refrigeration technologies," *Renewable and Sustainable Energy Reviews,* vol. 19, pp. 629-651, 2013.

[149] A. Basaran and L. Ozgener, "Investigation of the effect of different refrigerants on performances of binary geothermal power plants," *Energy Conversion and Management,* vol. 76, pp. 483-498, 2013.

[150] H. Chen, D. Y. Goswami, and E. K. Stefanakos, "A review of thermodynamic cycles and working fluids for the conversion of low-grade heat," *Renewable and Sustainable Energy Reviews,* vol. 14, pp. 3059-3067, 2010.

[151] E. Nehdi, L. Kairouani, and M. Elakhdar, "A solar ejector air-conditioning system using environment-friendly working fluids," *International Journal of Energy Research,* vol. 32, pp. 1194-1201, 2008.

[152] C. Pollerberg, A. H. H. Ali, and C. Dötsch, "Experimental study on the performance of a solar driven steam jet ejector chiller," *Energy Conversion and Management,* vol. 49, pp. 3318-3325, 2008.

[153] W. Pridasawas and P. Lundqvist, "An exergy analysis of a solar-driven ejector refrigeration system," *Solar Energy,* vol. 76, pp. 369-379, 2004.

[154] B. J. Huang, J. M. Chang, V. A. Petrenko, and K. B. Zhuk, "A SOLAR EJECTOR COOLING SYSTEM USING REFRIGERANT R141b," *Solar Energy,* vol. 64, pp. 223-226, 12/1/ 1998.

[155] B. J. Huang, V. A. Petrenko, I. Y. Samofatov, and N. A. Shchetinina, "Collector selection for solar ejector cooling system," *Solar Energy,* vol. 71, pp. 269-274, // 2001.

[156] H.-Y. Chan, S. B. Riffat, and J. Zhu, "Review of passive solar heating and cooling technologies," *Renewable and Sustainable Energy Reviews,* vol. 14, pp. 781-789, 2010.

[157] E. H. Amer, "Passive options for solar cooling of buildings in arid areas," *Energy,* vol. 31, pp. 1332-1344, 2006.

[158] G. A. Florides, S. A. Tassou, S. A. Kalogirou, and L. C. Wrobel, "Review of solar and low energy cooling technologies for buildings," *Renewable and Sustainable Energy Reviews,* vol. 6, pp. 557-572, 12// 2002.

[159] S. Wanphen and K. Nagano, "Experimental study of the performance of porous materials to moderate the roof surface temperature by its evaporative cooling effect," *Building and Environment,* vol. 44, pp. 338-351, 2009.

[160] H. Takebayashi and M. Moriyama, "Surface heat budget on green roof and high reflection roof for mitigation of urban heat island," *Building and Environment,* vol. 42, pp. 2971-2979, 8// 2007.

[161] A. Synnefa, M. Santamouris, and I. Livada, "A study of the thermal performance of reflective coatings for the urban environment," *Solar Energy*, vol. 80, pp. 968-981, 8// 2006.

[162] K. S. Ong and C. C. Chow, "Performance of a solar chimney," *Solar Energy*, vol. 74, pp. 1-17, 2003.

[163] K. S. Ong, "A mathematical model of a solar chimney," *Renewable Energy*, vol. 28, pp. 1047-1060, 6// 2003.

[164] P. Raman, S. Mande, and V. V. N. Kishore, "A passive solar system for thermal comfort conditioning of buildings in composite climates," *Solar Energy*, vol. 70, pp. 319-329, // 2001.

[165] G. Walker and J. R. Senft, *Free-piston Stirling engines*: Springer, 1985.

[166] J. D. Van de Ven and P. Y. Li, "Liquid piston gas compression," *Applied Energy*, vol. 86, pp. 2183-2191, 2009.

[167] K. Mahkamov, E. Orda, B. Belgasim, and I. Makhkamova, "A novel small dynamic solar thermal desalination plant with a fluid piston converter," *Applied Energy*, vol. 156, pp. 715-726, 2015.

[168] B. Belgasim and K. Mahkamov, "Theoretical Modelling of a Dynamic Solar Thermal Desalination Unit with a Fluid Piston Engine," in *2nd World Renewable Energy Congress (WREC)*, 2011.

[169] Y. A. Çengel and M. Boles, *Thermodynamics: an engineering approach*. London McGraw-Hill 2008.

[170] J. P. Holman, *Heat Transfer*, 10th ed. ed. New Tork: McGraw-Hill, 2010.

[171] I. Urieli and D. M. Berchowitz, *Stirling cycle engine analysis*. Bristol: A. Hilger 1984

[172] M. I. M. Shatat and K. Mahkamov, "Determination of rational design parameters of a multi-stage solar water desalination still using transient mathematical modelling," *Renewable Energy*, vol. 35, pp. 52-61, 2010.

[173] R. K. Mishra, V. Garg, and G. N. Tiwari, "Thermal modeling and development of characteristic equations of evacuated tubular collector (ETC)," *Solar Energy*, vol. 116, pp. 165-176, 2015.

[174] Y. Kim and T. Seo, "Thermal performances comparisons of the glass evacuated tube solar collectors with shapes of absorber tube," *Renewable Energy*, vol. 32, pp. 772-795, 2007.

[175] S. A. Kalogirou, "Solar thermal collectors and applications," *Progress in Energy and Combustion Science*, vol. 30, pp. 231-295, 2004.

[176] R. Perez. (2015, 05/06/2015). *Home Power*. Available: http://www.homepower.com/articles/solar-water-heating/equipment-products/solar-collectors-behind-glass

[177] T. C. P. Shop. (2015, 21/05/2015). *The Clear Acrylic Tube* Available: http://clearplastictube.co.uk/index.php?route=product/product&path=35_58&product_id=174

[178] G. S. C. Limited. (2015, 08/06/2015). *The R-Series liquid level sensor* Available: http://gillsc.com/content/datasheets/R-Series_datasheet.pdf?v=2.10.13

[179] L. OMEGA Engineering. (2015, 08/06/2015). *Insulated Wire Thermocouples with Stripped Ends*. Available: http://www.omega.co.uk/pptst/5tc.html

[180] G. m. control. (2015, 08/06/2015). *UNIK 5000 pressure sensor*. Available: https://www.gemeasurement.com/sensors-probes-transducers/pressure-transducerstransmitters/unik-5000#sthash.FeAZtktB.dpuf

[181] I. Solar Light Company. (2015, 08/06/2015). *PMA2200* Available: http://solarlight.com/product/pma2200-single-input-radiometer/

[182] N. Instruments. (2015, 08/06/2015). *NI 9213*. Available: http://sine.ni.com/nips/cds/view/p/lang/en/nid/208788

[183] N. Instruments. (2015, 08/06/2015). *NI 9222*. Available: http://sine.ni.com/nips/cds/view/p/lang/en/nid/209142

[184] N. Instruments. (2015, 08/06/2015). *NI cDAQ-9178*. Available: http://sine.ni.com/nips/cds/view/p/lang/en/nid/207534

[185] N. Instruments. (2013, 02/06/2015). *LabVIEW Getting Started with LabVIEW*. Available: http://www.ni.com/pdf/manuals/373427j.pdf

[186] T. L. Bergman, F. P. Incropera, and A. S. Lavine, *Fundamentals of heat and mass transfer*: John Wiley & Sons, 2011.

[187] C. Charcosset, "A review of membrane processes and renewable energies for desalination," *Desalination,* vol. 245, pp. 214-231, 9/15/ 2009.

[188] B. Riangvilaikul and S. Kumar, "Numerical study of a novel dew point evaporative cooling system," *Energy and Buildings,* vol. 42, pp. 2241-2250, 2010.

Appendix A

Published papers:

1. K. Mahkamov, G. Hashem, B. Belgasim, and I. Makhkamova. A Novel Solar Cooling system Based on a Fluid Piston Convertor. Proceedings of the 16th International Stirling Engine Conference(ISEC), Bilbao, Spain, 2014.
2. K. Mahkamov and G. Hashem. Development of a Solar Cooling System Based on a Fluid Piston Convertor. *Proceedings of The European Conference on Sustainability, Energy & the Environment 2015*, Brighton, UK, 2015.
3. K. Mahkhamov, G. Hashem, B. Belgasim, K Hossin, I. Mahkamova. Parametric Analysis of Dynamic Solar Cooling System Based on Liquid Piston Converter. *Proceedings of the 17th International Stirling Engine Conference(ISEC)*, Newcastle upon Tyne, UK, 2016.

A Novel Solar Cooling system Based on a Fluid Piston Convertor

Khamid Mahkamov[a], Gamal Hashem[a], Basim Belgasim[c], Irina Makhkamova[a]
[a] *Northumbria University, NE1 8ST, Newcastle upon Tyne, UK*
[b] *Mechanical Engineering Department, Benghazi University, Benghazi, Libya*

Keywords: *solar cooling system, fluid piston engine*

Abstract

About 15% of the global electricity production is used to actuate different kinds of conventional cooling systems. Numerous solar cooling systems are commercially available but their market penetration level is relatively low due to the high capital cost and R & D activities are ongoing to reduce these costs.

Operational principles of the systems for solar water pumping and dynamic water desalination were described previously which had been built around the fluid piston converter with a simple design and made of low cost materials. In water pump and desalination systems the fluid piston converter works as an engine driven by solar thermal energy accumulated by flat- plate or evacuated tube collectors.

The fluid piston converter can function as a cooling machine if the fluid piston oscillations are induced by an external source. The solar cooling system which is under investigation in this research project is made of two separate parts which are coupled together. In the first part the fluid piston converter is driven by the thermal energy accumulated by a solar collector. The kinetic energy of oscillations of the fluid piston in the engine is used to maintain oscillations of the second fluid piston converter which operates as a cooling machine in the second part of the system. Calculations carried out using a computational code in MATLAB/Simulink environment demonstrate that temperatures considerably below ambient can be achieved in the cooling part of such coupled system. The developed code can also be used to determine the rational set of design parameters of the cooling section. Preparations are underway for experimental testing and evaluation of performance of the solar cooling system.

Nomenclature

c = denotes to the cooler control volume
C_v = specific heat at constant volume
m = mass
P = pressure
$\dot{Q}$ = heat transfer rate
t = time
V = volume
γ = isentropic index
ω = angular velocity
C_p = specific heat at constant pressure
e = denotes to cooling space control volume
$\dot{m}$ = mass flow rate
p = denotes to fluid piston engine control volume
R = universal gas constant
T = temperature
X = displacement of the water level
ε = the cooler effectiveness

1. Introduction

A significant part of the electricity produced in the world is used to run the various types of refrigeration and air-conditioning machines [1]. The energy consumption by air conditioning systems has been estimated to be 45% of the energy used in households and commercial buildings around the world [2]. Furthermore, the conventional air conditioning is partially responsible for the ozone depletion that occurs due to the use of refrigerants containing CFC, HCFC and HFC [3].

In a number of recent papers authors investigated the feasibility of application and determined the coefficient of performance (COP) of cooling devices operating on the Stirling cycle. Tekin and Ataer [4] developed a computer programme in FORTRAN to simulate a V-type Stirling-cycle refrigerator (VSR). The COP was calculated for a range of working fluids including air, helium and hydrogen. The V-type integral

Stirling refrigerator system using helium or hydrogen as a working fluid was studied experimentally and theoretically by Le'an et al. in [5]. From early works, Walker et al [6] reported on estimation of the performance of Stirling cryo-coolers with a two-phase working fluid Schulz and Thomas presented experimental results on a free-piston Vuilleumier refrigerator in [7]. Heidrich et al. [8] presented a mathematical model for numerical simulations of free-piston Stirling coolers. As an alternative for conventional vapor compression cycles, a Stirling cooler for domestic refrigerators was developed and the Stirling cooler performance was evaluated. Experimental investigations were conducted on a hybrid cooling system by He et al. in [9]. This system consisted of an active magnetic refrigeration cycle linked to a Stirling gas refrigerator. By combining the above two effects a considerable improvement of the cooling effect was achieved. Otaka et al. [10] studied experimentally the β- type Stirling cycle refrigerator. Helium, hydrogen and nitrogen were considered and the effects of the dead space and phase angle on the refrigeration capacity were investigated.

In this study, the concept of a solar cooling system using the fluid piston converter as an actuator of the cooling process will be investigated. The fluid of the free-piston converter was described by Mahkamov and Belgasim in [11] and they investigated experimentally and theoretically a desalination system built around the fluid piston converter.

2. Physical and Mathematical Model

Figure 1 shows a schematic diagram of the system being investigates. It consist of two parts: engine and cooling machine parts. The engine part contains solar evacuated tube collectors to heat water in the cylindrical evaporator. In addition, it contains condenser and fluid piston engine. The produced steam drives the fluid piston engine. The external fluid column acts as a fly wheel. The system is self-starting and the frequency of oscillations is between 2 and 3 Hz. The pressure variation of the air in the space above the external water column of the engine drives the fluid piston of the cooling machine which has a U-shape. The engine part and its mathematical model are described in details by Mahkamov and Belgasim in [11]. Oscillations of the fluid piston of the cooling machine provide a cooling effect in the cooling space. The heat from the cooling machine cycle is rejected in its cooler.

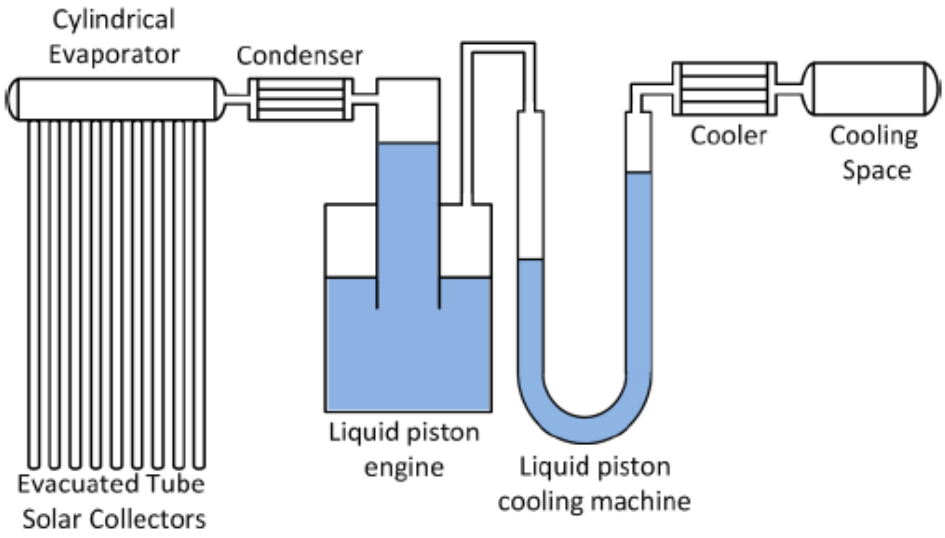

Fig 1. The schematic diagram of the fluid piston solar cooling system.

The calculation scheme of the cooling machine part of the system is presented in Figure 2 and it consists of three main parts which are fluid piston converter, cooler and cooling space. The working fluid in the system is

air which is assumed to behave as an ideal gas. The pressure and temperature of the air in the system varies due to the change in the volume caused by oscillations of the fluid piston with the expansion and compression processes taking place in the cycle. The heat generated during the compression process is rejected in the cooler and the cooling effect generated in the cooling space then can be transferred to the process heat carrier.

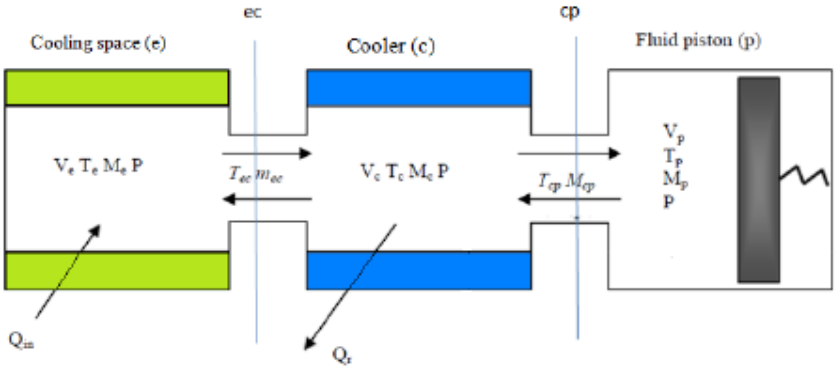

Fig. 2 The calculation diagram of the dynamic solar cooling system.

In deriving the mathematical model of the cooling part of the system all the above three components were considered to be control volumes.

For each control volume the general form of energy conservation equation is [10]:

$$\dot{Q} + (C_p \dot{m} T)_{in} - (C_p \dot{m} T)_{out} = P\frac{dV}{dt} + C_v \frac{d}{dt}(mT) \qquad (1)$$

where Cp and Cv are the specific heat capacities at the constant pressure and constant volume, respectively; T is the air temperature, P is the air pressure, V is the volume, m is the mass of air, $\dot{m}$ is mass flow rate into or out the control volume. The specific heats Cp, Cv can be calculated by using the universal gas constant R and isentropic index γ :

$$\left.\begin{aligned} C_p &= \frac{R\gamma}{\gamma - 1} \\ C_v &= \frac{R}{\gamma - 1} \end{aligned}\right\} \qquad (2)$$

In addition, the equation of state of the ideal gas is used in each control volume as follows:

$$PV = mRT \qquad (3)$$

The displacement of the fluid piston is calculated as

$$X = X_0 \cos(\omega t + \alpha) + L \qquad (4)$$

where ω is the angular velocity, α is the phase in the displacement which generally is assumed to be $\frac{\pi}{2}$; L is the starting position of the fluid piston. The volume of air in the fluid piston's cylinder can be calculated as

$$V_p = X * A_1 \qquad (5)$$

where A1 is the cross section of the cylinder.

The air pressure equation in the system can be found by summing the energy equation (1) written for each control volume:

$$\frac{V_t}{\gamma - 1}\frac{dP}{dt} = -\dot{Q}_r - \frac{\gamma}{\gamma - 1}P\frac{dV_p}{dt} + Q_e \tag{6}$$

Here V_t is the total air volume in the system and $\dot{Q}_r$ is the heat rejected in the cooler.

$$V_t = V_p + V_c + V_e \tag{7}$$

Indexes p, c and e refer to the control volumes of the fluid piston cyclinder; cooler and expansion (cooling) space, respectively. $\dot{Q}_r$ is calculated using the effectiveness-NTU method presented in [12]:

$$\dot{Q}_r = \varepsilon \dot{m}_{cp} C_p (T_{ci} - T_{cp}) \tag{8}$$

where T_{ci} is the temperature of the cooling water in the inlet to the cooler; T_{cp} is the temperature of the air at the plane between the cooler and expansion (cooling) space and ε is the effectiveness which depends on the type of the used heat exchanger. For the counter flow heat exchanger it is [12]:

$$\varepsilon = \frac{1 - \exp[-NTU(1 - C)]}{1 - C * \exp[-NTU(1 - C)]} \tag{9}$$

where

$$\left.\begin{aligned} C &= \dot{m}_{cp} Cp_{min} / \dot{m}_{ci} Cp_{max} \\ NTU &= \frac{UA_c}{\dot{m}_{cp} Cp_{air}} \end{aligned}\right\} \tag{10}$$

The value of T_{cp} in Eq (8) is defined as:

$$T_{cp} = \begin{cases} T_c, & \dot{m}_{cp} > 0 \\ T_p, & \dot{m}_{cp} < 0 \end{cases} \tag{11}$$

The equation of state is used to evaluate the temperature in each control volume:

$$\left.\begin{aligned} T_p &= \frac{PV_p}{Rm_p} \\ T_c &= \frac{PV_c}{Rm_c} \\ T_e &= \frac{PV_e}{Rm_e} \end{aligned}\right\} \tag{12}$$

The total mass of the air in the system is:

$$m_t = m_p + m_c + m_e \tag{13}$$

The mass flow rates in the control surfaces separating control volumes can be found using the following equation:

$$\frac{dm_p}{dt} + \frac{dm_c}{dt} + \frac{dm_e}{dt} = 0 \tag{14}$$

where

$$\left.\begin{aligned}\frac{dm_p}{dt} &= \dot{m}_{cp}\\ \frac{dm_e}{dt} &= -\dot{m}_{ec}\end{aligned}\right\} \tag{15}$$

Finally, the mass of air in the cooler can be defined in terms of the mass of air in the cooler from the previous time step m_c^i:

$$m_c = m_c^i + \frac{dm_c}{dt}dt \tag{16}$$

3. Methodology

The equations of the mathematical model of the dynamic solar cooling system have been solved using the Matlab/Simulink software. The developed Simulink model was built as a closed loop as shown in Figures 3 and 4. Such the model allows to consider influence of parameters of all three control volumes on each other during the integration process. As output it provides information on the variation of volumes, pressures and temperatures in every control volume. The Matlab/Simulinkl model also contains a set of criteria to establish whether the steady regime of operation is achieved during numerical integration (Figure 4). The model also takes into account the heat losses in the design of the system.

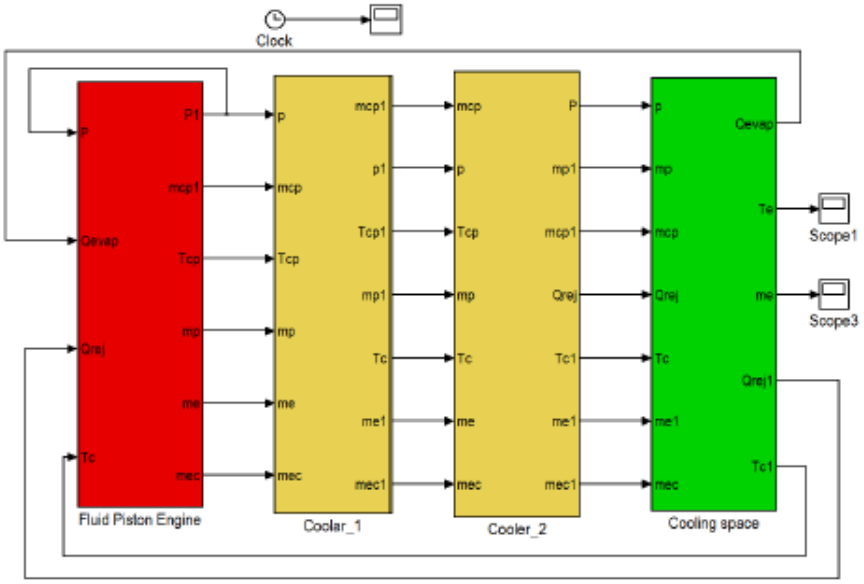

Fig. 3 The Simulink model of the dynamic solar cooling system.

4. Results and Discussion

The operation of the cooling system was simulated for the conditions in which the amplitude of the fluid piston on the engine side and its frequency of oscillations were 50 mm and 3 Hz, respectively. The temperature of the water in the inlet to the cooler was assumed to be 25 °C. These conditions correspond to the operation of the fluid piston engine, tested experimentally in [11]. The relationship between diameters of pipes of the cylinders of the engine and cooling machine would results in the amplitude of the fluid piston in the cooling machine being 150 mm.

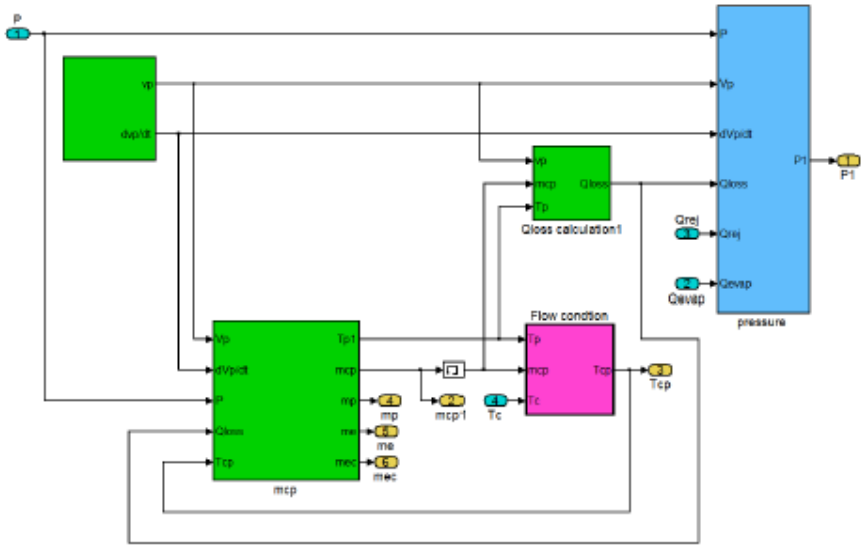

Fig. 4 The Simulink model of the fluid piston cooling system.

Figure 5 and 6 demonstrate the displacement of the fluid piston in the cylinder of the cooling machine and air pressure variation inside the cooling system, respectively. Amplitude of fluid piston is about 130 mm. Due to variation of the total volume of the cooling system the air pressure periodically changes between 1.06 and 0.958 bar.

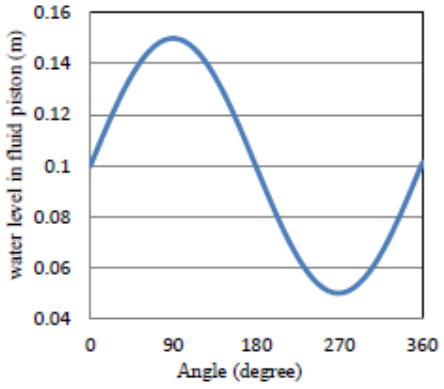

Fig. 5 The liquid piston displacement in the cylinder of the cooling system.

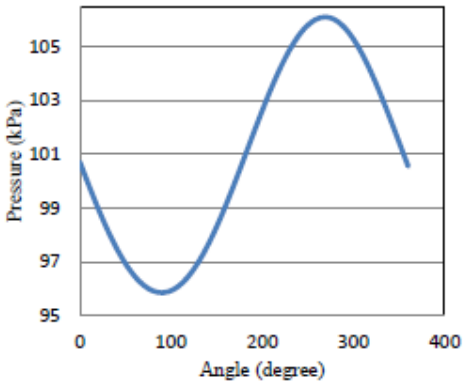

Fig. 6 The air pressure variation in the cooling system

Figures 7, 8 and 9 demonstrate the variation of the temperature of air in the cylinder, cooler and cooling space, respectively. It can be seen that the amplitude of the temperature variation in the cylinder is 15 K (the maximum and minimum temperatures are 304 and 289 K). The range of the temperature variations in the cooler and cooling space are about 22 K with maximum and minim temperatures being 303 and 281 K, respectively. Figure 10 demonstrates the influence of the temperature of the water in the inlet to the cooler and it

can be seen that the temperature close to 272 K can be obtained when the cooling water has the temperate of 283 K.

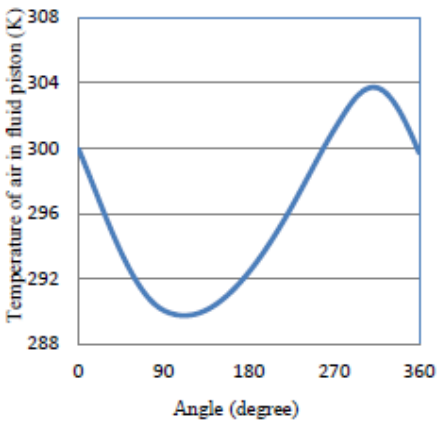

Fig. 7 The temperature of air in the cylinder of the cooling system.

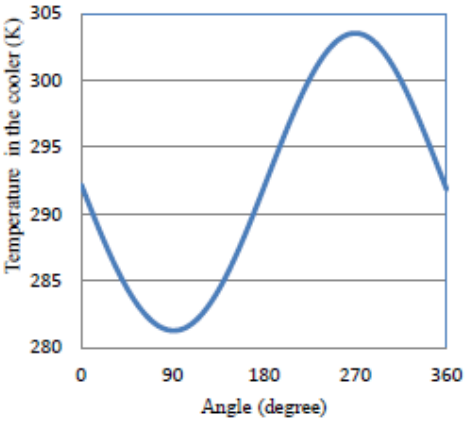

Fig. 8 The temperature of air in the cooler of the cooling system.

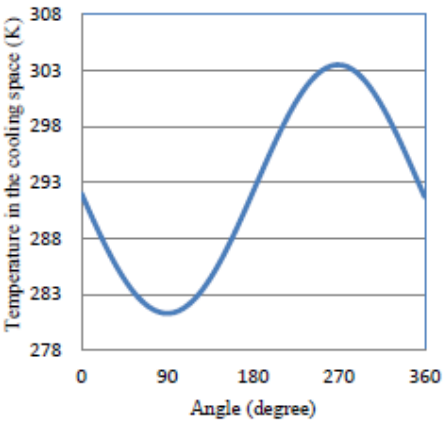

Fig. 9 The temperature of air in the cooling space of the cooling system.

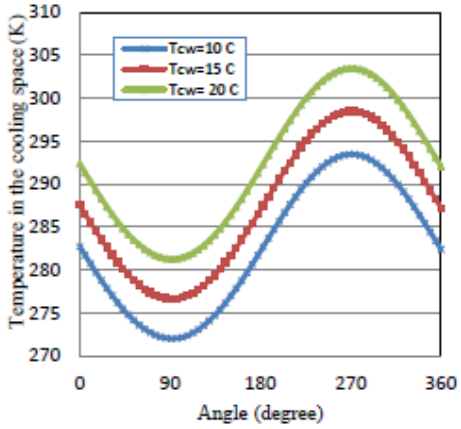

Fig. 10 effect of coolant temperature on air temperature.

The cooling capacity of the system depends on its dimensions and its cooling effect can be used for air-conditioning of buildings in regions with high solar radiation.

5. Conclusion

In this study, the physical model of a solar cooling system based on the fluid piston converter is presented. The mathematical model of this system was developed and its operation was simulated using Matlab/Simulink software. Preliminary results demonstrate that the cooling temperatures below water freezing point can be achieved and such systems could be used as a part of air-conditioning in the regions with hot climate.

6. References

[1] H. Hassan, "A Solar Powered Adsorption Freezer: A Case Study for Egypt's Climate," International Journal of Energy Engineering, vol. 3, pp. 21-29, 2013.

[2] B. Choudhury, P. Chatterjee, and J. Sarkar, "Review paper on solar-powered air-conditioning through adsorption route," Renewable and Sustainable Energy Reviews, vol. 14, pp. 2189-2195, 2010.

[3] H. Z. Hassan and A. A. Mohamad, "A review on solar cold production through absorption technology," Renewable and Sustainable Energy Reviews, vol. 16, pp. 5331-5348, 2012.

[4] Y. Tekin and O. E. Ataer, "Performance of V-type Stirling-cycle refrigerator for different working fluids," International Journal of Refrigeration, vol. 33, pp. 12-18, 2010.

[5] S. Le'an, Z. Yuanyang, L. Liansheng, and S. Pengcheng, "Performance of a prototype Stirling domestic refrigerator," Applied Thermal Engineering, vol. 29, pp. 210-215, 2009.

[6] T. Otaka, M. Ota, K. Murakami, and M. Sakamoto, "Study of performance characteristics of a small Stirling refrigerator," Heat Transfer—Asian Research, vol. 31, pp. 344-361, 2002.

[7] G. Walker, "Stirling cycle cooling engine with two-phase, two-component working fluid," Cryogenics, vol. 14, pp. 459-462, 1974.

[8] S. Schulz and B. Thomas, "Experimental investigation of a free-piston Vuilleumier refrigerator," International journal of refrigeration, vol. 18, pp. 51-57, 1995.

[9] X. N. He, M. Q. Gong, H. Zhang, W. Dai, J. Shen, and J. F. Wu, "Design and performance of a room-temperature hybrid magnetic refrigerator combined with Stirling gas refrigeration effect," International Journal of Refrigeration, vol. 36, pp. 1465-1471, 2013.

[10] J. W. F. Heidich and D. E. B. Prata, "Heat and fluid flow in a free piston Stirling refrigerator.," presented at the Fluid Mech. Group Inter. Conf. compressors syst. IMechE, 2005.

[11] K. Mahkamov and B. Belgasim, Experimental study of the performance of a dynamic water desalination system with a fluid piston engine, Proceedings of the 14th International Stirling Engine Conference, November 16-18, 2009, Groningen, Netherlands.

[12] J. P. Holman, Heat Transfer, 10th ed. ed. New Tork: McGraw-Hill, 2010.

Development of a Solar Cooling System Based on a Fluid Piston Convertor

Khamid Mahkamov, Northumbria University, UK
Gamal Hashem, Northumbria University, UK

The Third European Conference on Sustainability, Energy & the Environment 2015
Official Conference Proceedings

Abstract
Solar water pumping and dynamic water desalination based on fluid piston converter were developed at Northumbria University. The fluid piston converter has a simple design and made of low cost materials. In water pump and desalination systems, the fluid piston converter works as an engine, driven by solar thermal energy absorbed by flat-plate or evacuated tube collectors. If in the same design of the converter, its fluid piston is driven using external source of energy without heat input, then such the converter works as a cooling device.

In this study, the solar fluid piston engine is coupled with the cooling unit with the fluid piston of the latter driven by the fluid piston engine. This results in production of cooling effect using solar energy. The operation of such system has been investigated theoretically and experimentally. The thermodynamic model, consisting of a system of ordinary differential equations, was developed in the MATLAB/Simulink environment to simulate the operation of such the thermal auto-oscillation system. The theoretical results confirm that it is possible to achieve the temperature of the working fluid in the cycle of the cooling unit, which is below the ambient temperature. The cooling effect depends on the operational parameters of both the engine and cooling parts of the system.

Keywords: solar cooling system, fluid piston engine

iafor
The International Academic Forum
www.iafor.org

Nomenclature

Symbols

C_v - specific heat at constant volume
M - mass
P - pressure
$\dot{Q}$ - heat transfer rate
t - time
V - volume
γ - isentropic index
ω - angular velocity
C_p - specific heat at constant pressure
$\dot{m}$ - mass flow rate
p - denotes to fluid piston engine control volume
R - universal gas constant
T - temperature
X - displacement of the water level
ε - the cooler effectiveness

Indexes

c - denotes to the cooler control volume
e - denotes to cooling space control volume

Introduction

At present, a limited number of solar cooling systems are available commercially on the market and the scale of the practical applications is relatively small due to relatively high initial and running costs. Numerous studies have been carried out on different types of solar cooling systems including solar absorption and adsorption systems [1-5], the combined power and cooling [6, 7] and other types of solar cooling systems [8-10]. During the last few years, new test rigs for solar water pumping and dynamic water desalination unit were built and experimentally and theoretically investigated at Nortumbria University [11, 12]. These test rigs were built around the fluid piston converter/engine and solar evacuated tube collector with heat pipes. Heat input into the system was carried out using a solar simulator, made of 110 halogen floodlights, and controlled by an electrical three-phase transformer.

The concept of solar cooling system which has been built around the fluid piston engine and cooling machine is shown in Figure 1. The solar energy is used to drive the fluid piston engine which in its turn drives the cooling machine producing a cooling effect.

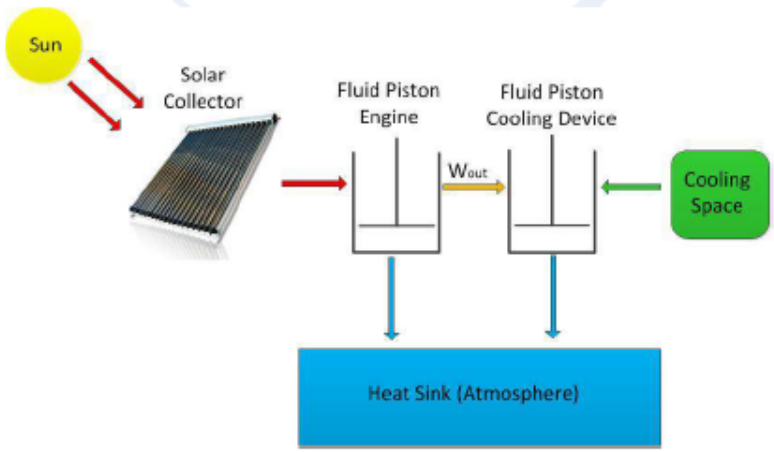

Figure 1: The concept of the solar cooling system.

Physical and Mathematical Model

Figure 2 shows a schematic diagram of the test rig with solar cooling system. It consists of two parts: engine and cooling machine parts. The engine part is made of the solar evacuated tube collector to heat water in the cylindrical evaporator and fluid piston engine. The evaporator is connected to the engine through the condenser. Steam produced by the solar collector drives the fluid piston engine. The fluid piston engine is made of two enclosed concentric plastic cylinders connected to each other in their bottom sections. The internal and external fluid columns act as a piston and fly wheel, respectively. The system is self-starting and the frequency of oscillations is about 1.5-3 Hz depending on the air volume above the external liquid column in the engine. The fluid piston is activated by the thermal energy generated in the evaporator. The pressure variation of air in the space above the external water column of the engine also drives the fluid piston of the cooling machine which has a U-shape. The condenser and cooler are used to reject the heat from the cycle of the engine and cooling machine.

The engine part and its mathematical model are described in details by Mahkamov et al. in [13].

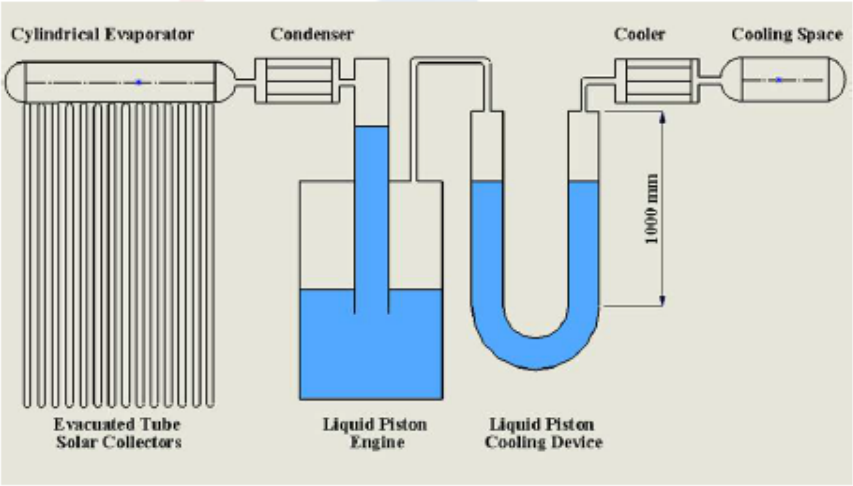

Figure 2: The fluid piston solar cooling system.

The calculation scheme for the mathematical modelling of the cooling part of the system is presented in Figure 3. It consists of three main control volumes, namely for fluid piston converter, cooler and cooling space. The working fluid in the system is air which is assumed to behave as an ideal gas. The pressure and temperature of the air in the system vary due to the change in the volume caused by oscillations of the fluid piston with the expansion and compression processes taking place in the cycle. The heat generated during the compression process is rejected in the cooler and the cooling effect generated in the cooling space during expansion process. The cold generated then can be transferred to the process heat carrier.

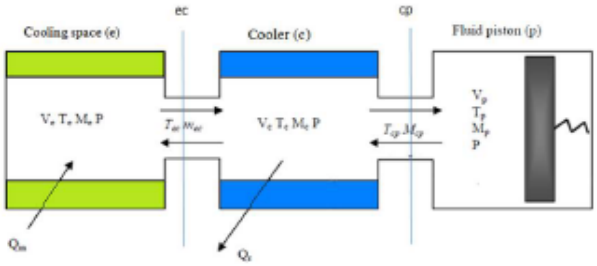

Figure 3: The calculation scheme of the cooling system.

The temperatures in the control volumes are affected by the direction of gas flow in interfaces between cooling space and cooler (denoted as ec) and cooler and fluid piston cylinder (shown as cp in Figure 3). For each of the control volumes mass and energy conservation equations are written.

The energy equation for the control volume can be presented as [14]:

$$\dot{Q} + (C_p \dot{m} T)_{in} - (C_p \dot{m} T)_{out} = P\frac{dV}{dt} + C_v \frac{d}{dt}(mT) \quad (1)$$

The displacement of the fluid piston is described as

$$X = X_0 \cos(\omega t) + L \quad (2)$$

where L is the starting position of the fluid piston.

The air pressure in the system is found by adding to each other energy equations (1) written for control volumes:

$$\frac{V_t}{\gamma - 1}\frac{dP}{dt} = -\dot{Q}_r - \frac{\gamma}{\gamma - 1} P \frac{dV_p}{dt} + Q_e \quad (3)$$

Here V_t is the total air volume in the system, Q_e are heat losses and $\dot{Q}_r$ is the heat rejected from the cooler, which calculated by applying the effectiveness-NTU method presented in [15].

MATLAB/Simulink environment

The above set of equations was solved in the MATLAB/Simulink environment. The developed Simulink model was built as a closed loop to simulate the proposed dynamic solar cooling system, as shown in Figure 4. After reaching the steady state condition, the variation in the fluid piston volume, the system air pressure and temperatures in every control volume are defined. The MATLAB/Simulink model also contains a set of criterion to establish whether the steady regime of operation is achieved during numerical integration. The heat losses in all three control volumes are calculated to produce more accurate results.

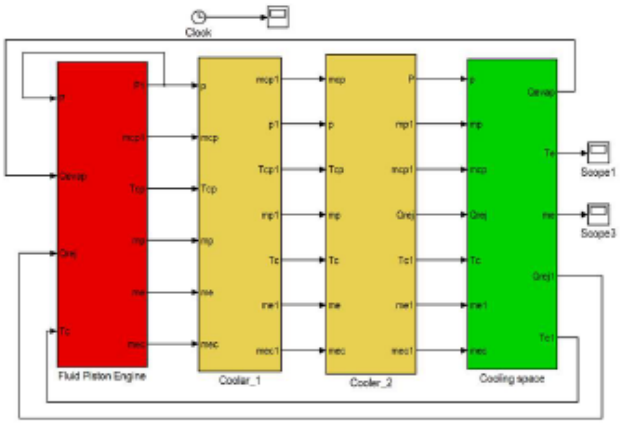

Figure 4: Simulink model of the solar cooling system.

Theoretical results

The operation of the cooling system was simulated for the specified amplitude of the fluid piston in the engine part and its frequency equal to 0.1 m and 3Hz, respectively. In addition, the temperature of the cooling water that enters the cooler was set to be 20° C. These conditions correspond to the operation of the fluid piston engine, tested experimentally in [11]. The displacement of the water column in cooling machine over the cycle is shown in Figure 5. Due to variation of the total volume of the cooling system the air pressure also periodically changes between 1.06 and 0.958 bar, see Figure 6.

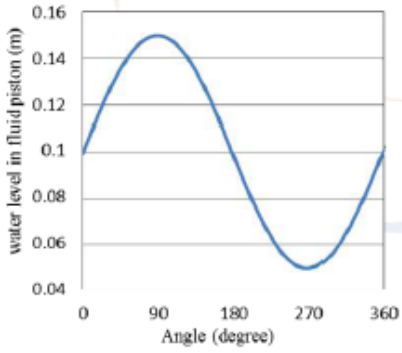

Figure 5: The liquid piston displacement.

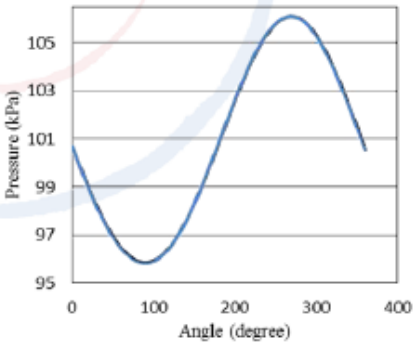

Figure 6: Air pressure variations.

Figures 7 and 8 demonstrate the variations of the temperature of air in the cylinder and cooling space, respectively. It can be seen in Figure 7 that the amplitude of the temperature variation in the cylinder is 15 degrees with maximum and minimum temperatures being 304 and 289 K. The range of the temperature variations in the cooling space are about 22 degrees with maximum and minimum temperatures being 303 and 281 K, respectively.

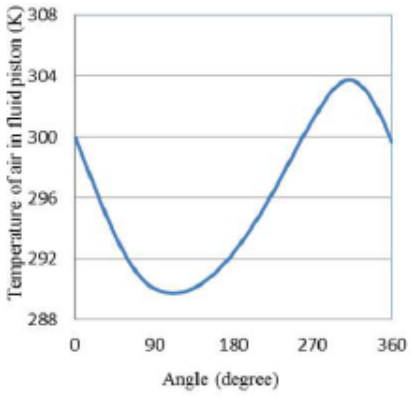

Figure 7: Air temperature in the cylinder.

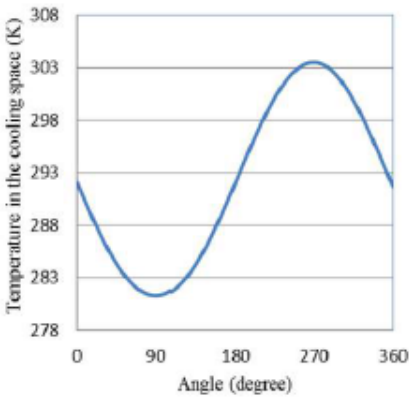

Figure 8: Air temperature in cooling space.

Experimental test rig

The engine test rig consists of the engine part with condenser, U-shaped cooling machine with cooler and heat pipe evacuated-tube solar collectors with the solar radiation simulator, see Figure 9

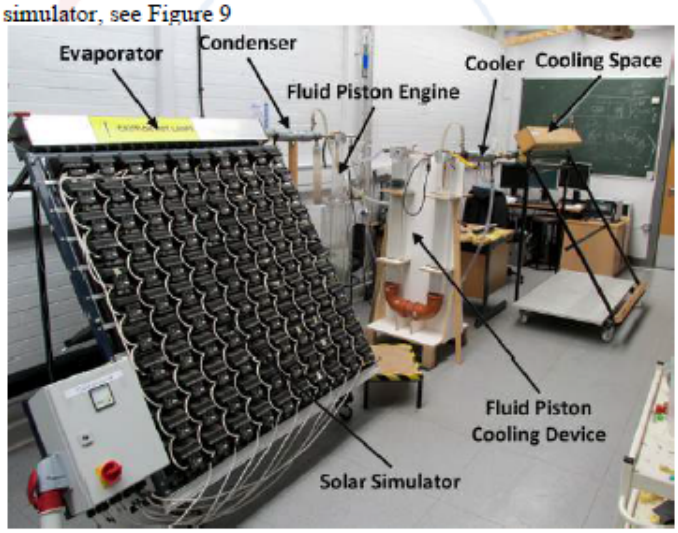

Figure 9: The test rig.

The evaporator is also the upper manifold of the solar collector which houses heads of heat pipes of the evacuated tube solar receivers. In this manifold the heat from head of heat pipes is transferred to the water and it is boiled producing steam. Generated steam is turned into the liquid in the condenser and returned back to the manifold. The pressure rise in the manifold initiates oscillations of water column (fluid piston) in the engine part. The solar simulator is made of 110 tungsten halogen lamps (150 W each) controlled by 3-phase variable transformer. The heat flux form halogen lamps onto the surface of the evacuated tubes was measured using a PMA 2200 photometer as a

function of the 3-phas transformer voltage. The changes in the temperatures, pressures and levels of water columns were recorded using National Instruments DAQ, as shown in Figure 10. The types and specifications of sensors together with their locations are presented in Table 1.

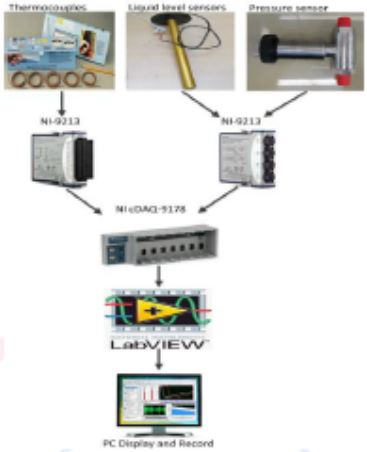

Figure 10: Data acquisition system.

Table 1: Specifications of the different sensors.

Component	Sensors	Description
Fluid piston engine	Water column level; Pressure; Temperature.	Level sensor: The aluminium R-series liquid level sensor by Gill Sensors (UK) with sampling rate of 80Hz. Pressure sensor: UNIK 5000 differential pressure transducer (-4 to +4 bar gauge), Druck Ltd Temperature sensor: The PFA insulated T-type thermocouples with thickness of 0.08mm.
U-Tube liquid piston cooling machine	Water column level; Pressure; Temperature.	
Cooling space	Temperature	

Experimental Results

The experimental results on oscillations fluid pistons in engine and cooling machine, cyclic variation in the air pressure and temperatures in the cylinders and cooling space are presented in Figures 11-15. It can be seen in Figures 11 and 12 that the amplitude of the fluid piston engine is about 5 cm whilst in the cooling machine this value is 1.6

cm. This difference is due to difference in diameters of plastic pipes used to make the engine and cooling machine (8.5 and 10 cm, respectively) frictional losses in the movement of the water columns in the internal and external cylinders of the fluid piston engine and the cylinder of the cooling machine. The changes in the air pressure in the engine and cooling parts over the cycle are shown in Figure 13.

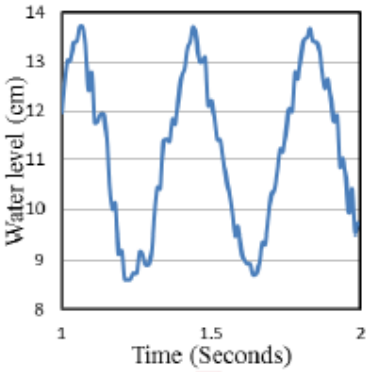

Figure 11: The engine liquid piston displacement.

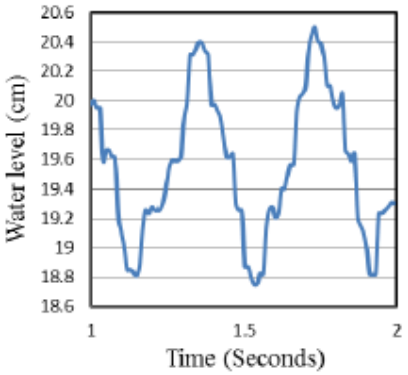

Figure 12: The cooling machine liquid piston displacement.

Before switching on the solar simulator, the air gage pressure in both the engine part and cooling part are set to be equal to the atmospheric pressure. By switching the set The oscillation of the air pressure and cooling parts is between 0.032 and -0.073 bar (gage) in the engine part and between 0.11 and 0.02 bar (gage) in the cooling machine.

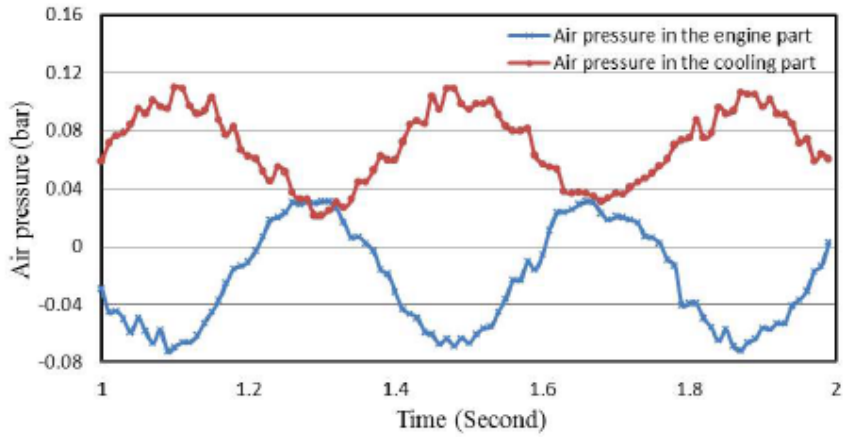

Figure 13: Air pressure in the engine part and cooling part.

Figures 14 and 15 show the variation in the air temperature in the cylinder of the cooling machine and in the cooling space. It can be seen that the average air temperature in the cylinder is 294.24 °K and this value in the cooling space is 292.7 °K. This demonstrates that the cooling effect takes place in the system with a 1.54 degrees reduction in the temperature of air.

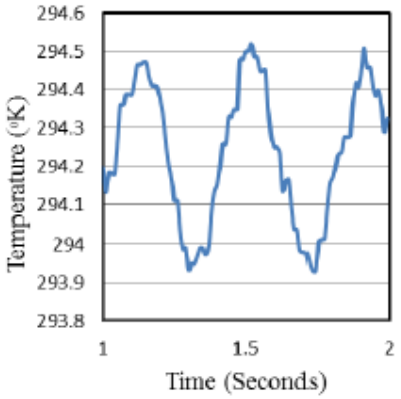

Figure 14: Air temperature in the cylinder of cooling machine.

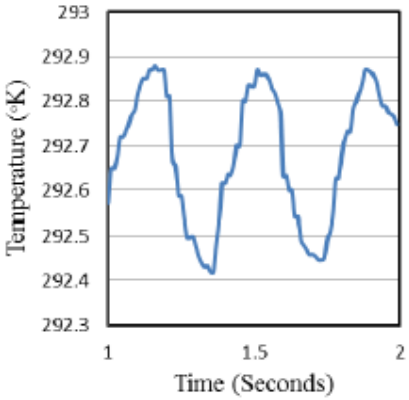

Figure 15: Air temperature in the cooling space.

Conclusions

In this study, the concept of the solar cooling system based on fluid piston converters is presented. The mathematical model of this cooling system was and numerical simulations were performed in MATLAB/Simulink environment. The possibility of producing the cooling effect in the system was demonstrated by means of numerical simulations and experiment. The theoretical reduction in the air temperature was about 3 degrees whilst in the experiment this value was found to be 1.54 degrees. The deviation between the theoretical and experimental results is due to unaccounted heat losses in the system.

References

[1] H. Z. Hassan and A. A. Mohamad, "A review on solar cold production through absorption technology," *Renewable and Sustainable Energy Reviews,* vol. 16, pp. 5331-5348, 2012.

[2] X. Yan, G. Chen, D. Hong, S. Lin, and L. Tang, "A novel absorption refrigeration cycle for heat sources with large temperature change," *Applied Thermal Engineering,* vol. 52, pp. 179-186, 2013.

[3] R. de Lieto Vollaro, F. Botta, A. de Lieto Vollaro, and G. Galli, "Solar cooling system for buildings: Thermal analysis of solid absorbents applied in low power adsorption system," *Energy and Buildings,* vol. 80, pp. 436-440, 2014.

[4] H. Z. Hassan, A. A. Mohamad, and R. Bennacer, "Simulation of an adsorption solar cooling system," *Energy,* vol. 36, pp. 530-537, 2011.

[5] H. Hassan, "A Solar Powered Adsorption Freezer: A Case Study for Egypt's Climate," *International Journal of Energy Engineering,* vol. 3, pp. 21-29, 2013.

[6] D. S. Ayou, J. C. Bruno, R. Saravanan, and A. Coronas, "An overview of combined absorption power and cooling cycles," *Renewable and Sustainable Energy Reviews,* vol. 21, pp. 728-748, 2013.

[7] S. Vijayaraghavan and D. Y. Goswami, "A combined power and cooling cycle modified to improve resource utilization efficiency using a distillation stage," *Energy,* vol. 31, pp. 1177-1196, 2006.

[8] F. Xu, D. Y. Goswami, and S. S. Bhagwat, "A combined power/cooling cycle," *Energy,* vol. 25, pp. 233-246, 2000.

[9] M. Sultan, I. I. El-Sharkawy, T. Miyazaki, B. B. Saha, and S. Koyama, "An overview of solid desiccant dehumidification and air conditioning systems," *Renewable and Sustainable Energy Reviews,* vol. 46, pp. 16-29, 2015.

[10] Y. Tekin and O. E. Ataer, "Performance of V-type Stirling-cycle refrigerator for different working fluids," *International Journal of Refrigeration,* vol. 33, pp. 12-18, 2010.

[11] K. Mahkamov and B. Belgasim, "Experimental study of the performance of a dynamic water desalination system with a fluid piston engine," in *The 14th international Stirling engine conference*, 2009.

[12] K. Mahkamov, E. Orda, B. Belgasim, and I. Makhkamova, "A novel small dynamic solar thermal desalination plant with a fluid piston converter," *Applied Energy,* vol. 156, pp. 715-726, 2015.

[13] K. Mahkamov, G. Hashem, B. Belgasim, and I. Makhkamova, "A Novel Solar Cooling system Based on a Fluid Piston Convertor," presented at the 16th International Stirling Engine Conference, Belbao, Spain, 2014.

[14] Y. A. Çengel and M. Boles, *Thermodynamics: an engineering approach*. London McGraw-Hill 2008.

[15] J. P. Holman, *Heat Transfer*, 10th ed. ed. New Tork: McGraw-Hill, 2010.

PARAMETRIC ANALYSIS OF A DYNAMIC SOLAR COOLING SYSTEM BASED ON A LIQUID PISTON CONVERTER

K. MAHKAMOV[a,*], G. HASHEM[a,b], B. BELGASIM[b], K. HOSSIN[a,b], I. MAKHKAMOVA[a]

[a] Faculty of Engineering & Environment, Northumbria University, Newcastle upon Tyne, UK

[b] Faculty of Engineering, University of Benghazi, Benghzi, Libya

*Corresponding author: khamid.mahkamov@northumbria.ac.uk

Keywords: Solar thermal collectors; fluid piston engine, cooling machine.

ABSTRACT

Various solar-powered cooling technologies exist, yet their business sector penetration level is relatively low because of the high capital costs involved with a long pay-back period. Extensive R & D activities are in progress to enhance performance and reduce capital and running costs of existing and future solar-powered systems.

Solar water pumping and dynamic water desalination based on application of the liquid piston converter were investigated in the Energy Laboratory at Northumbria University. The liquid piston converter has a simple design and made of non-expensive materials. In the water pump and desalination systems, the fluid piston converter works as an engine, driven by solar thermal energy absorbed by flat plate or evacuated tube collectors. A combination of the liquid piston engine driving a similar converter with reversed cycle can operate as a solar cooling system.

A thermodynamic model consisting of a set of ordinary differential equations, describing fluid piston motions, energy and mass conversion processes inside the working gas circuits of the engine and cooling part, was developed in the MATLAB/Simulink environment to simulate the operation of such the thermal auto-oscillation system and to compare to experimental results. In this study, the effect of the cooling water temperature and its flow rate in the cooler on the performance of the system is studied. It is shown that the reduction of water temperature, circulated across the cooler, which is the good effect, is positively affected with the drop in cooling water temperature, and to a lesser extent positive with increasing cooling water flowrate.

INTRODUCTION

The International Energy Agency (IEA) reported that the world's total final energy consumption in 2010 was 8677 million tonnes of oil equivalent (Mtoe) or 363 Exajoules (EJ) [1, 2]. In 2011, the International Energy Outlook predicted that the world's energy consumption is expected to rise from 533 EJ in 2008 to 812 EJ in 2035, with a growth of 53% [3]. The growth of energy demand occurs predominantly in countries outside of the Organization for Economic Cooperation and Development (non-OECD). Based on the report issued by the Renewable Energy Policy Network for the 21st Century, currently about 81% of the world's energy consumption is satisfied by using fossil fuels, while 16% is provided by renewable sources and the remainder comes from nuclear industry.

Numerous studies have been carried out on different types of solar cooling systems including solar absorption and adsorption systems [4-8], the combined power and cooling [9,

10] and other wide range of solar cooling systems [11-13]. Yet, a limited number of solar cooling systems are available commercially and the scale of their practical application is relatively small due to high initial and running costs.

Mahkamov et al. [14-16] developed and tested in laboratory conditions a dynamic solar water desalination plant. The system is a combination of a heat pipe evacuated tube solar collector, conventional condenser and novel fluid piston converter. A small fraction of the solar energy supplied to the plant is used to drive the fluid piston converter. Oscillations of the fluid piston are periodical and result in the near harmonic change of the volume of the engine and pressure in the plant. The fluid piston converter drives a pump which provides lifting of saline water from a well and pumps this through the cooling jacket of the condenser to a saline water storage tank. The proposed novel system with greater fresh water production capacity has a simple design and is easy to manufacture using low cost materials and therefore can be mass deployed for small scale saline water pumping and desalination across different regions with the relatively high solar radiation and shortage in the drinking water supply.

Based on this dynamic solar water desalination plant, Mahkamov et al. proposed and presented a preliminary theoretical study of a solar cooling system [17]. In that study, the physical model consisted of just cooling part and in the modelling the liquid piston movement was assumed to be an input parameter. The proposed model of the cooling system consisted of three control volumes namely, liquid piston cylinder in the cooling device, cooler and cooling space. The preliminary findings showed promising results and confirmed that the cooling effect could be achieved in the cooling space. Furthermore, Mahkamov and Hashem [18] illustrated the possibility of producing the cooling effect in the proposed solar cooling system by means of numerical simulations and experiment. The experimental work has been carried out at Northumbria University by connecting the solar energy converter to a reversed machine, which is a new solar cooling system, to produce the cooling effect.

DESIGN AND OPERATIONAL PRINCIPLE OF THE PLANT

The schematic diagram of the dynamic solar cooling unit is illustrated in Figure 1. The system consists of two main parts: engine/converter and cooling machine. The engine part contains evacuated tube solar collector, cylindrical evaporator, condenser and liquid piston engine which is the left side of the U-shaped tube. The cooling part contains the liquid piston machine, which is the right side of the U-shaped tube, cooler and cooling space. The system is self-starting and the frequency of oscillations is about 3 Hz.

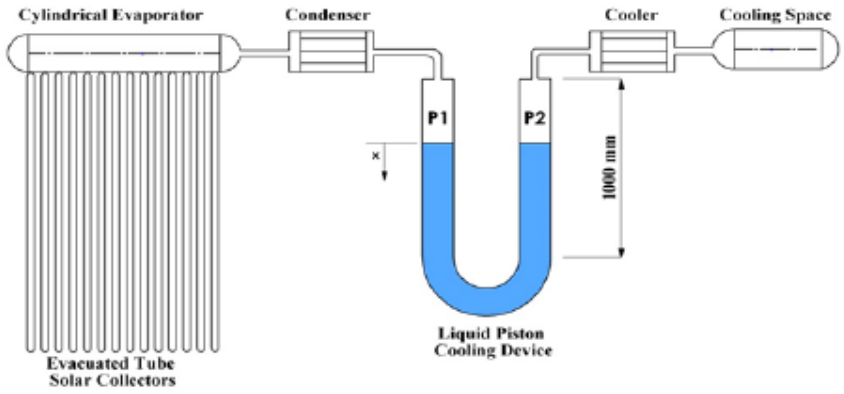

Figure 1. The schematic diagram of the solar cooling system.

The system receives the solar radiation through the evacuated tube solar collectors which is used to boil water in the cylindrical evaporator. In its turn steam heats up air in the system and turns into liquid in the condenser. Increase in the air pressure results in the initiation of the liquid piston oscillations. The outcome of these oscillations are alternate compression and expansion of air in the cooling part of the system. The heat generated during compression process is dissipated in the cooler and as a result the air temperature in the cooling part is reduced below the ambient temperature.

MATHEMATICAL MODEL

To derive the mathematical model of the system, it has been divided into two main parts, namely: the engine and cooling parts. The link between the two parts is the reciprocating movement of the water column (liquid piston), as shown in Figure 1. The engine and cooling parts are further divided into three control volumes, as shown in Figures 2 and 3 to include evaporator, condenser and cylinder space on the engine side and the cylinder space, cooler and cooling space on the cooling machine side. In these Figures, index *e* denotes the evaporator and cooling space, *c* denotes the condenser and cooler and *p* denotes the cylinder spaces. Additionally, the two control surfaces between the three control volumes are denoted as *ec* and *cp*. The evaporator has a volume of two litres but it is normally filled with one litre of water whilst the remaining part is filled with air. The generation of saturated stream is a continuous process in the evaporator, therefore, in this control volume, the working fluid is assumed to be only generated steam. In the control volume of the condenser, the working fluid consists of the mixture of steam, coming out the evaporator, and air. In the cylinders the working fluid is assumed to be air because all steam passing through the condenser is converted to liquid and collected in the water trap. On the cooling machine side, the working fluid is just air. The mixture of water vapour and air are assumed to behave as an ideal gas. The fluid piston engine is treated as a mass-spring oscillating system with a rigid piston and a dumper. By using such calculation scheme, the lumped parameter mathematical model of the system can be derived which includes the system of energy and the mass conservation equations, written for each control volume in the form of ordinary differential equations, toped up by dynamics equation of the liquid piston. By solving these equations, the information on the cyclic change of the air pressure and temperatures in the two parts of the system can be obtained.

In the modelling process, the temperature in the evaporation space is assumed to be equal to the saturation temperature, defined by value of the instantaneous pressure value in the system. Temperatures T_{ec} and T_{cp} depend on the direction of the flow.

The Engine Part

The general form of energy conservation equation for unsteady flow in the control volume can be described as [19]:

$$\dot{Q} + (C_p \dot{m} T)_{in} - (C_p \dot{m} T)_{out} = P\frac{dV}{dt} + C_v \frac{d}{dt}(mT) \quad (1)$$

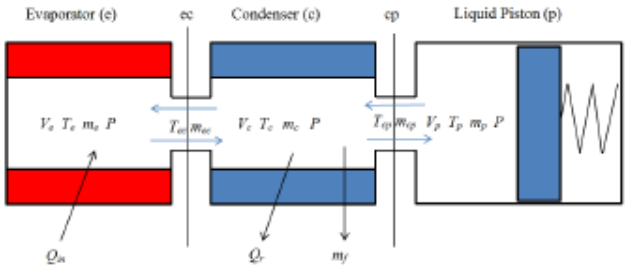

Figure 2. The calculation scheme of the engine part.

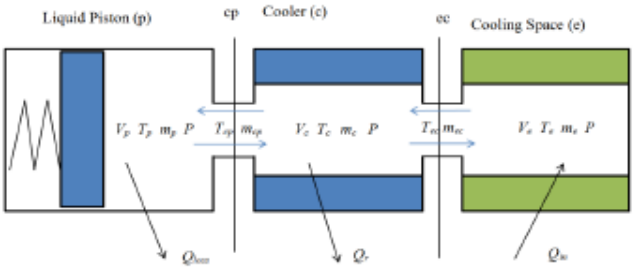

Figure 3. The calculation scheme of the cooling part.

Control Volume of the Evaporator

The evaporator contains two different fluids - water and steam. Therefore, the entire volume of the evaporator has been divided into two control volumes as shown in Figure 4.

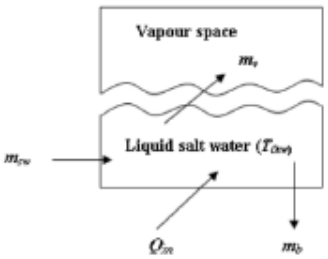

Figure 4. The control volume of the evaporator.

Application of the energy equation (1) to the vapour space of the evaporator results in:

$$\frac{V_e}{\gamma_v - 1}\frac{dP_1}{dt} = \dot{m}_v h_g - \dot{m}_{ec} h_g \qquad (2)$$

where $\dot{m}_v$ is the vapour mass production rate inside the evaporator, $\dot{m}_{ec}$ is the vapour mass flow rate from the evaporator to the condenser, h_g is the enthalpy of the vapour; γ_v is isentropic index of vapour and P_1 is the vapour pressure in the engine part.

The mass balance equation for the vapour space is

$$\frac{dM_g}{dt} = m_v - m_{ec} \qquad (3)$$

In this equation m_v can be obtained from the energy equation of the liquid salt water (if such is used) in the evaporator:

$$m_v\left[h_{fg} - C_{psw}(T_{0sw} - T_{sat})\right] = Q_{in} \tag{4}$$

T_{0sw} is the boiling point of the saline water, which is assumed to be constant during the operation of the system: $T_{0sw} = 103$ °C.

Control Volume of the Condenser

For the control volume of the condenser, the energy equation takes the following form:

$$\frac{V_c}{\gamma - 1}\frac{dP_1}{dt} = \dot{m}_{ec}h_g - \dot{m}_f h_f - \left(\dot{m}_{cp}C_pT_{cp}\right)_v - \left(\dot{m}_{cp}C_pT_{cp}\right)_a - \dot{Q}_r \tag{5}$$

where, $\dot{m}_f$ and h_f are the mass and enthalpy of the condensed fresh water, $\dot{Q}_r$ is the heat rejected from the working fluid in the condenser, Cp_v and Cp_a are the heat capacity of the water vapour and air, respectively.

The temperature of the working fluid in the condenser is Tc equal to saturation temperature.

The temperature of the working fluid on control surface T_{cp} depends on the direction of the flow between the two control volumes:

$$T_{cp} = \begin{cases} T_c, & \dot{m}_{cp} > 0 \\ T_p, & \dot{m}_{cp} < 0 \end{cases} \tag{6}$$

The heat exchanged in the condenser, which is concentric double pipe counter flow heat exchanger, is calculated by using the effectiveness-NTU method described in [20]:

$$\dot{Q}_r = \varepsilon\dot{m}_{cool}C_{pcool}(T_{sat} - T_{ci}) \tag{7}$$

In this equation, ε is the heat exchanger effectiveness, $\dot{m}_{cool}$ and C_{pcool} are the mass flow rate and heat capacity of cooling water in the water jacket, respectively, T_{ci} is the inlet temperature of the cooling water.

$$NTU = \frac{UA_c}{\dot{m}_{cool}C_{pcool}} \tag{8}$$

where A_c denotes to contact surface area between the two fluids, and U is the overall heat transfer coefficient which is defined as:

$$U = \frac{h_o h_i}{h_o + h_i} \tag{9}$$

Here, the outer and inner heat transfer coefficients h_o , h_i are the convective heat transfer coefficients on the condensation and water jacket sides, respectively.

$$h_i = 0.555\left[\frac{g\rho_l(\rho_l - \rho_v)k_l^3 h'_{fg}}{\mu_l(T_{sat} - T_s)D}\right]^{1/4} \tag{10}$$

where the term h'_{fg} denotes to the modified value of the condensation heat.

$$h'_{fg} = h_{fg} + \frac{3}{8}C_{p,l}(T_{sat} - T_s) \tag{11}$$

The outer convective heat transfer coefficient h_o is usually determined as a function of Nusselt number Nu in a heat transfer correlation [21].

Control Volume of the Cylinder of the Liquid Piston Engine

The energy equations for the cylinder of the liquid piston engine can be written as

$$\frac{V_p}{\gamma-1}\frac{dP_1}{dt} = \left(\dot{m}_{cp}C_pT_{cp}\right)_v + \left(\dot{m}_{cp}C_pT_{cp}\right)_a - \frac{\gamma}{\gamma-1}P_1\frac{dV_p}{dt} - \dot{Q}_{loss} \quad (12)$$

where, V_p is the volume of the cylinder, $\dot{Q}_{loss}$ is the heat exchange rate between the cylinder walls and the surrounding. To obtain the pressure variation inside the engine part, equations (2), (5) and (12) are added and rearranged so

$$\frac{dP_1}{dt} = \frac{\gamma-1}{V_t}\left[\dot{m}_v h_g - \dot{m}_f h_f - \frac{\gamma}{\gamma-1}P_1\frac{dV_p}{dt} - \dot{Q}_r - \dot{Q}_{loss}\right] \quad (13)$$

where V_t is the total volume of the engine part:

$$V_t = V_e + V_C + V_p \quad (14)$$

The Cooling Part

The calculation scheme for the cooling part of the system is shown in Figure 3.

Control Volume of the Cooling Device Cylinder

The energy equation for the cylinder is:

$$\frac{V_p}{\gamma-1}\frac{dP_2}{dt} = \dot{m}_{cp}c_pT_{cp} - \frac{\gamma}{\gamma-1}P_2\frac{dV_p}{dt} + \dot{Q}_{losses} \quad (15)$$

Equation (15) is used to calculate the mass $\dot{m}_{cp}$ which is the mass rate of working fluid flow between the cylinder and cooler. The temperature T_{cp} depends on the direction of the flow:

$$T_{cp} = \begin{cases} T_c, & \dot{m}_{cp} > 0 \\ T_p, & \dot{m}_{cp} < 0 \end{cases} \quad (16)$$

Control Volume of the Cooler

The configuration and geometrical dimensions of the cooler are identical to the condenser on the engine part. The energy equation for the cooler is

$$\frac{V_c}{\gamma-1}\frac{dP_2}{dt} = -\dot{m}_{cp}c_pT_{cp} + \dot{m}_{ec}c_pT_{ec} - \dot{Q}_r \quad (17)$$

The effectiveness-NTU method is used in order to calculate the heat rejected in the cooler [20]:

$$\dot{Q}_r = \varepsilon\dot{m}_{cp}C_p\left(T_{ci} - T_{cp}\right) \quad (18)$$

where the effectiveness ε is calculated from the formula

$$\varepsilon = \frac{1 - exp[-NTU(1-C)]}{1 - C * exp[-NTU(1-C)]} \quad (19)$$

In this equation

$$C = \dot{m}_{cp} Cp_{air} / \dot{m}_{cl} Cp_{water} \tag{20}$$

$$NTU = \frac{UA_c}{\dot{m}_{cp} Cp_{air}} \tag{21}$$

Control Volume of Cooling Space

The cooling space has the same geometry and dimensions as evaporator. For the control volume of the cooling space, the energy equation is

$$\frac{V_e}{\gamma - 1}\frac{dP_2}{dt} = -\dot{m}_{ec} c_p T_{ec} + \dot{Q}_{CS} \tag{22}$$

The air pressure in the cooling part can be calculated by adding and rearranging the energy equations written for the cylinder, cooler and cooling space:

$$\frac{V_t}{\gamma - 1}\frac{dP_2}{dt} = -\frac{\gamma}{\gamma - 1} P_2 \frac{dV_p}{dt} + \dot{Q}_{losses} - \dot{Q}_r + \dot{Q}_{cs} \tag{23}$$

where V_t is the total air volume confined in the cooling part.

$$V_t = V_p + V_c + V_e \tag{24}$$

The temperature in each control volume can be calculated from the ideal gas state equation:

$$T_p = \frac{P_2 V_p}{R\ m_p} \tag{25}$$

$$T_c = \frac{P_2 V_c}{R m_c} \tag{26}$$

$$T_e = \frac{P_2 V_e}{R m_e} \tag{27}$$

Since the cooling part is confined system, the total mass of the air in the cooling part is constant:

$$m_t = m_p + m_c + m_e \tag{28}$$

then, in accordance with [22]

$$\frac{dm_p}{dt} + \frac{dm_c}{dt} + \frac{dm_e}{dt} = 0 \tag{29}$$

Here the term $\frac{dm_p}{dt}$ and $\frac{dm_e}{dt}$ are defined as:

$$\left.\begin{aligned} \frac{dm_p}{dt} &= \dot{m}_{cp} \\ \frac{dm_e}{dt} &= -\dot{m}_{ec} \end{aligned}\right\} \tag{30}$$

Finally, the mass of air in the cooler can be calculated as

$$m_c = m_c^i + \frac{dm_c}{dt} * dt \tag{31}$$

where m_c^i is the initial mass of the air in the cooler.

Displacement of the Liquid Column

The displacement of the water column can be written as

$$M_{lp2}\ddot{x} + C_2\dot{x} + (K_2 + 2A_2\rho g)x = (P_1 - P_2)A_2 \quad (32)$$

where, x is the displacement of the water column, M_{lp2} is the water mass inside the liquid piston. The spring stiffness on the cooling side can be calculated as [23]:

$$K_2 = \frac{\gamma P_2 A_2^2}{V_2} \quad (33)$$

The abovementioned equations describing the operation of the dynamic solar cooling unit were solved simultaneously using Matlab/Simulink environment. The time step of simulation was set to 0.005 seconds and the simulations would be terminated when solutions reach the stabilisation.

DISCUSSION OF NUMERICAL RESULTS

The effect of the cooling water temperature and the cooling water flow rate on the performance of the system was investigated. The modelling input parameters are the heat input to the evaporator and design parameters of the system parts (evaporator, condenser, U-tube, cooler and cooling space) in the laboratory prototype of the system. The heat input to the evaporator is constant and equal to 700 W which is the same provided by solar radiation in summer day in Benghazi, Libya.

The Effect of the Cooling Water Temperature

The heat rejected in the cooling part is defined by the temperature of the cooling water. The cooling water temperatures were set as 20, 15 and 10 °C. The temperature of the cooling water in the condenser, which is the heat sink in the engine part, is kept at a constant value of 20 °C. Figures 5 to 9 show the influence of the cooling water temperature on the amplitude of the water column oscillations in the cylinder, pressure variations on the engine and cooling parts, the air temperature in the cylinder of the cooling part and in the cooling space. The cooling water flow rate was kept constant at 270 kg/hr.

The effect of the cooling water temperature on the amplitude of the water column oscillations in the cylinder is shown in Figure 5. It can be seen that the amplitude of oscillations stays approximately constant with value of 2.5 cm. The frequency of oscillations is about 3.3 Hz for all three cases. The variables stay constant since the cooling water temperature in the condenser is kept constant which means that the engine operates with constant heat source and heat sink temperatures.

The effect of the cooling water temperature on the engine pressure variations is demonstrated in Figure 6. The engine pressure gradually decreases with the decrease in the cooling water temperature. The average values of the engine pressure are 106410, 106100 and 105770 Pa for cases when the cooling water temperature values are 20, 15 and 10 °C, respectively.

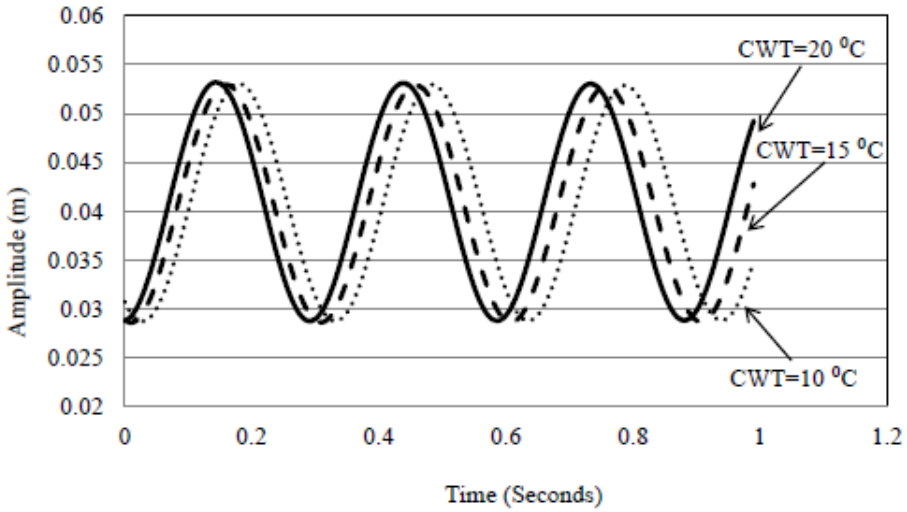

Figure 5. The effect of the cooling water temperature on the water column oscillations.

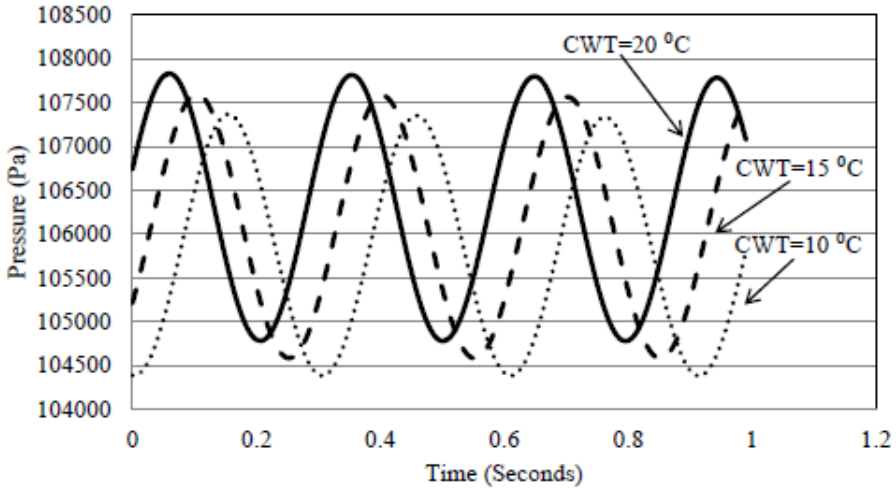

Figure 6. The effect of the cooling water temperature on the pressure in engine part.

The water cooling temperature has the same effect on the pressure variations in the cooling part of the system, as shown in Figure 7. The cooling part pressure decreases with the drop in the cooling water temperature. The average values of the pressure in the cooling part are 100670, 99080 and 97470 Pa for the cooling water temperature of 20, 15 and 10 °C.

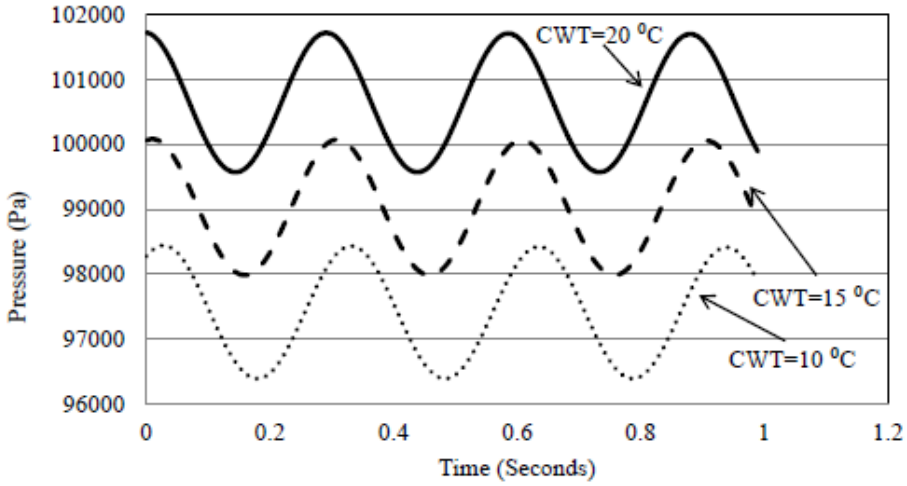

Figure 7. The effect of the cooling water temperature on the pressure variation in the cooling part of the system.

Figure 8 shows the effect of the cooling water temperature on the temperature change in the cooling cylinder. It can be observed that the air temperature gradually decreases with the reduction of the cooling water temperature. The average values of the air temperature in the cooling cylinder are found to be 293.8, 288.8 and 284.6 K for the cooling water temperatures of 20, 15, 10 °C, respectively.

Figure 9 shows the effect of the cooling water temperature on the temperature change in the cooling space. By lowering the cooling water temperature from 20 to 15 and then to 10 °C, the air temperature in the cooling space is decreased from 291.8 to 287.4 and then to 282.6 K.

The Effect of the Cooling Water Flow Rate

The cooling water flow rate affects the amount of the heat rejected in both the condenser and the cooler. The effect of the cooling water flow rate on the oscillations of water column, engine and cooling part pressures and temperatures were studied. In the theoretical model, the cooling water flow rate was set to 180, 220 and 270 kg/hr. The heat input rate to the evaporator and the cooling water temperature were kept at 700 W and 20 °C, respectively.

Figure 10 shows the effect of the cooling water flow rate on the amplitude and frequency of the water column oscillations in the cylinder. It can be seen that the amplitude of the water column oscillations decreases from 2.9 cm at the cooling water flow rate of 180 kg/hr to 2.2 cm at the flow rate of 220 kg/hr and then increases to 2.4 cm at the cooling water flow rate of 270 kg/hr.

The effect of the cooling water flow rate on the engine pressure variations is illustrated in Figure 11 which clearly shows that the engine pressure gradually decreases with the increase in the cooling water flow rate. The average pressure decreases from 139390 Pa at the cooling water flow rate of 180 kg/hr to 123100 Pa at the flow rate of 220 kg/hr and then to 106410 Pa at the cooling water flow rate of 270 kg/hr.

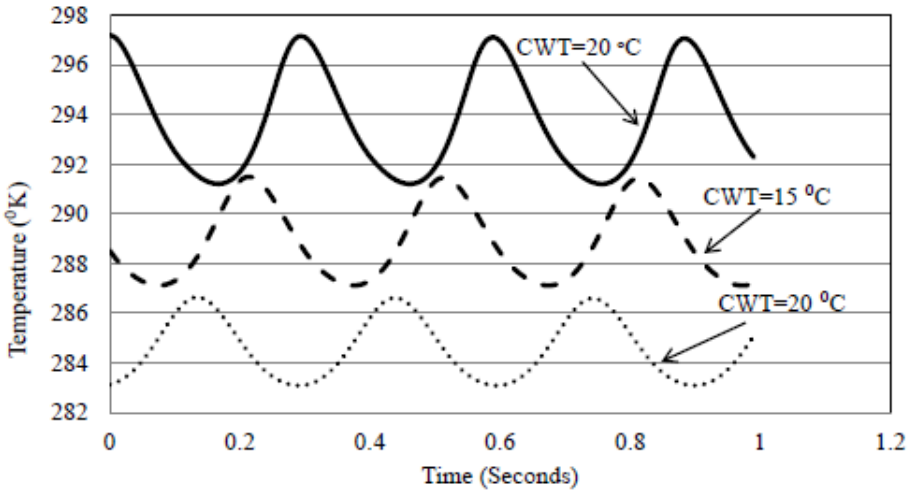

Figure 8. The effect of the cooling water temperature on the temperature change in the cooling cylinder.

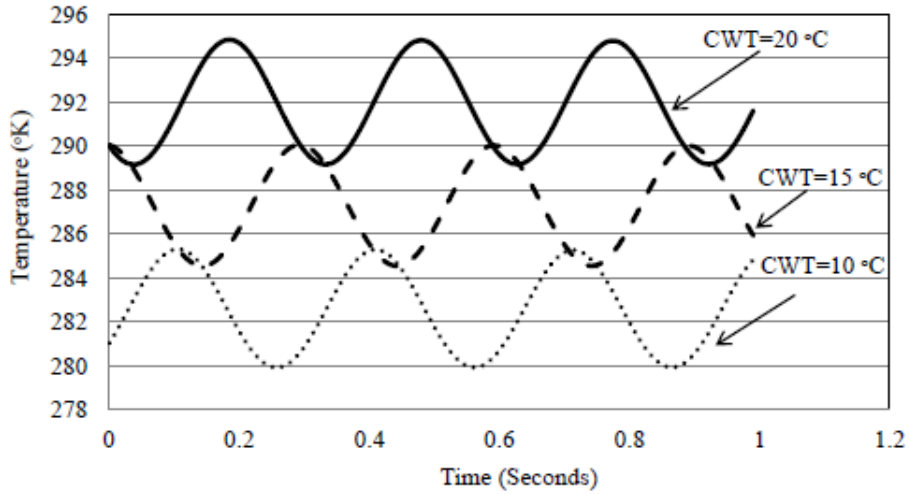

Figure 9. The effect of the cooling water temperature on the temperature change in the cooling space.

It can be seen in Figure 12 that the average cooling part pressure increases from 100160 Pa at the cooling water flow rate of 180 kg/hr to 100600 Pa at the flow rate of 220 kg/hr. The average cooling pressure increases to reach 100670 Pa at the flow rate of 270 kg/hr. This increase in the cooling part pressure leads to an increase in the average value of the air temperature in the cooling cylinder, as shown in Figure 13. The average air temperatures in the cooling cylinder are 291.4, 292.4 and 293.8 K at flow rates of 180, 220 and 270 kg/hr, respectively.

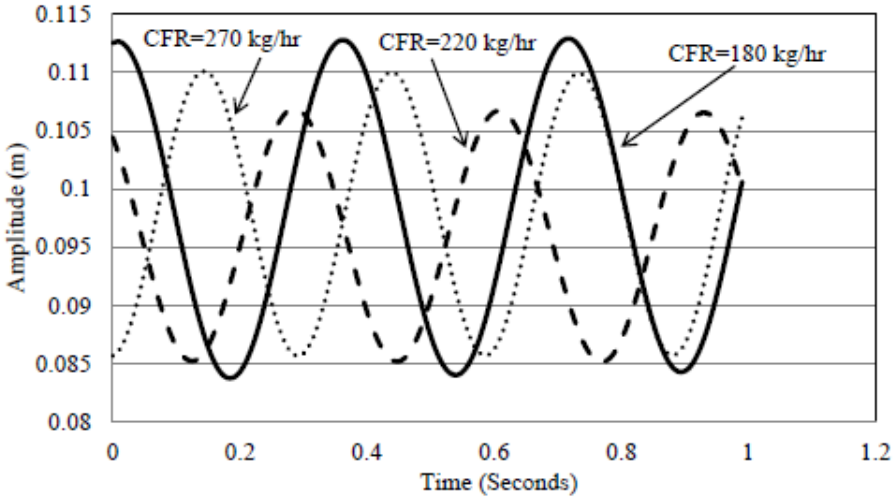

Figure 10. The effect of the cooling water flow rate on the water column oscillations.

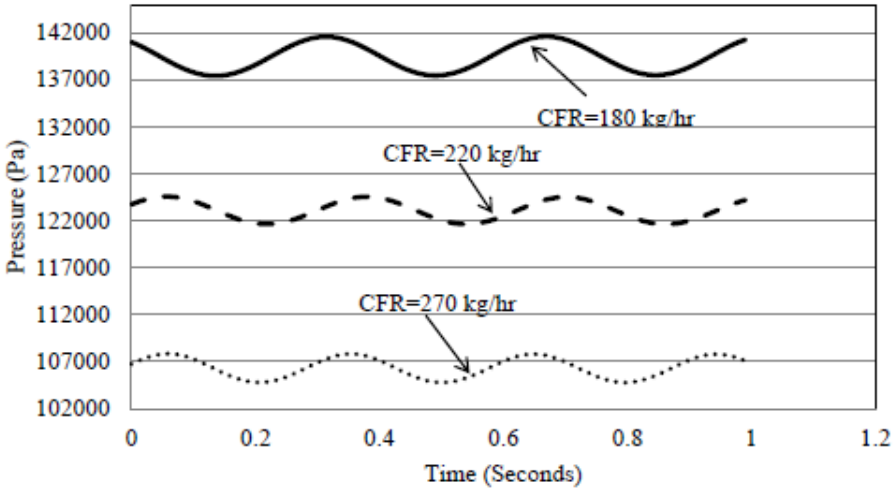

Figure 11. The effect of the cooling water flow rate on the engine pressure.

Figure 14 shows the effect of cooling water flow rate on the air temperature in the cooling space. It was found that the air temperature rises with the increase in the cooling water flow rate and is 290.7, 292 and 292.05 K, respectively

70

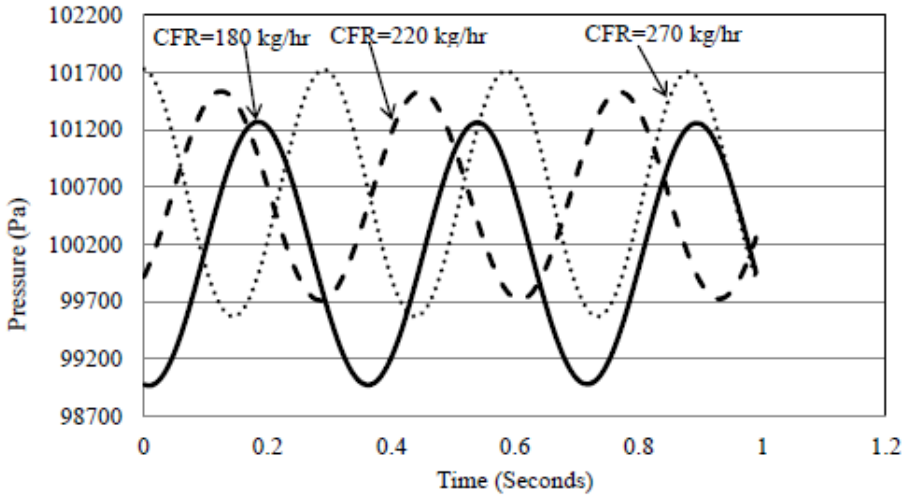

Figure 12. The effect of the cooling water flow rate on the cooling part pressure.

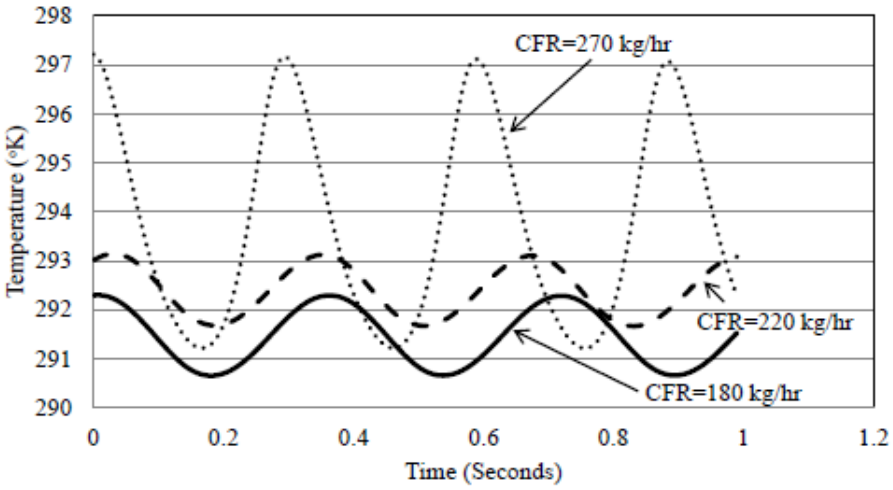

Figure 13. The effect of the cooling water flow rate on the temperature in the cooling cylinder.

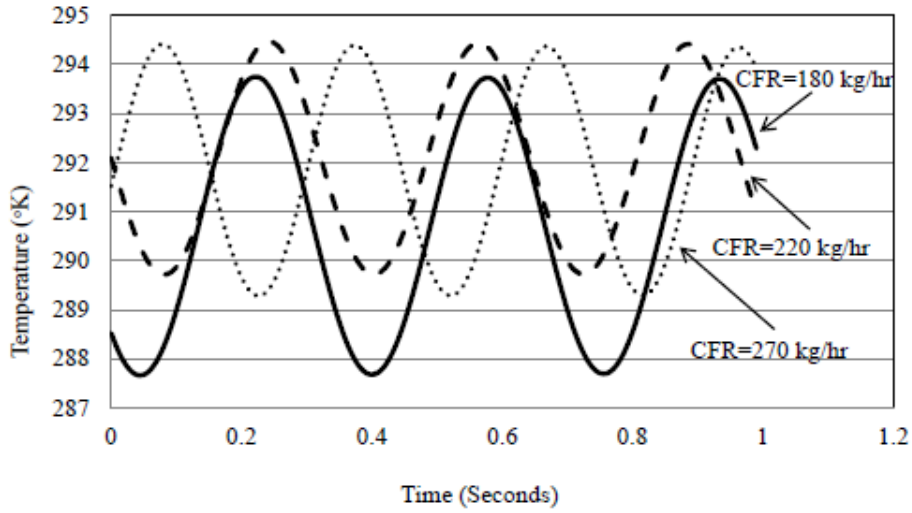

Figure 14. The effect of the cooling water flow rate on the temperature in cooling space.

CONCLUSIONS

In this study, a mathematical mode of the solar cooling system based on the liquid piston converter is developed and its operation is simulated. The thermodynamic equations of the working process and water column dynamic equation were solved in MATLAB/Simulink environment to obtain numerical results on the performance of such thermal auto-oscillating system. Furthermore, the impact of some factors on the operation of the system was investigated.

Using water and air as working fluids in such unpressurised system it is possible to obtain about two degrees reduction in the average temperature of the working fluid on the cooling side of the system, compared to the ambient temperature.

To achieve higher levels of cooling capacity usage of other gases such helium and more volatile liquids instead of water should be studied.

ACKNOWLEDGEMENTS

The authors would like to acknowledge the PhD financial provision by the Cultural attaché at the Libyan Embassy in London, UK.

REFERENCES

[1] M. Beerepoot, "Technology Roadmap Solar Heating and Cooling," *International Energy Agency, Paris, France,* 2012.

[2] S. LANGDON-ARMS, M. GSCHWENDTNER, and M. NEUMAIER, "Performance of Heat-powered Unconstrained 4 Cylinder Double-acting Alpha-type Liquid Piston Stirling Cooler," presented at the The 16th International Stirling Engine ISEC, Bilbao, Spain, 2014.

[3] F. Muhammad-Sukki, A. B. Munir, R. Ramirez-Iniguez, S. H. Abu-Bakar, S. H. Mohd Yasin, S. G. McMeekin, *et al.*, "Solar photovoltaic in Malaysia: The way forward," *Renewable and Sustainable Energy Reviews,* vol. 16, pp. 5232-5244, 2012.
[4] H. Z. Hassan and A. A. Mohamad, "A review on solar cold production through absorption technology," *Renewable and Sustainable Energy Reviews,* vol. 16, pp. 5331-5348, 2012.
[5] X. Yan, G. Chen, D. Hong, S. Lin, and L. Tang, "A novel absorption refrigeration cycle for heat sources with large temperature change," *Applied Thermal Engineering,* vol. 52, pp. 179-186, 2013.
[6] R. de Lieto Vollaro, F. Botta, A. de Lieto Vollaro, and G. Galli, "Solar cooling system for buildings: Thermal analysis of solid absorbents applied in low power adsorption system," *Energy and Buildings,* vol. 80, pp. 436-440, 2014.
[7] H. Z. Hassan, A. A. Mohamad, and R. Bennacer, "Simulation of an adsorption solar cooling system," *Energy,* vol. 36, pp. 530-537, 2011.
[8] H. Hassan, "A Solar Powered Adsorption Freezer: A Case Study for Egypt's Climate," *International Journal of Energy Engineering,* vol. 3, pp. 21-29, 2013.
[9] D. S. Ayou, J. C. Bruno, R. Saravanan, and A. Coronas, "An overview of combined absorption power and cooling cycles," *Renewable and Sustainable Energy Reviews,* vol. 21, pp. 728-748, 2013.
[10] S. Vijayaraghavan and D. Y. Goswami, "A combined power and cooling cycle modified to improve resource utilization efficiency using a distillation stage," *Energy,* vol. 31, pp. 1177-1196, 2006.
[11] F. Xu, D. Y. Goswami, and S. S. Bhagwat, "A combined power/cooling cycle," *Energy,* vol. 25, pp. 233-246, 2000.
[12] M. Sultan, I. I. El-Sharkawy, T. Miyazaki, B. B. Saha, and S. Koyama, "An overview of solid desiccant dehumidification and air conditioning systems," *Renewable and Sustainable Energy Reviews,* vol. 46, pp. 16-29, 2015.
[13] Y. Tekin and O. E. Ataer, "Performance of V-type Stirling-cycle refrigerator for different working fluids," *International Journal of Refrigeration,* vol. 33, pp. 12-18, 2010.
[14] K. Mahkamov and B. Belgasim, "Experimental study of the performance of a dynamic water desalination system with a fluid piston engine," in *The 14th international Stirling engine conference*, 2009.
[15] K. Mahkamov, E. Orda, B. Belgasim, and I. Makhkamova, "A novel small dynamic solar thermal desalination plant with a fluid piston converter," *Applied Energy,* vol. 156, pp. 715-726, 2015.
[16] B. Belgasim and K. Mahkamov, "Theoretical Modelling of a Dynamic Solar Thermal Desalination Unit with a Fluid Piston Engine," in *2nd World Renewable Energy Congress (WREC)*, 2011.
[17] K. Mahkamov, G. Hashem, B. Belgasim, and I. Makhkamova, "A Novel Solar Cooling system Based on a Fluid Piston Convertor," presented at the 16th International Stirling Engine Conference, Belbao, Spain, 2014.
[18] [18] K. Mahkamov and G. Hashem, "Development of a Solar Cooling System Based on a Fluid Piston Convertor," presented at the The European Conference on Sustainability, Energy & the Environment 2015, Brighton, UK, 2015.
[19] Y. A. Çengel and M. Boles, *Thermodynamics: an engineering approach*. London McGraw-Hill 2008.
[20] J. P. Holman, *Heat Transfer*, 10th ed. ed. New Tork: McGraw-Hill, 2010.
[21] T. L. Bergman, F. P. Incropera, and A. S. Lavine, *Fundamentals of heat and mass transfer*: John Wiley & Sons, 2011.

[22] I. Urieli and D. M. Berchowitz, *Stirling cycle engine analysis*. Bristol: A. Hilger 1984
[23] G. Walker and J. R. Senft, *Free-piston Stirling engines*: Springer, 1985.

NOMENCLATURE

A	area, m^2
C	damping coefficient, N s m^{-1}
C_p, C_v	specific heat at constant pressure and volume J kg^{-1} K^{-1}
D	diameter, m
G	solar radiation, Wm^{-2}
g	gravitational acceleration, m s^{-2}
H	water column height, m
h_o, h_i	outer and inner convection heat transfer coefficients, W m^{-2} K^{-1}
K	gas spring stiffness, Nm^{-1}
M	mass, kg
$\dot{m}$	mass flow rate, kg s^{-1}
NTU	number of heat transfer unit
P	pressure, Pa
Q_r	heat rejected, W
Q_{in}	heat input, W
R	gas constant, J kg .K^{-1}
R_b	geometric factor
T	temperature, K
t	time, seconds
U	overall convection heat transfer coefficient, $Wm^{-2}K^{-1}$
V	volume, m^3
X	displacement of water column in the liquid piston, m

Subscripts

a	air
b	brine
c	condenser of the engine part or cooler of the cooling part
cool	cooling water
cp	interface between condenser and liquid piston
e	evaporator of the engine part or cooling space of the cooling part
ec	interface between condenser and evaporator
p	liquid piston cylinder
sw	seawater
v	vapour
1	inner cylinder
2	outer cylinder

Greek symbols

γ	isentropic index
ε	effectiveness
μ	viscosity, kg $m^{-1}s^{-1}$
ρ	density, kg m^{-3}

Appendix B

Theoretical and experimental data for the second and third configurations of the dynamic solar cooling unit

1. Second configuration

1.1 Theoretical and experimental values of the amplitude of the liquid piston engine

Sampling time (Second)	theoretical amplitude (m)	experimental amplitude (m)
0	0.086296296	0.087387101
0.01	0.086672225	0.091594638
0.02	0.087793427	0.091212101
0.03	0.089640161	0.089044638
0.04	0.092179562	0.096439565
0.05	0.095365734	0.091594638
0.06	0.099139907	0.099372101
0.07	0.103430682	0.104472029
0.08	0.108154416	0.104089565
0.09	0.113215812	0.113779493
0.1	0.118508779	0.114289493
0.11	0.123917679	0.113779493
0.12	0.129319041	0.118241957
0.13	0.134583843	0.117349493
0.14	0.139580436	0.12244942
0.15	0.144178139	0.126911884
0.16	0.148251452	0.12856942
0.17	0.151684742	0.132649348
0.18	0.154377149	0.134051884
0.19	0.156247332	0.13009942
0.2	0.15723765	0.134944348
0.21	0.157317276	0.13009942
0.22	0.15648394	0.13009942
0.23	0.154764051	0.13086442

0.24	0.152211204	0.12117442
0.25	0.148903242	0.122066957
0.26	0.14493825	0.118496957
0.27	0.140429883	0.114161957
0.28	0.135502463	0.114161957
0.29	0.130286237	0.110337029
0.3	0.124913067	0.106257029
0.31	0.119512722	0.103197029
0.32	0.114209835	0.099372101
0.33	0.109121512	0.094782101
0.34	0.10435552	0.096567101
0.35	0.100008973	0.091977101
0.36	0.096167407	0.094272101
0.37	0.092904137	0.094399565
0.38	0.090279834	0.089172101
0.39	0.08834226	0.092487101
0.4	0.0871261	0.087259638
0.41	0.086652866	0.089299638

1.2 Theoretical and experimental amplitude of the liquid piston cooling machine

Sampling time (Second)	theoretical amplitude (m)	experimental amplitude (m)
0	0.120121867	0.12048553
0.01	0.120253804	0.12048553
0.02	0.119917032	0.120010826
0.03	0.119119025	0.119536122
0.04	0.117877141	0.119536122
0.05	0.116218394	0.111465878
0.06	0.114179092	0.1138394
0.07	0.111804333	0.104819748
0.08	0.109147336	0.104819748
0.09	0.106268597	0.097224209
0.1	0.103234849	0.096749504
0.11	0.100117809	0.091527487
0.12	0.096992712	0.090578078
0.13	0.093936617	0.089153965
0.14	0.091026537	0.091527487
0.15	0.088337376	0.091527487
0.16	0.085939771	0.092476896
0.17	0.08389789	0.090103374
0.18	0.082267299	0.092002191

0.19	0.081093011	0.091527487
0.2	0.08040782	0.090578078
0.21	0.080231046	0.088204557
0.22	0.08056777	0.091052783
0.23	0.081408634	0.091527487
0.24	0.082730211	0.098173617
0.25	0.084495891	0.099123026
0.26	0.086657252	0.105294452
0.27	0.089155799	0.105769157
0.28	0.091924986	0.103870339
0.29	0.094892389	0.110991174
0.3	0.09798192	0.112889991
0.31	0.101115999	0.111940583
0.32	0.104217586	0.112889991
0.33	0.10721206	0.120010826
0.34	0.110028871	0.120960235
0.35	0.112602966	0.119536122
0.36	0.114875993	0.120960235
0.37	0.116797294	0.121434939
0.38	0.118324696	0.118586713
0.39	0.119425119	0.120010826
0.4	0.120075021	0.118586713
0.41	0.120260701	0.120010826

1.3 Theoretical and experimental pressure in the engine part

Sampling time (Second)	theoretical pressure (Pa)	experimental pressure (Pa)
0	105161.6811	104890.7
0.01	104952.4804	104694.1
0.02	104580.7495	104580.7495
0.03	104055.8093	103928.5
0.04	103391.1819	102945.6
0.05	102605.3585	101910.9
0.06	101719.7635	101962.6
0.07	100758.0223	101497
0.08	99745.20948	101031.4
0.09	98702.63462	99686.4
0.1	97659.23439	99376
0.11	96641.46668	98134.4
0.12	95673.56135	96996.2
0.13	94778.12544	96634.1
0.14	93975.73108	96375.4
0.15	93287.48021	95392.5

0.16	92727.80467	95237.3
0.17	92306.66467	94000
0.18	92033.52753	93300
0.19	91913.0884	92700
0.2	91947.45584	92700
0.21	92134.75617	94000
0.22	92470.48458	95237
0.23	92946.78208	95651.1
0.24	93554.05177	95754.6
0.25	94277.09239	96789.3
0.26	95100.22832	97668.8
0.27	96008.10902	98962.1
0.28	96980.53269	98962.1
0.29	97995.25985	100255.4
0.3	99028.41843	99686.4
0.31	100056.2157	100721
0.32	101055.2458	102428.2
0.33	101996.182	103669.8
0.34	102854.3698	103669.8
0.35	103606.8091	103876.8
0.36	104232.9407	104187.2
0.37	104715.3995	104715.3995
0.38	105038.4955	105038.4955
0.39	105193.6685	105193.6685
0.4	105179.4313	105179.4313
0.41	105179.4313	105179.4313

1.4 Theoretical and experimental pressure in the cooling part

Sampling time (Second)	theoretical pressure (Pa)	experimental pressure (Pa)
0	98817.66794	97723.35
0.01	98835.54168	97904.5
0.02	98892.10309	98189.15
0.03	98986.20667	98008
0.04	99115.90344	98266.75
0.05	99278.57759	98887.85
0.06	99470.90611	98887.85
0.07	99688.82759	99276
0.08	99927.6246	99793.55
0.09	100181.9835	100492.25
0.1	100446.0792	99638.3

0.11	100713.7036	100259.35
0.12	100978.0298	100854.55
0.13	101232.3428	100983.9
0.14	101469.9922	100906.3
0.15	101684.5543	101837.85
0.16	101870.0636	101372.1
0.17	102021.2264	102122.55
0.18	102133.6639	102122.55
0.19	102204.0724	101605
0.2	102230.3736	101372.1
0.21	102211.5135	101605
0.22	102147.6281	101579.1
0.23	102040.707	101682.6
0.24	101894.0554	101190.95
0.25	101712.1637	100828.65
0.26	101500.4342	100647.5
0.27	101264.9435	100155.85
0.28	101012.2584	100725.15
0.29	100749.1785	99819.4
0.3	100482.5588	99508.9
0.31	100218.8183	99405.4
0.32	99964.17444	99327.75
0.33	99724.48525	98577.3
0.34	99505.01106	98499.65
0.35	99310.36769	98525.55
0.36	99144.48716	98473.8
0.37	99010.60195	98396.15
0.38	98911.3024	98215
0.39	98848.34537	98215
0.4	98822.84555	98499.65
0.41	98822.84555	98499.65

1.5 Theoretical and experimental temperature in engine cylinder

Sampling time (Second)	theoretical temperature (K)	experimental temperature (K)
0	357.5102809	358.1720109
0.01	357.7845274	358.09356
0.02	357.8918191	358.4505164
0.03	357.9707914	357.9668509
0.04	357.9312902	357.5976436
0.05	357.7272982	357.9847564

0.06	357.3619992	357.6447527
0.07	356.8480701	357.8937891
0.08	356.2052203	356.7225273
0.09	355.4576999	355.9713055
0.1	354.5114488	355.1614764
0.11	353.5095523	354.6382327
0.12	352.4930966	354.0351091
0.13	351.4901922	353.3334945
0.14	350.527441	352.8046036
0.15	349.6295509	351.6733273
0.16	348.8800358	351.0959418
0.17	348.2616195	351.3101127
0.18	347.7497756	351.5121127
0.19	347.3588401	350.73728
0.2	347.0629079	350.0461564
0.21	346.8812812	349.9231236
0.22	346.8542174	351.6774327
0.23	346.958357	352.9193127
0.24	347.1787006	353.0111236
0.25	347.5131962	353.9003927
0.26	347.8923394	355.3496982
0.27	348.3246206	356.2180545
0.28	348.8402427	355.7330582
0.29	349.4298526	355.4442618
0.3	350.082566	355.6211855
0.31	350.7862755	355.6682509
0.32	351.5666691	356.6242473
0.33	352.4528859	357.1191564
0.34	353.3412727	357.9652073
0.35	354.2143766	357.8539091
0.36	355.0539117	357.4949891
0.37	355.8405427	357.6799527
0.38	356.5538639	357.3054764
0.39	357.0870722	356.9200545
0.4	357.4565778	356.7698545
0.41	357.4565778	356.7698545

1.6 Theoretical and experimental temperature in the cylinder of the cooling machine

Sampling time (Second)	theoretical temperature (K)	experimental temperature (K)

0	290.8931051	290.300128
0.01	290.9018241	291.0937218
0.02	290.94286	290.8505878
0.03	291.0154612	291.6018244
0.04	291.1194092	291.0866503
0.05	291.2526798	291.198128
0.06	291.4128154	291.7004093
0.07	291.5969682	291.6724137
0.08	291.8019399	291.5027575
0.09	292.0242003	292.2676459
0.1	292.2595808	291.9440566
0.11	292.5038643	291.8491816
0.12	292.7523978	292.5372843
0.13	293.000107	293.1635878
0.14	293.2414704	293.051561
0.15	293.470038	293.3129718
0.16	293.6798828	293.6
0.17	293.8648923	293.65
0.18	294.0193254	293.8
0.19	294.1430175	293.45
0.2	294.2392423	293.88907
0.21	294.3008611	293.1380521
0.22	294.3205421	293.1209405
0.23	294.2934594	293.062253
0.24	294.2162472	292.9210119
0.25	294.0870367	292.6187575
0.26	293.908425	292.4546682
0.27	293.6859175	292.4546682
0.28	293.4274249	292.2194673
0.29	293.1421831	292.0646994
0.3	292.8407001	291.8647039
0.31	292.5337187	291.7873066
0.32	292.2317022	291.7567753
0.33	291.9443941	291.6956101
0.34	291.6804964	291.42357
0.35	291.4474644	291.42357
0.36	291.2536744	291.1495164
0.37	291.1014538	291.0122485
0.38	290.9935834	290.9813244
0.39	290.9278715	290.8983378
0.4	290.8974739	291.1244539
0.41	290.8974739	291.1244539

1.7 Theoretical and experimental temperature in the cooling space

Sampling time (Second)	theoretical temperature (K)	experimental temperature (K)
0	286.9275544	288.2643086
0.01	286.9761362	287.8203257
0.02	287.1371122	288.5912571
0.03	287.4072089	288.7262571
0.04	287.7808363	287.6410286
0.05	288.2504433	288.0071314
0.06	288.80645	289.85
0.07	289.4371232	289.5488571
0.08	290.1288224	289.2574457
0.09	290.8661718	289.5
0.1	291.6323054	290.25
0.11	292.4092345	291.0778457
0.12	293.1771624	291.75
0.13	293.9166061	291.5255486
0.14	294.6082501	291.13704
0.15	295.2334189	291.8236629
0.16	295.7747465	292.75
0.17	296.2167965	293.95
0.18	296.5467685	294.53412
0.19	296.7549675	295.25
0.2	296.8352433	295.25
0.21	296.7843867	294.85
0.22	296.6026947	294.6885771
0.23	296.2958396	294.3914914
0.24	295.8733135	294.3372514
0.25	295.3480593	293.2813543
0.26	294.7356992	292.0273543
0.27	294.0538173	293.1305314
0.28	293.3214453	291.6780686
0.29	292.5583094	292.52364
0.3	291.7843152	291.2097771
0.31	291.0181138	291.8784686
0.32	290.27779	290.25
0.33	289.5803923	290.85
0.34	288.9412422	289.65
0.35	288.373796	289.4858743
0.36	287.889529	288.3622114

0.37	287.4978882	288.3784629
0.38	287.2064516	287.75
0.39	287.0203983	287.6316857
0.4	286.9430249	287.5030114
0.41	286.9430249	287.5030114

2. Third configuration

2.1 Theoretical and experimental amplitudes of the liquid piston engine oscillations

Sampling time (Second)	theoretical amplitude (m)	experimental amplitude (m)
0	0.009692	0.008521
0.01	0.01016	0.008521
0.02	0.011169	0.009049
0.03	0.01267	0.011336
0.04	0.014592	0.0139
0.05	0.016845	0.0145
0.06	0.019324	0.016
0.07	0.021914	0.018
0.08	0.024498	0.022
0.09	0.026958	0.0245
0.1	0.029185	0.027
0.11	0.031081	0.029
0.12	0.032564	0.0305
0.13	0.033569	0.03
0.14	0.034052	0.0325
0.15	0.033994	0.0325
0.16	0.033398	0.031
0.17	0.032289	0.030691
0.18	0.030716	0.029
0.19	0.028747	0.027524
0.2	0.026467	0.025
0.21	0.023978	0.0235
0.22	0.021391	0.02
0.23	0.01882	0.016791
0.24	0.016385	0.013976
0.25	0.014197	0.0138
0.26	0.012357	0.011336
0.27	0.010953	0.007993

0.28	0.010051	0.008345
0.29	0.009693	0.008873

2.2 Theoretical and experimental pressure in the engine part

Sampling time (Second)	theoretical pressure (Pa)	experimental pressure (Pa)
0	104780	104779.8
0.01	104806	104779.8
0.02	104896	105169.2
0.03	105046.6	104909.6
0.04	105251.8	105125.9
0.05	105503.4	105666.7
0.06	105790.8	105883
0.07	106101.8	106294
0.08	106422.6	106380.5
0.09	106738.9	106575.2
0.1	107035.9	106986.2
0.11	107299.6	107375.5
0.12	107517.2	107159.2
0.13	107677.9	107159.2
0.14	107773.7	107764.9
0.15	107799.9	107764.9
0.16	107754.7	107527
0.17	107640.1	107332.3
0.18	107462.1	107137.6
0.19	107229.6	106986.2
0.2	106954.3	106683.4
0.21	106649.3	106358.9
0.22	106329.2	105947.9
0.23	106008.6	105702
0.24	105702.1	105385.5
0.25	105422.9	105209.6
0.26	105183.1	104992
0.27	104992.7	104823.1
0.28	104859.5	104755
0.29	104789	104688
0.3	104784.4	104655

2.3 Theoretical and experimental pressure in the cooling part

Sampling time (Second)	theoretical pressure (Pa)	experimental pressure (Pa)

0	101728.3	101735.1
0.01	101685	101772.3
0.02	101593.1	101571.4
0.03	101457	101370.5
0.04	101283.8	101266.4
0.05	101082	101221.7
0.06	100861.4	100872.1
0.07	100632.5	100604.2
0.08	100405.6	100291.8
0.09	100190.7	99815.65
0.1	99997.07	99890.06
0.11	99832.94	99837.98
0.12	99705.02	99518.08
0.13	99618.42	99562.72
0.14	99576.51	99599.91
0.15	99581.03	99644.56
0.16	99632.28	99666.87
0.17	99728.26	99592.48
0.18	99865.07	99904.93
0.19	100037	100098.4
0.2	100236.8	100306.7
0.21	100455.9	100529.8
0.22	100684.5	100827.4
0.23	100912.4	101028.3
0.24	101128.7	101348.2
0.25	101323.2	101519.3
0.26	101486.7	101705.3
0.27	101611.2	101727.6
0.28	101690.7	101824.3
0.29	101721.6	101965.7
0.3	101702.3	101742.5

2.4 Theoretical and experimental engine cylinder temperature

Sampling time (Second)	theoretical temperature (K)	experimental temperature (K)
0	356.6876	356.7782
0.01	356.7684	358.1481
0.02	357.0065	357.3872
0.03	357.4355	358.3286
0.04	358.0887	358.1975
0.05	358.9852	358.8498

0.06	360.1103	358.8872
0.07	361.4114	359.6762
0.08	362.7845	359.7357
0.09	363.8869	360.2046
0.1	364.5869	360.5058
0.11	364.8618	360.8959
0.12	364.7829	361.2423
0.13	364.4501	361.2678
0.14	363.9526	361.4718
0.15	363.3578	361.3781
0.16	362.7126	362.041
0.17	362.0489	361.2955
0.18	361.3875	362.1415
0.19	360.7426	361.5684
0.2	360.1239	361.4453
0.21	359.5403	360.1886
0.22	359.0164	360.7758
0.23	358.5285	359.5342
0.24	358.0551	359.1425
0.25	357.6308	359.2897
0.26	357.2701	358.0089
0.27	356.984	358.0835
0.28	356.7834	357.4358
0.29	356.6821	357.0603
0.3	356.6984	356.8779
0.31	356.8574	356.8779

2.5 Theoretical and experimental temperature in the cylinder of the cooling machine

Sampling time (Second)	theoretical temperature (K)	experimental temperature (K)
0	297.2163	296.0193
0.01	297.0726	296.6597
0.02	296.7302	296.6151
0.03	296.2516	296.7329
0.04	295.6922	296.4597
0.05	295.0963	296.0121
0.06	294.4982	295.1612
0.07	293.9238	295.4312
0.08	293.3923	295.1138
0.09	292.9172	295.0477

0.1	292.5074	294.5933
0.11	292.1677	293.9969
0.12	291.885	293.722
0.13	291.6433	293.9464
0.14	291.449	292.7321
0.15	291.3084	293.1424
0.16	291.2285	292.4379
0.17	291.2169	292.3312
0.18	291.2831	292.1987
0.19	291.4383	292.7448
0.2	291.6956	292.7962
0.21	292.0687	293.5542
0.22	292.5687	293.2955
0.23	293.1983	293.5376
0.24	293.944	293.7886
0.25	294.7699	294.7671
0.26	295.6178	295.3347
0.27	296.3694	295.2715
0.28	296.8983	295.9917
0.29	297.1472	296.5008
0.3	297.1226	296.8185

2.6 Theoretical and experimental temperature in the cooling space

Sampling time (Second)	theoretical temperature (K)	experimental temperature (K)
0	294.8411	294.8497556
0.01	294.8392	295.0418556
0.02	294.7046	294.8616389
0.03	294.4438	295.0724
0.04	294.07	294.4371722
0.05	293.6019	293.7406
0.06	293.0624	294.1348222
0.07	292.4775	293.3516056
0.08	291.8747	292.7100667
0.09	291.2808	292.7304722
0.1	290.7221	292.3575333
0.11	290.2229	291.6032889
0.12	289.8042	291.5023444
0.13	289.4834	291.3492111
0.14	289.2732	290.6769444

0.15	289.182	290.6935833
0.16	289.214	290.5612
0.17	289.3689	290.5252056
0.18	289.6406	290.7742556
0.19	290.0177	290.9688056
0.2	290.4844	292.0556944
0.21	291.0208	291.8313833
0.22	291.6036	292.0482056
0.23	292.2071	291.6996833
0.24	292.8032	292.5133556
0.25	293.364	293.6258611
0.26	293.8632	294.1412389
0.27	294.277	294.7982167
0.28	294.5854	295.0797722
0.29	294.7737	295.0277833
0.3	294.8333	295.3185611